الجمهورية الجزائرية الديمقراطية الشعبية
REPUBLIQUE ALGERIENNE DEMOCRATIQUE POPULAIRE
وزارة التعليم العالي و البحث العلمي
MINISTERE DE L'ENSEIGNEMENT SUPERIEUR ET DE LA RECHERCHE SCIENTIFIQUE

Université 20 Aout 1955-Skikda
Faculté des sciences
Département de Chimie
réf :……

جامعة 20 أوت 1955 سكيكدة
كلية العلوم
قسم الكيمياء
المرجع:..... .....

Thèse de Doctorat en sciences

Spécialité : Chimie

Option : **ELECTROCHIMIE ET CORROSION**

Réalisée par

Mr : KAHLOUCHE ABDESALEM

Intitulée :

Etude du mécanisme d'action et de l'efficacité d'inhibiteurs de corrosion naturels dans les milieux agressifs

Devant le jury composé de :

Messaoud LEGOUERA	Professeur	Président.	Université 20 Août 1955 - Skikda
Ferial KRID	MCA	Rapporteur	Université 20 Août 1955 - Skikda
Amel DELIMI	MCA	Co-Rapporteur	Université 20 Août 1955 - Skikda
Djamel BERDJANE	MRA	Examinateur	CRTI - Alger
Yamina BOUDINAR	MCA	Examinateur	Université 20 Août 1955 – Skikda
Linda TOUKAL	MCA	Examinateur	Université Ferhat Abbas -1 - Sétif
Amel SEDIK	MRA	Examinateur	CRAPC – Annaba
Hana FERKOUS	MCA	Invitée	Université 20 Août 1955 - Skikda

2023

الجمهورية الجزائرية الديمقراطية الشعبة
PEOPLE'S DEMOCRATIC REPUBLIC OF ALGERIA
وزارة التعليم العالي و البحث العلمي
MINISTRY OF HIGHER EDUCATION AND SCIENTIFIC RESEARCH

August 20, 1955 Skikda University
Faculty of Sciences
Chemistry Departement
ref :……

جامعة 20 أوث 1955 سكيكدة
كلية العلوم
قسم الكيمياء
المرجع:..... .....

Thesis of Doctorate in sciences

Speciality : Chemitry
Option : **ELECTROCHEMISTRY AND CORROSION**

Realized by :

Mr : KAHLOUCHE ABDESALEM

Entitled :

Study of the mechanism of action and effectiveness of natural corrosion inhibitors in aggressive environments

Thesis Committee:

Messaoud LEGOUERA	Professor	Chairman	University of August 20, 1955-Skikda
Ferial KRID	Assistant Lecturer	Thesis Director	University of August 20, 1955-Skikda
Amel DELIMI	Assistant Lecturer	Thesis Co-Director	University of August 20, 1955-Skikda
Djamel BERDJANE	Senior Researcher	Examiner	CRTI - Alger
Yamina BOUDINAR	Assistant Lecturer	Examiner	University of August 20, 1955-Skikda
Linda TOUKAL	Assistant Lecturer	Examiner	Ferhat Abbas University-1 - Setif
Amel SEDIK	Senior Researcher	Examiner	CRAPC – Annaba
Hana FERKOUS	Assistant Lecturer	Guest of Honor	University of August 20, 1955-Skikda

2023

أهدي عملي هذا

إلى أبي و أمي اللذين علماني الحياة حفظهما الله

إلى زوجتي التي ساندتني و صبرت كثيرا

إلى بنتي العزيزتين سدرة المنتهى و ماريا لينا

إلى إخوتي و أخواتي و كل العائلة الكريمة

إلى كل من ساعدني من قريب أو بعيد

Acknowledgements

Without the support and advice of many people, I would not have made it to this point, and it is here that I intend to express my gratitude.

My sincere thanks are addressed to the members of the jury: Mr. M. LAGOUERA; Professor at the University of Skikda; who made me a great honor to chair the jury of this work. To Mrs Y. BOUDINAR Assistant Lecturer class A university of Skikda, Mrs. A. SADIK; Sinior researcher at CRAPC-Annaba, Mr. Dj. BERDJANE; Sinior researcher at CRTI - Annaba; and L. TOUKAL Assistant Lecturer class A Setif-1 university for having accepted to be the examiners of this thesis.

First of all, I would like to express my gratitude to my thesis director, Mrs Ferial KRID Assistant Lecturer class A university of Skikda, who gave me the opportunity to work on a very current subject.

I would like to thank especially Mrs Amel DELIMI Assistant Lecturer class A, who was the first to introduce me to the subject that guided my thesis. I would like to thank her sincerely for her patience, her availability and especially her judicious advices, which contributed to feed my reflection.

I want to express my profound gratitude to Mme.Hana FERKOUS Assistant Lecturer class A, for her understanding, her availability, and especially her wise counsel, which helped to inspire my reflection. I also want to thank Mrs. Cherifa BOULECHFAR for her assistance and advice to me. I want to thank Mr Yacine BENGUERBA Professor Setif-1 University for her assistance to me.

The major part of this work was carried out at the Unit Research Additive Manufacturing Research Unit - Sétif. I would like to thank both the director of the unit Mr. Halim MERABTI and the division directors Dr. Boussaha BOUCHOUL and Dr. Farouk LAIDOUDI for the facilities that were granted to me.

The part of this work was carried out at the Research Unit of Emerging Materials at the University of Ferhat Abbas-Setif-1. I would like to thank both the current director of the unit Mr. Abdelghani MERDAS and the previous director Mr. Mohamed HAMIDOUCHE for the facilities that were granted to me.

I would like to thank all my friends who shared with me these moments. I Mention them, Abelghani Kenzour, Mohamed Hamidouche,Ammar Kassaa, Ammar Haboussi, Hassen Nezzari, Khaled Hamdi-cherif and Moussa Athmani.

Finally, a very big ***thank you*** *to all my family who have flooded me with their love, prayers and motivations that have made my endeavors successful. My heartfelt gratitude goes out to them.*

Abstract

This work investigates the corrosion inhibition of XC48 Carbon steel and 304L stainless steel, in sulfuric acid 1M to which green and nontoxic inhibitors such as Cytisus multiflorus extract (CMFE) and Punica granatum extract (PGPE) were added at different concentrations. Potentiodynamic and electrochemical impedance spectroscopy measurements were used to characterize each inhibitors mode of action. Quantum chemical parameters were also calculated, which provided a reasonable theoretical explanation for the adsorption and inhibition behavior of CMFE and PGPE on the metal surface.

The CMFE and PGPE are a mixed-type corrosion inhibitors, have been shown inhibit the cathodic and anodic reactions of XC48 carbon steel and 304L stainless steel in electrochemical studies. At 500 ppm, CMFE had an anti-corrosion efficiency of 95.91% and 92.91% of XC48 carbon steel and 304L stainless steel, respectively. In contrast, PGPE exhibits a maximum inhibitory efficiency of approximately 97.40% and 95.91%, at a concentration of 500 ppm in XC48 carbon steel and 304L stainless steel, respectively.

The adsorption of CMFE and PGPE leads to the formation of a protective film revealed by the Scanning Electron Microscope (SEM), Fourier-transform infrared spectroscopy with attenuated total reflectance (FTIR-ATR), X-ray photoelectron spectroscopy (XPS) and X-ray diffraction (XRD) analysis.

The theoretical findings of quantum chemistry calculations were compared with experimental data as part of our study to better understand corrosion mechanisms.

Key words: Carbon steel, Stainless steel, Corrosion Inhibitor, PDP, EIS and DFT.

Résumé

Ce travail étudie l'inhibition contre la corrosion de l'acier au carbone XC48 et de l'acier inoxydable 304L, dans l'acide sulfurique 1M auquel des inhibiteurs verts et non toxiques tels que l'extrait de cytise multiflore (CMFE) et l'extrait de Punica Grenadier (PGPE) ont été ajoutés à différentes concentrations. Des mesures de spectroscopie d'impédance potentiodynamique et électrochimique ont été utilisées pour caractériser le mode d'action de chaque inhibiteur. Les paramètres de la chimie quantique ont également été calculés, ce qui a fourni une explication théorique raisonnable du comportement d'adsorption et d'inhibition du CMFE et du PGPE sur la surface métallique.

Le CMFE et le PGPE sont des inhibiteurs de corrosion de type mixte, il a été démontré qu'ils bloquent les réactions cathodiques et anodiques de l'acier au carbone XC48 et de l' acier inoxydable 304L par des études électrochimiques. À 500 ppm, le CMFE avait une efficacité anti-corrosion de 95,91 % et 92,91 % de l'acier au carbone XC48 et de l'acier inoxydable 304L, respectivement. En revanche, le PGPE présente une efficacité inhibitrice maximale d'environ 97,40 % et 95,91 % , à une concentration de 500 ppm dans l'acier au carbone XC48 et l'acier inoxydable 304L, respectivement.

L'adsorption de CMFE et de PGPE conduit à la formation d'un film protecteur monté par le Microscope Electronique à Balayage (MEB), la spectroscopie infrarouge à transformée de Fourier à réflectance totale atténuée (FTIR-ATR), la spectroscopie photoélectronique à rayons X (XPS) et X analyse par diffraction des rayons (DRX).

Les résultats théoriques des calculs de chimie quantique ont été confrontés aux données expérimentales dans le cadre de notre étude afin de mieux comprendre les mécanismes de corrosion.

Mots clés : acier au carbone, acier inoxydable, inhibiteur de corrosion, PDP, EIS et DFT.

الملخص

هذا العمل يتضمن دراسة في تثبيط ضد تآكل الفولاذ الكربوني XC48 والفولاذ المقاوم للصدأ 304L، في حمض الكبريتيك بتركيز M1 الذي أضيف إليه مثبطات خضراء وغير سامة مثل مستخلص اللـزان متعدد الأزهار (CMFE) ومستخلص قشور الرمان (PGPE) بتركيزات مختلفة. تم استخدام قياسات التحليل الطيفي للمعاوقة الديناميكية والكهروكيميائية لوصف طريقة عمل كل مثبط. تم أيضًا حساب معلمات الكيمياء الكمية ، والتي قدمت تفسيرًا نظريًا معقولًا لسلوك الامتزاز والتثبيط لـ CMFE و PGPE على سطح المعدن.

يُعد كل من CMFE و PGPE من مثبطات التآكل من النوع المختلط ، وقد ثبت أنهما يثبطان التفاعلات الكاثودية والأنودية للفولاذ الكربوني XC48 والفولاذ المقاوم للصدأ 304L من خلال الدراسات الكهروكيميائية . عند 500 جزء في المليون ، كان لدى CMFE كفاءة مقاومة للتآكل تبلغ95.91 ٪ و92.91 ٪ للفولاذ الكربوني XC48 وللفولاذ المقاوم للصدأ 304L على التوالي .في المقابل ، تُظهر PGPE أقصى كفاءة مثبطة تقارب 97.40 ٪ و95.91 ٪ ، بتركيز 500 جزء في المليون للفولاذ الكربوني XC48 وللفولاذ المقاوم للصدأ304L على التوالي.

يؤدي امتزاز CMFE و PGPE إلى تكوين فيلم واقٍ تم الكشف عنه بواسطة المسح المجهري الإلكتروني (MEB) ، والتحليل الطيفي للأشعة تحت الحمراء بتحويل فورييه مع الانعكاس الكلي المخفف (FTIR-ATR) ، والتحليل الطيفي الضوئي للأشعة السينية (XPS) و تحليل حيود الأشعة السينية (DRX)

تمت مقارنة النتائج النظرية لحسابات الكيمياء الكمية مع النتائج التجريبية كجزء من دراستنا لفهم آليات التآكل بشكل أفضل.

الكلمات المفتاحية :الفولاذ الكربوني ، **الفولاذ المقاوم** للصدأ ، مانع التآكل ، PDP ، EIS و.DFT

Abbreviations & Symbols used

βa : Tafel anodic slop

βc : Tafel cathodic slop

Cdl : Double layer capacitance

CMFE : Cytisus Multiflorus Flowers Extract

Conc. : Concentration.

CPE : Constant phase element

CR : Corrosion rate

CS : Carbon steel

DFT : Density Functional Theory

Ecorr : Corrosion potential

EEC: Equivalent circuit electric

EIS: Electrochemical impedance spectroscopy

EOCP : Open circuit potential

Fe: Iron

FTIR: Fourier transform infrared spectroscopy

HOMO : Highest Occupied Molecular Orbital

Hz : Hertz.

icorr: Corrosion current density

ISO: International Standard Organization

***IE*:** Inhibition efficiency

LUMO: Lowest Unoccupied Molecular Orbital

MEP : Molecular electrostatic potential

MD: Molecular dynamics simulation

OCP : Open circuit potential

PDP: potentiodynamic polarization

PGPE : Punica Granatum Peel Extract

ppm: parts per million

Rdt : yeild

Rp : Polarization resistance

Rs : Solution resistance

RDF: Radial distribution function

SEM : Scanning electron microscope

SS : Stainless Steel

VCI: Volatil corrosion inhibitors

XPS: X-ray photoelectron spectroscopy

XRD: X-Ray diffraction

θ: Surface coverage

HBD: hydrogen bond donor

HBA: hydrogen bond acceptor

HB: hydrogen bonding

Eads: adsorption energies

QMDs : quantum molecular descriptors

$\mathbf{E_{Rad}}$:Rigid adsorption energy

$\mathbf{E_{def}}$ **:** DeformationEnergy

List of Figures

List of Tables

Table of Contents

General Introduction

Problematic

Steel alloys are the most widely used metals in various fields in the daily life of people worldwide. Due to their physical and mechanical excellent properties [1-2] and their high carbon content, they are extremely hard and appropriate for applications requiring great wear and abrasion resistance [3]. Due to their low cost, they are used in different industrial sectors such as the automobile industry and machinery in the military and aerospace industries [3-4].

However, some manufacturing operations and other industrial procedures, such as acid cleaning, oil well cleaning, acid de-scaling, and acid pickling, heavily rely on strong acids for various objectives [5]. This led to some risks that conducted to fatal consequences and issues that harm industries, the environment, and humans because of using such as hazardous compounds such as Nitric, sulfuric, hydrochloric, formic, and acetic acids, which are widely employed in these applications [6].

Because metals tend to retreat to their ground states during the corrosion process, it is regarded as one of the difficult-to-solve recurrent problems. In general, corrosion is a process in which the structure of metals deteriorates due to heterogeneous chemical interactions in particular environments [7]. This phenomenon is widespread in many industries, mainly where the acidic medium is commonly utilized, which accelerates the rate of it. It also must be mentioned that water, liquid and gaseous acids, air humidity, sulfur, base salts, ammonia, particular lubricants, and rigorous metal polishing are all known corrosion agents [8], as previously stated. Many industries are affected by corrosion, including the oil and gas sector, fertilizer manufacturing, civil engineering infrastructure such as buildings and bridges, power plants, and petrochemical [9]. As a result, billions of dollars are spent each year to repair infrastructure that has been harmed by corrosion and to control and reduce the consequences of corrosion [10].

Nowadays, one of the essential topics in industrial and academic studies is the corrosion phenomenon of Steel and alloys in acidic media [11]. Corrosion inhibitors can be classified into three classes cathodic, anodic, or mixed [12]. During the past last decades, various types of anti-corrosion methods used plasma electrolytic oxidation [13-14], physical vapor and chemical vapor deposition [15-16], electrodeposition [17-18], applying polymeric and organic coatings [19-20], and using corrosion inhibitors [21-22], are among the most widely used methods of protecting metals from corrosion in acidic environments. Due to their low cost, non-toxic

nature, and the presence of different heterocyclic atoms, double conjugate bonds, polar groups, and aromatic rings, plant extracts are highly effective environmental inhibitors in various industries [15]. The corrosion inhibition property of organic compounds with highly electron-dense hetero-atoms such as N, S, and O is well established. To date, a large number of plant extracts have been reported. Various plant parts, such as seeds, leaves, flowers, and fruits, have been used as anti-corrosion factors [23]. Apricot juice [17], Calendula officinalis flower heads [24], Dardagan Fruit [25] Garlic, Glycine max meal [15], Hymenaea stigonocarpa fruit shell [26], Cytisus Multiflorus is a species (Leguminosae cytiseae), a broad and diverse genus found around the Mediterranean countries, particularly in North Africa and Europe. This genus of plants has bioactive, antiparasitic, and antioxidant properties with a high concentration of phenolic compounds [27].

The aim of this work an investigation on the inhibitory effect of Cytisus Multiflorus extract (CMFE) and Punica Granatum extract (PGPE) regarding corrosion of XC48 Carbon steel and 304L stainless steel (304L SS) in sulfuric acid 1M H_2SO_4.

The present work has been broken down into four chapters.

In the ***first chapter***, a more detailed presentation of the context of this study, as well as general information on the corrosion of metals with essential notions of their protection by corrosion inhibitors. We then present bibliographical reminders of polyphenols and their applications.

The ***second chapter*** is dedicated to the characterization techniques used in this study.

First, we presented the extraction methods of Cytisus multiflorus extract (CMFE) and Punica Granatum extract (PGPE). Then, we explained the principles of the experimental techniques used in applying our extracts by potentiodynamic polarization (PDP) experiments and electrochemical impedance spectroscopy (EIS).

Surface analyzes are carried out by scanning electron microscopy (SEM), X-ray diffraction (XRD), and X-ray photoelectron spectroscopy (XPS). Fourier-transform infrared spectroscopy with attenuated total reflectance (FTIR/ATR) was applied to investigate the adsorption behavior.

In the ***third chapter***, we present the results of our study. These results confirm; the good corrosion-inhibiting power of our extracts.

The fourth chapter is devoted to the quantum description of the series of inhibitors chosen using different computational methods, particularly DFT and dynamic molecular simulation (DMS).

At the end of this manuscript, we present a general conclusion.

References

[1] H. El-Lateef, M. Abo Riya, et A. Tantawy, « Empirical and Quantum Chemical Studies on the Corrosion Inhibition Performance of Some Novel Synthesized Cationic Gemini Surfactants on Carbon Steel Pipelines in Acid Pickling Processes », *Corrosion Science*, vol. 108, mars 2016, doi: 10.1016/j.corsci.2016.03.004.

[2] X. Li et S. Deng, « Inhibition effect of Dendrocalamus brandisii leaves extract on aluminum in HCl, H3PO4 solutions », *Corrosion Science*, vol. 65, p. 299‑308, 2012.

[3] K. Cronin et R. Cocker, « Plant and Equipment| Materials and Finishes for Plant and Equipment », 2011.

[4] S. A. Abd El-Maksoud, « The effect of organic compounds on the electrochemical behavior of steel in acidic media. A review », *International Journal of Electrochemical Science*, vol. 3, nº 5, p. 528‑555, 2008.

[5] V. S. Sastri, *Corrosion inhibitors: principles and applications*, vol. 1. Wiley New York, 1998.

[6] H. Ferkous, S. Djellali, R. Sahraoui, Y. Benguerba, H. Behloul, et A. Çukurovali, « Corrosion inhibition of mild steel by 2-(2-methoxybenzylidene) hydrazine-1-carbothioamide in hydrochloric acid solution: Experimental measurements and quantum chemical calculations », *Journal of Molecular Liquids*, vol. 307, p. 112957, juin 2020, doi: 10.1016/j.molliq.2020.112957.

[7] W. Sun et S. Nesic, « A mechanistic model of H2S corrosion of mild steel », in *CORROSION 2007*, OnePetro, 2007.

[8] O. S. I. Fayomi, I. G. Akande, et S. Odigie, « Economic impact of corrosion in oil sectors and prevention: An overview », in *Journal of Physics: Conference Series*, IOP Publishing, 2019, p. 022037.

[9] K. Zakaria, N. A. Negm, E. A. Khamis, et E. A. Badr, « Electrochemical and quantum chemical studies on carbon steel corrosion protection in 1 M H2SO4 using new eco-friendly Schiff base metal complexes », *Journal of the Taiwan Institute of Chemical Engineers*, vol. 61, p. 316‑326, 2016.

[10] W. Ebdelly, S. Ben Hassen, X. R. Nóvoa, et Y. Ben Amor, « Inhibition of carbon steel corrosion in neutral calcareous synthetic water by Eruca sativa extract », *protection of metals and physical chemistry of surfaces*, vol. 55, nº 3, p. 591‑602, 2019.

[11] M. Behpour, S. M. Ghoreishi, N. Soltani, M. Salavati-Niasari, M. Hamadanian, et A. Gandomi, « Electrochemical and theoretical investigation on the corrosion inhibition of mild steel by thiosalicylaldehyde derivatives in hydrochloric acid solution », *Corrosion Science*, vol. 50, nº 8, Art. nº 8, août 2008, doi: 10.1016/j.corsci.2008.06.020.

[12] A. Miralrio et A. Espinoza Vázquez, « Plant extracts as green corrosion inhibitors for different metal surfaces and corrosive media: a review », *Processes*, vol. 8, nº 8, p. 942, 2020.

[13] R. C. Barik, J. A. Wharton, R. J. K. Wood, K. R. Stokes, et R. L. Jones, « Corrosion, erosion and erosion–corrosion performance of plasma electrolytic oxidation (PEO) deposited Al2O3 coatings », *Surface and coatings technology*, vol. 199, nº 2‑3, p. 158‑167, 2005.

[14] A. L. Yerokhin, X. Nie, A. Leyland, et A. Matthews, « Characterisation of oxide films produced by plasma electrolytic oxidation of a Ti–6Al–4V alloy », *Surface and Coatings Technology*, vol. 130, nº 2, Art. nº 2, août 2000, doi: 10.1016/S0257-8972(00)00719-2.

[15] M. P. Asfia, M. Rezaei, et G. Bahlakeh, « Corrosion prevention of AISI 304 stainless steel in hydrochloric acid medium using garlic extract as a green corrosion inhibitor: Electrochemical and theoretical studies », *Journal of Molecular Liquids*, vol. 315, p. 113679, oct. 2020, doi: 10.1016/j.molliq.2020.113679.

[16] C. Keawhan, P. Wongpanya, N. Witit-Anun, et P. Songsiriritthigul, « Corrosion behavior of AISI 4140 steel surface coated by physical vapor deposition », *Journal of Metals, Materials and Minerals*, vol. 22, nº 1, 2012.

[17] R. T. loto, C. A. Loto, et M. Akinyele, « Effect of ginger, pomegranate and celery extracts on zinc electrodeposition, surface morphology and corrosion inhibition of mild steel », *Alexandria Engineering Journal*, vol. 59, nº 2, Art. nº 2, avr. 2020, doi: 10.1016/j.aej.2020.03.014.

[18] C.-X. Wang et X.-F. Zhang, « A non-particle and fluorine-free superhydrophobic surface based on one-step electrodeposition of dodecyltrimethoxysilane on mild steel for corrosion protection », *Corrosion Science*, vol. 163, p. 108284, 2020.

[19] A. F. Baldissera et C. A. Ferreira, « Coatings based on electronic conducting polymers for corrosion protection of metals », *Progress in Organic Coatings*, vol. 75, nº 3, p. 241‑247, 2012.

[20] R. Selvaraj, M. Selvaraj, et S. V. K. Iyer, « Studies on the evaluation of the performance of organic coatings used for the prevention of corrosion of steel rebars in concrete structures », *Progress in Organic Coatings*, vol. 64, nº 4, Art. nº 4, mars 2009, doi: 10.1016/j.porgcoat.2008.08.005.

[21] C. Verma, L. O. Olasunkanmi, E. E. Ebenso, et M. A. Quraishi, « Substituents effect on corrosion inhibition performance of organic compounds in aggressive ionic solutions: A review », *Journal of Molecular Liquids*, vol. 251, p. 100‑118, févr. 2018, doi: 10.1016/j.molliq.2017.12.055.

[22] A. S. Yaro, A. A. Khadom, et R. K. Wael, « Apricot juice as green corrosion inhibitor of mild steel in phosphoric acid », *Alexandria Engineering Journal*, vol. 52, nº 1, Art. nº 1, mars 2013, doi: 10.1016/j.aej.2012.11.001.

[23] M. Prabakaran, S.-H. Kim, K. Kalaiselvi, H. Venkatesan, et I.-M. Chung, « Highly efficient Ligularia fischeri green extract for the protection against corrosion of mild steel in acidic medium: Electrochemical and spectroscopic investigations », *Journal of the*

Taiwan Institute of Chemical Engineers, vol. 59, sept. 2015, doi: 10.1016/j.jtice.2015.08.023.

[24] M. A. El-Hashemy et A. Sallam, « The inhibitive action of Calendula officinalis flower heads extract for mild steel corrosion in 1 M HCl solution », *Journal of Materials Research and Technology*, vol. 9, nº 6, Art. nº 6, nov. 2020, doi: 10.1016/j.jmrt.2020.09.078.

[25] A. Sedik *et al.*, « Dardagan Fruit extract as eco-friendly corrosion inhibitor for mild steel in 1 M HCl: Electrochemical and surface morphological studies », *Journal of the Taiwan Institute of Chemical Engineers*, vol. 107, p. 189‑200, févr. 2020, doi: 10.1016/j.jtice.2019.12.006.

[26] E. de Britto Policarpi et A. Spinelli, « Application of Hymenaea stigonocarpa fruit shell extract as eco-friendly corrosion inhibitor for steel in sulfuric acid », *Journal of the Taiwan Institute of Chemical Engineers*, vol. 116, p. 215‑222, 2020.

[27] O. R. Pereira, A. M. S. Silva, M. R. M. Domingues, et S. M. Cardoso, « Identification of phenolic constituents of Cytisus multiflorus », *Food Chemistry*, vol. 131, nº 2, Art. nº 2, mars 2012, doi: 10.1016/j.foodchem.2011.09.045.

Chapter I :

Literature review

CHAPTER I: LITERATURE REVIEW

I.1. Introduction

Corrosion is an unwanted phenomenon that destroys the brightness and perfection of the materials and diminishes their life. Corrosion is the deterioration of metals arising from the interaction of metals with their surroundings. It is a consistent issue and often can't be discarded entirely. Prevention is more sensible and achievable than complete disposal [1].

Corrosion is not always restricted to metals; it could likewise occur on distinct materials, such as polymers and plastic manufacturing. Amongst many metals, corrosion is experienced firmly in iron and steel. The formation of oxides in the process of oxidation no longer holds immovably to the surface of a metal. As a result, it gets off the metal effortlessly. Corrosion is an irreversible interfacial response of a material with its surroundings or disintegration into the segments as the material can't return to its most thermodynamically steady state. It consists of an electrochemical procedure that depends on vital environmental factors like pH, temperature, pressure, etc. [2].

I.2. Corrosion

I.2.1. Definition

Corrosion can be defined as the eating away of metal or degradation and deterioration of valuable properties of metal due to chemical, electrochemical, and biochemical reactions with environmental factors. Corrosion of metals is also defined as the spontaneous damage of metals due to their chemical, electrochemical and biochemical exchanges with the environment [3]. The technical definition of corrosion given by the International Standard Organization (ISO) denotes that it is the "Physicochemical interaction between a metal and its surrounding conditions which result in changes in the properties of the metal and which may often lead to mutilation of the function of the technical system of which these form a part" [4]. But as per the International Union of Pure and Applied Chemistry IUPAC, "Corrosion is an irreversible interfacial reaction of a material (metal, ceramic, and polymer) with its environment which results in its consumption or dissolution into the environment" [5]. In the other side, the ASTM terminology (G15), corrosion is defined as, "the chemical or

electrochemical reaction between a material, usually a metal, and its environment that produces a deterioration of the material and its properties" [6].

I.2.2 Different forms of corrosion

Different forms of corrosion affect metals. They go under various categories:

I.2.2.1. Uniform corrosion

Corrosion most frequently takes the form of uniform degradation. It is typically characterized by an electrochemical or chemical reaction that spreads evenly across a significant fraction of the exposed surface.

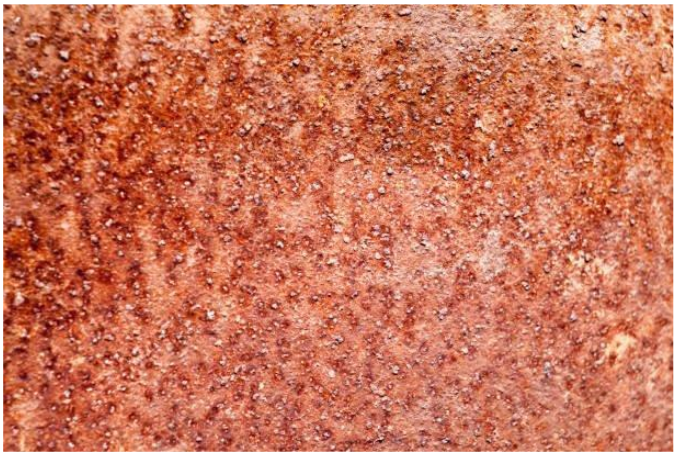

Figure I.1. Schematic representation of uniform corrosion [7].

I.2.2.2. Galvanic or Two metal corrosion

Usually, when two dissimilar metals are submerged in a corrosive or conductive fluid, a potential difference arises between them. If these metals touch one another, the potential difference causes electron flow.

I.2.2.3. Crevice corrosion

Intense localized corrosion frequently occurs in protected areas on metal surfaces exposed to corrosives. Small volumes of stagnant solution brought on by holes, cracks, surface deposits, and rivet heads are typically connected with this attack. Crevice or narrow crack corrosion are two names for this type of corrosion.

I.2.2.4. Pitting corrosion

A copper pipe that handled potable water failed after several years because of stagnant water. It had created pits or holes. This is pitting corrosion. Pitting is a form of extremely localized attack that results in holes in the metal. These holes frequently only have a small size, despite their diameters being small or enormous. Pits can occasionally be isolated or so close together that they resemble an uneven surface. Pitting is one of the most dangerous forms of corrosion. The result of localized corrosion is pitting.

Figure I.2. Schematic representation of pitting corrosion [8].

I.2.2.5. Erosion corrosion

When a corrosive fluid and the metal's surface move close to one another, it causes corrosion, which is the acceleration of a metal's degradation or attack. Erosion corrosion results when the protective surfaces are damaged and the metal and alloy are attacked rapidly. All types of equipment exposed to moving fluids are subjected to erosion corrosion. For example, piping systems, bends, elbows, pumps, and equipment are subject to spray.

I.2.2.6. Intergranular corrosion

This is a localized attack at and near grain boundaries. This relatively little corrosion of the grains is intergranular. This type of corrosion can be caused by impurities at the grain boundaries, the enrichment of an alloying element, or the depletion of an alloying element in the grain-boundary regions can all lead to intergranular corrosion.

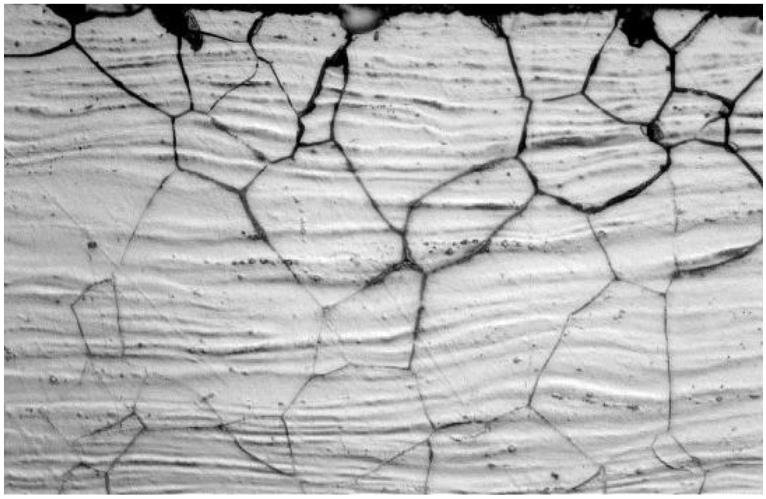

Figure I.3. Schematic representation of intergranular corrosion [9]

I.2.2.7. Fretting corrosion

Fretting corrosion products where materials are in touch and are being loaded while being subjected to vibration and slide. It appears as corrosion products surrounding pits in the metal. Friction oxidation is another name for fretting. It has been noted in machinery, automotive parts, and parts of engines. An excellent example of fretting corrosion is the bolted tie plates on a track when a heavy train moves over it[10].

I.2.2.8. Stress corrosion

Tensile stress (including residual stress left over from fabrication) and localized corrosion combine to form stress corrosion, which causes metal to fracture brittlely under specific circumstances. Examples of conditions that promote stress corrosion include high pH amine solutions for most common steels and chloride-bearing solutions for most stainless steels and specific aluminum alloys [10].

I.3. Corrosion Inhibitor

I.3.1. Definition

A corrosion inhibitor is a substance added in a small amount to a corrosive medium that decreases the rate of corrosion of metal exposed to that environment. Inhibitors often participate significantly in the oil extraction and processing industries where these are always considered the first line of defense against corrosion.

I.3.2. Classification of corrosion inhibitors

Corrosion inhibitors can be classified on different bases, for example:

Based on the information of polarization data, inhibitors are classified into anodic, cathodic, and mixed. The anodic inhibitor changes the corrosion potential toward the anodic side, and the cathodic inhibitor alters the corrosion potential toward the cathodic side. In contrast, a mixed inhibitor reverses both types of corrosion potential value [11].

Corrosion inhibitors can be classified based on mechanism, environment, and mode of protection [8,9, 12,13].

I.3.2.1. Based on the electrode process

I.3.2.1.1. Anodic Inhibitors

Anodic inhibitors typically function by producing a protective oxide layer on the metal's surface, which results in a significant anodic shift of the corrosion potential. This shift brings out the metallic surface into the passivation region. These are also sometimes called passivation. Chromatic, nitrates, tungstate, and molybdates are examples of anodic inhibitors.

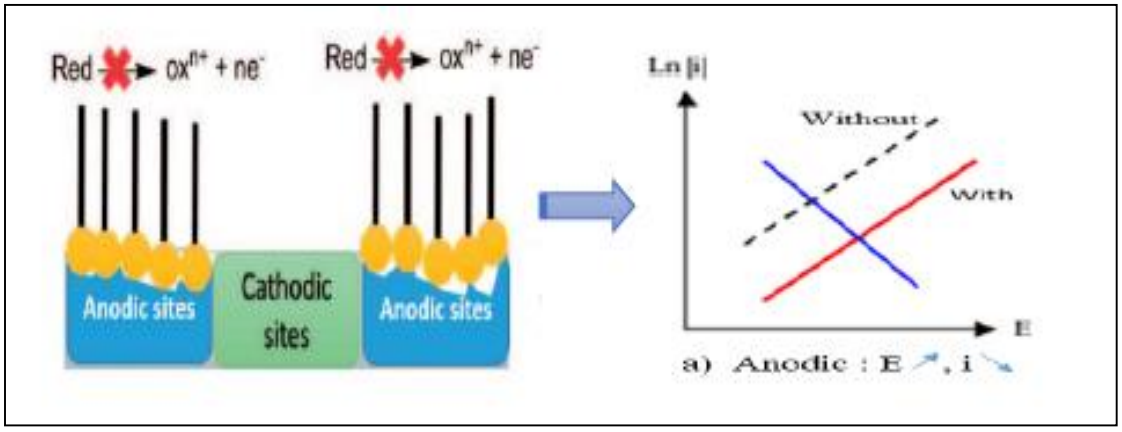

Figure I.4. Effect of the addition of the anodic inhibitor [14]

I.3.2.1.2. Cathodic Inhibitors

Cathodic inhibitors work by either reducing the cathodic reaction itself or selectively precipitating on cathodic areas to limit the movement of species that undergo reduction towards the surface. Some

substances can reduce the rates of cathodic reactions, called cathodic poisons. However, metal susceptibility to hydrogen-induced cracking can be increased by cathodic poisons since the metal absorbs hydrogen during aqueous corrosion. Oxygen scavengers can also decrease corrosion rates by reacting with dissolved oxygen. Examples of oxygen scavengers are sulfite and bisulfite ions, which can combine with oxygen to form sulfate.

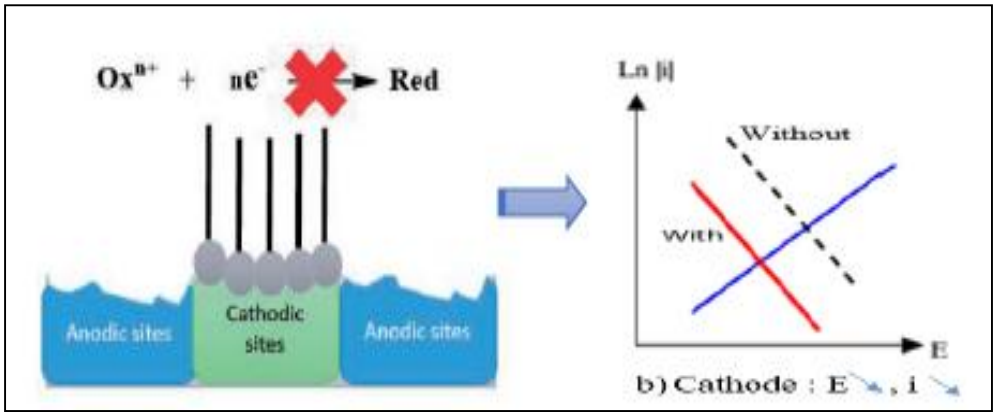

Figure I.5. Effect of addition of the cathodic inhibitor [14].

I.3.2.1.3 Mixed Inhibitors

Mixed inhibitors reduce both reactions, i.e., oxidation and reduction. These inhibitors are adsorbed on the surface, forming a film that causes the formation of precipitates on the surface of metal or alloy, blocking both anodic and cathodic areas indirectly. Hard water with a high composition of calcium and magnesium is less corrosive than soft water because the salts tend to precipitate on the surface of the metal forming a protective film compared to soft water. The most common examples of this category of inhibitors are phosphates and silicates. For example, sodium silicate is used in many domestic water softeners to prevent rusting. Sodium silicate protects steel, copper, and brass in aerated hot water systems. However, protection is not always accurate and depends mainly on ph. Phosphates require oxygen for effective inhibition of corrosion. The protection capability is suitable for chromates and nitrites, but these are toxic. Although Silicates and phosphates are not efficient, they are beneficial in situations where non-toxic additives are needed [15-16].

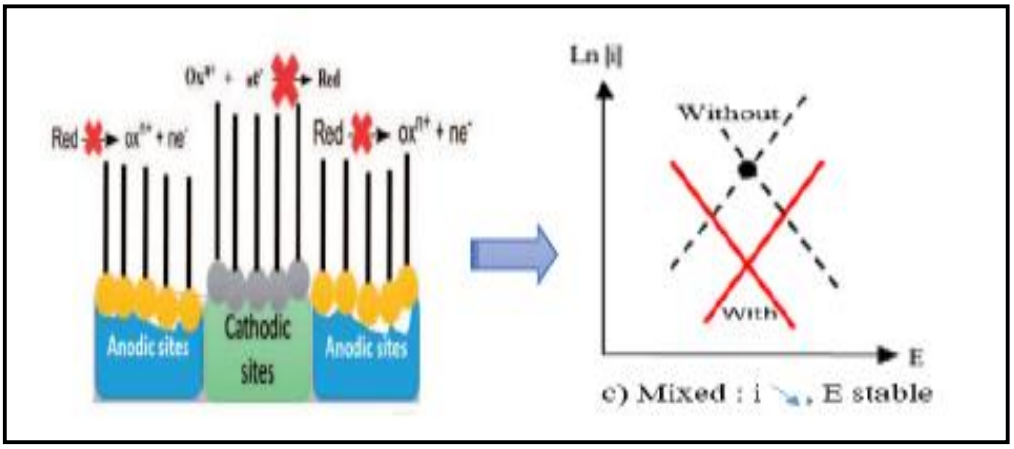

Figure I.6. Effect of addition of the mixed inhibitor [14].

I.3.2.2. Based on the environment

I.3.2.2.1. Acidic environment inhibitors

 Inorganic inhibitors: The oxides such as As_2O_3 and Sb_2O_3 have been reported as inhibitors in acid media. These substances deposit as metal oxide, increasing the hydrogen overvoltage and reducing the corrosion rate. [17]. The addition of heavy metal ions like Pb^{2+}, Mn^{2+}, and Cd^{2+} inhibit iron corrosion in acids due to the deposition of these metal ions over the iron surface [18].

 Organic inhibitors: Organic inhibitors are substances with at least one functional group considered the reaction center for adsorption. Organic compounds containing oxygen, nitrogen, and sulfur with multiple bonds were considered suitable corrosion inhibitors [19-21]. Organic inhibitors can be anodic, cathodic, and mixed based on their reaction at the metal surface and potential. Cruz et al. [22] have shown that the effectiveness of an organic inhibitor is related to its adsorption properties, which depend on the nature and surface condition of the metal, as well as the corrosive environment.

I.3.2.2.2. Alkaline inhibitors

Metals are susceptible to corrosion in alkaline solutions. Many organic compounds are often utilized as metal inhibitors in essential solutions. Compounds such as thiourea, substituted phenols, naphthol, β-diceton, etc., have been used as effective inhibitors in basic solutions because of the formation of metallic complexes.

I.3.2.2.3. Neutral inhibitors

Because the mechanisms in the two solutions are different, inhibitors that are effective in acid solutions do not operate successfully in neutral solutions [23-25]. The interaction of inhibitors with oxide-coated metal surfaces in neutral fluids suppresses the oxygen reduction reaction at cathode sites. These inhibitors guard against aggression on the surface layers. In near-neutral solutions, it has been discovered that some active surface chelation inhibitors are effective [26].

I.3.2.2.4. Vapor phase inhibitors

Like organic adsorption-type inhibitors, vapor-phase or volatile corrosion inhibitors (VCIs) have an extremely high vapor pressure. When used, these inhibitors are positioned close to the metal that needs to be protected because they are transferred to the metal surface via sublimation, followed by condensation. The inhibitor then adsorbs Figure I.7. For example, copper is protected by benzothiazole and dicyclohexyl ammonium nitrite, while brass is protected by phenylthiourea and cyclohexylamine chromate. Ferrous and non-ferrous metals and alloys are both protected by dicyclohexylamine nitrite [14].

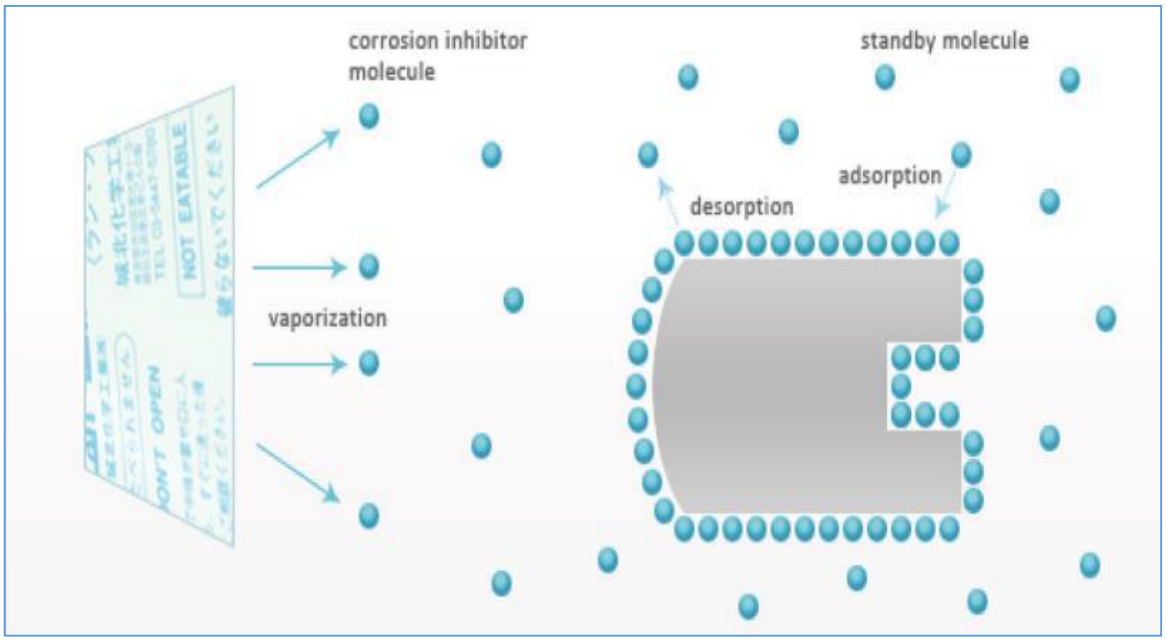

Figure I.7. Schematic representation of volatile inhibitors [14].

I.3.3. Based on the mode of protection

I.3.3.1. Adsorption inhibitors

This class of inhibitors represents the largest class of corrosion-inhibiting substances. They are organic compounds that are adsorbed on the metal surface and suppress metal dissolution and reduction reactions. They typically have an equal impact on cathodic and anodic reactions [14]. Examples: substances with lone pairs of electrons, including those with nitrogen, sulfur, and oxygen atoms.

I.3.3.2. Pickling inhibitors

Pickling inhibitors generally produce an adsorbed coating on the metal surface, thereby preventing H+ ion discharge and metal ion dissolution. In general, pickling inhibitors need a polar group or groups that are advantageous for the molecule to adhere to the metal surface.

I.3.3.3. Precipitation inhibitors

These substances precipitate on metal surfaces and create a barrier of protection [27]. Because hard water contains more calcium and magnesium than soft water, its salts precipitate on the metal surface to form a protective coating, making it less corrosive. The silicates and phosphates are the most typical precipitation inhibitors.

I.3.3.4. Synergistic inhibitors

Single inhibitors, for example, are very infrequent to utilize in cooling water systems. Anodic and cathodic inhibitors are frequently employed in conjunction to achieve greater corrosion protection. Blends created by mixing multiple inhibitors are synergistic inhibitors [18]. Examples include chromate-phosphates, polyphosphate-silicate, zinc-tannins, and zinc-phosphates.

I.3.3.5. Environment-friendly or green corrosion inhibitors

Traditional corrosion inhibitors are now limited due to the growing concept of "green chemistry" in science, technology, and engineering [28-30]. In practical terms, studies on corrosion inhibition have focused on human health and safety considerations. Researchers are focusing on using environmentally friendly substances, like plant extracts rich in organic components. As environmentally friendly replacements for dangerous and poisonous substances, alkaloids, amino

acids, pigments, and tannins are used. The extracts of some common plants and plant products have been investigated as corrosion inhibitors for various metals and alloys under diverse settings due to their biodegradability, ecofriendliness, cheap cost, and ease of availability [30-31].

I .4. Adsorption of corrosion inhibitors onto metals

The percentage of the surface the inhibitor has adsorbed to is typically inversely correlated with its inhibitive efficacy. The efficiency of adsorbed inhibitor species in slowing the corrosion reactions may be better at low surface coverage (0.1) than at high surface coverage. Adsorption-type corrosion inhibitors (mainly organic compounds) are widely used for corrosion inhibition. Most organic compounds possessing electron rich species such as nitrogen, phosphorus, oxygen and sulfur in their moieties are called adsorption centers, essential in inhibiting metal corrosion. They inhibit metal corrosion by forming a thin adsorption layer on the electrode (metal) surface through chemical or physical adsorption mode [14].

I.4.1. Physical adsorption (physisorption)

Physical adsorption results from attractive electrostatic forces between the inhibition of organic ions or dipoles and the electro-charged surface of the metal. The interaction between the inhibitor and the metal surface is weak (Van der Waals forces), and the process is rapid because it involves relatively low, almost temperature-independent activation energies. Moreover, it is reversible, characterized by low adsorption energy (typically 20 kJ/mol), which tends to decrease at increasing temperatures [32-33].

I.4.2. Chemical adsorption (chemisorption)

This type of adsorption involves charge transfer or sharing from the organic corrosion inhibitor with a metal, which leads to a coordinate covalent bond formation. The chemisorption process takes place more slowly than electrostatic adsorption and with higher activation energy. It is irreversible, with free adsorption energies as high as 40 kJ/mol or more [34]. This absorption type occurs when heteroatoms such as S, N, and O are present with lone pair electrons and/or aromatic rings in the adsorbed molecules. The adsorption strength depends on the corrosion inhibitor's electron density and polarity. An increase in temperature may increase the protection efficiency of the corrosion inhibitor. Due to the irreversibility of chemisorption, these inhibitors can act as pre-filming substances which

form protective films capable of persisting in uninhibited solutions. Some inhibiting molecules may offer coupled physical and chemical adsorption with enhanced inhibiting effects.

I.5. Corrosion of carbon steel

I.5.1. Corrosion of steels in aqueous environments

Corrosion is a complicated process, but the basic process of metallic corrosion in an aqueous solution involves the following steps [35]

- Electrons are lost when a metal is exposed to an aggressive environment, and positively charged ions are produced.
- As a result of the formation of positively charged ions, electrons are released to flow through the steel to the cathodic area.

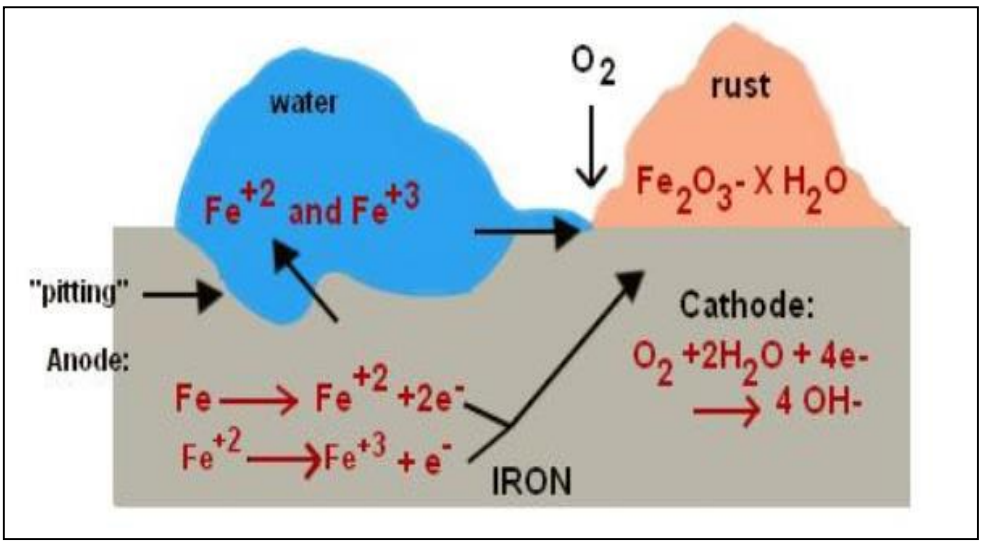

Figure I.8. Reaction occurring during steel corrosion [14].

- Oxygen in the aqueous solution moves to the cathode. It completes the electric circuit by utilizing the electrons that flow to the cathode to produce OH- at the surface of the metal.

Anodic reaction: $Fe \rightarrow Fe^{2+} + 2e^-$ **(I.1)**

Cathodic reaction: $O_2 + 2H_2O + 4e^- \rightarrow 4OH^-$ **(I.2)**

In the absence of oxygen, hydrogen ion participates in the reaction at the cathode instead of oxygen and completes the electrical circuit as follows:

$$2H^+ + 2e^- \rightarrow H_2\uparrow \quad \textbf{(I.3)}$$

Ferrous ions produced by the dissolution of the metal combine with hydroxyl ions as follow:

$$Fe^{2+}+2OH^{-} \rightarrow (OH)_2\downarrow \quad \textbf{(I.4)}$$

The ferrous hydroxide produced has very low solubility and quickly precipitates

$$4(OH)_2 + O_2+2H_2O \rightarrow 4Fe(OH)_3 \quad \textbf{(I.5)}$$

Dehydrolysis of this product leads to the formation of the corrosion products usually seen on the metal surface **(Eq. I.6 and I.7).**

$$2(OH)_3 \rightarrow Fe_2O_3\downarrow+3H_2O \quad \textbf{(I.6)}$$

$$(OH)_3 \rightarrow FeO(OH)\downarrow+H_2O \quad \textbf{(I.7)}$$

Figure I.9 shows a diagram of the Pourbaix of iron in water, drawn considering the only corrosion products the Fe, Fe_3O_4, and Fe_2O_3 [36].

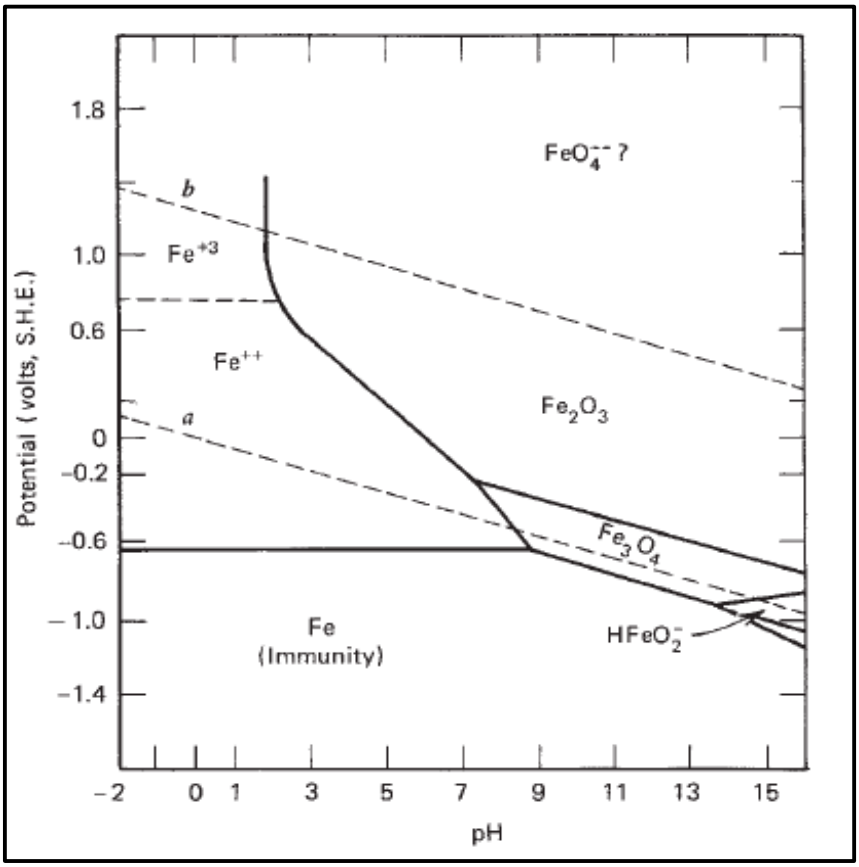

Figure I.9. Pourbaix diagram for the iron – water system at 25 ° C, considering Fe, Fe_3O_4, and Fe_2O_3 as the only solid substances [36].

I.5.2. Effect of green inhibitors on the XC48 Carbon Steel corrosion

XC48 carbon steel, like other alloys and metals, has been widely utilized in various industries, making it susceptible to corrosion, and the search for methods to inhibit these phenomena is a critical topic to avoid significant economic losses due to corrosion. Over the years, many researchers have developed various ways to inhibit and stop the development of the phenomenon of corrosion, one of which is to develop and use green corrosion inhibitors from multiple sources, which has proven to be an efficient method to limit the XC48 Carbon steel corrosion rate.

(L Toukal, 2022) used 1-(4-Methoxybenzyl)-2-(4-methoxyphenyl)-1H-benzimidazole (MMBI) as XC48 Carbon steel green corrosion inhibitor in different acidic mediums, which results in an inhibition efficiency in HCl (97%) and (92%) in H_2SO_4, this inhibition has been demonstrated by Benzimidazole (MMB) adsorption on carbon steel surface followed the Langmuir adsorption isotherm. These findings have been validated by SEM pictures, which show the creation of a protective coating on the surface of XC48 carbon steel. Also, (Chaimae Merimi, 2023) used acetylsalicylic acid molecule (aspirin) as an environmentally and cost-effective inhibitor for XC48 carbon steel corrosion in an acidic medium of 1M HCl. This resulted in a 96% inhibition efficiency, with the inhibition increasing as the inhibitor concentration increased. With the exact mechanism utilized in the previous work, the surface morphology study revealed that the acetylsalicylic acid molecule was exposed on the surface, forming a protective layer.

On the other hand (Belakhdar A, 2020) used the methanolic extract of Rosmarinus officinalis for XC48 corrosion inhibition in 2M HCl solution, which was obtained by the extraction of fresh leaves of Rosmarinus officinalis conduct to an 89.18% inhibition efficiency at 200ppm concentration. The inhibition of corrosion by the methanolic extract of Rosmarinus officinalis is accomplished by forming a protective layer on the steel surface. Challouf (Hassen Challouf, 2016) prepared an inhibitor from Origanum majorana Extracts and used it in an aqueous Chloride Medium for XC48 Mild steel, results indicated that this green corrosion inhibitor led to 90% inhibition efficiency, and this inhibition done by the adsorption of the extract on the surface of mild steel.

As a result, for XC48 corrosion inhibition, the use of green inhibitors is still one of the most effective ways to prevent this phenomenon. As shown in the previous studies, green corrosion inhibition helped to limit the corrosion rate by exposing the surface of the steel and forming a protective layer that prevents corrosion.

I.6. Corrosion of Stainless Steel

I.6.1. Introduction

The Sheffield, England-based Brown-Firth research laboratory's Harry Brearleyis credited with developing stainless steel in 1913. Most major sectors, including chemical, construction, petroleum, power, process, and others, frequently employ stainless steel alloys as building materials for essential rust-resistant components.

Alloy steels resistant to corrosion are collectively referred to as stainless steel. Iron-based alloys with at least 11 weight percent chromium make up these stainless steels [36]. With this much chromium, stainless steel can create a passive or protective coating that prevents corrosion. The corrosion resistance of stainless steel is due to this protective coating, which self-forms and self-heals [37]. Increasing the chromium content improves the stability of the passive film [38]. A thin coating forms at about 10.5% chromium and will offer minimal atmospheric protection. The stability of the passive coating is much improved, and consequently, more corrosion resistance is acquired. Raising the chromium content to 17–20% is typical for concentration in the type 300 series of austenitic stainless steels. Stainless steels, however, cannot be said to be completely corrosion-resistant. Under specific circumstances, the passive state can degrade, and corrosion may occur [39].

As previously mentioned, stainless steel has considerable corrosion resistance, although it is not impervious to all environments and may experience specific types of corrosion in some media. Several types of corrosion can occur in stainless steel, including galvanic corrosion, stress corrosion cracking, intergranular corrosion, pitting corrosion, and crevice corrosion [40].

The most frequent type of corrosion is general corrosion, which attacks uniformly. It is distinguished by a chemical or electrochemical reaction that spreads evenly across the exposed material's surface. Typically, during the active and transpassive dissolution of materials, this general corrosion occurs when none of the alloying elements in the material can form a protective layer [41]. Consequently, the metal gets thinner and eventually breaks. The corrosion resistance of stainless steel typically rises with increasing quantities of chromium, nickel, and molybdenum. In general, the corrosion of stainless steels typically occurs in acids and hot caustic solutions.

Additional alloying elements are added to the alloys to change the structure of the stainless steel alloys and improve qualities like formability, strength, and cryogenic toughness.

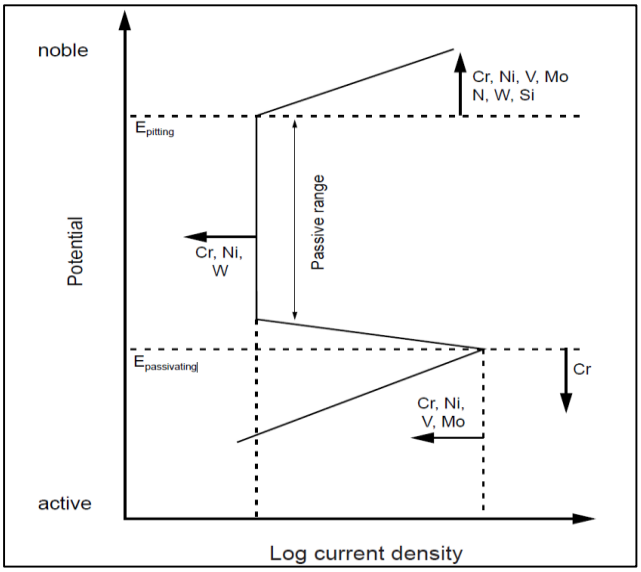

Figure I.10. Schematic summary of the effects of alloying elements on the anodic polarization curve of stainless steel [38].

I.6.2. Passive Films of Stainless Steels

The passive protective film that forms with a few nanometers thickness on the alloy's surface gives stainless steel alloys excellent corrosion resistance [39-40]. The surface of the alloy is kept safe from corrosive surroundings by this layer, which serves as a barrier. However, the film adapts to its surroundings. Therefore it may expand or disintegrate as well as absorb or adsorb anions. [41].

The composition of the alloy is one of the key elements influencing the characteristics (composition, protectiveness, thickness) of the passive film. The film structure, layers, composition, chemical states of the elements, species distribution in the film, and thickness of the passive films created on various types of stainless steel have all been the subject of numerous research. A general agreement in the previously studies is that chromium and molybdenum have a more significant influence on the stainless steel passive film formation than the other alloying elements. The passive film formed on the stainless steel consists of chromium oxide and/or hydroxide [42-45]. Also, significant evidence suggests a dual structure consisting of an inner oxide and an outer hydroxide layer [46-48].

A bilayer structure model described the passive films formed on pure chromium and Fe-Cr alloy in sulphuric acid (0.5M H2SO4) [44-45]. The authors proposed that the passive films were composed of an exterior layer of chromium hydroxide, $Cr(OH)_3$, and an interior layer of mixed chromium Cr(III) and Fe(III) oxide that was enriched with Cr_2O_3. Similar results for passive layers electrochemically generated on Fe-Cr stainless steel alloy in 0.5M H2SO4 solution were seen by

Keller and Strehblow [46]. However, it was discovered that the composition of the layer changed in the transpassive potential range. The outside portion of the transpassive layer comprises Fe (III) species, while the interior part still has a significant enrichment of Cr_2O_3. In research by Marcus et al. [47] for comparable alloys in the same environment (0.5M H2SO4), the analyses demonstrated chromium enrichment in the passive films generated on the surface of these alloys.

I.7. Green Corrosion inhibitors from polyphenols

I.7.1. Introduction

Over the last decades, green chemistry has emphasized the significance of defending and preserving human and environmental safety in an economically advantageous strategy that aims to avoid toxic compounds [49]. Green chemistry is generally described as "*the design of chemical products and processes that reduce or eliminate the use and generation of hazardous substances*" [50]. Political influence for its advancement has been reported to be substantial, wherein the 1990 Pollution Prevention Act informally provided as the political reference point. However, green chemistry dates back well before 1990. Several environmental concepts integrated the chemical industry throughout the late 1980s and early 1990s—for instance, clean, environmental, green, sustainable, and benign chemistry [51].

Lately, "green chemistry" has become an important emerging subject of study in the science field. Numerous European and non-European nations, including Italy, the United Kingdom, and Japan, initiated significant green chemistry strategies, where several research, educational, and awareness programs have been designated as core initiatives. Consequently, green chemistry has shown that even the most basic scientific methods may have positive economic outcomes for society while also safeguarding human health and the environment, including polymers [52-53], solvents [54-56], catalysis [57-58], and advanced method development [59-60]. Overall, the development of eco-friendly materials with a heightened awareness of environmental influence [61]. Metals are the most common materials in modern society and various industries. However, because of interaction with its environment, its quality deteriorates slowly, undoubtedly, and permanently due to this susceptibility. Metals costs reach up to just a few percent of the overall product of the world's most industrialized nations, where their primary industrial challenge has, in recent years, drawing a significant number of researchers [62-63]. Before this observation, it was suggested that the main technique for avoiding metal corrosion is isolating metals from corrosive chemicals. Inhibitors are currently one of the only viable solutions for protection against corrosion. Numerous attempts have been conducted to

determine chemicals appropriate for corrosion inhibitors in diverse corrosive conditions to prevent or slow the corrosion of metals. Recent research has been conducted on the metal corrosion inhibition by synthetic organic compounds, which is typically ecologically hazardous [64-65]. Frequently, organic compounds are utilized as corrosion inhibitors.

Nevertheless, the combined toxicity of organic chemicals negatively affects the ecosystem. Moreover, environmental protection must replace organic substances with biodegradable inhibitors, which are ecologically friendly to nature and have no adverse effect on biological entities [66-67]. Environmental concern necessitates replacing organic compounds with biodegradable and environmental inhibitors; hence, natural materials have become a practical corrosion inhibitor alternative.

In the field of corrosion research, eco-friendly or "green" corrosion inhibitors are getting a lot of interest because they are harmless, biodegradable, environmentally desirable, and can be recycled [68]. Although a significant proportion of innovative studies have been performed and numerous research publications have been published, the green inhibitors field is still largely unexplored. The highly elevated interest in the concept increased the number of investigated compounds. The researchers describe the selected inhibitors as green, environmentally sustainable, or suitable [63]. Several natural-based compounds have been studied as potential corrosion inhibitors for mild steel, carbon steel, and aluminum materials. Almost the majority of these investigations have focused on extracts from natural sources. Thus, according to studies, the essential components of these extracts include a range of organic compounds.

Consequently, almost all of these compounds have multiple bonds and atoms of O, N, S, and P, which function as bonding sites for their adsorption on the surface of the metal. This usually involves, for instance, amino acids [69], alkaloids [70], polyphenols [62], and often extracts of plants [71-72] widespread despite it having little commercial value; there is also potential it can be utilized for corrosion protection if indeed the demand increases. Thus, there has been a lot of interest in studying the effects of using these natural compounds with excellent inhibitor capabilities in metal corrosion protection, particularly in the current ecological situation. Different plant extracts have been discussed in the literature [73-74], leave extracts [75], and fruit peel extracts [76-77], which have been investigated and shown to be effective in inhibiting the corrosion of metals. Tannins, a type of polyphenolic compound that naturally occur, harmless and biodegradable, were the first naturally occurring corrosion inhibitors to be introduced to the market. However, natural extracts include a large

number and diversity of compounds, and it is complicated to understand the processes associated with corrosion inhibition [78].

Polyphenol-based extracts seem to fulfill the majority of requirements for a combination inhibition and bio-deterioration of materials, besides being less harmful than most other plant extracts, including alkaloid extracts [63]. Polyphenols have a phenolic attribute, while their structural variety results in distinct physicochemical properties. Extraction, isolation, characterization, and measurement of polyphenols are even more outstanding; however, recent technological advances are in a high prevalence of polyphenols in plants and their structural diversity. Complicated glycosyl and polymerization processes prevent the development of a standardized approach for polyphenols. Also, it has been found that phenolic displacement in plants varies across tissue, cellular, and sub-cellular levels. Polyphenols may be classified into a wide variety of families based on their chemical structure; this structural variety potentially leads to a wide range of physicochemical properties that influence polyphenol extraction and renders them a promising candidate for the protection of metal corrosion [79].

I.7.2. Polyphenols

Phenolic compounds, or polyphenols, are one of the most diverse and widely dispersed substances in the plant kingdom, identified by a phenyl ring and various attached hydroxyl groups ($-OH$). Polyphenols are natural components of plants' secondary metabolism that protect against pathogens, free radicals, UV radiation, and parasites [80]. Polyphenols cover a large and varied class of over 10,000 known compounds with at least one phenyl ring with one or even more $-OH$ groups in their chemical composition [81]. Polyphenols may take on many forms, ranging from simple molecules like phenolic acids to highly polymerized molecules like tannins. They are most commonly found conjugated, with one or more sugar by-products associated with $-OH$ groups, however, there are significant associations between the sugar group and the phenyl's carbon atom. The attached sugars can therefore be monosaccharides, disaccharides, or even oligosaccharides, galactose, rhamnose, and xylose are also considered as well as glucuronic and galacturonic acids, among many others, although glucose is the most prevalent sugar residue [82]. The structure of polyphenols in some plant products, such as exotic fruits or cereals, is still unidentified [83]. Besides, polyphenols frequently link with other molecules, such as carboxylic or organic acids, amines, and fatty acids, as well as with other phenols. The degree of oxidation, hydroxylation, methylation, and glycosylation are the most common differences in the compound's skeleton. Thus, the primary classes of

polyphenols include non-flavonoids, flavonoids, phenolic acids, and coumarins, as illustrated in Figure I.11, where the basic structure of each class is provided [84-85].

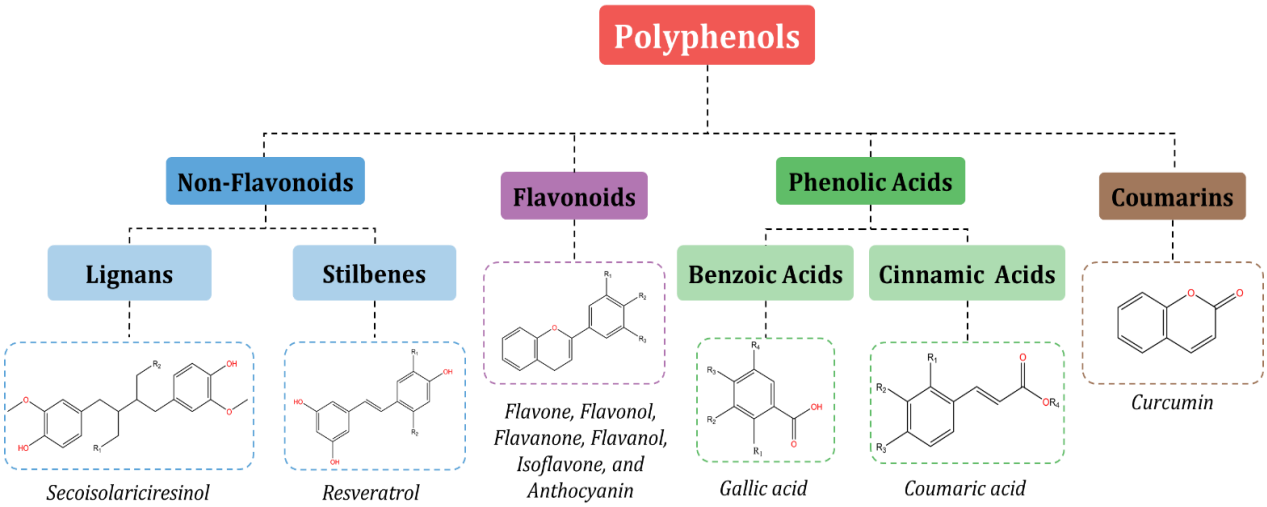

Figure I.11. Schematic representation of different classes of polyphenols [84-85].

Examples of the important subclasses of each class are also shown in Figure I.12, 1) Flavonoids, which include flavone, flavonol, flavanone, flavanol, and anthocyanin; Phenolic acids subclass, which is split into substances derived from: 2) benzoic acids, including *p*-Hydroxy benzoic acid, as well as ones derived from 3) cinnamic acids, such as caffeic and ferulic acid; and 4) Lignans, 5) Stilbenes and 6) Coumarins [86-88]. Furthermore, additional subclasses, such as alkylphenols, hydroxybenzaldehydes, hydroxybenzoketones, tyrosols, etc., are not currently listed [89]. Regarding green corrosion inhibition, utilizing such naturally occurring compounds with favorable molecular properties, including polyphenols, is an exciting research topic. In the present environmental perspective, natural plant extracts appear as an alternative to fulfilling the requirements of the "Registration, Evaluation, Authorization and Restriction of Chemicals" regulation (REACH) and European directives on wastewater refusal [78]. Recently, numerous publications have been on isolating and extracting polyphenols from plants, food, or natural resources. Modern techniques are increasingly challenging conventional methods for sample preparation, separation or isolation, surveillance, and identification [90]. In the following section, traditional and contemporary techniques for polyphenols extraction are described.

1) Flavonoids

Flavone

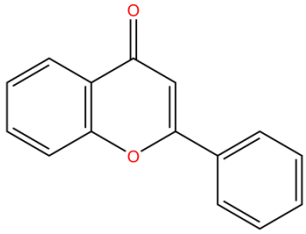

Flavonol

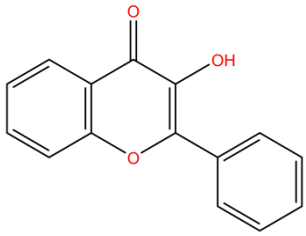

Flavanone

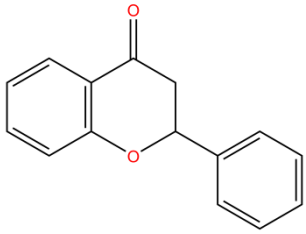

Flavanol

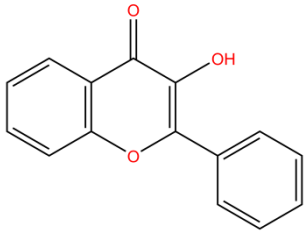

Cyanidin

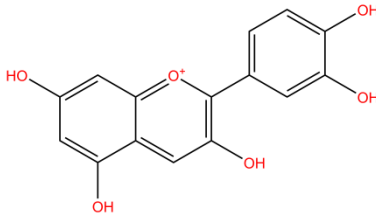

2) Benzoic Acids

p-Hydroxy benzoic acid

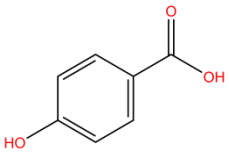

Vanillic acid

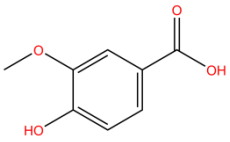

Gallic acid

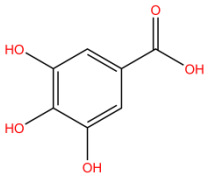

3) Cinnamic Acids

Coumaric acid

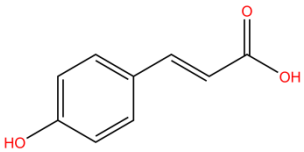

Caffeic acid

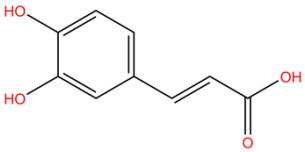

Ferulic acid

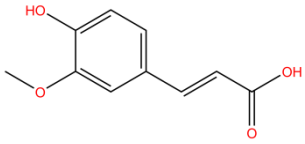

4) Lignans

Secoisolariciresinol

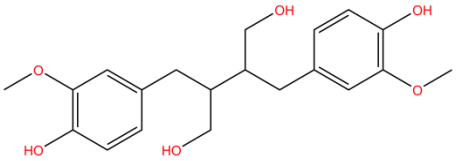

5) Stilbenes

Resveratrol

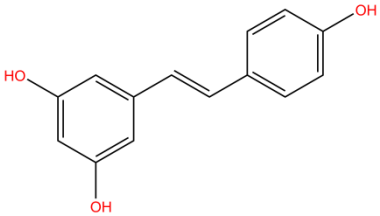

6) Coumarins

Curcumin

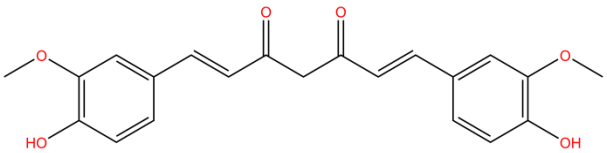

Figure I.12. Basic chemical structures of various classes of polyphenols [87-88].

I.7.3. Polyphenols Extraction Techniques

Typically, the appropriate extraction technique should be considered in the first process, where the molecular structures of the substance, specimen particle shape, and the involvement of interferents

influence the selected extraction technique. Furthermore, extraction time, temperature, solvent ratio, number of repeated extractions, and extraction solvent selection are the critical parameters influencing extraction efficiency. Extraction time and temperature both affect solubility. A higher temperature substantially expands solubility and mass and heat transfer velocity profile while decreasing solvent viscosity and surface tension, increasing the speed extraction rate [91]. Several steps are required to extract polyphenols from vegetable products, including feed preparation, extraction, purification, and drying, which can be removed from fresh, refrigerated, or dried selected plants. Processing steps include grinding, crushing, drying, and blending on the plant before extraction. The drying procedure selected affects the total polyphenols. However, Freeze-drying maintains more polyphenol content in selected plants than air-drying [92]. The technique and solvent are critical factors in extraction efficiency. For instance, an acidified organic solvent can also be used to obtain polyphenol extracts with such a high anthocyanin content, meanwhile, in selective recovery, attempting to avoid harmful substances [93].

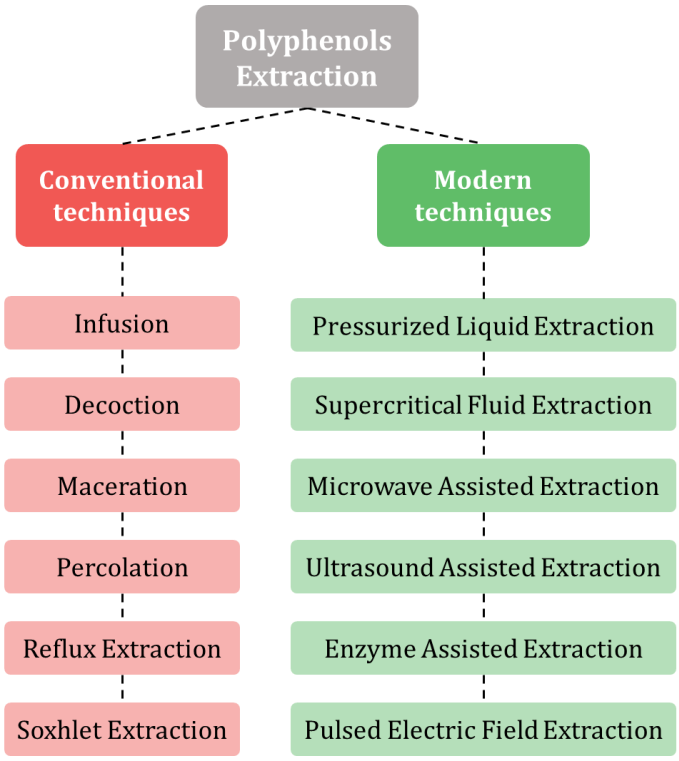

Figure I.13. Different extraction techniques for polyphenols [94].

Traditional methods use simple equipment, and extraction performance, amount, and duration are frequently interrogated. These techniques have evolved to increase extraction efficiency and decrease extraction time. Numerous complex methods have been developed for rapid, simple, and

targeted extraction with minimal solvent [94]. Figure I.13 highlights the most frequently used extraction techniques.

I.7.3.1. Traditional extraction technologies

Conventional techniques have mainly been accepted for many years owing to their usability, effectiveness, and extensive applicability [95-96]. Despite several drawbacks, liquid-liquid and solid-liquid extraction remains the most frequent extraction methods [97]. In such operations, common solvents such as methanol, ethanol, acetone, diethyl ether, and ethyl acetate are often combined with water in various ratios. In addition to providing a hazard to human health, these solvents may also leave behind residues in the end product. This necessitates extra, time-consuming purification processes that impact the entire cost of the process.

Additionally, incomplete extraction of extremely polar phenolic acids such as benzoic or cinnamic acids is observed when employing pure organic solvents. In such conditions, alcohol/water or acetone/water mixes are recommended. Highly nonpolar substances, such as waxes, oils, sterols, and chlorophyll, may be removed from a substance by less polar solvents, including dichloromethane, chloroform, hexane, and benzene [98]. Nevertheless, several phenolic compounds are susceptible to degradation or undesired oxidative reaction. Therefore, the phenolic content in the extract is dramatically reduced, and it is recommended to avoid high process temperatures. Extraction is commonly performed at a temperature range of 20−50 °C; temperature over 70 °C is also unfavorable and results in rapid polyphenols (i.e., anthocyanin) degradation. Long and complex extraction durations are another drawback of conventional extraction techniques. In particular, the most prominent and usual traditional extraction techniques are maceration and Soxhlet extraction. However, they are highly inefficient and may represent environmental risks since of the apparent massive amount of organic solvents they require [99]. However, Soxhlet extraction is commonly known as solid-liquid extraction. It is among the earliest acknowledged techniques for extracting polyphenolic substances [100].

Furthermore, as aforementioned, this technique of extraction is often challenged due to the enormous amount of solvent used, which causes environmental issues in addition to a higher price tag, long processing time, and thermal reduction owing to excessive heat exposure throughout extraction and evaporation of extracted molecules, since the solvent is removed at its boiling point. Additionally, high tolerance to light and oxygen results in the destruction of other sensitive compounds [101]. Consequently, numerous alternative enhanced extraction techniques are

investigated and rapidly developed, emphasizing reducing the amount of organic solvent, reducing processing time or energy, and increasing production.

I.7.3.2. Modern Extraction Techniques

According to challenges accompanied by high operating temperatures and extended procedure durations in traditional extraction approaches, it is essential to accelerate the development, including innovative phenolic compound extraction techniques. Alternatives recently attracted significant interest include ultrasound extraction, microwave extraction, ultrasound-microwave-assisted extraction, supercritical fluid extraction, and subcritical water extraction since they are uncomplicated, require less time to extract and use less organic solvent [99-102].

I.7.3.2.1. Ultrasound Extraction

Ultrasound extraction offers significant advantages over conventional techniques, increasing extraction efficiency while decreasing the time. It could also exhibit good biological activity. As a result, it has been widely acknowledged as an easy and effective technique for extracting bioactive components. The ultrasonic extraction process is typically considered substantially controlled by the mechanical impact, cavitation, and heat effects [103]. Ultrasound extraction has been frequently utilized in extracting and isolating numerous useful compounds from natural plants, generally with favorable performance [94]. This technique uses ultrasonic waves to generate mechanical vibrations in a liquid medium. Sound wave transmission generates compression and rarefaction spaces in the medium. As a result, numerous bubbles form and blow up at the subsequent level. A phenomenon known as acoustic cavitation is produced when these bubbles collapse. Various instruments and equipment may be used depending on the desired use of ultrasound techniques. This variation potentially includes using conventional ultrasonic water baths to modern high-power ultrasonic generators [104]. A generalized scheme of the extraction of polyphenols using ultrasound is shown in Figure I.14.

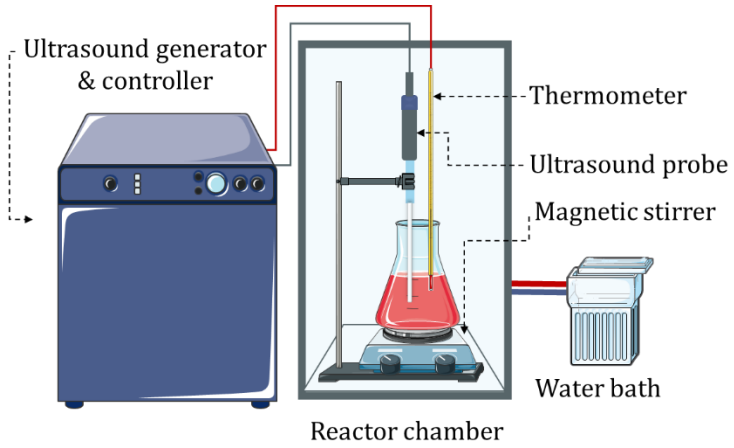

Figure I.14. Schematic illustration of ultrasound extraction of polyphenols [105].

Numerous publications on the isolation of polyphenols *via* ultrasound extraction have occurred in the last twenty years. For instance, *Garcia-Castello et al.* [106] extracted flavonoid molecules from grapefruit residuals using conventional solid-liquid and ultrasonic extraction. The total polyphenol contents and antioxidant properties of ultrasound extraction extracts were approximately 1.7 times that of traditional solid-liquid extraction extracts when isolating flavonoids from grapefruit (*Citrus paradisi L.*) residuals under the same parameters. *El Kantar et al.* [107] integrated infrared pre-treatment with ultrasound extraction and compared it to traditional solid-liquid extraction to increase the extraction of polyphenols from orange peels. They reported that the ultrasound technique enhanced polyphenols extraction from untreated peels by 62.5 %. Another study was written by *Martínez-Ramos et al.* [108] for increasing the extraction of phenolic compounds from various agro-food sources. The total polyphenol contents were obtained with the "60% ethanol, 40% acetone" mixture *via* ultrasound extraction.

I.7.3.2.2. Microwave Extraction

Microwave extraction was introduced in the late 1980s as a technique that requires heating a solvent in interface with a sample using microwave energy to recover polyphenols from food residuals towards the solvent utilized [109]. This technique provides many advantages owing to its high extraction rate, short extraction time, relatively less solvent content, and high product services at an affordable cost [110-111]. In addition, microwave extraction could adapt quickly to the existing extraction process. For instance, considering the published research by *Alara et al.* for extracting bioactive molecules from *Vernonia amygdalina* leaf tissue, the efficiencies from microwave extraction and soxhlet techniques were compared [112]. The results show that plant metabolites can

be extracted using microwave technique in a short time while the extract also can possess a high capacity of inhibiting antioxidants compared with conventional extraction technique. *Li et al.* [113-114] investigated the effects of focused microwave extraction on the extraction of phenolic acids, including gallic, chlorogenic, and caffeic acids, from *Eucommia Ulmodies*, which is a plant with antibacterial, antimutagenic, and antioxidant properties that are extensively used in Chinese medicine. The optimal extraction parameters were reported to be the use of 50% microwave power for 30 seconds, as well as a solvent capacity to solid ratio of 10 mL/g. For optimal extraction efficiency, the samples should be dried and powdered prior to microwave extraction. If the particle size is insufficient, it interferes with the extraction and may require an additional washing process [115]. Microwave drying and extraction has recently developed as a revolutionary concept in which microwave drying is integrated with a condensate. Polyphenol-containing vapours evaporated from the dried sample migrate via condenser and condensed to form the liquid extract. Using this technique, the bioactive components are isolated and extracted without adding extra solvents, which is more effective for the long-term extraction of bioactive substances from various fruits, vegetables, and herbal products after dry [116-117]. Figure I.15 shows a schematic illustration of polyphenol extraction *via* the microwave extraction technique utilizing a condenser.

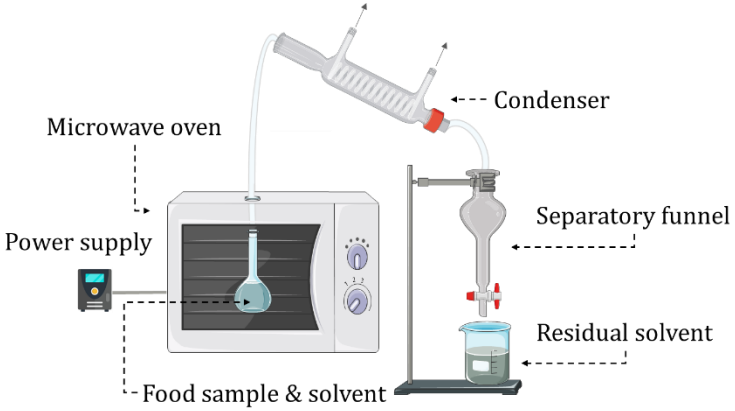

Figure I.15. Schematic illustration of microwave extraction of Polyphenols using a condenser [105].

I.7.3.2.3. Enzyme Extraction

Enzyme extraction is an environmentally friendly approach for increasing productivity by introducing enzymes to a mixture. The cell wall of wastages fruit material acts as a barrier, blocking polyphenols from escaping the cell. Cellulases, β-Glucosidases, Xylanases, and pectinases are only a few enzymes that may decompose cell walls and allow for the release of their components. Therefore, the primary technique involved the hydrolysis of food material's cell wall utilizing an enzyme as

catalysis at optimal parameters for the extraction of bioactive components [118-119], as illustrated in Figure I.16. Owing to these parameters, enzyme extraction can be used in combination with other extraction techniques as a pre-treatment process or as a powerful extraction technique using various enzymes for extracting the target compounds [120-121]. In addition, this technique produces unique advantages for extracting polyphenols from fruit waste. It destroys the cell wall more efficiently than mechanical treatment and can also avoid losing active substances [122]. This extraction also occurs at a lower temperature and consumes minimal power, preserving polyphenols from decomposition, primarily used in extracting polyphenols from fruits and vegetables like cabbage [123]. *Mushtaq et al.* [124] utilized a 3.8% enzyme mixture to pre-treat pomegranate peels at pH 6.8 and 41 °C for 85 min, and the extraction efficiency reached three times more than that of conventional solvent extraction. Compared to the ultrasonic extraction of polyphenols from orange peels, It was found that the enzyme extraction produced multiple times as many polyphenols *via* ultrasound extraction [125]. Consequently, recent investigations have demonstrated that the effectiveness of enzyme phenolics extraction is significantly superior to that of conventional techniques [119].

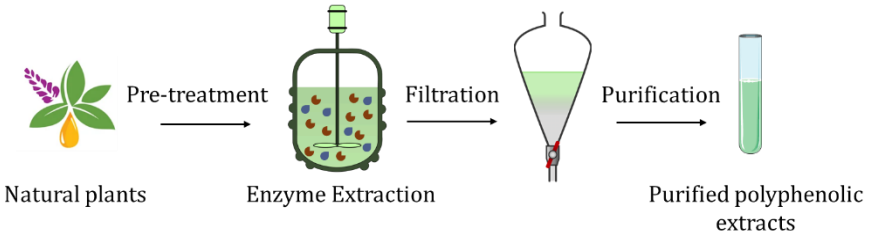

Figure I.16. Schematic illustration of Enzyme extraction of Polyphenols [105-126].

I.7.3.2.4. Membrane separation technique

The extraction and purification of phenolic compounds by molecular weight using membrane separation technology have attracted considerable attention, which other techniques cannot accomplish. The technology provides a considerably superior alternative, as they have lower operating costs, easy adaptability, and improved product quality than traditional techniques such as Soxhlet extraction. In the agro-food industry, pressure-driven membrane processes, namely ultrafiltration, microfiltration, and nanofiltration, have been extensively investigated recently [127]. Numerous strategies for extracting polyphenols from fruit waste via membrane separation have been produced. Papaioannou et al. [128] successfully extracted polyphenols from pomegranate peels with 98% using nanofiltration. *Conidi et al.* [129] investigated the nanofiltration extraction of phenols from orange press liquid. The findings indicate that flavonoids and anthocyanins have been recovered to the extent

of 70 and 89.2 %, respectively. Hence, this technique has been identified as appropriate for separating phenolic compounds from nutrients.

I.7.3.2.5. Accelerated Solvent Extraction

Accelerated solvent extraction, often pressured liquid extraction, is a trendy technique used extensively to extract polyphenol molecules from natural sources. This technique has several advantages, including a rapid extraction time, increased pressure and temperature, process automation, and minimal solvent utilization [130-131]. The desired extract can be recovered through an organic solvent using molecular diffusion, heat transfer, and pressure evaporation. Accelerated solvent extraction performs better than standard solvent extraction regarding extraction yields, time, and organic solvent usage [132]. Therefore, this procedure requires a solvent container, an oven containing an extraction cell, a pump, blocking valves, and a collection vial, as illustrated in Figure I.17. specific Accelerated solvent extraction devices are accessible on the markets [133]. Compared to ultrasound-assisted or microwave-assisted extraction, it has non-thermal treatment, sustainable energy, and a low cost. Consequently, this technology has been used to extract polyphenols from agricultural wastes, where they can be taken advantage of for large-scale industrial manufacturing [134-135].

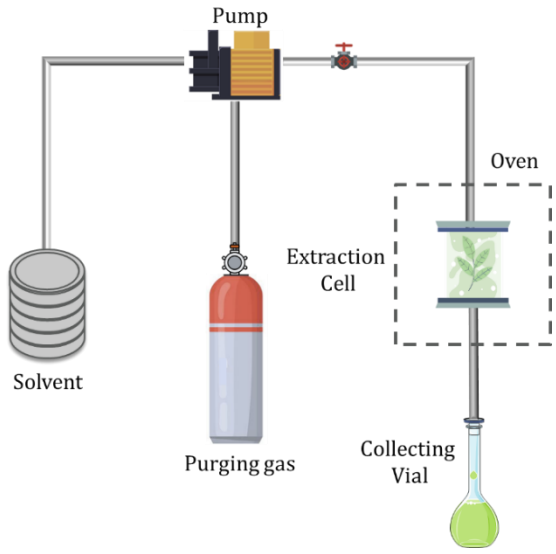

Figure I.17. Polyphenols extraction *via* Accelerated Solvent Extraction [105].

I.7.3.6. Supercritical fluid extraction

In recent years, supercritical fluid extraction has attracted particular attention for the extraction of active compounds from plants at atmospheric temperatures without thermal denaturation, where it

is an eco-friendly process that utilizes supercritical fluid, such as carbon dioxide (CO_2), as an extraction procedure to extract active compounds from waste [110]. This technique is increasingly becoming popular due to its extremely low or elimination of organic solvent, innovative, high-valued, and high-quality final product, faster extraction time, and increased selectivity. However, it is often criticized for its expensive investment cost. At critical pressure and temperature, fluid functions as a supercritical fluid with intermediate properties such as diffusivity, solubility, or density between a gas and a liquid [136]. However, there are also a few drawbacks when considering further extraction studies. For a susceptible process with many possible operating conditions, phase equilibrium is crucial to consider during the design phase. Before separation studies can initiate, considerable pressure and specific environmental conditions must have been achieved [137]. In contrast to traditional extraction techniques, supercritical fluid extraction has excellent selectivity and a rapid extraction time. Furthermore, since it is performed in the darkness of night and oxygen, supercritical fluid extraction considerably minimizes the oxidation of compounds [138].

I.7.3.7. Pulsed Electric Field Extraction

The pulsed electric field is among the most recent non-thermal processes extensively explored in industrial applications. This technique improves the extraction of bioactive compounds from plant cells by electro-permeabilization of plants *via* enhancing mass transfer even at the reduced electromagnetic current [139], as illustrated in Figure I.18. Considering that biological membranes are more conductive than their environments, they serve a crucial function in amplifying electrical impulses (cytoplasm and extracellular medium). Compared with conventional extraction technologies, pulsed electric field-assisted extraction can improve the extraction efficiency of natural compounds while being ecologically safe, cheap, and rapid [140-141]. Pulsed electric field treatment is a promising technique for increasing polyphenol content and quality in food processing [142-143].

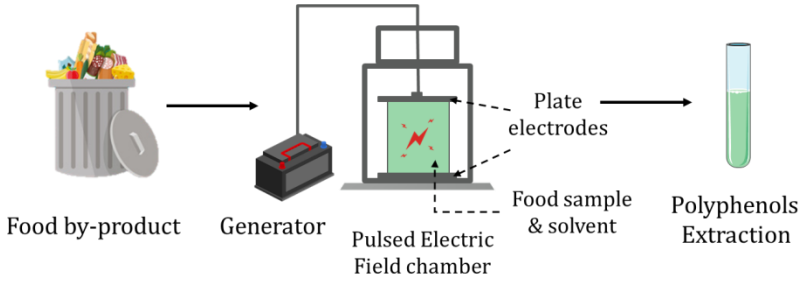

Figure I.18. Extracting polyphenols *via* Pulsed electric field technique [105].

I.7.4. Polyphenols detection and quantification techniques

Due to the structural variety and low quantities of polyphenols, as well as the complexity of the plant matrix, their study remains difficult. Currently, the investigation of polyphenols in plants and foods necessitates the development of sensitive and reliable techniques. Scientists have used cutting-edge procedures in the last several decades, including liquid chromatography (LC), mass spectrometry (MS), and spectroscopic approaches. Figure I.19 shows a general scheme of polyphenols extraction, detection, and quantification steps. Extraction-followed qualitative and quantitative research of polyphenols has recently advanced with analytical technologies. In particular, the significance of high-resolution mass spectrometry in the targeted/untargeted chemometric study of polyphenols is also highlighted [144]. Since polyphenols are naturally chromophoric, high-pressure liquid chromatography (HPLC) remains the most popular analytical method for identifying and quantifying [80,145-146].

Depending on the compound's physicochemical structure, HPLC's detection mechanism can be used to record certain features of the eluted polyphenols. For instance, using authenticated standards, UV/VIS absorption spectra can be plotted in parallel to the retention time, contributing to identifying polyphenols in *Lamiaceae herbs* [147].

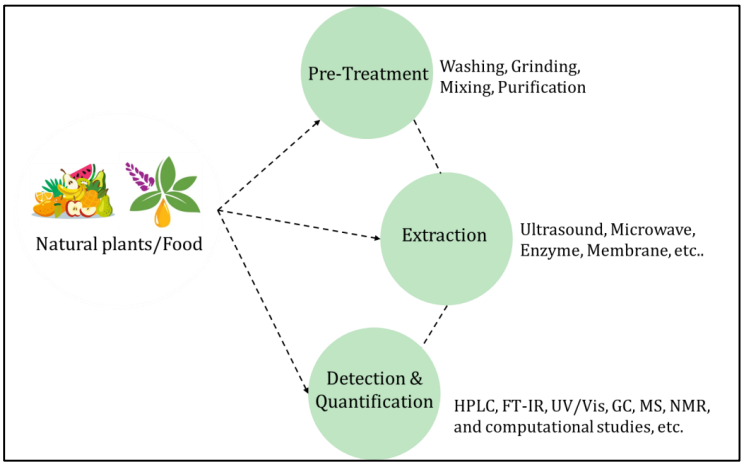

Figure I.19. General diagram of polyphenol treatment, extraction, detection, and quantification [148]

Typically, HPLC accuracy and identification rely on the purification of phenolics and the pre-concentration of crude plant extracts from complicated matrices. Meanwhile, there is no chromatographic technique capable of separating the various forms of phenolic chemicals. The

stationary phase, mobile phase, gradient elution, temperature, and flow rate must be optimized according to each group of compounds. Additionally, other factors such as the stereochemistry, molecular weight, polarity, and degree of polymerization of polyphenols should be considered since they influence the retention of the molecules [149-151]. Gas chromatography (GC) is another method to separate, identify, and quantify phenolic substances, such as phenolic acids [152]. When integrated with MS, HPLC, and GC provide increased sensitivity and selectivity [153]. For instance, When high-temperature–high-resolution GC–MS was performed, conventional GC's challenges associated with flavonoid glycoside assessment were eliminated [154]. According to another research, GC-MS evaluation of polyphenolic compounds is more effective than HPLC analysis, performing a precise detection with improved resolution and separation of all standards with minimal co-elution [155]. *Naczk and Shahidi* [156] discussed various techniques for analyzing polyphenols, including chromatographic approaches and others, for chromatography paper and thin-layer chromatography methods using multiple solvent systems. Gas chromatography is another technique that can isolate and identify polyphenols While requiring a selection of different preparation procedures before the analysis [157].

On the other hand, MS may be used to analyze polyphenols owing to its analytical power resulting from employing ionizing chemical substances by generating charged molecules or fragments and measuring their mass-load relationships. The potential advantages of MS include its high sensitivity and outstanding versatility in the identification, quantification, characterization, and structural analysis of molecules [158]. Furthermore, nuclear magnetic resonance (NMR) spectroscopy is further applied to evaluate and identify polyphenols [158]. These innovative approaches potentially play a pivotal role in polyphenols analysis. However, it is difficult to identify and characterize these compounds owing to the lack of available analytical standards and their structural variety.

I.7.4.1. Corrosion inhibition

Considering corrosion is a surface reaction, adding a much lower concentration of corrosion inhibitor to an interlayer can avoid or minimize the corrosion rate of an exposed metal in an aggressive environment. In general, the attached inhibitor molecules can form a surface layer referred to as a protective layer, which might also function as a protective border to the metal surface owing to the diffusion of ions or water molecules that subsequently react with inhibitor molecules, as highlighted in Figure I.20 [159-160].

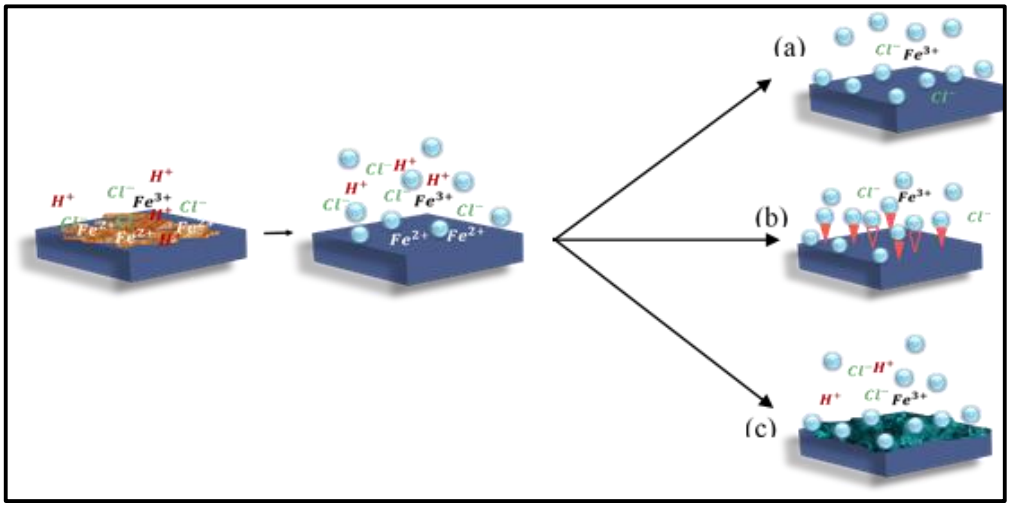

Figure I.20. Adsorption inhibition mechanisms: 1) physical adsorption, 2) chemical adsorption, and 3) surface coating [161].

Regarding Figure I.20, the adsorption of inhibitors can protect the metal in three different mechanisms: 1) physical adsorption, 2) chemical adsorption, and 3) surface coating. Physical or electrostatic adsorption occurs due to the electrostatic attraction between the inhibitor and the metal surface. Inhibitors that are physically adsorbable have an accelerated interaction rate but are also easy to desorb. Chemically adsorbed inhibitors are the most effective due to charge exchange or transfer between inhibitor molecules and metal surfaces. Moreover, chemical adsorption is more time-consuming and less adaptable than physical adsorption [162]. The mechanism of the surface coating depends on the surface reactions of inhibitor molecules and the production of a thin film on the surface blocking both anodic and cathodic areas. On the metal surface, organic inhibitors can create a protective hydrophobic coating. Specifically, the organic molecules' polar group is covalently bonded to the metal, whereas the nonpolar end is perpendicular to the metallic surface. This makes them efficient as a barrier against chemical and electrochemical attacks and the diffusion of corrosion products. Corrosion inhibitors may be categorized into cathodic, anodic, and mixed or adsorption forms based on their action method. Inhibitors of corrosion that inhibit the cathodic process are called cathodic inhibitors. Similar to cathodic inhibitors, anodic inhibitors interrupt the anodic process. Mixed inhibitors are those compounds that affect both the cathodic and anodic processes, and they are so-called adsorption inhibitors since they often function *via* an adsorption mechanism. Cathodic or anodic behaviors are typical of inorganic inhibitors, while organic inhibitors may do both [159].

Corrosion inhibition typically consists of organic or inorganic substances that adsorb on a metal part to separate it from its surrounding environment and interrupt the oxidation reactions [163]. Inorganic inhibitors function as anodic inhibitors, and their metal molecules are coated on the surface to increase corrosion resistance.

Most reported inorganic corrosion inhibitors are hazardous and present significant environmental problems when removed. Accordingly, ecological rules have restricted their usage. Besides that, inorganic inhibitors play an important role in corrosion protection, although their limited applicability is due to toxicity [164]. Organic inhibitors reduce corrosion by adsorbing their molecules to the surface of the metal or alloy, forming a protective layer by physically blocking or prolonging the electro-chemical processes [165-166]. Consequently, these are much more efficient than inorganic substances for protecting steels, particularly in acid conditions; they typically contain heteroatoms such as O, N, or S, in which their effectiveness is correlated with the existence of these atoms, heterocyclic compounds, and electrons. Attributed to the reason that O, N, and S have stronger oxidation states and electron density, they are the essential active sites for the adsorption mechanism on the metal surface [167-168]. In addition, a study of previous literature reveals that organic compounds comprising multiple bonds and these heteroatoms in cyclic rings and polar functional groups, including $-NH_2$, $-OH$, $-NO_2$, $-OMe_2$, $-NMe$, $-CN$, $-N=O$, $-N=C<$, $-N=N-$, $>C=O$, $>C=S$ etc. Function as effective corrosion inhibitors [169-170].

The majority of organic inhibitors have at minimum one functional group. The polarity of this group determines the adsorption strength of organic inhibitors rather than the presence of heteroatoms in the compound. The charge density of the functional group is further influenced by the composition of the remainder of all molecules [159,168]. Common organic inhibitors come from a wide variety of classes of compounds, including imidazole [171], amino acids and their derivatives [172], pyridines [173], and polymers [174-175] shown to be exceptionally effective corrosion inhibitors. Although many other inorganic and organic molecules can be applied as inhibitors, most provide disadvantages regarding environmental protection standards, cost, and toxicology if they have been placed into practical applications. Thereby, there is a critical need to develop corrosion inhibitors that are both effective and ecologically benign. Green inhibitors are the best alternative to the conventional expensive, harmful, synthetic organic corrosion inhibitors, including many components that can absorb and protect against metal corrosion [176].

I.7.4.2. Green corrosion inhibitors

As aforementioned, there is an increase in the research and the use of corrosion inhibitors, which are less hazardous and biodegradable than conventional inhibitors. Therefore, corrosion inhibitors with a "green" designation are receiving more attention. These inhibitors have demonstrated high effectiveness and promote sustainable compatibility, which will undoubtedly be the most prominent in the future [177]. There are several types of eco-friendly corrosion inhibitors, which may be categorized depending on their manufacturing processes as natural corrosion inhibitors or synthetic corrosion inhibitors [178].

Green corrosion inhibitors are derived from or produced from natural substances. This category includes several organic corrosion inhibitors and polymers. Leaves, herbs, flowers, fruits, seeds, pericarp, and other plant parts can contain effective inhibitory compounds. Polyphenols are readily available and straightforward to extract from a variety of sources. These compounds have oxygen groups that most are complexation with metallic surfaces, such as iron. The−OH groups can establish tannates with metal ions to form a black substance that helps to stabilize the surface oxides [177].

I.7.4.3. Polyphenols as green corrosion inhibitors

Polyphenols are recognized to be additional types of essential plant-based natural chemicals. Their anticorrosion properties are primarily responsible for the appearance of aromatic −OH groups. Furthermore, heteroatoms can contribute electrons to fill vacant *d*-orbitals in metal, coordinating interactions. Adsorption of molecules onto metal surfaces is also facilitated by interactions with rings, including conjugated bonds or electrons [61]. Table I.1 presents an overview of several publications on the different extracted Polyphenols utilized as environmentally friendly inhibitors reporting most of the articles mentioned on this topic.

In an experiment, *Chaieb et al.* [179] employed weight loss measurements, potentiodynamic polarization (PDP), and electrochemical impedance spectroscopy (EIS) techniques to measure the influence of eugenol and its derivative acetyl eugenol on the corrosion of steel in 1 M hydrochloric acid (HCl) medium. The naturally available compounds reduce the rate of corrosion, and it was observed that acetyl eugenol increased the inhibitory efficacy by 91% at 0.17 g L^{-1}whereeugenol compounds function primarily as mixed-type inhibitors. The correlation between temperature and steel's corrosion characteristic shows that the natural component's capability to inhibit corrosion grows

as temperature increases. *EL-Etre* [180] released a study on the corrosion protection properties of olive leaves (*Olea Europaea L.)* extract on carbon steel. The inhibition of acidic corrosion of steel was attributable to the unshared electrons adsorption of O atoms producing a protective coating and functioning as a barrier between the surface of the steel and the corrosive medium.

Moreover, the configuration of O atoms around the aromatic rings of phenols can conclude that phenolic compounds are promoted to be adsorbed horizontally over the steel surface. Olive leaves extract contains polyphenolic substances with antioxidant properties where the primary components were determined as *Olea Europaea* in and hydroxytyrosol. Since oleuropein can be easily decomposed to hydroxytyrosol, oleanolic acid or hydroxytyrosol perhaps is the primary responsible for the inhibition process. Nevertheless, there was no experimental evidence verifying these assumptions concerning the mechanism of inhibitory action, and the activity of individual compounds was not confirmed in this study. *Arab et al.* [181] the synergistic effect of iodide ions on the corrosion inhibition of aluminum in the presence of *Azadirachia Indica* leaf extracts in a corrosive medium containing 0.5 M HCl. The PDP and EIS approaches were utilized, revealing that Azadirachia Indica extracts inhibit aluminum corrosion with increased effectiveness as the inhibitor concentrations increase. In the presence of a constant concentration of iodide ions, the inhibitor forms an insoluble compound at decreasing *Azadirachia Indica* extract concentrations through combined adsorption.

Umoren et al. [182] reported that *Vigna Unguiculata* had adsorption and corrosive inhibiting properties in alkaline and acidic environments. The weight loss technique was utilized to test the inhibitory effect of the plant extract at 30 and 60 °C. The tendency of inhibition efficacy with temperature was used to describe the inhibition mechanisms and the adsorption type. Thus, the extract of *Vigna Unguiculata* successfully inhibited aluminum corrosion in both alkaline and acidic conditions, in which temperature and inhibitor concentration significantly improved the inhibition effectiveness. *Using weight loss and galvanostatic techniques, Foudaa and Ellithy [183] evaluated several 4-phenyl thiazole derivatives as corrosion inhibitors for 304L stainless steel in 3 M HCl*. The results show that increasing the concentration of 4-phenyl thiazole derivatives increases the inhibition activity, as demonstrated by the PDP test. These compounds are inhibitors of mixed type. Numerous thermodynamic properties were measured, and the weight loss approach was employed to investigate how temperature impacts corrosion. Abdallah et al. [184] used an alternative strategy by choosing four commercial phenols and assessing how effective their individual inhibitory properties are against steel corrosion. The molecules were characterized by the presence of $-NH_2$, $-OH$, $-CHO$, or $-COOH$

groups in *ortho*-position regarding the phenol. The order of inhibition efficiency was by the following ranking $-NH_2 > -OH > -CHO > -COOH$. It was concluded from the specific order that compounds with electron-donating groups are more effective as inhibitors than those with acceptors groups. The electron-donating groups promote adsorption and add electronegativity to the molecule, producing it more nucleophilic and, as a result, increasing the efficacy of inhibition. Furthermore, HOMO-LUMO orbital theoretical computations were also reported. Using ESI, linear polarization resistance (LPR), and PDP experiment evaluations at different concentrations, *Yıldız et al.* [185] determined the corrosion behavior of 4-amino-3-hydroxynaphthalene-1-sulphonic acid on mild steel in 0.1 M HCl. The surface morphology of mild steel was analyzed by scanning electron microscopy (SEM) in the presence and absence of an inhibitor and a corrosive medium containing 10 mM of inhibitor. In addition, at the metal-interface, the inhibitory mechanism was identified by measuring the potential of the zero charge. From the *Cryptostegiagrandiflora* plant methanolic extracts, *Prabakaran et al.* [186] investigated mild steel's polyphenol content and anti-corrosion properties. The largest concentrations of myricetin, quercetin, and rutin were found in the extract. However, single inhibition actions were negligible. Furthermore, many research studies, such as the extract of *Gongronemena latifolium* [187], exhibited optimum inhibition effectiveness of 90.66% at 1.0 gL^{-1} concentration, *Curcuma longa* extract [188] obtained excellent effectiveness of 95.65% at 30 °C. In contrast, *Pennisetum purpureum* extract [189] exhibited a high inhibition of 81.7% at 5.0 g L^{-1}. Besides, *Bitter kola* extract [190] has an inhibition efficacity of 86.81% at 0.9 g L^{-1}.

Recently, using an electrochemical impedance spectroscopy technique, *Bourazmi et al.* [191] analyzed the corrosion inhibition properties of *Salvia Officinalis* extracted from mild steel in 1 M HCl medium. The findings demonstrate that at 1.2 g L^{-1} concentration, the inhibitor successfully interrupted mild steel corrosion at approximately 86%. *Haddadi et al.* [192] studied the effectiveness of *Juglans Regia* extract as an efficient corrosion inhibitor for carbon steel, reaching a superior corrosion efficiency of 94 % with 1000 ppm of inhibitor. *Haldhar et al.* [193] investigate the efficacy of *Gloriosa superba* seed extract as a carbon steel corrosion inhibitor in a corrosive solution of sulfuric acid (0.5 M H_2SO_4). Electrochemical methods have been used, followed by a weight loss evaluation. With the addition of 700 mg L^{-1} of inhibitor, PDP achieved an exceptional corrosion efficiency of 93 %, confirming the presence of mixed adsorption on low-carbon steel. Tan et al. [194] also employed *Betel* leaves extracts as an environment-conscious corrosion inhibitor for mild steel in 1 M HCl medium. According to electro-chemical measurements, the inhibitor prevented the anode and cathode

reactions of Q235 steel at a concentration of 400 mg L^{-1}, and approximately 90 % anti-corrosion efficacy was achieved. Using the mass loss method, *Belakhdar et al.* [195] evaluated the performance and corrosion inhibition behavior of the extract derived from *Rosmarinus officinalis* on XC48 steel in 1 M HCl medium at varying temperatures. They characterized *using EIS, SEM, PDP, FTIR, and LC–MS chromatography techniques*. Results indicate that inhibitor-based extract functions as a mixed-type inhibitor. Specifically, the inhibition efficacy increases with increasing inhibitor concentration and decreases as the temperature rises from 30 to 60 °C. SEM results demonstrated that adsorbed inhibitor molecules entirely limit HCl operations at the steel intergranular, validating the reported results. Quantum chemical calculations also showed that, among the most prominent components detected in the *Rosmarinus officinalis* extract, carnosic acid has a more potent inhibitory potential than carnosol. *Echihi et al.* [196] tested the inhibition effect of polyphenols derived from *Artemisia Herba alba* on mild steel corrosion in a 1 M HCl solution using EIS, PDP, and weight loss experiments. SEM, atomic force microscopy (AFM), X-ray diffraction (XRD), with X-ray photoelectron spectroscopy (XPS) are used to evaluate the surface shape and chemical composition of a sample of mild steel after contact with *Artemisia Herba alba* secondary metabolites in the corrosive medium. According to the results of PDP curves, *Artemisia Herba Alba* extract works as a mixed-type inhibitor. For all examined inhibitor-based extract concentrations, inhibitory efficacy is related to extract concentration, reaching 92.9% at 900 ppm. Experiments on the metal surface demonstrate that the applied inhibitor molecules effectively block HCl effects at steel grain boundaries, proving the integrity of these results. Lastly, molecular modeling simulations demonstrate that dicaffeoylquinic acids, among most common *Artemisia Herba Alba* extract constituents, are efficient corrosion inhibitors. *Tehrani et al.* [197] investigated an innovative green corrosion inhibitor coating produced on mild steel employing *Malva Sylvestris* extracts and evaluated by various techniques. The generated film provided an inhibitory effectiveness of 91 % in the saline medium, where 1000, 1500, and 2000 ppm, respectively, resulted in the formation of this inhibition coating with a total resistance of 12, 14, and 16 K cm^2. Additionally, electro-chemical analysis showed that *Malva Sylvestris* extracts significantly reduced the anodic reaction. Theoretical studies based on quantum chemistry and molecular modeling were also provided to confirm the adsorption of *Malva Sylvestris* based extracted molecules on the metallic surface through their reactive sites.

I.7.4.4. Computational approaches and polyphenolic compounds

In order to explore the processes of corrosion inhibition, computational calculations are essential for understanding experimental results. After the practical parts, a computational study, considering each molecule separately, would be required to accomplish the research. Recent research emphasizes the significance of theoretical studies. Still, it lacks a specific methodology and ends up providing data of corrosion inhibition of various compounds, then conducting computer calculations on a single component of the molecules [198-201]. Computational chemistry techniques were performed to investigate and comprehend how the molecule of polyphenols influences their inhibitory efficacy.

For this reason, according to many investigations, researchers have focused on the polyphenolic molecule functioning as a green corrosion inhibitor by itself in vacuum or aqueous phase in its neutral, protonated, or un-protonated forms depending on the pH of a corrosive medium by using these quantum chemical calculations. Typically, approaches deriving from density functional theory, such as the DFT/B3LYP method with multiple basis sets, are utilized. After that, researchers tried to use specific characteristics of both large and small reactivity to integrate one or more characteristics to estimate the inhibition efficiency using a mathematical model. Nevertheless, corrosion inhibition is a multidimensional phenomenon involving numerous competing effects, such as the inhibitor-metal surfaces interaction (adsorption energy), inhibitor solubility, inhibitor complexation with metal ions in solution, etc., [202-203]. Some of the most valuable DFT-based parameters are E_{HOMO} (energy of highest occupied molecular orbital), E_{LUMO} (energy of lowest unoccupied molecular orbital), energy band gap ($\Delta E=E_{LUMO}-E_{HOMO}$), hardness ($\eta$), electronegativity ($\chi$), softness ($\sigma$), dipole moment ($\mu$), nucleophilicity ($\omega$) and a fraction of electron transfer (DN), etc.

Furthermore, the use of DFT to study corrosion inhibition has been addressed previously [204]. It is significant to mention that the capacity to donate electrons improves with increasing E_{HOMO} levels and decreases with increasing E_{LUMO} levels. Typically, the protection efficiency of organic compounds increases as the energy band gap decreases. Higher levels of softening and nucleophilicity are associated with effective corrosion inhibition and *vice versa*. Conversely, low levels of electronegativity and hardness are related to high inhibitory efficacy. Molecular sites involved in donating electrons and electron acceptation can be readily observed in corrosion using the DFT approach, which will help the design and develop exceptional corrosion inhibitors. A literature study demonstrates that DFT-based theoretical calculations are infrequently utilized to identify polyphenolic

compounds' corrosion inhibition effect [205-212]. Recently, the adsorption energy has been calculated using Molecular Dynamic (MD) modeling with periodic boundary conditions *via* using the Metropolis Monte Carlo statistical method (MC) to determine the adsorption arrangement with the lowest energy for a variety of polyphenols on metallic surfaces [213-215]. For the largest systems, the tendency is toward using MD simulations because of the time savings compared to quantum chemical techniques. The *ab initio* force field COMPASS (Condensed phase Optimized Molecular Potentials for Atomistic Simulation Studies) is widely used during MD calculations to determine the energy of all system components [216-217]. For instance, the findings of an MD simulation revealed that the conjugated $C = C$, $C = O$, and $-OH$ groups of phenolic compounds were drawn directly from the metal surface and into the solution, which may contribute to its decreased adsorption energy in a neutral state. In specific investigations on polyphenol compounds, the interaction energy between molecule and metal surface was determined using DFT and MD techniques, for example, Colchicine and Colchicoside on Fe (110) surface [193]. Overall, most papers in this type of method performed only a standard series of experiments and rarely explored the underlying mechanisms. Given these findings, researchers should use this approach more frequently when analyzing polyphenols and related compounds in corrosion inhibition studies.

Table I.1. Summary of the primary characteristics of the Polyphenols extracted as green corrosion inhibitors.

	Extract Source	Extraction Method& Solvent	Main constituents	Metal/Alloy	Corrosive Medium	Inhibitor Concentration	Inhibition Efficiency (%)	Year	*Ref.*
1	*Hibiscus Sabdariffa* leaves	Reflux extraction in 1M H_2SO_4	[a]	Mild steel	1 M H_2SO_4	50% v/v	93.30	**2008**	[218]
2	*Hibiscus Sabdariffa* leaves	Water extraction	Thiamine, Niacine, Ascorbic acid, and Anthocyanins	Aluminum	0.5 M NaOH	1.5 g L^{-1}	84.68	**2009**	[219]
3	Henna Leaves	Water extraction	Lawsone, Gallic acid, α-D-Glucose, and Tannic acid	Mild steel	1 M HCl	1.2 g L^{-1}	92.06	**2009**	[220]
	Red onion skin bulb	Solvent Extraction using a water/acetone mixture	Quercetin	Aluminum	2 M HCl	-	90.00		[221]
4	*Jasminum Nnudiflorum* Lindl Leaves	Reflux extraction in methanol	Phillyrin, Verbascoside, and Jasnudifloside	Cold rolled steel	1 M HCl	50 mg L^{-1}	93.00	**2010**	[222]
5	*Rhizophora apiculata* Bark	Maceration in 9 different solvents	Tannin	Mild steel	1 M HCl	0.1 g L^{-1}	57.90	**2011**	[223]
6	*Gossypium Hirsutum* Leaves	Reflux extraction in 1 M HCl	Gossypol, Phenylalanine, Cystine, and Methionine	Aluminum	1 M HCl	2.5% w/v	92.40	**2011**	[224]
7	*Schinopsis Lorentzii* tree powder	Water extraction	Flavan-3-ol	Low carbon Steel	1 M HCl	0.2 g L^{-1}	63.00	**2012**	[225]
8	*Piper guineense* Seeds	Reflux extraction in 1 M HCl	Piperine, Safrole, and Dihydrocubebin	Mild steel	1 M HCl	0.9 g L^{-1}	88.40	**2012**	[226]
9		Reflux extraction in 0.5 M H_2SO_4			0.5 M H_2SO_4	0.9 g L^{-1}	97.70		
10	*Acacia mearnsii* Mimosa tree powder	Water extraction	Mimosa tannin	Brass-MM55	0.5 M H_2SO_4	2 g L^{-1}	60.24	**2012**	[227]
11	*Rhizophora Apiculate* Mangrove barks	Soxhlet extraction and Maceration method	Tannin and (+)-catechin	Mild steel	1 M HCl	0.5 g L^{-1}	91.80	**2012**	[228]
12	*Olive mill* wastewater	Solvents Extraction	Not determined	Carbon steel	1 M HCl	4 g L^{-1}	92.90	**2013**	[229]
13	*Punica granatum Linne husk*	Water extraction	Gallic acid, Ellagic acid, Gallagic acid, Punicalin, and Punicalagin	Q235A steel	1 M HCl	1 mg L^{-1}	87.40	**2013**	[230]
14	*Kleinia Grandiflora* Leaves	Solvent Extraction using ethanol	Quinic acid, 6-deoxy D-galactose, Hexadecanoic acid, and Linolenic acid	Mild steel	1 M H_2SO_4	1.5 g L^{-1}	81.68	**2014**	[231]
15	*Capsicum Annuum* Fruit	Reflux extraction in water	Capsaicin and Ascorbic acid	Copper	3 M HNO_3	0.3 g L^{-1}	88.00	**2015**	[232]
16	*Musa paradisica (Banana)* peels	Solvent Extraction using a water/acetone mixture	Gallocatechin	Mild steel	1 M HCl	300 mg L^{-1}	90.00	**2015**	[233]
17	*Ceratonia Siliqua* Carob tree	Solvents Extraction	[a]	α-brass (Copper-Zinc) Copper	1 M HNO_3	300 mg L^{-1}	97.00 82.80	**2015**	[234]

18	*Palisota hirsute* leaves	Reflux extraction	[a]	Aluminum Alloy AA8011	0.25 M KOH	0.4 g L^{-1}	74.10	**2016**	[235]
19	*Cryptostegia grandiflora* Leaves	Solvent Extraction using methanol	Myricetin, Rutin, and Quercetin,	Mild steel	1 M H_2SO_4	0.5 g L^{-1}	83.54	**2016**	[186]
20	*Diospyros kaki* leaves	Soxhlet Extraction using ethanol	Uvao, Oleanolic acid, Betulinic acid, 19 α Hydroxyursolic acid, and 19 α, 24 Dihydroxyursolic acid	St37 steel	1 M HCl	0.225 g L^{-1}	91.00	**2016**	[236]
21	*glycine max* leaves	Water extraction	Genestein and Daidzein	Mild steel	0.5 M HCl	0.5 g L^{-1}	84.94	**2016**	[237]
22	*Lannea Coromandelica* leaves	Water extraction	Flavonoids, Glucosides, Carbohydrates, Phenols, and Tannins	Mild steel	1 M H_2SO_4	250 mg L^{-1}	88.50	**2017**	[238]
23	*Moringa Oleifera* leaves	Soxhlet Extraction using double distilled water	Quercetin and Luteolin	Copper	1 M (HNO_3+ H_3PO_4)	0.3 mol L^{-1}	89.30	**2018**	[239]
24	*Myristica Fragrans* fruit	Reflux extraction in ethanol	5 different phenolic compounds	Mild steel	0.5 M H_2SO_4	0.5 g L^{-1}	87.81	**2018**	[240]
25	*Rosa canina* fruit	Water extraction	Marein, Ascorbic acid, Pectin, and Tannin	Mild steel	1 M HCl	0.8 g L^{-1}	80.57	**2019**	[213]
26	*Punica Granatum B*ark waste	Soxhlet Extraction using methanol	Phenols, Flavonoids, Saponosides, Sterols, and Polyterpenes	Mild steel	1 M HCl	1 g L^{-1}	88.00	**2020**	[241]
27	*Garcinia Indica* fruit rind	Reflux extraction in water	Cyanidin and Anthocyanin	Mild steel	1 M HCl	4% v/v	93.94	**2020**	[242]
28	*Rosmarinus Officinalis P*lant	Solvent Extraction using a water/ethanol mixture	Carnosol and Carnosic acid	XC48 steel	1 M HCl	0.4 g L^{-1}	91.00	**2020**	[195]
29	Green tea	Reflux extraction in Dimethyl formamide	[a]	Carbon steel	1 M HCl	0.08 g L^{-1}	78.80	**2021**	[243]
30	*Artemisia Herba Alba* leaves	Solvent Extraction using a water/methanol mixture	Dicaffeoylquinic acid isomers	Mild steel	1 M HCl	0.9 g L^{-1}	92.90	**2021**	[244]
31	*Gloriosa superba* seeds	Soxhlet Extraction using distilled water	Colchicine, and Colchicoside	Low carbon steel	0.5 M H_2SO_4	700 mg L^{-1}	93.00	**2021**	[193]
32	*Passiflora edulia Sims* shell	Solvent Extraction using a water/ethanol mixture	Isoorientin, Schaftoside, and Apigenin	Mild steel	1 M HCl	0.5 g L^{-1}	95.82	**2022**	[245]
33	*Cytisus multiflorus* flowers	Solvent Extraction using ethanol	Chrysin-7-O-b-D-glucopyranoside, Dihydroxyflavone, and Rutin	Carbon steel	1 M H_2SO_4	0.5 g L^{-1}	95.91	**2022**	[205]

[a] *Not Determined*

Conclusion

Metallic materials are extensively applied in industrial applications, susceptible to corrosion damage when interacting with an acid medium in various engineering processes. Corrosion may be decreased with the use of inhibitors, providing for damage limitation. The interest in natural products has been growing in recent years. This interest is manifested by a growing demand for active natural products without harmful effects and the need to protect the environment. The Mediterranean region, in a general way, Algeria in particular, with its mild and sunny climate, is particularly favorable to the culture of natural and aromatic plants. Natural plants owe their action to one or more active principles that can be analyzed chemically. The main ones are essential oils, alkaloids, flavonoids, heterosides, polyphenols, etc. Despite the development of chemistry, which has arrived at the synthesis of compounds identical to the natural ones, some of these compositions remain impossible to be synthesized, from where we resort to the methods of extraction of the general matter.

For several years, research on corrosion inhibitors has been increasing for several reasons: ecological constraints, which require the search for new "green" formulations that can replace toxic compounds. Therefore, the effectiveness of these compounds in inhibiting corrosion depends on their chemical structure, concentration, corrosion medium, metal surface type, and other parameters. Although some polyphenols can be effective corrosion inhibitors, they can also reverse the corrosion reaction, depending on the operational parameters. Recent surveys on using polyphenols as corrosion inhibitors have focused on synthesizing novel derivatives more effectively than their analogous molecules (i.e., phenolic acid). They describe their inhibitory mechanism using quantum chemistry computation with molecular mechanical modeling. Density functional theory (DFT) has been used extensively in this field to study these substances, for instance, their interaction with a metal surface, referring to simulations of molecular mechanics (based on classical mechanics) because of their accessibility and accuracy. In addition, DFT approaches are limited by their time-consuming aspect and their restriction on the size of the studied structures, particularly when considering the "inhibitor molecule-metal surface" complex. For this reason, we recommend that the researchers focus more on this topic.

Reference

[1] M. Acharya, J. S. Chouhan, A. Dixit, et D. K. Gupta, « Green inhibitors for prevention of metal and alloys corrosion: an overview », *Chem Mater Res*, vol. 3, n° 6, Art. n° 6, 2013.

[2] N. I. Kairi et J. Kassim, « The effect of temperature on the corrosion inhibition of mild steel in 1 M HCl solution by Curcuma longa extract », *Int. J. Electrochem. Sci.*, vol. 8, n° 5, Art. n° 5, 2013.

[3] M. G. Fontana et N. D. Greene, *Corrosion Engineering I*. McGraw Hill, New York, 1978.

[4] C. Fiaud, C. Lemaitre, et N. Pébère, « Corrosion et anticorrosion, chapitre 13 », *Lavoisier Paris*, 2002.

[5] K. E. Heusler, D. Landolt, et S. Trasatti, « Electrochemical corrosion nomenclature », *J. Electroanal. Chem. Interfacial Electrochem.*, vol. 274, n° 1‑2, Art. n° 1‑2, 1989.

[6] A. Norma, « G15 », *Stand. Terminol. Relat. Corros. Corros. Test. Corros. Corros. Test. Des. G 15*, vol. 7.

[7] M. G. Fontana et N. D. Greene, « Corrosion Engineering McGraw-Hill book Company », *N. Y.*, p. 8‑29, 1987.

[8] B. Wiersma, « A Structural Integrity Evaluation of the Tank Farm Waste Transfer System », Savannah River Site (SRS), Aiken, SC (United States), 2006.

[9] G. Palanisamy, *Corrosion inhibitors. Corrosion inhibitors: Ambrish Singh, IntechOpen; 2019*.

[10] M. G. Fontana, N. D. Greene, et J. Klerer, « Corrosion Engineering », *J. Electrochem. Soc.*, vol. 115, n° 5, p. 142C, 1968.

[11] O. L. Riggs Jr et C. C. Nathan, *Corrosion inhibitors*. CC Nathan, Houston, Tx, 1973.

[12] M. G. Fontana et N. D. Greene, « Corrosion Engineering McGraw-Hill book Company », *N. Y.*, p. 8‑29, 1987.

[13] R. W. Revie, *Corrosion and corrosion control: an introduction to corrosion science and engineering*. John Wiley & Sons, 2008.

[14] T. K. Chaitra, « Synthesis and corrosion inhibition behaviour of some new heterocyclic derivatives on mild steel in acid media ».

[15] Y. El Aoufir *et al.*, « Understanding the adsorption of benzimidazole derivative as corrosion inhibitor for carbon steel in 1 M HCl: experimental and theoretical studies », *J Mater Env. Sci*, vol. 8, n° 9, Art. n° 9, 2017.

[16] C. Verma, M. A. Quraishi, E. E. Ebenso, I. B. Obot, et A. El Assyry, « 3-Amino alkylated indoles as corrosion inhibitors for mild steel in 1M HCl: Experimental and theoretical studies », *J. Mol. Liq.*, vol. 219, p. 647‑660, 2016.

[17] A. El Rehim, « Corrosion inhibition and adsorption behaviour of 4-aminoantipyrine on mild steel in H 2 SO 4 », *Corros. Prev. Control*, vol. 46, n° 6, Art. n° 6, 1999.

[18] G. Palanisamy, « Corrosion inhibitors », *Corros. Inhib.*, p. 24, 2019.

[19] M. Chafiq *et al.*, « Unveiled understanding on corrosion inhibition mechanisms of hydrazone derivatives based on naproxen for mild steel in HCl: A joint experimental/theoretical study », *J. Mol. Liq.*, vol. 320, p. 114442, 2020.

[20] A. Chaouiki *et al.*, « New benzohydrazide derivative as corrosion inhibitor for carbon steel in a 1.0 M HCl solution: electrochemical, DFT and Monte Carlo simulation studies », *Port. Electrochimica Acta*, vol. 37, n° 3, Art. n° 3, 2019.

[21] V. Srivastava *et al.*, « Amino acid based imidazolium zwitterions as novel and green corrosion inhibitors for mild steel: Experimental, DFT and MD studies », *J. Mol. Liq.*, vol. 244, p. 340‑352, 2017.

[22] J. Cruz, R. Martınez, J. Genesca, et E. Garcıa-Ochoa, « Experimental and theoretical study of 1-(2-ethylamino)-2-methylimidazoline as an inhibitor of carbon steel corrosion in acid media », *J. Electroanal. Chem.*, vol. 566, n° 1, Art. n° 1, 2004.

[23] K. F. Khaled, « Molecular simulation, quantum chemical calculations and electrochemical studies for inhibition of mild steel by triazoles », *Electrochimica Acta*, vol. 53, n° 9, Art. n° 9, 2008.

[24] B. M. Mistry, N. S. Patel, S. Sahoo, et S. Jauhari, « Experimental and quantum chemical studies on corrosion inhibition performance of quinoline derivatives for MS in 1N HCl », *Bull. Mater. Sci.*, vol. 35, n° 3, Art. n° 3, 2012.

[25] S. A. Umoren, Y. Li, et F. H. Wang, « Synergistic effect of iodide ion and polyacrylic acid on corrosion inhibition of iron in H2SO4 investigated by electrochemical techniques », *Corros. Sci.*, vol. 52, n° 7, Art. n° 7, 2010.

[26] S. Aejitha et P. K. Asthuri, « Geethamani,"Inhibition effect of Antigonon leptopus extract on mild steel in sulphuric acid medium," » *Indian J. Appl. Res.*, vol. 4, n° 12, Art. n° 12, 2014.

[27] S. H. Kumar et S. Karthikeyan, « Amoxicillin as an efficient green corrosion inhibitor for mild steel in 1M sulphuric acid », *J Mater Env. Sci*, vol. 4, n° 5, Art. n° 5, 2013.

[28] K. Hu *et al.*, « Effect of novel cytosine-l-alanine derivative based corrosion inhibitor on steel surface in acidic solution », *J. Mol. Liq.*, vol. 222, p. 109‑117, 2016.

[29] S. A. Umoren et U. M. Eduok, « Application of carbohydrate polymers as corrosion inhibitors for metal substrates in different media: a review », *Carbohydr. Polym.*, vol. 140, p. 314‑341, 2016.

[30] C. Verma, E. E. Ebenso, I. Bahadur, et M. A. Quraishi, « An overview on plant extracts as environmental sustainable and green corrosion inhibitors for metals and alloys in aggressive corrosive media », *J. Mol. Liq.*, vol. 266, p. 577‑590, 2018.

[31] C. Verma, M. A. Quraishi, E. E. Ebenso, et I. Bahadur, « A green and sustainable approach for mild steel acidic corrosion inhibition using leaves extract: experimental and DFT studies », *J. Bio- Tribo-Corros.*, vol. 4, n° 3, Art. n° 3, 2018.

[32] M. A. Ferro-Garcia, J. Rivera-Utrilla, I. Bautista-Toledo, et C. Moreno-Castilla, « Adsorption of humic substances on activated carbon from aqueous solutions and their effect on the removal of Cr (III) ions », *Langmuir*, vol. 14, n° 7, Art. n° 7, 1998.

[33] K. F. Khaled, « Experimental and atomistic simulation studies of corrosion inhibition of copper by a new benzotriazole derivative in acid medium », *Electrochimica Acta*, vol. 54, n° 18, Art. n° 18, 2009.

[34] N. Hackerman et A. C. Makrides, « Action of polar organic inhibitors in acid dissolution of metals », *Ind. Eng. Chem.*, vol. 46, n° 3, Art. n° 3, 1954.

[35] M. P. Chakravarthy, « Synthesis and corrosion inhibition study of isoniazide nicotinamide and dapsone derivatives for mild steel in acid media ».

[36] M. Pourbaix, « Atlas of electrochemical equilibria in aqueous solutions », *NACE*, 1966.

[37] P. A. Schweitzer, *Fundamentals of metallic corrosion: atmospheric and media corrosion of metals*. Crc, 2006.

[38] P. R. Roberge, *Handbook of corrosion engineering*. McGraw-Hill Education, 2019.

[39] E. Cho, S. Ahn, et H. Kwon, « Effects of EDTA on the electronic properties of passive film on Fe–20Cr in pH 8.5 buffer solution », *Electrochimica Acta*, vol. 50, n° 16‑17, Art. n° 16‑17, 2005.

[40] Y. X. Qiao, Y. G. Zheng, W. Ke, et P. C. Okafor, « Electrochemical behaviour of high nitrogen stainless steel in acidic solutions », *Corros. Sci.*, vol. 51, n° 5, Art. n° 5, mai 2009, doi: 10.1016/j.corsci.2009.02.026.

[41] C.-O. Olsson et D. Landolt, « Passive films on stainless steels—chemistry, structure and growth », *Electrochimica Acta*, vol. 48, n° 9, Art. n° 9, 2003.

[42] P. Keller et H.-H. Strehblow, « XPS investigations of electrochemically formed passive layers on Fe/Cr-alloys in 0.5 M H2SO4 », *Corros. Sci.*, vol. 46, n° 8, Art. n° 8, août 2004, doi: 10.1016/j.corsci.2004.01.007.

[43] P. Marcus et I. Olefjord, « Round Robin on combined electrochemical and AES/ESCA characterization of the passive films on Fe□Cr and Fe□Cr□Mo alloys », *Surf. Interface Anal.*, vol. 11, n° 11, Art. n° 11, 1988, doi: 10.1002/sia.740111106.

[44] V. Maurice, W. P. Yang, et P. Marcus, « XPS and STM Study of Passive Films Formed on Fe-22Cr(110) Single-Crystal Surfaces », *J. Electrochem. Soc.*, vol. 143, n° 4, Art. n° 4, avr. 1996, doi: 10.1149/1.1836616.

[45] V. Maurice, W. P. Yang, et P. Marcus, « XPS and STM investigation of the passive film formed on Cr (110) single-crystal surfaces », *J. Electrochem. Soc.*, vol. 141, n° 11, Art. n° 11, 1994.

[46] C. R. Clayton et Y. C. Lu, « A Bipolar Model of the Passivity of Stainless Steel: The Role of Mo Addition », *J. Electrochem. Soc.*, vol. 133, n° 12, Art. n° 12, déc. 1986, doi: 10.1149/1.2108451.

[47] I. Olefjord, B. Brox, et U. Jelvestam, « Surface Composition of Stainless Steels during Anodic Dissolution and Passivation Studied by ESCA », *J. Electrochem. Soc.*, vol. 132, n° 12, Art. n° 12, déc. 1985, doi: 10.1149/1.2113683.

[48] I. Olefjord et L. Wegrelius, « Surface analysis of passive state », *Corros. Sci.*, vol. 31, p. 89‑98, janv. 1990, doi: 10.1016/0010-938X(90)90095-M.

[49] E. S. Beach, Z. Cui, et P. T. Anastas, « Green Chemistry: A design framework for sustainability », *Energy Environ. Sci.*, vol. 2, n° 10, p. 1038‑1049, 2009.

[50] M. J. Mulvihill, E. S. Beach, J. B. Zimmerman, et P. T. Anastas, « Green chemistry and green engineering: a framework for sustainable technology development », *Annu. Rev. Environ. Resour.*, vol. 36, n° 1, p. 271‑293, 2011.

[51] J. A. Linthorst, « An overview: origins and development of green chemistry », *Found. Chem.*, vol. 12, n° 1, p. 55‑68, 2010.

[52] M. A. Dube et S. Salehpour, « Applying the principles of green chemistry to polymer production technology », *Macromol. React. Eng.*, vol. 8, n° 1, p. 7‑28, 2014.

[53] A. Boublia, S. El, I. Lebouachera, et N. Haddaoui, *State ‑of ‑the ‑art review on recent advances in polymer engineering : modeling and optimization through response surface methodology approach*, n° 0123456789. Springer Berlin Heidelberg, 2022. doi: 10.1007/s00289-022-04398-6.

[54] Y. Gu et F. Jérôme, « Glycerol as a sustainable solvent for green chemistry », *Green Chem.*, vol. 12, n° 7, p. 1127‑1138, 2010.

[55] T. Lemaoui *et al.*, « Predicting the Surface Tension of Deep Eutectic Solvents Using Artificial Neural Networks », 2022, doi: 10.1021/acsomega.2c03458.

[56] A. Boublia *et al.*, « Molecular-based artificial neural network for predicting the electrical conductivity of deep eutectic solvents », *J. Mol. Liq.*, vol. 366, p. 120225, 2022, doi: https://doi.org/10.1016/j.molliq.2022.120225.

[57] R. A. Sheldon, I. Arends, et U. Hanefeld, *Green chemistry and catalysis*. John Wiley & Sons, 2007.

[58] G. Centi et S. Perathoner, « Catalysis and sustainable (green) chemistry », *Catal. Today*, vol. 77, n° 4, p. 287‑297, 2003.

[59] T. Lemaoui *et al.*, « Simultaneous dearomatization, desulfurization, and denitrogenation of diesel fuels using acidic deep eutectic solvents as extractive agents: A parametric study », *Sep. Purif. Technol.*, vol. 256, p. 117861, 2021, doi: 10.1016/j.seppur.2020.117861.

[60] A. S. Darwish *et al.*, « Green Extraction of Volatile Fatty Acids from Fermented Wastewater Using Hydrophobic Deep Eutectic Solvents », *Fermentation*, vol. 7, n° 4, p. 226, 2021.

[61] S. Marzorati, L. Verotta, et S. P. Trasatti, « Green corrosion inhibitors from natural sources and biomass wastes », *Molecules*, vol. 24, n° 1, p. 48, 2018.

[62] K. Xhanari, M. Finšgar, M. K. Hrnčič, U. Maver, Ž. Knez, et B. Seiti, « Green corrosion inhibitors for aluminium and its alloys: a review », *RSC Adv.*, vol. 7, n° 44, p. 27299‑27330, 2017.

[63] M. Aliofkhazraei, *Developments in corrosion protection*. BoD–Books on Demand, 2014.

[64] H. Elmsellem *et al.*, « Inhibition of mild steel corrosion in hydrochloric acid solution by new synthesized Schiff Base », *Pharma Chem*, vol. 7, n° 7, p. 353‑364, 2015.

[65] Y. E. Louadi *et al.*, « Theoretical and experimental studies on the corrosion inhibition potentials of two tetrakis pyrazole derivatives for mild steel in 1.0 M HCl », *Electrochim Acta*, vol. 35, n° 3, p. 159‑178, 2017.

[66] Y. El Ouadi *et al.*, « Evaluation of Pelargonium extract and oil as eco-friendly corrosion inhibitor for steel in acidic chloride solutions and pharmacological properties », *Res. Chem. Intermed.*, vol. 41, n° 10, p. 7125‑7149, 2015.

[67] A. Nahle *et al.*, « Evaluation of Melissa officinalis extract and oil as eco-friendly corrosion inhibitor for carbon steel in acidic chloride solutions », *Orient. J. Chem.*, vol. 32, n° 4, p. 1909, 2016.

[68] D. Darling et R. Rakshpal, « Green chemistry applied to corrosion and scale inhibitors », in *CORROSION 98*, OnePetro, 1998.

[69] B. El Ibrahimi, A. Jmiai, L. Bazzi, et S. El Issami, « Amino acids and their derivatives as corrosion inhibitors for metals and alloys », *Arab. J. Chem.*, vol. 13, n° 1, p. 740‑771, 2020, doi: 10.1016/j.arabjc.2017.07.013.

[70] C. Verma, E. E. Ebenso, et M. A. Quraishi, « Alkaloids as green and environmental benign corrosion inhibitors: An overview », *Int. J. Corros. Scale Inhib.*, vol. 8, n° 3, p. 512‑528, 2019.

[71] Y. P. Asmara, T. Kurniawan, A. G. E. Sutjipto, et J. Jafar, « Application of plants extracts as green corrosion inhibitors for steel in concrete-A review », *Indones. J. Sci. Technol.*, vol. 3, n° 2, p. 158 ‑170, 2018.

[72] C. Verma, E. E. Ebenso, I. Bahadur, et M. A. Quraishi, « An overview on plant extracts as environmental sustainable and green corrosion inhibitors for metals and alloys in aggressive corrosive media », *J. Mol. Liq.*, vol. 266, p. 577‑590, 2018.

[73] M. Lebrini, F. Robert, A. Lecante, et C. Roos, « Corrosion inhibition of C38 steel in 1 M hydrochloric acid medium by alkaloids extract from Oxandra asbeckii plant », *Corros. Sci.*, vol. 53, n° 2, p. 687‑695, 2011.

[74] A. M. Abdel-Gaber, B. A. Abd-El-Nabey, I. M. Sidahmed, A. M. El-Zayady, et M. Saadawy, « Inhibitive action of some plant extracts on the corrosion of steel in acidic media », *Corros. Sci.*, vol. 48, n° 9, p. 2765‑2779, 2006.

[75] S. Deng et X. Li, « Inhibition by Ginkgo leaves extract of the corrosion of steel in HCl and H2SO4 solutions », *Corros. Sci.*, vol. 55, p. 407‑415, 2012.

[76] J. C. Da Rocha, J. A. da C. P. Gomes, et E. D'Elia, « Corrosion inhibition of carbon steel in hydrochloric acid solution by fruit peel aqueous extracts », *Corros. Sci.*, vol. 52, n° 7, p. 2341‑2348, 2010.

[77] M. Behpour, S. M. Ghoreishi, M. Khayatkashani, et N. Soltani, « Green approach to corrosion inhibition of mild steel in two acidic solutions by the extract of Punica granatum peel and main constituents », *Mater. Chem. Phys.*, vol. 131, n° 3, p. 621‑633, 2012.

[78] D. Veys-Renaux, S. Reguer, L. Bellot-Gurlet, F. Mirambet, et E. Rocca, « Conversion of steel by polyphenolic model molecules: Corrosion inhibition mechanism by rutin, esculin, esculetol », *Corros. Sci.*, vol. 136, p. 1‑8, 2018, doi: https://doi.org/10.1016/j.corsci.2018.02.015.

[79] K. Rajbhar, H. Dawda, et U. Mukundan, « Polyphenols: Methods of extraction », *Sci Revs Chem Commun*, vol. 5, n° 1, p. 1‑6, 2015.

[80] M. Naczk et F. Shahidi, « Extraction and analysis of phenolics in food », *J. Chromatogr. A*, vol. 1054, n° 1‑2, p. 95‑111, 2004.

[81] A.-N. Li, S. Li, Y.-J. Zhang, X.-R. Xu, Y.-M. Chen, et H.-B. Li, « Resources and biological activities of natural polyphenols », *Nutrients*, vol. 6, n° 12, p. 6020‑6047, 2014.

[82] L. Bravo, « Polyphenols: chemistry, dietary sources, metabolism, and nutritional significance », *Nutr. Rev.*, vol. 56, n° 11, p. 317‑333, 1998.

[83] C. Manach, A. Scalbert, C. Morand, C. Rémésy, et L. Jiménez, « Polyphenols: food sources and bioavailability », *Am. J. Clin. Nutr.*, vol. 79, n° 5, p. 727‑747, 2004.

[84] F. Truzzi, C. Tibaldi, Y. Zhang, G. Dinelli, et E. D'Amen, « An Overview on Dietary Polyphenols and Their Biopharmaceutical Classification System (BCS) », *International Journal of Molecular Sciences*, vol. 22, n° 11. 2021. doi: 10.3390/ijms22115514.

[85] T. F. Rambaran, « Nanopolyphenols: A review of their encapsulation and anti-diabetic effects », *SN Appl. Sci.*, vol. 2, n° 8, p. 1‑26, 2020.

[86] X. Han, T. Shen, et H. Lou, « Dietary polyphenols and their biological significance », *Int. J. Mol. Sci.*, vol. 8, n° 9, p. 950‑988, 2007.

[87] P. C. H. Hollman *et al.*, « The biological relevance of direct antioxidant effects of polyphenols for cardiovascular health in humans is not established », *J. Nutr.*, vol. 141, n° 5, p. 989S-1009S, 2011.

[88] S. Quideau, D. Deffieux, C. Douat-Casassus, et L. Pouységu, « Plant polyphenols: chemical properties, biological activities, and synthesis », *Angew. Chem. Int. Ed.*, vol. 50, n° 3, p. 586‑621, 2011.

[89] S. Lacroix *et al.*, « A computationally driven analysis of the polyphenol-protein interactome », *Sci. Rep.*, vol. 8, n° 1, p. 1‑13, 2018.

[90] Ž. Knez, « Food processing using supercritical fluids », in *Emerging and Traditional Technologies for Safe, Healthy and Quality Food*, Springer, 2016, p. 413‑442.

[91] E. Brglez Mojzer, M. Knez Hrnčič, M. Škerget, Ž. Knez, et U. Bren, « Polyphenols: Extraction Methods, Antioxidative Action, Bioavailability and Anticarcinogenic Effects », *Mol. Basel Switz.*, vol. 21, n° 7, 2016, doi: 10.3390/molecules21070901.

[92] K. Abascal, L. Ganora, et E. Yarnell, « The effect of freeze-drying and its implications for botanical medicine: a review », *Phytother. Res. Int. J. Devoted Pharmacol. Toxicol. Eval. Nat. Prod. Deriv.*, vol. 19, n° 8, p. 655‑660, 2005.

[93] C. M. Ajila, S. K. Brar, M. Verma, R. D. Tyagi, S. Godbout, et J. R. Valéro, « Extraction and analysis of polyphenols: recent trends », *Crit. Rev. Biotechnol.*, vol. 31, n° 3, p. 227‑249, 2011.

[94] P. Panja, « Green extraction methods of food polyphenols from vegetable materials », *Curr. Opin. Food Sci.*, vol. 23, p. 173‑182, 2018, doi: https://doi.org/10.1016/j.cofs.2017.11.012.

[95] S. E. E. Warrag, A. S. Darwish, I. A. Adeyemi, M. K. Hadj-Kali, M. C. Kroon, et I. M. Alnashef, « Extraction of pyridine from n-alkane mixtures using methyltriphenylphosphonium bromide-based deep eutectic solvents as extractive denitrogenation agents », *Fluid Phase Equilibria*, vol. 517, p. 112622, 2020, doi: 10.1016/j.fluid.2020.112622.

[96] A. S. Darwish *et al.*, « Multicomponent extraction of aromatics and heteroaromatics from diesel using acidic eutectic solvents: Experimental and COSMO-RS predictions », *J. Mol. Liq.*, vol. 336, p. 116575, 2021, doi: 10.1016/j.molliq.2021.116575.

[97] F. A. Hatab *et al.*, « Extraction of Thiophene, Pyridine, and Toluene from n ‑ Decane as a Diesel Model Using Betaine-Based Natural Deep Eutectic Solvents », 2020, doi: 10.1021/acs.jced.0c00579.

[98] C. D. Stalikas, « Extraction, separation, and detection methods for phenolic acids and flavonoids », *J. Sep. Sci.*, vol. 30, n° 18, p. 3268‑3295, 2007.

[99] E. Brglez Mojzer, M. Knez Hrnčič, M. Škerget, Ž. Knez, et U. Bren, « Polyphenols: Extraction methods, antioxidative action, bioavailability and anticarcinogenic effects », *Molecules*, vol. 21, n° 7, p. 901, 2016.

[100] M. D. Luque de Castro et L. E. García-Ayuso, « Soxhlet extraction of solid materials: an outdated technique with a promising innovative future », *Anal. Chim. Acta*, vol. 369, n° 1, p. 1‑10, 1998, doi: https://doi.org/10.1016/S0003-2670(98)00233-5.

[101] M. A. López-Bascón et M. D. L. De Castro, « Soxhlet extraction », in *Liquid-phase extraction*, Elsevier, 2020, p. 327‑354.

[102] M. Solana, I. Boschiero, S. Dall'Acqua, et A. Bertucco, « A comparison between supercritical fluid and pressurized liquid extraction methods for obtaining phenolic compounds from Asparagus officinalis L », *J. Supercrit. Fluids*, vol. 100, p. 201‑208, 2015, doi: https://doi.org/10.1016/j.supflu.2015.02.014.

[103] C. Wen *et al.*, « Advances in ultrasound assisted extraction of bioactive compounds from cash crops – A review », *Ultrason. Sonochem.*, vol. 48, p. 538‑549, 2018, doi: https://doi.org/10.1016/j.ultsonch.2018.07.018.

[104] G. V Barbosa-Cánovas, F. Donsì, S. Yildiz, K. Candoğan, P. R. Pokhrel, et A. Y. Guadarrama-Lezama, « Nonthermal processing technologies for stabilization and enhancement of bioactive compounds in foods », *Food Eng. Rev.*, p. 1‑37, 2021.

[105] P. Ebrahimi et A. Lante, « Environmentally Friendly Techniques for the Recovery of Polyphenols from Food By-Products and Their Impact on Polyphenol Oxidase: A Critical Review », *Appl. Sci. Switz.*, vol. 12, n° 4, 2022, doi: 10.3390/app12041923.

[106] E. M. Garcia-Castello, A. D. Rodriguez-Lopez, L. Mayor, R. Ballesteros, C. Conidi, et A. Cassano, « Optimization of conventional and ultrasound assisted extraction of flavonoids from grapefruit (Citrus paradisi L.) solid wastes », *LWT - Food Sci. Technol.*, vol. 64, n° 2, p. 1114‑1122, 2015, doi: https://doi.org/10.1016/j.lwt.2015.07.024.

[107] S. El Kantar, H. N. Rajha, R. G. Maroun, et N. Louka, « Intensification of polyphenols extraction from orange peels using infrared as a novel and energy saving pretreatment », *J. Food Sci.*, vol. 85, n° 2, p. 414‑420, 2020.

[108] T. Martínez-Ramos, J. Benedito-Fort, N. J. Watson, I. I. Ruiz-López, G. Che-Galicia, et E. Corona-Jiménez, « Effect of solvent composition and its interaction with ultrasonic energy on the

ultrasound-assisted extraction of phenolic compounds from Mango peels (Mangifera indica L.) », *Food Bioprod. Process.*, vol. 122, p. 41‑54, 2020, doi: https://doi.org/10.1016/j.fbp.2020.03.011.

[109] M. Letellier et H. Budzinski, « Microwave assisted extraction of organic compounds », *Analusis*, vol. 27, p. 259‑271, 1999.

[110] H. Cai *et al.*, « Novel extraction methods and potential applications of polyphenols in fruit waste: a review », *J. Food Meas. Charact.*, vol. 15, n° 4, p. 3250‑3261, 2021.

[111] J. Xi, B. Xiang, et Y. Deng, « Comparison of batch and circulating processes for polyphenols extraction from pomelo peels by liquid-phase pulsed discharge », *Food Chem.*, vol. 340, p. 127918, 2021.

[112] O. R. Alara, N. H. Abdurahman, et O. A. Olalere, « Optimization of microwave-assisted extraction of flavonoids and antioxidants from Vernonia amygdalina leaf using response surface methodology », *Food Bioprod. Process.*, vol. 107, p. 36‑48, 2018, doi: https://doi.org/10.1016/j.fbp.2017.10.007.

[113] H. Li, B. Chen, L. Nie, et S. Yao, « Solvent effects on focused microwave assisted extraction of polyphenolic acids from Eucommia ulmodies », *Phytochem. Anal. Int. J. Plant Chem. Biochem. Tech.*, vol. 15, n° 5, p. 306‑312, 2004.

[114] H. Li, B. Chen, Z. Zhang, et S. Yao, « Focused microwave-assisted solvent extraction and HPLC determination of effective constituents in Eucommia ulmodies Oliv.(E. ulmodies) », *Talanta*, vol. 63, n° 3, p. 659‑665, 2004.

[115] X. Pan, G. Niu, et H. Liu, « Microwave-assisted extraction of tea polyphenols and tea caffeine from green tea leaves », *Chem. Eng. Process. Process Intensif.*, vol. 42, n° 2, p. 129‑133, 2003, doi: https://doi.org/10.1016/S0255-2701(02)00037-5.

[116] M. K. I. Khan, M. Ansar, A. Nazir, et A. A. Maan, « Sustainable dehydration of onion slices through novel microwave hydro-diffusion gravity technique », *Innov. Food Sci. Emerg. Technol.*, vol. 33, p. 327‑332, 2016, doi: https://doi.org/10.1016/j.ifset.2015.12.010.

[117] L. Zhang, Y. Wang, D. Wu, M. Xu, et J. Chen, « Microwave-assisted extraction of polyphenols from Camellia oleifera fruit hull », *Molecules*, vol. 16, n° 6, p. 4428‑4437, 2011.

[118] A. Sridhar, M. Ponnuchamy, P. S. Kumar, A. Kapoor, D. V. N. Vo, et S. Prabhakar, *Techniques and modeling of polyphenol extraction from food: a review*, vol. 19, n° 4. Springer International Publishing, 2021. doi: 10.1007/s10311-021-01217-8.

[119] S. S. Nadar, P. Rao, et V. K. Rathod, « Enzyme assisted extraction of biomolecules as an approach to novel extraction technology: A review », *Food Res. Int.*, vol. 108, p. 309‑330, 2018, doi: https://doi.org/10.1016/j.foodres.2018.03.006.

[120] G. Domínguez-Rodríguez, M. L. Marina, et M. Plaza, « Enzyme-assisted extraction of bioactive non-extractable polyphenols from sweet cherry (Prunus avium L.) pomace », *Food Chem.*, vol. 339, p. 128086, 2021.

[121] G. Singh, A. K. Verma, et V. Kumar, « Catalytic properties, functional attributes and industrial applications of β-glucosidases », *3 Biotech*, vol. 6, n° 1, p. 1‑14, 2016.

[122] N. Saad *et al.*, « Enzyme-assisted extraction of bioactive compounds from raspberry (Rubus idaeus L.) pomace », *J. Food Sci.*, vol. 84, n° 6, p. 1371‑1381, 2019.

[123] N. T. Huynh, G. Smagghe, G. B. Gonzales, J. Van Camp, et K. Raes, « Enzyme-assisted extraction enhancing the phenolic release from cauliflower (Brassica oleracea L. var. botrytis) outer leaves », *J. Agric. Food Chem.*, vol. 62, n° 30, p. 7468‑7476, 2014.

[124] M. Mushtaq, B. Sultana, S. Akram, A. Adnan, R. K. O. Apenten, et P. S.-N. Nigam, « Enzyme-assisted Extraction of Polyphenols from Pomegranate (Punicagranatum) Peel », *Res. Rev. J. Microbiol. Biotechnol.*, vol. 5, n° 2, p. 27‑34, 2016.

[125] J. Nishad, S. Saha, et C. Kaur, « Enzyme-and ultrasound-assisted extractions of polyphenols from Citrus sinensis (cv. Malta) peel: a comparative study », *J. Food Process. Preserv.*, vol. 43, n° 8, p. e14046, 2019.

[126] S. Nigam *et al.*, « Perspective on the therapeutic applications of algal polysaccharides », *J. Polym. Environ.*, p. 1‑25, 2021.

[127] R. Castro-Muñoz, J. Yáñez-Fernández, et V. Fíla, « Phenolic compounds recovered from agro-food by-products using membrane technologies: An overview », *Food Chem.*, vol. 213, p. 753‑762, 2016.

[128] E. H. Papaioannou, S. T. Mitrouli, S. I. Patsios, M. Kazakli, et A. J. Karabelas, « Valorization of pomegranate husk–Integration of extraction with nanofiltration for concentrated polyphenols recovery », *J. Environ. Chem. Eng.*, vol. 8, n° 4, p. 103951, 2020.

[129] C. Conidi, A. Cassano, et E. Drioli, « Recovery of phenolic compounds from orange press liquor by nanofiltration », *Food Bioprod. Process.*, vol. 90, n° 4, p. 867‑874, 2012, doi: https://doi.org/10.1016/j.fbp.2012.07.005.

[130] D. Mihaylova, A. Lante, et A. I. Krastanov, « A study on the antioxidant and antimicrobial activities of pressurized-liquid extracts of Clinopodium vulgare and Sideritis scardica », *Agro Food Ind Hi Tech*, vol. 25, p. 55‑58, 2014.

[131] N. Petkova, I. Ivanov, D. Mihaylova, et A. Lante, « Effect of pressure liquid extraction and ultrasonic irradiation frequency on inulin, phenolic content and antioxidant activity in burdock (Arctium lappa L.) roots », *Acta Sci. Pol. Hortorum Cultus*, vol. 19, n° 3, p. 125‑133, 2020.

[132] A. Mustafa et C. Turner, « Pressurized liquid extraction as a green approach in food and herbal plants extraction: A review », *Anal. Chim. Acta*, vol. 703, n° 1, p. 8‑18, 2011.

[133] P. R. Toledo-Merma *et al.*, « Phenolic Compounds Recovery from Pomegranate (Punica granatum L.) By-Products of Pressurized Liquid Extraction », *Foods*, vol. 11, n° 8, p. 1070, 2022.

[134] R. Mateos, J. R. Pérez-Correa, et H. Domínguez, « Bioactive properties of marine phenolics », *Mar. Drugs*, vol. 18, n° 10, p. 501, 2020.

[135] K. Ameer, H. M. Shahbaz, et J. Kwon, « Green extraction methods for polyphenols from plant matrices and their byproducts: A review », *Compr. Rev. Food Sci. Food Saf.*, vol. 16, n° 2, p. 295‑315, 2017.

[136] M. Herrero, A. Cifuentes, et E. Ibañez, « Sub- and supercritical fluid extraction of functional ingredients from different natural sources: Plants, food-by-products, algae and microalgae: A review », *Food Chem.*, vol. 98, n° 1, p. 136‑148, 2006, doi: https://doi.org/10.1016/j.foodchem.2005.05.058.

[137] J. O. Chaves *et al.*, « Extraction of flavonoids from natural sources using modern techniques », *Front. Chem.*, vol. 8, p. 507887, 2020.

[138] A. Al-Otoom *et al.*, « Extraction of oil from uncrushed olives using supercritical fluid extraction method », *J. Supercrit. Fluids*, vol. 95, p. 512‑518, 2014.

[139] F. Donsì, G. Ferrari, et G. Pataro, « Applications of pulsed electric field treatments for the enhancement of mass transfer from vegetable tissue », *Food Eng. Rev.*, vol. 2, n° 2, p. 109‑130, 2010.

[140] H. N. Rajha *et al.*, « Comparison of aqueous extraction efficiency and biological activities of polyphenols from pomegranate peels assisted by infrared, ultrasound, pulsed electric fields and high-voltage electrical discharges », *Innov. Food Sci. Emerg. Technol.*, vol. 58, p. 102212, 2019.

[141] C. M. Galanakis, F. J. Barba, et K. N. Prasad, « Cost and safety issues of emerging technologies against conventional techniques », in *Food waste recovery*, Elsevier, 2015, p. 321‑336.

[142] S. El Kantar *et al.*, « Pulsed electric field treatment of citrus fruits: Improvement of juice and polyphenols extraction », *Innov. Food Sci. Emerg. Technol.*, vol. 46, p. 153‑161, 2018.

[143] R. Ostermeier, K. Hill, A. Dingis, S. Töpfl, et H. Jäger, « Influence of pulsed electric field (PEF) and ultrasound treatment on the frying behavior and quality of potato chips », *Innov. Food Sci. Emerg. Technol.*, vol. 67, p. 102553, 2021.

[144] E. R. Chiriac, C. L. Chiţescu, E.-I. Geană, C. E. Gird, R. P. Socoteanu, et R. Boscencu, « Advanced analytical approaches for the analysis of polyphenols in plants matrices—A review », *Separations*, vol. 8, n° 5, p. 65, 2021.

[145] K. M. Kalili et A. de Villiers, « Recent developments in the HPLC separation of phenolic compounds », *J. Sep. Sci.*, vol. 34, n° 8, p. 854‑876, 2011.

[146] H. M. Merken et G. R. Beecher, « Measurement of food flavonoids by high-performance liquid chromatography: a review », *J. Agric. Food Chem.*, vol. 48, n° 3, p. 577‑599, 2000.

[147] K. Tzima, N. P. Brunton, et D. K. Rai, « Qualitative and quantitative analysis of polyphenols in Lamiaceae plants—A review », *Plants*, vol. 7, n° 2, p. 25, 2018.

[148] B. Sik, R. Székelyhidi, E. Lakatos, V. Kapcsándi, et Z. Ajtony, « Analytical procedures for determination of phenolics active herbal ingredients in fortified functional foods: an overview », *Eur. Food Res. Technol.*, vol. 248, n° 2, p. 329‑344, 2022, doi: 10.1007/s00217-021-03908-6.

[149] N. Alonso-Carrillo, Ma. de los Á. Aguilar-Santamaría, E. J. Vernon-Carter, R. Jiménez-Alvarado, F. Cruz-Sosa, et A. Román-Guerrero, « Extraction of phenolic compounds from Satureja macrostema using microwave-ultrasound assisted and reflux methods and evaluation of their antioxidant activity and cytotoxicity », *Ind. Crops Prod.*, vol. 103, p. 213‑221, 2017, doi: https://doi.org/10.1016/j.indcrop.2017.04.002.

[150] N. M'hiri, I. Ioannou, N. Mihoubi Boudhrioua, et M. Ghoul, « Effect of different operating conditions on the extraction of phenolic compounds in orange peel », *Food Bioprod. Process.*, vol. 96, p. 161‑170, 2015, doi: https://doi.org/10.1016/j.fbp.2015.07.010.

[151] K. Pyrzynska et A. Sentkowska, « Recent developments in the HPLC separation of phenolic food compounds », *Crit. Rev. Anal. Chem.*, vol. 45, n° 1, p. 41‑51, 2015.

[152] A. Khoddami, M. A. Wilkes, et T. H. Roberts, « Techniques for analysis of plant phenolic compounds », *Molecules*, vol. 18, n° 2, p. 2328‑2375, 2013, doi: 10.3390/molecules18022328.

[153] I. Ignat, I. Volf, et V. I. Popa, « A critical review of methods for characterisation of polyphenolic compounds in fruits and vegetables », *Food Chem.*, vol. 126, n° 4, p. 1821‑1835, 2011.

[154] A. dos Santos Pereira, M. C. Padilha, et F. R. de Aquino Neto, « Two decades of high temperature gas chromatography (1983–2003): what's next? », *Microchem. J.*, vol. 77, n° 2, p. 141‑149, 2004.

[155] I. Deslauriers, « Recovery, separation and characterization of phenolic compounds and flavonoids from maple products », 2000.

[156] M. Naczk et F. Shahidi, « Phenolics in cereals, fruits and vegetables: Occurrence, extraction and analysis », *J. Pharm. Biomed. Anal.*, vol. 41, n° 5, p. 1523‑1542, 2006.

[157] R. Amarowicz *et al.*, « Influence of postharvest processing and storage on the content of phenolic acids and flavonoids in foods », *Mol. Nutr. Food Res.*, vol. 53, n° S2, p. S151‑S183, 2009.

[158] C. S. Cutrim et M. A. S. Cortez, « A review on polyphenols: Classification, beneficial effects and their application in dairy products », *Int. J. Dairy Technol.*, vol. 71, n° 3, p. 564‑578, 2018.

[159] C. G. Dariva et A. F. Galio, « Corrosion inhibitors–principles, mechanisms and applications », *Dev. Corros. Prot.*, vol. 16, p. 365‑378, 2014.

[160] O. Benali, O. Cherkaoui, et A. Lallam, « Adsorption and corrosion inhibition of new synthesized Pyridazinium-Based Ionic Liquid on Carbon steel in 0.5 MH2so4 », *J Mater Env. Sci*, vol. 6, p. 598‑606, 2015.

[161] I. A. Ma, S. Ammar, S. S. A. Kumar, K. Ramesh, et S. Ramesh, « A concise review on corrosion inhibitors: types, mechanisms and electrochemical evaluation studies », *J. Coat. Technol. Res.*, p. 1‑28, 2021.

[162] R. W. Revie, *Corrosion and corrosion control: an introduction to corrosion science and engineering*. John Wiley & Sons, 2008.

[163] A. Zakeri, E. Bahmani, et A. S. R. Aghdam, « Plant extracts as sustainable and green corrosion inhibitors for protection of ferrous metals in corrosive media: A mini review », *Corros. Commun.*, vol. 5, p. 25‑38, 2022, doi: https://doi.org/10.1016/j.corcom.2022.03.002.

[164] V. S. Saji, « A review on recent patents in corrosion inhibitors », *Recent Pat. Corros. Sci.*, vol. 2, n° 1, 2010.

[165] K. E. Heusler, D. Landolt, et S. Trasatti, « Electrochemical corrosion nomenclature », *J. Electroanal. Chem. Interfacial Electrochem.*, vol. 274, n° 1, p. 345‑348, 1989, doi: https://doi.org/10.1016/0022-0728(89)87063-9.

[166] E. Bardal, *Corrosion and protection*. Springer, 2004.

[167] E.-S. M. Sherif, « Effects of 2-amino-5-(ethylthio)-1,3,4-thiadiazole on copper corrosion as a corrosion inhibitor in 3% NaCl solutions », *Appl. Surf. Sci.*, vol. 252, n° 24, p. 8615‑8623, 2006, doi: https://doi.org/10.1016/j.apsusc.2005.11.082.

[168] A. S. Yaro, A. A. Khadom, et R. K. Wael, « Apricot juice as green corrosion inhibitor of mild steel in phosphoric acid », *Alex. Eng. J.*, vol. 52, n° 1, p. 129‑135, 2013, doi: https://doi.org/10.1016/j.aej.2012.11.001.

[169] B. E. Brycki, I. H. Kowalczyk, A. Szulc, O. Kaczerewska, et M. Pakiet, « Organic corrosion inhibitors », *Corros. Inhib. Princ. Recent Appl.*, vol. 3, p. 33, 2018.

[170] L. T. Popoola, « Organic green corrosion inhibitors (OGCIs): a critical review », *Corros. Rev.*, vol. 37, n° 2, p. 71‑102, 2019.

[171] M. A. Quraishi, M. Z. A. Rafiquee, S. Khan, et N. Saxena, « Corrosion inhibition of aluminium in acid solutions by some imidazoline derivatives », *J. Appl. Electrochem.*, vol. 37, n° 10, p. 1153‑1162, 2007.

[172] B. El Ibrahimi, A. Jmiai, L. Bazzi, et S. El Issami, « Amino acids and their derivatives as corrosion inhibitors for metals and alloys », *Arab. J. Chem.*, vol. 13, n° 1, p. 740‑771, 2020, doi: https://doi.org/10.1016/j.arabjc.2017.07.013.

[173] C. Verma, K. Y. Rhee, M. A. Quraishi, et E. E. Ebenso, « Pyridine based N-heterocyclic compounds as aqueous phase corrosion inhibitors: A review », *J. Taiwan Inst. Chem. Eng.*, vol. 117, p. 265‑277, 2020, doi: https://doi.org/10.1016/j.jtice.2020.12.011.

[174] D. E. Arthur, A. Jonathan, P. O. Ameh, et C. Anya, « A review on the assessment of polymeric materials used as corrosion inhibitor of metals and alloys », *Int. J. Ind. Chem.*, vol. 4, n° 1, p. 1‑9, 2013.

[175] S. A. Umoren et U. M. Eduok, « Application of carbohydrate polymers as corrosion inhibitors for metal substrates in different media: a review », *Carbohydr. Polym.*, vol. 140, p. 314‑341, 2016.

[176] N. Hossain, M. Asaduzzaman Chowdhury, et M. Kchaou, « An overview of green corrosion inhibitors for sustainable and environment friendly industrial development », *J. Adhes. Sci. Technol.*, vol. 35, n° 7, p. 673‑690, avr. 2021, doi: 10.1080/01694243.2020.1816793.

[177] M. F. Montemor, *Fostering green inhibitors for corrosion prevention*, vol. 233. 2016. doi: 10.1007/978-94-017-7540-3_6.

[178] Z. Shang et J. Zhu, « Overview on plant extracts as green corrosion inhibitors in the oil and gas fields », *J. Mater. Res. Technol.*, vol. 15, p. 5078‑5094, 2021, doi: https://doi.org/10.1016/j.jmrt.2021.10.095.

[179] E. Chaieb, A. Bouyanzer, B. Hammouti, et M. Benkaddour, « Inhibition of the corrosion of steel in 1M HCl by eugenol derivatives », *Appl. Surf. Sci.*, vol. 246, n° 1, p. 199‑206, 2005, doi: https://doi.org/10.1016/j.apsusc.2004.11.011.

[180] A. Y. El-Etre, « Inhibition of acid corrosion of carbon steel using aqueous extract of olive leaves », *J. Colloid Interface Sci.*, vol. 314, n° 2, p. 578‑583, 2007, doi: https://doi.org/10.1016/j.jcis.2007.05.077.

[181] S. T. Arab, A. M. Al-Turkustani, et R. H. Al-Dhahiri, « Synergistic effect of Azadirachta Indica extract and iodide ions on the corrosion inhibition of aluminium in acid media », *J. Korean Chem. Soc.*, vol. 52, n° 3, p. 281‑294, 2008.

[182] S. A. Umoren, I. B. Obot, L. E. Akpabio, et S. E. Etuk, « Adsorption and corrosive inhibitive properties of Vigna unguiculata in alkaline and acidic media », *Pigment Resin Technol.*, 2008.

[183] A. S. Fouda et A. S. Ellithy, « Inhibition effect of 4-phenylthiazole derivatives on corrosion of 304L stainless steel in HCl solution », *Corros. Sci.*, vol. 51, n° 4, p. 868‑875, 2009.

[184] M. Abdallah, B. H. Asghar, I. Zaafarany, et A. S. Fouda, « The inhibition of carbon steel corrosion in hydrochloric acid solution using some phenolic compounds », *Int J Electrochem Sci*, vol. 7, n° 1, p. 282‑304, 2012.

[185] R. Yıldız, T. Doğan, et İ. Dehri, « Evaluation of corrosion inhibition of mild steel in 0.1 M HCl by 4-amino-3-hydroxynaphthalene-1-sulphonic acid », *Corros. Sci.*, vol. 85, p. 215‑221, 2014.

[186] M. Prabakaran, S.-H. Kim, V. Hemapriya, et I.-M. Chung, « Evaluation of polyphenol composition and anti-corrosion properties of Cryptostegia grandiflora plant extract on mild steel in acidic medium », *J. Ind. Eng. Chem.*, vol. 37, p. 47‑56, 2016, doi: https://doi.org/10.1016/j.jiec.2016.03.006.

[187] C. O. Akalezi, C. E. Ogukwe, E. A. Ejele, et E. E. Oguzie, « Corrosion inhibition properties of Gongronema latifollium extract in acidic media », *Int. J. Corros. Scale Inhib.*, vol. 5, n° 3, p. 232‑247, 2016.

[188] A. A. Khadom, A. F. Hassan, et B. M. Abod, « Evaluation of environmentally friendly inhibitor for galvanic corrosion of steel–copper couple in petroleum waste water », *Process Saf. Environ. Prot.*, vol. 98, p. 93‑101, 2015.

[189] E. B. Ituen, A. O. James, et O. Akaranta, « Elephant grass biomass extract as corrosion inhibitor for mild steel in acidic medium », *J Mater Env. Sci*, vol. 8, p. 1498‑1507, 2017.

[190] P. E. Alvarez, M. V. Fiori-Bimbi, A. Neske, S. A. Brandán, et C. A. Gervasi, « Rollinia occidentalis extract as green corrosion inhibitor for carbon steel in HCl solution », *J. Ind. Eng. Chem.*, vol. 58, p. 92‑99, 2018, doi: https://doi.org/10.1016/j.jiec.2017.09.012.

[191] H. Bourazmi, M. Tabyaoui, L. Hattabi, Y. El Aoufir, et M. Taleb, « Methanolic extract of salvia officinalis plant as a green inhibitor for the corrosion of carbon steel in 1 M HCl », *J Mater Env. Sci*, vol. 9, p. 928‑938, 2018.

[192] S. A. Haddadi, E. Alibakhshi, G. Bahlakeh, B. Ramezanzadeh, et M. Mahdavian, « A detailed atomic level computational and electrochemical exploration of the Juglans regia green fruit shell extract as a sustainable and highly efficient green corrosion inhibitor for mild steel in 3.5 wt% NaCl solution », *J. Mol. Liq.*, vol. 284, p. 682‑699, 2019, doi: https://doi.org/10.1016/j.molliq.2019.04.045.

[193] R. Haldhar, D. Prasad, I. Bahadur, O. Dagdag, et A. Berisha, « Evaluation of Gloriosa superba seeds extract as corrosion inhibition for low carbon steel in sulfuric acidic medium: A combined experimental and computational studies », *J. Mol. Liq.*, vol. 323, p. 114958, 2021, doi: https://doi.org/10.1016/j.molliq.2020.114958.

[194] B. Tan *et al.*, « Insight into anti-corrosion nature of Betel leaves water extracts as the novel and eco-friendly inhibitors », *J. Colloid Interface Sci.*, vol. 585, p. 287‑301, 2021, doi: https://doi.org/10.1016/j.jcis.2020.11.059.

[195] A. Belakhdar *et al.*, « Computational and experimental studies on the efficiency of Rosmarinus officinalis polyphenols as green corrosion inhibitors for XC48 steel in acidic medium », *Colloids Surf. Physicochem. Eng. Asp.*, vol. 606, p. 125458, 2020, doi: https://doi.org/10.1016/j.colsurfa.2020.125458.

[196] S. Echihi *et al.*, « Performance of methanolic extract of artemisia herba alba as a potential green inhibitor on corrosion behavior of mild steel in hydrochloric acid solution », *Biointerface Res Appl Chem*, vol. 11, n° 6, p. 14751‑14763, 2021.

[197] M. E. H. N. Tehrani, P. Ghahremani, M. Ramezanzadeh, G. Bahlakeh, et B. Ramezanzadeh, « Theoretical and experimental assessment of a green corrosion inhibitor extracted from Malva sylvestris », *J. Environ. Chem. Eng.*, vol. 9, n° 3, p. 105256, 2021.

[198] C. Boulechfar *et al.*, « Synthesis, electrochemical, and quantum chemical studies of some metal complexes: Mn(II), Co(II), and Zn(II) with 2-furaldehyde semicarbazone », *J. Mol. Struct.*, vol. 1271, p. 134007, janv. 2023, doi: 10.1016/j.molstruc.2022.134007.

[199] A. Sedik *et al.*, « Experimental and theoretical insights into copper corrosion inhibition by protonated amino-acids », *RSC Adv.*, vol. 12, n° 36, p. 23718‑23735, 2022, doi: 10.1039/D2RA03535A.

[200] M. Damej *et al.*, « New epoxy resin as a corrosion inhibitor for the protection of carbon steel C38 in 1M HCl. experimental and theoretical studies (DFT, MC, and MD) », *J. Mol. Struct.*, vol. 1254, p. 132425, 2022, doi: https://doi.org/10.1016/j.molstruc.2022.132425.

[201] B. Ould Abdelwedoud *et al.*, « Inhibition effect of N-propargyl saccharin as corrosion inhibitor of C38 steel in 1 M HCl, experimental and theoretical study », *J. Mol. Liq.*, vol. 354, p. 118784, 2022, doi: https://doi.org/10.1016/j.molliq.2022.118784.

[202] C. Verma, H. Lgaz, D. K. Verma, E. E. Ebenso, I. Bahadur, et M. A. Quraishi, « Molecular dynamics and Monte Carlo simulations as powerful tools for study of interfacial adsorption behavior of corrosion inhibitors in aqueous phase: A review », *J. Mol. Liq.*, vol. 260, p. 99‑120, 2018, doi: 10.1016/j.molliq.2018.03.045.

[203] G. Gece, « The use of quantum chemical methods in corrosion inhibitor studies », *Corros. Sci.*, vol. 50, n° 11, p. 2981‑2992, 2008.

[204] I. B. Obot, D. D. Macdonald, et Z. M. Gasem, « Density functional theory (DFT) as a powerful tool for designing new organic corrosion inhibitors. Part 1: An overview », *Corros. Sci.*, vol. 99, p. 1‑30, 2015, doi: https://doi.org/10.1016/j.corsci.2015.01.037.

[205] A. Kahlouche *et al.*, « Molecular insights through the experimental and theoretical study of the anticorrosion power of a new eco-friendly Cytisus multiflorus flowers extract in a 1 M sulfuric acid », *J. Mol. Liq.*, vol. 347, p. 118397, 2022, doi: https://doi.org/10.1016/j.molliq.2021.118397.

[206] H. Ferkous, M. Zerroug, M. A. Chaouch, M. Radjai, H. Majdoub, et A. Bouzid, « Green corrosion inhibitor for carbon steel in 1 m hcl: A comparative study of polysaccharides extracted from prickly pear nopals of opuntia ficus-indica (peel and pulp) », *Adv. Sci. Technol. Innov.*, p. 1293‑1296, 2018, doi: 10.1007/978-3-319-70548-4_380.

[207] Z. Meriem *et al.*, « Experimental and theoretical evaluation of the adsorption process of some polyphenols and their corrosion inhibitory properties on mild steel in acidic media », *J. Environ. Chem. Eng.*, vol. 9, n° 6, p. 106482, déc. 2021, doi: 10.1016/j.jece.2021.106482.

[208] W. Zhang *et al.*, « Chemically modified resveratrol as green corrosion inhibitor for Q235 steel: Electrochemical, SEM, UV and DFT studies », *J. Mol. Liq.*, vol. 343, p. 117672, 2021, doi: https://doi.org/10.1016/j.molliq.2021.117672.

[209] X. Chen, Y. Chen, J. Cui, Y. Li, Y. Liang, et G. Cao, « Molecular dynamics simulation and DFT calculation of “green” scale and corrosion inhibitor », *Comput. Mater. Sci.*, vol. 188, p. 110229, 2021, doi: https://doi.org/10.1016/j.commatsci.2020.110229.

[210] Q. Wang *et al.*, « Experimental, DFT and MD evaluation of Nandina domestica Thunb. extract as green inhibitor for carbon steel corrosion in acidic medium », *J. Mol. Struct.*, vol. 1265, p. 133367, 2022, doi: https://doi.org/10.1016/j.molstruc.2022.133367.

[211] A. Berrissoul *et al.*, « Exploitation of a new green inhibitor against mild steel corrosion in HCl: Experimental, DFT and MD simulation approach », *J. Mol. Liq.*, vol. 349, p. 118102, 2022, doi: https://doi.org/10.1016/j.molliq.2021.118102.

[212] D. Kumar, V. M. K, V. Jain, et B. Rai, « Integrating experiments, DFT and characterization for comprehensive corrosion inhibition studies – A case for cinnamaldehyde as an excellent green inhibitor for steels in acidic media », *Corros. Sci.*, vol. 208, p. 110623, 2022, doi: https://doi.org/10.1016/j.corsci.2022.110623.

[213] Z. Sanaei, M. Ramezanzadeh, G. Bahlakeh, et B. Ramezanzadeh, « Use of Rosa canina fruit extract as a green corrosion inhibitor for mild steel in 1M HCl solution: A complementary experimental, molecular dynamics and quantum mechanics investigation », *J. Ind. Eng. Chem.*, vol. 69, p. 18‑31, 2019, doi: https://doi.org/10.1016/j.jiec.2018.09.013.

[214] S. Pal, G. Ji, H. Lgaz, I.-M. Chung, et R. Prakash, « Lemon seeds as green coating material for mitigation of mild steel corrosion in acid media: Molecular dynamics simulations, quantum chemical calculations and electrochemical studies », *J. Mol. Liq.*, vol. 316, p. 113797, 2020, doi: https://doi.org/10.1016/j.molliq.2020.113797.

[215] K. O. Sulaiman, A. T. Onawole, O. Faye, et D. T. Shuaib, « Understanding the corrosion inhibition of mild steel by selected green compounds using chemical quantum based assessments and molecular dynamics simulations », *J. Mol. Liq.*, vol. 279, p. 342‑350, 2019, doi: https://doi.org/10.1016/j.molliq.2019.01.136.

[216] A. Delimi *et al.*, « Corrosion protection performance of silicon-based coatings on carbon steel in NaCl solution: a theoretical and experimental assessment of the effect of plasma-enhanced chemical vapor deposition pretreatment », *RSC Adv.*, vol. 12, n° 24, p. 15601‑15612, 2022, doi: 10.1039/D1RA08848C.

[217] C. Boulechfar *et al.*, « DFT/molecular scale, MD simulation and assessment of the eco-friendly anti-corrosion performance of a novel Schiff base on XC38 carbon steel in acidic medium », *J. Mol. Liq.*, vol. 344, p. 117874, 2021, doi: https://doi.org/10.1016/j.molliq.2021.117874.

[218] E. E. Oguzie, « Corrosion inhibitive effect and adsorption behaviour of Hibiscus sabdariffa extract on mild steel in acidic media », *Port. Electrochimica Acta*, vol. 26, n° 3, p. 303‑314, 2008, doi: 10.4152/pea.200803303.

[219] E. A. Noor, « Potential of aqueous extract of Hibiscus sabdariffa leaves for inhibiting the corrosion of aluminum in alkaline solutions », *J. Appl. Electrochem.*, vol. 39, n° 9, p. 1465‑1475, 2009.

[220] A. Ostovari, S. M. Hoseinieh, M. Peikari, S. R. Shadizadeh, et S. J. Hashemi, « Corrosion inhibition of mild steel in 1M HCl solution by henna extract: A comparative study of the inhibition by henna and its constituents (Lawsone, Gallic acid, α-d-Glucose and Tannic acid) », *Corros. Sci.*, vol. 51, n° 9, p. 1935‑1949, 2009, doi: https://doi.org/10.1016/j.corsci.2009.05.024.

[221] A. O. James et O. Akaranta, « Corrosion inhibition of aluminum in 2.0 M hydrochloric acid solution by the acetone extract of red onion skin », *Afr. J. Pure Appl. Chem.*, vol. 3, n° 12, p. 262‑268, 2009.

[222] X.-H. Li, S.-D. Deng, et H. Fu, « Inhibition by Jasminum nudiflorum Lindl. leaves extract of the corrosion of cold rolled steel in hydrochloric acid solution », *J. Appl. Electrochem.*, vol. 40, n° 9, p. 1641‑1649, 2010.

[223] K. W. Tan et M. J. Kassim, « A correlation study on the phenolic profiles and corrosion inhibition properties of mangrove tannins (Rhizophora apiculata) as affected by extraction solvents », *Corros. Sci.*, vol. 53, n° 2, p. 569‑574, 2011, doi: https://doi.org/10.1016/j.corsci.2010.09.065.

[224] O. K. Abiola, E. M. Odin, D. N. Olowoyo, et T. A. Adeloye, « Gossipium hirsutum L. extract as green corrosion inhibitor for aluminum in HCl solution », *Bull. Chem. Soc. Ethiop.*, vol. 25, n° 3, 2011.

[225] H. Gerengi et H. I. Sahin, « Schinopsis lorentzii extract as a green corrosion inhibitor for low carbon steel in 1 M HCl solution », *Ind. Eng. Chem. Res.*, vol. 51, n° 2, p. 780‑787, 2012.

[226] E. E. Oguzie, C. B. Adindu, C. K. Enenebeaku, C. E. Ogukwe, M. A. Chidiebere, et K. L. Oguzie, « Natural Products for Materials Protection: Mechanism of Corrosion Inhibition of Mild Steel by Acid Extracts of Piper guineense », *J. Phys. Chem. C*, vol. 116, n° 25, p. 13603‑13615, juin 2012, doi: 10.1021/jp300791s.

[227] H. Gerengi, K. Schaefer, et H. I. Sahin, « Corrosion-inhibiting effect of Mimosa extract on brass-MM55 corrosion in 0.5 M H2SO4 acidic media », *J. Ind. Eng. Chem.*, vol. 18, n° 6, p. 2204‑2210, 2012, doi: https://doi.org/10.1016/j.jiec.2012.06.019.

[228] K. W. Tan, Mohd. J. Kassim, et C. W. Oo, « Possible improvement of catechin as corrosion inhibitor in acidic medium », *Corros. Sci.*, vol. 65, p. 152‑162, 2012, doi: https://doi.org/10.1016/j.corsci.2012.08.012.

[229] M. Larif *et al.*, « An investigation of carbon steel corrosion inhibition in hydrochloric acid medium by an environmentally friendly green inhibitor », *Res. Chem. Intermed.*, vol. 39, n° 6, p. 2663‑2677, 2013.

[230] G. Chen, M. Zhang, M. Pang, X. Hou, H. Su, et J. Zhang, « Extracts of Punica granatum Linne husk as green and eco-friendly corrosion inhibitors for mild steel in oil fields », *Res. Chem. Intermed.*, vol. 39, n° 8, p. 3545‑3552, 2013.

[231] M. Pitchaipillai, K. Raj, J. Balasubramanian, et P. Periakaruppan, « Benevolent behavior of Kleinia grandiflora leaf extract as a green corrosion inhibitor for mild steel in sulfuric acid solution », *Int. J. Miner. Metall. Mater.*, vol. 21, n° 11, p. 1083‑1095, 2014.

[232] N. C. Savita, M. Punita, V. K. Singh, et M. M. Singh, « Fruit extract as a green inhibitor for copper corrosion in nitric acid solution », *Int. J. Innov. Res. Sci. Eng. Technol.*, vol. 4, n° 6, p. 4545‑4553, 2015.

[233] G. Ji, S. Anjum, S. Sundaram, et R. Prakash, « Musa paradisica peel extract as green corrosion inhibitor for mild steel in HCl solution », *Corros. Sci.*, vol. 90, p. 107‑117, 2015, doi: https://doi.org/10.1016/j.corsci.2014.10.002.

[234] A. S. Fouda, K. Shalabi, et A. A. Idress, « Ceratonia siliqua extract as a green corrosion inhibitor for copper and brass in nitric acid solutions », *Green Chem. Lett. Rev.*, vol. 8, n° 3‑4, p. 17‑29, 2015.

[235] A. NNANNALebe, K. O. UCHENDU, et G. IKWUAGWU, « Inhibition of corrosion of aluminum alloy AA8011 in alkaline medium using palisota hirsute extract », *relation*, vol. 4, n° 5, p. 10, 2016.

[236] H. Gerengi, I. Uygur, M. Solomon, M. Yildiz, et H. Goksu, « Evaluation of the inhibitive effect of Diospyros kaki (Persimmon) leaves extract on St37 steel corrosion in acid medium », *Sustain. Chem. Pharm.*, vol. 4, p. 57‑66, 2016.

[237] D. K. Verma et F. Khan, « Corrosion inhibition of mild steel in hydrochloric acid using extract of glycine max leaves », *Res. Chem. Intermed.*, vol. 42, n° 4, p. 3489‑3506, 2016.

[238] P. Muthukrishnan, B. Jeyaprabha, et P. Prakash, « Adsorption and corrosion inhibiting behavior of Lannea coromandelica leaf extract on mild steel corrosion », *Arab. J. Chem.*, vol. 10, p. S2343‑S2354, 2017, doi: https://doi.org/10.1016/j.arabjc.2013.08.011.

[239] F. I. El-Dossoki, H.-A. El-Nadr, et A. El-Hussein, « Moringa oleifera plant extract as a copper corrosion inhibitor in binary acid mixture (HNO3+ H3PO4) », *Zašt. Mater.*, vol. 59, n° 3, p. 422‑435, 2018.

[240] R. Haldhar, D. Prasad, et A. Saxena, « Myristica fragrans extract as an eco-friendly corrosion inhibitor for mild steel in 0.5 M H2SO4 solution », *J. Environ. Chem. Eng.*, vol. 6, n° 2, p. 2290‑2301, 2018.

[241] A. Marsoul, M. Ijjaali, F. Elhajjaji, M. Taleb, R. Salim, et A. Boukir, « Phytochemical screening, total phenolic and flavonoid methanolic extract of pomegranate bark (Punica granatum L): Evaluation of the inhibitory effect in acidic medium 1 M HCl », *Mater. Today Proc.*, vol. 27, p. 3193‑3198, 2020, doi: https://doi.org/10.1016/j.matpr.2020.04.202.

[242] A. Thomas, M. Prajila, K. M. Shainy, et A. Joseph, « A green approach to corrosion inhibition of mild steel in hydrochloric acid using fruit rind extract of Garcinia indica (Binda) », *J. Mol. Liq.*, vol. 312, p. 113369, 2020, doi: https://doi.org/10.1016/j.molliq.2020.113369.

[243] T. Brindha, R. Rathinam, et S. Dheenadhayalan, « Antibacterial, Antifungal and Anticorrosion Properties of Green Tea Polyphenols Extracted Using Different Solvents », *Asian J. Biol. Life Sci.*, vol. 10, n° 1, p. 63, 2021.

[244] Z. Meriem *et al.*, « Experimental and theoretical evaluation of the adsorption process of some polyphenols and their corrosion inhibitory properties on mild steel in acidic media », *J. Environ. Chem. Eng.*, vol. 9, n° 6, 2021, doi: 10.1016/j.jece.2021.106482.

[245] B. Fan, X. Zhao, Z. Liu, Y. Xiang, et X. Zheng, « Inter-component synergetic corrosion inhibition mechanism of Passiflora edulia Sims shell extract for mild steel in pickling solution: Experimental, DFT and reactive dynamics investigations », *Sustain. Chem. Pharm.*, vol. 29, p. 100821, 2022, doi: https://doi.org/10.1016/j.scp.2022.100821.

Chapter II :

Experimental methods

II. Materials and methods

Introduction

This chapter details the different investigative methods adopted to evaluate the corrosion-inhibiting effect of carbon steel of a plant extract of (CMFE and PGPE) in an acidic medium. Three main approaches exist to investigate the corrosion phenomenon and inhibitor efficiency in a corrosive medium.

- ✓ Inhibitor extraction
- ✓ Samples and solution preparation
- ✓ Electrochimical analyses
- ✓ Characterization methods
- ✓ Theoretical study

II.1. Inhibitor extracted

II.1.1. Cytisus multiflorus flowers and Punica granatum peel

The cytisus multiflorous flowers (CMF) and Punica granatum peel (PGP) have been selected as inhibitors of XC 48 steel and 304L stainless steel corrosion. Figure.II.1.(a) and Figure.II.1.(b) show two plants used for the study.

The Cytisus multiflorus flowers (CMF) were collected in March 2017 from the region of Collo in Northeastern Algeria, and Punica granatum fruit peel was collected from in fresh state.

II.1.2. Extraction method of corrosion inhibitor

In our study, we used maceration extraction for both plants. The flowers of Cytisus multiflorus (or Punica Granatum Peel) (5 g) were grounded and degreased with 150 ml of n-hexane three times. The residue was extracted with 150 ml of an 80% ethanol solution (v/v) at room temperature for 1 h then the resulting mixture was filtered. The residue was removed in the same conditions thrice, and the filtrated solutions were combined, concentrated, and freeze-dried. For subsequent use, the dried extract (ethanolic extract) of C. multiflorus was stored in a vacuum at a desiccator in the dark. This procedure was performed three times [1].

The Major chemical components of CMFE and PGPE are presented in Table II.1 and Table II.2.

(a) (b)

Figure II.1. (a) Cytisus multiflorus flowers, (b) Punica granatum peel

Table II.1. Major chemical structures of CMF components [2].

	CGP	**DHF**	**Rutin**
name	chrysin-7-O-b-D-glucopyranoside (Molecular Formula: $C_{21}H_{18}O_{10}$ Molecular Weight 430,4 g/mol)	(7) Dihydroxyflavone isomer of chrysin (Molecular Formula: $C_{15}H_{10}O_4$ Molecular Weight: 254.2 g/mol)	(4.5) Rutin (Molecular Formula: $C_{27}H_{30}O_{16}$ Molecular Weight: 610.5 g/mol)
Compound	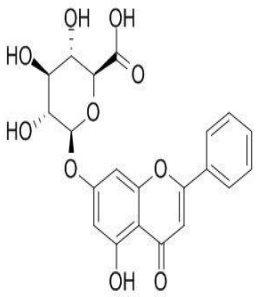	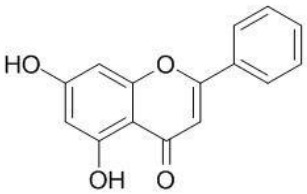	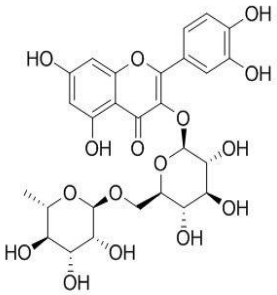

Table II.2. Major chemical structures of Punica granatum peel extract components [3].

name	Gallic Acid	Ellagic acid	Callagic acid
Compound	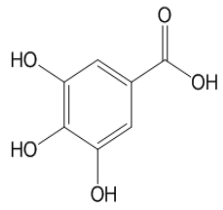	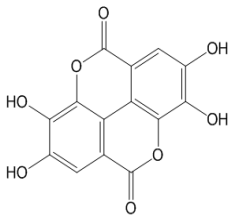	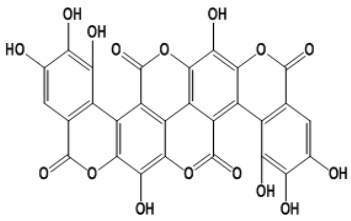
Compound	Punicalgin 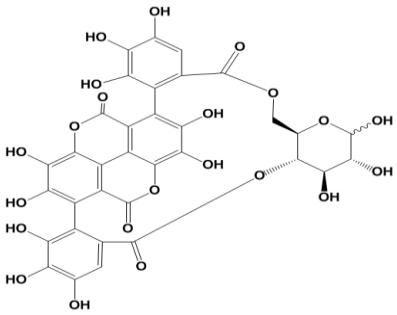	Punicallin 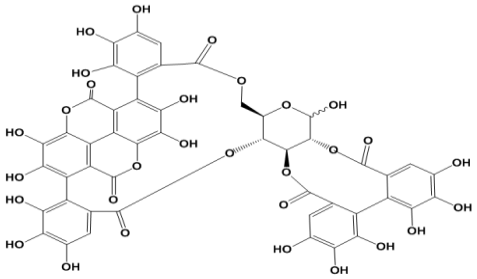	

II.2. Metals and solutions

II.2.1. Metal samples

In the experiments to regarding the corrosion process, XC48 carbon steel (EN 10278) and 304L stainless steel (EN 1.4307) are used to prepare specimens and the working electrode. The Marcegaglia company has manufactured steel.

They contributed to the application of electrochemical studies. Before each experiment, samples were mechanically polished (using abrasive paper from 400 to 2400), cleaned with bidistilled water and acetone, and dried in hot air before being immersed in the corrosive electrolyte. For electrochemical studies, the samples have been prepared for placement in a sample holder with an exposed area of 0.5 cm^2 (Fig.II.2.(a)).

The samples are rubbed and cleaned according to the previous procedure for characterization. They have entirely immersed themselves in the solution. Samples of carbon steel and 304L stainless steel are cylindrical (diameter: D = 15 mm and thickness H = 2 mm) (Fig.II.2.(b)). The samples were immersed in an acid solution without and with inhibitor at 298 K for 24 h.

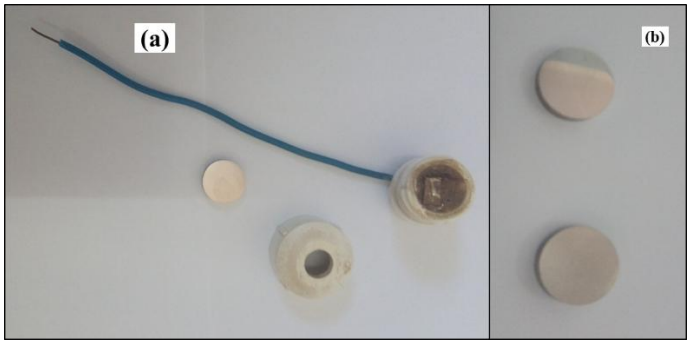

Figure II.2. Work electrode composition : (a) sample holder (b) samples

XC48 carbon steel used in mechanical engineering, intended for heat treatment, is Ideal for parts subjected to shocks and requires good resistance (axes, gears, worms, bearings, sprockets, bolts, forging) [4].

Austenitic type Iron-Chromium-Nickel alloys are widely used and are characterized by a range of nuance with grades of between 17 and 20% chromium, between 9 and 14% nickel, and optionally contain between 2 and 4.5% molybdenum by weight [5]. Alloys in this group of stainless steels have excellent general corrosion resistance. However, in specific environments, they are very susceptible to localized corrosion such as pitting, crevice, and stress corrosion cracking [6].

The nominal elemental compositions of these two alloys are listed in Table II.3.

Table II.3. Chemical composition of XC48 carbon steel and 304L stainless steel [7]:

Element (Wt%)	C	Cr	Ni	Si	Mn	P	Mo	S	N	Fe
XC48	0.440	0.040	0.011	0.187	0.610	0.0090	0.001	--	--	Balance
304L	0.03	18-20	8-10.5	0.75	2	0.045	--	0.03	0.1	Balance

The microstructure of xc48 steel, observed under an optical microscope, is illustrated in Figure II.3.(a) after a chemical attack by a Nital solution (4%). The dark and striated grains characteristic of the pearlite pseudo-phase and the clear ferrite grains are observed. Figure II.3.(a) shows a very fine ferritic-pearlitic microstructure [8].

After an electrolytic attack with oxalic acid on the prepared 304L stainless steel for a few seconds, a typical austenitic microstructure can be observed in the presence of annealing twins in a few places (Fig.II.3-b) [8].

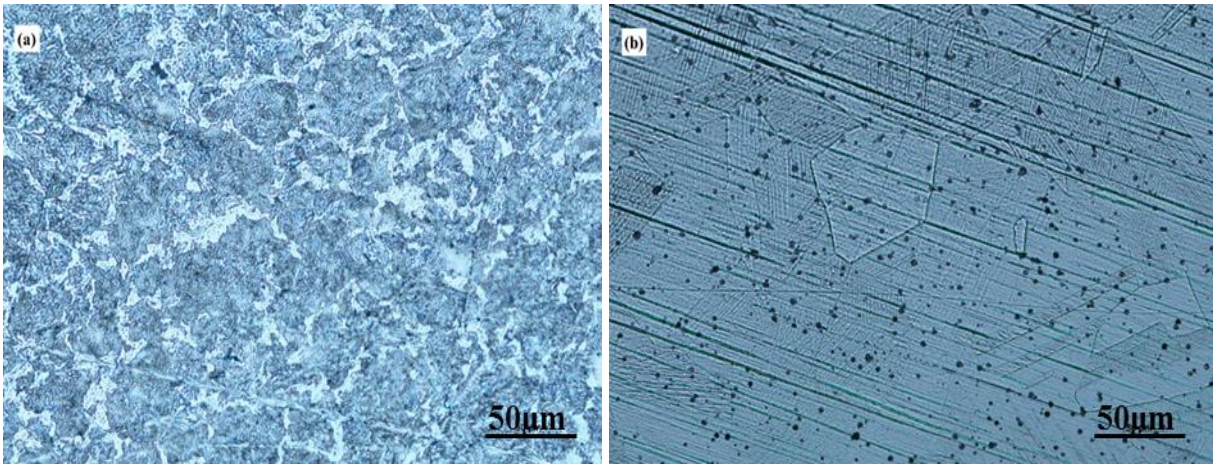

Figure II.3. Microstructures of metals studied (a) XC 48 carbon steel, (b) 304L stainless steel

II.2.2. Corrosive solutions

A solution of 1M H_2SO_4 was prepared from analytical grade H_2SO_4 (purity 98%) and distilled water in the presence and absence of the inhibitor to be the aggressive electrolyte solution. A variety of 50 ppm to 500 ppm was considered the working concentration of inhibitors in 1M H_2SO_4. Double distilled water was employed in the preparation of several concentration test solutions.

II.3. Instruments and technics

II.3.1. Electromechanical measurements

The electrochemical tests were carried out using a traditional 3-electrode (carbon steel or 304L SS are a working electrode WE, the platinum counter-electrode CE, and a saturated Ag/AgCl as the reference electrode RE). EIS measurements were carried out on a potentiostat–galvanostat (SP-150e) coupled with a computer equipped with EC-Lab software. Before the measurement, the working electrode was immersed in the corrosive solution (1M H_2SO_4) (Figure II.4). A great aid in achieving the curves of potentiodynamic polarization was the automatic change in the potential from -200 to +200 mV with a scan rate of 0.5 $mV.s^{-1}$.

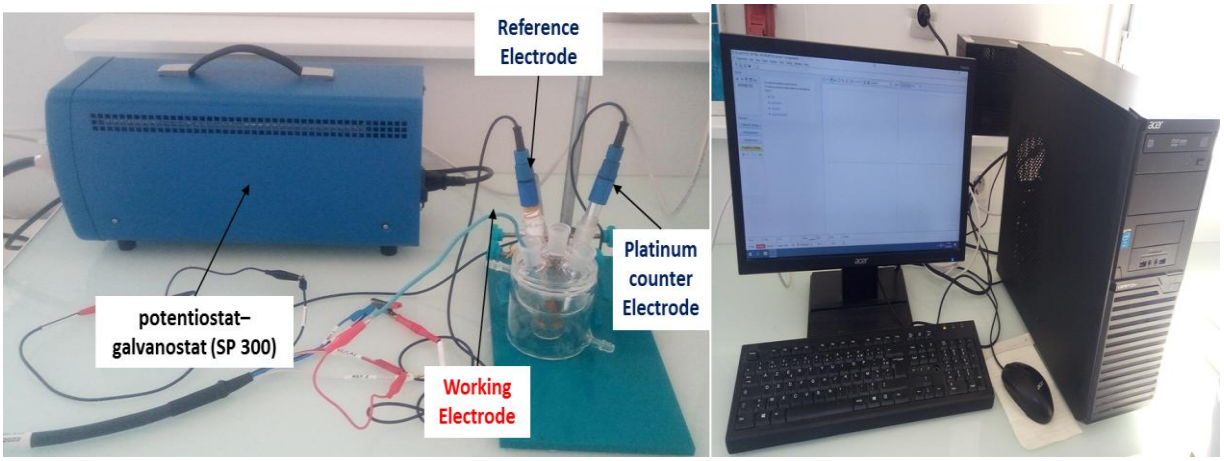

Figure II.4. The experimental setup used for the electrochemical tests

Following equation (II.1), corrosion inhibition efficiency was calculated, and the Tafel exploration approach was used [9] :

$$E_{icorr}(\%) = \frac{(i^0_{corr} - i_{corr})}{i^0_{corr}} \times 100 \quad \text{(II.1)}$$

Where i^0_{corr} is the uninhibited solution current density and i_{corr} is the inhibited solution current density.

The Stern-Geary correlation was employed as shown by the equation to indicate the polarization resistance R_p (Ωcm^2):

$$R_p = \frac{\beta_a \beta_c}{2.30\, i_{corr}\, (\beta_a + \beta_c)} \quad \text{(II.2)}$$

Where β_a and β_c, respectively, are the anodic and cathodic Tafel slopes.

The Values of polarization resistance were employed according to the equation to determine CMFE inhibition efficiency:

$$E_{Rp}(\%) = \frac{(R_p - R^0_p)}{R_p} \times 100 \quad \text{(II.3)}$$

R^0_p and R_p represent the system's polarization resistance values before and after inhibitor addition.

II.3.2. Electrochemical Impedance Spectroscopy (EIS)

Electrochemical impedance spectroscopy is a non-stationary technique that differentiates the reactive phenomena by their relaxation time. The electrochemical system is submitted to a sinusoidal voltage perturbation of low amplitude and variable frequency. The various processes evolve at different rates at each frequency, enabling us to distinguish them.

A weak amplitude sinusoidal perturbation is generally superimposed on the corrosion potential or open circuit potential [10]:

$$\Delta \boldsymbol{U} = |\Delta U| sin\omega t \quad \text{withe } \omega = 2\pi \tag{II.4}$$

Where f is the frequency (Hz) of the applied signal.

This perturbation induces a sinusoidal current $\Delta \boldsymbol{I}$ superimposed to the stationary current I and has a phase shift with respect to the potential:

$$\Delta \boldsymbol{I} = |\Delta I| \sin(\omega t - \varphi) \tag{II.5}$$

These values can be represented in the complex plane:

$$\Delta U = \Delta U_{re} + i\Delta U_{im} \tag{II.6}$$

$$\Delta I = \Delta I_{re} + i\Delta I_{im} \tag{II.7}$$

The complex impedance is defined as:

$$\boldsymbol{Z} = \frac{\Delta \boldsymbol{U}}{\Delta \boldsymbol{I}} = \boldsymbol{Z_{re}} + \boldsymbol{Z_{im}} \tag{II.8}$$

The impedance can also be represented by a modulus and a phase angle shift φ:

$$|Z| = \sqrt{z_{re}^2 + z_{im}^2} \tag{II.9}$$

$$\boldsymbol{tg\varphi} = \frac{\boldsymbol{Z_{im}}}{\boldsymbol{Z_{re}}} \tag{II.10}$$

The impedance data can be represented in two ways:

- Nyquist spectrum: $-Z_{im}$ as a function of Z_{re}

- Bode spectrum: log $|Z|$ and phase angle $\boldsymbol{\varphi}$ as a function of log f

II.3.4. Data presentation

There are different ways to illustrate the response of an electrochemical system to an applied AC potential or current. The most common plots are the Nyquist plot and the Bode plot. If, at each excitation frequency, the real part is plotted on the x-axis and the imaginary part is plotted on the y-axis of a chart, a 'Nyquist plot' is formed. A simple corroding system can be assumed as solution resistance, in series, with a combination of a resistor and a capacitor,

representing the polarization resistance and double-layer capacitance, respectively. This simple representation is called a Randles cell and is shown in Figure II.5 [11].

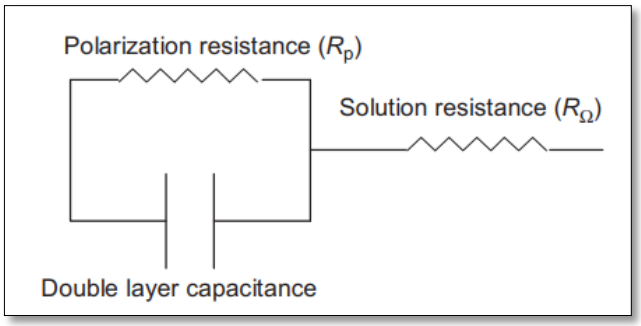

Figure II.5. Equivalent circuit for a simple electrochemical system.

The Nyquist plot represents Z(x) in the complex plane, while the Bode plot represents Z(x) and phase angle h(x) in the frequency domain. The Nyquist plot is data presentation in a complex impedance plane consisting of a real part on the X-axis and an imaginary part on the Y-axis. As shown in Figure II.6, this plot has the shape of a semicircle. Notice that in this plot, the y-axis was chosen as negative notation and that each point on the Nyquist plot is the impedance at one frequency [12]. On the Nyquist plot, the impedance can be represented as a vector of length | Z |, and the angle between this vector and the x-axis is the phase angle 'θ. At high frequencies, at the leftmost end of the semicircle, where the semicircle touches the x-axis, the impedance of the Randles cell is entirely produced by the ohmic resistance, R_Ω. The frequency reaches its lower limit at the rightmost end of the semicircle. The Randles cell also approximates a pure resistance at this frequency, but now the value is (R_Ω + Rp).

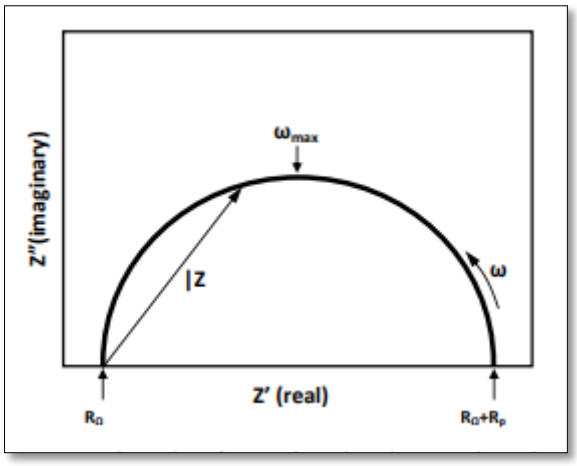

Figure II.6. Nyquist plot for a simple electrochemical system

The Nyquist plot has some limitations [13] :

- The frequency is not clearly shown on the plot, and it is not possible to determine, for a specific point, the frequency used to record that point;
- The ohmic and polarization resistances can be directly determined from the plot, but the electrode capacitance can be only calculated if the frequency information is known, using eq. (II.11):

$$C = \frac{1}{\omega_{max} + R_p} \qquad \text{(II.11)}$$

-If the circuit has high and low impedance components, the larger impedance controls plot scaling, and distinguishing the low impedance semicircle would probably be impossible.

A Bode plot is another popular presentation method for the impedance data. In the Bode plot, the data are plotted with a log of frequency on the abscissa and both the log of the absolute value of the impedance (|Z|) and phase-shift (θ) on the ordinate [14]. Figure II.7 schematically shows a Bode Plot for the same system shown in Figure II.6. Since the frequency appears as one of the axes in the Bode plot, it is easy to understand the dependence of impedance on the frequency from the plot. The log |Z| vs. log ω curve can be used to determine the values of Rp and R_Ω. |Z| becomes independent of frequency at very high and very low frequencies. At the highest frequencies, the ohmic resistance controls the impedance, and log (R_Ω) can be read from the high-frequency horizontal level. On the other hand, at the lowest frequencies, polarization resistance contributes, and log (Rp + R_Ω) can be read from the low-frequency horizontal portion.

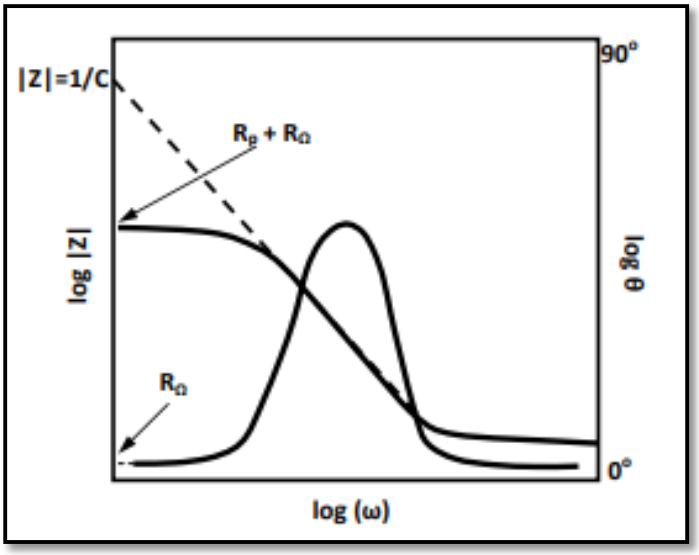

Figure II.7. Schematically shows a Bode Plot.

The Bode format is advantageous when data scatter prevents good fitting of the Nyquist semicircle. In general, the Bode plot provides a more understandable description of the electrochemical system's frequency-dependent behavior than the Nyquist plot, which has unclear frequency values.

In our research, the impedance measurements were performed using an AC voltage equal to ± 10 mV by varying the frequency from 0.1 Hz to 50 kHz at the OCP. All the impedance data were reproduced by adopting a fitting procedure that minimizes the χ^2 function as reported elsewhere [15]. The fitting quality q was determined as [16] :

$$q = \sqrt{\frac{\chi^2}{2n_f}} \tag{II.12}$$

Where n_f represents the number of frequencies. If the q value is close to 1, then the mean difference between the experimental and numerical figures is about 1% of the impedance modulus. The efficiency of the corrosion inhibition was also evaluated by electrochemical impedance spectroscopy (EIS) analyses following Eq. (II.13) [17]:

$$IE_Z(\%) = (1 - \frac{R_{ct}}{R_{ct}^0}) \times 100 \tag{II.13}$$

Rct and Rct 0 are the charge transfer resistance in the H_2SO_4 medium in the presence and absence of CMF and PGP extract, respectively. Consequently, for comparison purposes, independent measurements were adopted to assess the performances of the inhibition agent in determining a reduction of the corrosion attitude of the steel sample: weight loss (via Eq. II.3 and electrochemical measurements (through Eqs. (II.5), (II.6) and (II.13)).

II.4. Surface characterization

II.4.1. SEM analysis

SEM allows studying the surface morphology of practically all solid materials at scales ranging from the magnifying glass (x10) to the transmission electron microscope (x500,000 or more). The operation principle of scanning electron microscopy is based on an electron beam (electron sonde) scanning the sample's surface to be analyzed. Figure II.8 [18] illustrates the principle scheme of SEM, where the interaction between the electron beam and the sample generates secondary low-energy electrons that are accelerated towards a secondary electron detector that amplifies the signal. At each point of impact, there is an electrical signal. The intensity of this electrical signal depends on the nature of the sample at the point of impact which determines the secondary electron yield and on the sample's topography at the point

under consideration. It is thus possible, by scanning the beam over the sample, to obtain cartography of the scanned area. For conventional SEM, the analyzed material must be conductive to avoid charging phenomena due to electrons, so the metallization must be carried out, for example, with carbon or gold for the insulations. SEM at controlled pressure (known as an environmental or low vacuum) allows observation in a vacuum of up to 30 mbar, thus making it possible to examine wet or greasy samples and insulators without prior metallization (ceramics, polymers and corroded metals) or even in the presence of liquid.

In the present work, the elaborated coatings' morphology and microstructure were observed using FEI Quanta 250 model instrument while applying an acceleration voltage of 20 kVolts. SEM could be used to monitor the change in the corrosion process on the carbon steel and 304L SS surface in both inhibitor existence and non-existence cases.

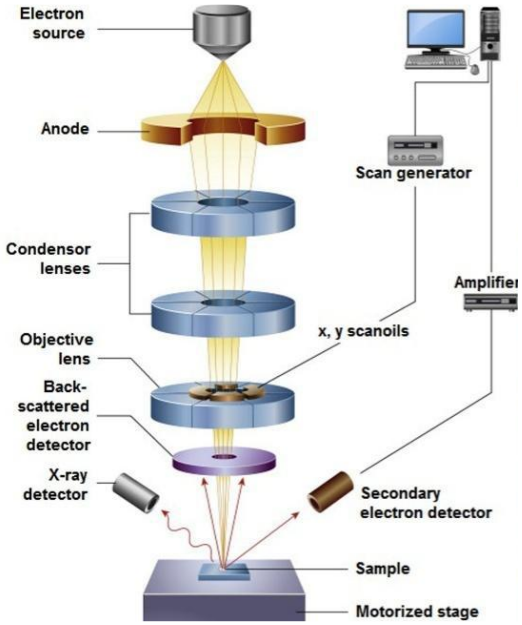

Figure II.8. The principle scheme of scanning electron microscope

II.4.2. Fourier transform infrared spectroscopy (FTIR)

The Fourier transform infrared spectroscopic analysis is a standout amongst the essential methods for elucidating the phenomenon of adsorbed inhibitor molecules. Numerous specialists have considered infrared spectral information as direct evidence of the presence of inhibitors on the metal surface [19-21].

Fourier transform infrared spectroscopy analysis was adopted to detect the presence of the specific functional groups of the CMF and PGP extract inhibitor. Attenuated Total Reflectance Fourier transform infrared spectroscopy (ATR-FTIR) measurements were performed with an FT/IR 4200 Jasco operated in the wavelength range 4000–400 cm^{-1} (Fig.II.9.(a) and Fig.II.9.(b))

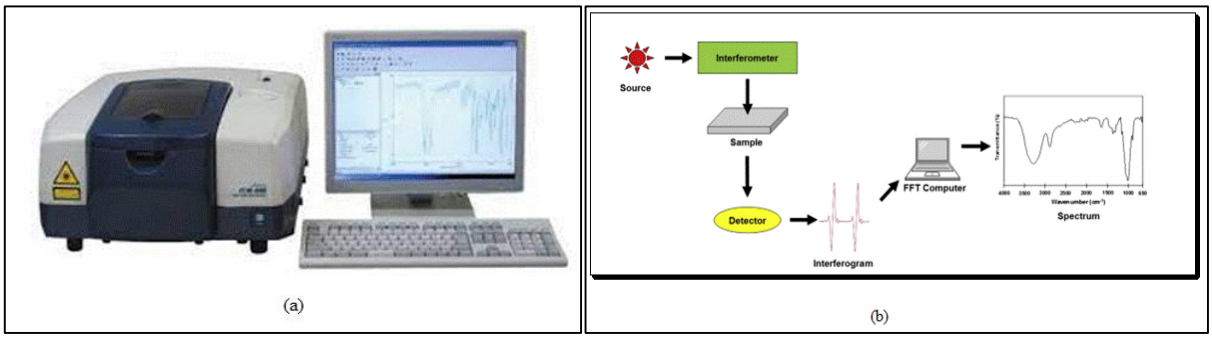

Figure II.9. (a) FT/IR 4200 Jasco, **(b)** Basic Fourier transform infrared spectrometer component.

II.4.3. X-Ray diffraction (XRD)

X-ray diffraction is a technique whose use ranges from the simple identification of crystals to determining their atomic structure. It can provide precious crystallographic information (atoms arrangement, lattice parameters, etc.) on various materials (metals, polymers, ceramics, and composites). It makes it possible to identify the composition of the phases in their presence as well as their evolution and transformations, the quantitative portions of the phases in some cases (within the precision limits of the technique), the size of the crystallites (grains) and their orientation on the surface layers of the material (about 10 µm), as well as the macro/micro stresses. The X-ray diffraction technique is based on a crystal lattice consisting of a stack of families of parallel and equidistant reticular planes. The incident X-ray beam is partially reflected from the foreground. The unreflected beam "falls" onto the second plane to be partially reflected again. For the waves scattered by the different planes to be in phase and for the total intensity of the scattered wave to be significant, Bragg's law [22] in relation (eq.II.14) must be verified:

$$n\lambda = 2d\,sin\theta \qquad \text{(II.14)}$$

Where d is the distance of the reticular planes, λ is the wavelength, and n the order of reflection. This relationship shows that it is sufficient to measure the Bragg angles θ to determine the dimensions and shape of the crystal's elementary lattice (Figure II.10.(a)). The amplitudes of

the reflected waves are used to determine the atomic structure of the pattern. The operating principle of the x-ray diffractometer is shown in Figure II.10.(b) [23].

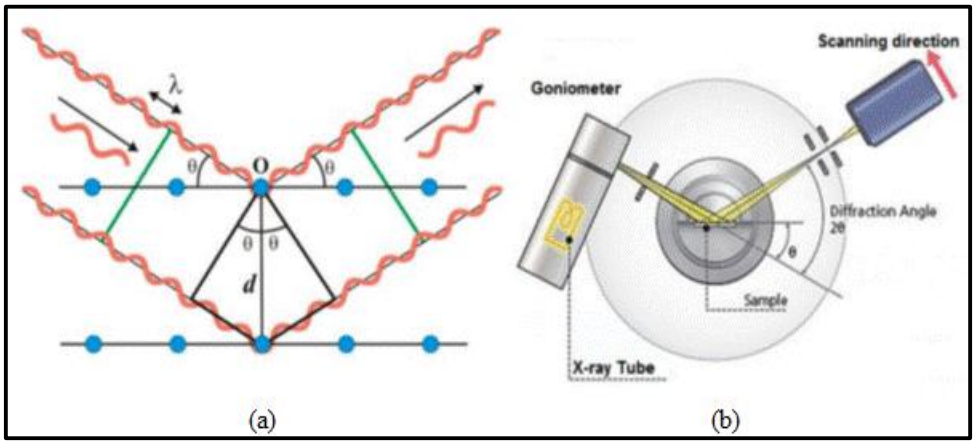

Figure II.10. (a) Schematic representation of the Bragg equation (b) the operating principle of the x-ray diffractometer.

Our theoretical study has characterized the XC48 carbon steel and the 304L SS surfaces before immersion in aggressive solutions in the presence and absence of the inhibitor by X-ray diffraction using the Bruker D8 Advance A25 instrument.

II.4.4. X-ray photoelectron spectroscopy (XPS)

X-ray photoelectron spectroscopy (XPS) is based on the photoelectric effect. X-Rays of fixed energy are focused on the sample surface [24]. As a result of the photoelectric effect, electrons are ejected from the core shells of the atoms present in the sample. For a given element, electrons in various shells are bound to the atom nucleus with well-defined energies. An electron ejected by an incident photon will escape with energy equal to the incident photon energy minus the electron binding energy E_b [25]. The energies of the emitted photoelectrons are measured using an electron energy analyzer to obtain an electron binding energy spectrum for the sample, as illustrated in Figure II.11. XPS is a very surface-sensitive technique as the escape depth of photoelectrons is only on the order of a few nanometers. XPS is also very quantitative as the number of electron counts for a given element is proportional to the concentration of that element in the sample. By normalizing the counts from different atoms by the sensitivity factors, an accurate measure of the surface composition can be obtained XPS was used in this work to characterize the chemical compositions of fracture surfaces to determine the locus of failure within thin film structures [26].

Figure II.11. instrement of X-ray photoelectron spectroscopy XPS

in the present work, the X-ray photoelectron spectroscopy (XPS) spectra were obtained via XPS Kratos Axis-Ultra mode with the monochromatized Al–Kα X-ray source ($h\nu$ = 1486.71 eV) radiation. High-resolution spectra were acquired at 20 eV pass energy with an energy resolution of 0,9 eV. The C 1s (284.4 eV) binding energy (*BE*) was used as an internal reference. XPS spectra were deconvoluted using a non-linear least-squares algorithm with a Shirley baseline and a Gaussian–Lorentzian combination. Casa-XPS software was mainly applied to complete all spectra deconvolution. XPS analyses were applied on the protected and non-protected steel surfaces. The carbon steel specimen was pretreated through the same gravimetric test method.

II.5. Theoretical study

II.5.1. Quantum chemical calculations

The reactivity of a chemical species is very much characterized as far as Frontier orbitals; the highest occupied molecular orbital (HOMO) and the lowest unoccupied molecular orbitals (LUMO) [27-28]. As indicated by the Frontier sub-atomic orbital (FMO) hypothesis of chemical reactivity, a transition state is formed because of the interaction between HOMO and LUMO of responding species. The smaller the energy gap (ΔE) between HOMO and LUMO, the stronger the interaction between the two responding species [29-30]. The quantum chemical parameters, for example, the energy of the highest occupied molecular orbital (E_{HOMO}), the energy of the lowest unoccupied molecular orbital (E_{LUMO}), and the energy gap (ΔE) were figured utilizing following equations (II.15) [31].

$$\Delta E = E_{LUMO} - E_{HOMO} \qquad \text{(II.15)}$$

As E_{HOMO} is frequently connected with the electron donating capacity of the molecule, high EHOMO values will probably demonstrate an inclination of a molecule to donate electrons to fitting acceptor molecules with low energy and empty molecular orbital.

Similarly, the low energy gap values ΔE will render great inhibition efficiencies since the energy to remove an electron from the last occupied orbital will be minimized. It has been reported that suitable inhibitors indicate a higher value of E_{HOMO} and a lower value of ΔE. Therefore, DFT made it possible for corrosion scientists to accurately predict organic compounds' corrosion inhibition capabilities based on electronic/molecular properties and reactivity indices. Previous researchers have also used the DFT study to study the interaction of inhibitor molecules with metal surfaces [32-35].

The DFT-B3LYB method was employed to optimize the CMFE compound and carry out the Quantum chemical calculations; with the basis set TZVP while using the Turbomole program package [36]. On the other hand, Materials Studio (MS) for further DFT computations at the level of generalized gradient approximation (GGABP) and the basis for double numeric polarization (DNP) are to be carried out [37]. Calculations were conducted in a liquid phase as a conductor-like screening model for real solutions (COSMO-RS) [36-37]. Combined with dual description calculation, Fukui functions were calculated using the Dmol3 module to investigate nucleophilicity and electrophilicity [37].

Equations of hardness η and electronegativity χ (chemical potential μ) have been given based on the ground state energies of ionization (I) and the electron affinity (A) values for CMF and PGFP extract [37].

$$\chi = -\mu = \frac{I+A}{2} \quad \text{(II.16)}$$

$$\eta = \frac{I-A}{2} \quad \text{(II.17)}$$

$$I = -E_{HOMO} \quad \text{(II.18)}$$

$$A = -E_{LUMO} \quad \text{(II.19)}$$

Softness (σ), known as the multiplicative inverse of hardness, is commonly recognized as a parameter closely related to polarizability.

$$\sigma = 1/\eta \quad \text{(II.20)}$$

The chemical proton affinity (PA) is proportional to the chemical potential value, which means calculating the chemical potential is considered a test for proton affinity. The electrophilicity index (ω) of ions, atoms, and molecules is calculated from the electronegativity and hardness values [37].

$$\omega = \frac{\chi^2}{2\eta} \quad \text{(II.21)}$$

The next formula calculates the fraction of electrons transferred (ΔN) in corrosion studies [37].

$$\Delta N = [\chi_{Fe} - \chi_{inh}]/[2(\eta_{Fe} + \eta_{inh})] \quad \text{(II.22)}$$

χ_{Fe}, χ_{inh}, η_{inh}, and η_{Fe} are the work function, electronegativity of inhibitor, the hardness of inhibitor, and hardness of (Fe) metal, respectively. η_{Fe} value is taken equal to 0 (I=A for bulk metals). The work function for Fe (110) surface is 4.82 eV [37].

II.5.2. Molecular Dynamics (MD) simulations

The Material Studio's Forcite module was used to carry out MD [37]. The iron structure was imported from the software database. It was then cleaved along (110) plane, and a slab of 15 Å length was obtained. The MD model consists of two layers: a top layer for the solvent; and a frozen bottom layer of Fe(110). The solvent layer was constructed using one inhibitor molecule, chloride (10) ions with their counter ions, hydronium (10), and water molecules (100). Both layers were placed in a simulation box (15.20× 18.169 × 43.43 $Å^3$). The system was first optimized using the SMART minimizer algorithm until the energies and temperature reached steady under periodic boundary conditions and the COMPASS force field. Electrostatic interactions were calculated using the Ewald summation technique with an Ewald precision of 1.0×10^{-4} kcal mol^{-1} and a buffer width of 0.5 Å. The atom-based summation approach was used to calculate the Van der Waals interactions, a cut-off of 15.5 Å, and the buffer width of 0.5 Å. After the optimization step, the simulation model was submitted to MD using the Andersen thermostat method under the canonical NTV set (constant N, T, and V) at T = 298K [37]. The simulation was performed with a time step of 1fs and a full time of 2ns. On MD's trajectory after simulation, the radial distribution function, also known as the pair correlation function, was determined to study the interaction between the inhibitory molecule and the iron surface.

II.5.3. Programs used

In our theoretical study, we used several programs.

II.5.3.1. material's studio

Materials Studio is software for the simulation and computation of materials. It is used by universities, research centers, and high-tech companies in advanced research on various

materials, such as drugs, polymers, carbon nanotubes, catalysts, metals, ceramics, etc., [38]. It is used to:

- Find the most stable adsorption sites for various materials, including carbon nanotubes, silica gel, and activated charcoal [39];
- Predicting electronic, optical, and structural properties;
- Predicting the properties of materials by methods of quantum mechanics;
- Calculating at high speed a variety of physical and chemical molecular properties, for example, for rapid screening when a drug is discovered;
- Identifying compounds with optimal physicochemical properties [40].
- Construct and characterize models of isolated chains or bulk polymers and predict their properties [41].

II.5.3.2. COSMOtherm

COSMOtherm is a universal tool for calculating the predictive properties of liquids. It uniquely combines quantum chemistry and thermodynamics. It calculates the chemical potential of most molecules in almost all pure or mixed liquids at a variable temperature. This is the key to predicting many properties required in industrial applications or academic research, including solubility, Log(P), vapor pressure, and complete phase diagrams [42]. Unlike many other methods, COSMOtherm can predict concentration and temperature properties by applying thermodynamically consistent equations [43].

II.5.3.3 TURBOMOLE

It is an ab-initio computational chemistry program that implements various quantum chemistry methods. It was developed in 2007 by the group of Professor Reinhart Ahlrichs from the University of Karlsruhe [44]. This program is one of the valuable tools in many fields of research, including homogeneous and heterogeneous catalysis, chemistry organic and inorganic, spectroscopy, and biochemistry [45].

CONCLUSION

This chapter describes the way in which the plants studied in the following chapters were selected. It presents the different selection criteria, their relative importance and the conclusions obtained concerning the choices we made. The first part of this work is a screening stage that should allow us to select two plants; the study of corrosion inhibitors can be done in many ways. In our work, we used electrochemical methods (polarization curves and electrochemical impedance spectroscopy) as well as the method of the lost mass for the inhibitor of two inhibitor of an plant extract of (CMFE and PGPE) . Surface analysis is performed by optical microscopy (OM) and scanning electron microscopy (SEM)

to examine the micrograph of the mild steel and stainless steel 304L surface before and after time of immersion in 1M H_2SO_4 medium in the absence and presence of (CMFE and PGPE) inhibitor. X-ray diffraction and Fourier transform infrared spectroscopic analysis and X-ray photoelectron spectroscopy (XPS) have allowed us to elucidate the phenomenon of adsorbed inhibitor molecules and their atomic structures. The experimental and analytical techniques used in this study ensure good reproducibility of results.

Reference

[1] O. R. Pereira *et al.*, « Cytisus multiflorus: source of antioxidant polyphenols », *11º Encontro Química dos Alimentos*, 2012, Consulté le: 6 septembre 2021. https://bibliotecadigital.ipb.pt/handle/10198/8268

[2] O. R. Pereira, A. M. S. Silva, M. R. M. Domingues, et S. M. Cardoso, « Identification of phenolic constituents of Cytisus multiflorus », *Food Chemistry*, vol. 131, nº 2, p. 652‑659, mars 2012, doi: 10.1016/j.foodchem.2011.09.045.

[3] S. K. Middha, T. Usha, et V. Pande, « HPLC Evaluation of Phenolic Profile, Nutritive Content, and Antioxidant Capacity of Extracts Obtained from Punica granatum Fruit Peel », *Adv Pharmacol Sci*, vol. 2013, p. 296236, 2013, doi: 10.1155/2013/296236.

[4] G. MURRY, « Les aciers de construction mécanique pour traitements thermiques: évolution de leur normalisation: Normalisation », *Traitement thermique (Paris)*, nº 299, p. 24‑26, 1997.

[5] P.-J. Cunat, « Aciers inoxydables. critères de choix et structure », *Techniques de l'ingénieur. Matériaux métalliques*, nº M4540, p. M4540. 1-M4540. 17, 2000.

[6] V. Shankar Rao et L. K. Singhal, « Corrosion behavior and passive film chemistry of 216L stainless steel in sulphuric acid », *Journal of materials science*, vol. 44, nº 9, p. 2327‑2333, 2009.

[7] « Marcegaglia - steel for green growth », *Marcegaglia*. https://www.marcegaglia.com/officialwebsite/en/ (consulté le 24 avril 2023).

[8] S. ANGELICA et R. ADOLF, *De Ferri Metallographia: Structure of Steels v. 2:*, vol. 2. MAX-PLANCK-INSTITUT FÜR EISENFORSCHUNG, 1966. Consulté le: 25 avril 2023. [En ligne]. Disponible sur: https://www.abebooks.fr/9783514004337/Ferri-Metallographia-Structure-Steels-3514004331/plp

[9] Z. Tao, S. Zhang, W. Li, et B. Hou, « Corrosion inhibition of mild steel in acidic solution by some oxo-triazole derivatives », *Corrosion Science*, p. 2588‑2595, novembre 2009.

[10] G. L. Goh *et al.*, « Potential of Printed Electrodes for Electrochemical Impedance Spectroscopy (EIS): Toward Membrane Fouling Detection », *Advanced Electronic Materials*, vol. 7, nº 10, p. 2100043, 2021, doi: 10.1002/aelm.202100043.

[11] A. Poursaee, « Corrosion sensing for assessing and monitoring civil infrastructures », in *Sensor Technologies for Civil Infrastructures*, Elsevier, 2014, p. 357‑382. doi: 10.1533/9780857099136.357.

[12] M. S. Abdul Rahman, S. C. Mukhopadhyay, et P.-L. Yu, « Experimental Investigation: Impedance Characterization », in *Novel Sensors for Food Inspection: Modelling,*

Fabrication and Experimentation, in Smart Sensors, Measurement and Instrumentation, vol. 10. Cham: Springer International Publishing, 2014, p. 37‑71. doi: 10.1007/978-3-319-04274-9_3.

[13] A. Poursaee, « Corrosion measurement and evaluation techniques of steel in concrete structures », in *Corrosion of Steel in Concrete Structures*, Elsevier, 2016, p. 169‑191. doi: 10.1016/B978-1-78242-381-2.00009-2.

[14] C. Fernández-Sánchez, C. J. McNeil, et K. Rawson, « Electrochemical impedance spectroscopy studies of polymer degradation: application to biosensor development », *TrAC Trends in Analytical Chemistry*, vol. 24, nº 1, p. 37‑48, janv. 2005, doi: 10.1016/j.trac.2004.08.010.

[15] Wahiba Ebdelly, S. Ben Hassen, X. R. Nóvoa, et Y. Ben Amor, « Inhibition of Carbon Steel Corrosion in Neutral Calcareous Synthetic Water by Eruca sativa Extract », *Prot Met Phys Chem Surf*, vol. 55, nº 3, p. 591‑602, mai 2019, doi: 10.1134/S2070205119030110.

[16] Y. B. Amor *et al.*, « Electrochemical study of the tarnish layer of silver deposited on glass », *Electrochimica acta*, vol. 131, p. 89‑95, 2014.

[17] F. S. de Souza et A. Spinelli, « Caffeic acid as a green corrosion inhibitor for mild steel », *Corrosion science*, vol. 51, nº 3, p. 642‑649, 2009.

[18] B. J. Inkson, « Scanning electron microscopy (SEM) and transmission electron microscopy (TEM) for materials characterization », in *Materials characterization using nondestructive evaluation (NDE) methods*, Elsevier, 2016, p. 17‑43.

[19] N. K. Piracha, F. Ito, et T. Nakanaga, « Infrared depletion spectroscopy of aniline–toluene cluster: the investigation of the red shifts of the NH2 stretching vibrations of aniline–aromatic clusters », *Chemical physics*, vol. 297, nº 1‑3, p. 133‑138, 2004.

[20] A. Chetouani, B. Hammouti, T. Benhadda, et M. Daoudi, « Inhibitive action of bipyrazolic type organic compounds towards corrosion of pure iron in acidic media », *Applied Surface Science*, vol. 249, nº 1‑4, p. 375‑385, 2005.

[21] C. Unterberg, A. Gerlach, A. Jansen, et M. Gerhards, « Structures and vibrations of neutral and cationic 3-and 4-aminophenol », *Chemical physics*, vol. 304, nº 3, p. 237‑244, 2004.

[22] W. L. Bragg, « The structure of some crystals as indicated by their diffraction of X-rays », *Proceedings of the Royal Society of London. Series A, Containing papers of a mathematical and physical character*, vol. 89, nº 610, p. 248‑277, 1913.

[23] Y. Park, H. J. Kim, J. R. Skuza, K. Lee, G. C. King, et S. H. Choi, *X-ray diffraction (XRD) characterization methods for sigma= 3 twin defects in cubic semiconductor (100) wafers*. Google Patents, 2017.

[24] Y.-W. Zhang, *Bimetallic Nanostructures: Shape-Controlled Synthesis for Catalysis, Plasmonics, and Sensing Applications*. John Wiley & Sons, 2018.

[25] D. Fang, F. He, J. Xie, et L. Xue, « Calibration of Binding Energy Positions with C1s for XPS Results », *J. Wuhan Univ. Technol.-Mat. Sci. Edit.*, vol. 35, nº 4, Art. nº 4, août 2020, doi: 10.1007/s11595-020-2312-7.

[26] P. Eriksson, *Cerium Oxide Nanoparticles and Gadolinium Integration: Synthesis, Characterization and Biomedical Applications*. Linköping University Electronic Press, 2019.

[27] P. Singh, V. Srivastava, et M. A. Quraishi, « Novel quinoline derivatives as green corrosion inhibitors for mild steel in acidic medium: electrochemical, SEM, AFM, and XPS studies », *Journal of Molecular Liquids*, vol. 216, p. 164‑173, 2016.

[28] J. Cruz, T. Pandiyan, et E. Garcia-Ochoa, « A new inhibitor for mild carbon steel: electrochemical and DFT studies », *Journal of Electroanalytical Chemistry*, vol. 583, nº 1, p. 8‑16, 2005.

[29] H. Ju, Z.-P. Kai, et Y. Li, « Aminic nitrogen-bearing polydentate Schiff base compounds as corrosion inhibitors for iron in acidic media: A quantum chemical calculation », *Corrosion Science*, vol. 50, nº 3, p. 865‑871, mars 2008, doi: 10.1016/j.corsci.2007.10.009.

[30] J. Bhawsar, P. K. Jain, et P. Jain, « Experimental and computational studies of Nicotiana tabacum leaves extract as green corrosion inhibitor for mild steel in acidic medium », *Alexandria Engineering Journal*, vol. 54, nº 3, p. 769‑775, sept. 2015, doi: 10.1016/j.aej.2015.03.022.

[31] Z. Salarvand, M. Amirnasr, M. Talebian, K. Raeissi, et S. Meghdadi, « Enhanced corrosion resistance of mild steel in 1M HCl solution by trace amount of 2-phenyl-benzothiazole derivatives: Experimental, quantum chemical calculations and molecular dynamics (MD) simulation studies », *Corrosion Science*, vol. 114, p. 133‑145, janv. 2017, doi: 10.1016/j.corsci.2016.11.002.

[32] L. L. Liao, S. Mo, H. Q. Luo, et N. B. Li, « Longan seed and peel as environmentally friendly corrosion inhibitor for mild steel in acid solution: Experimental and theoretical studies », *Journal of Colloid and Interface Science*, vol. 499, p. 110‑119, août 2017, doi: 10.1016/j.jcis.2017.03.091.

[33] H. Lgaz, R. Salghi, S. Jodeh, et B. Hammouti, « Effect of clozapine on inhibition of mild steel corrosion in 1.0M HCl medium », *Journal of Molecular Liquids*, vol. C, nº 225, p. 271‑280, 2017, doi: 10.1016/j.molliq.2016.11.039.

[34] P. B. Raja, A. K. Qureshi, A. A. Rahim, H. Osman, et K. Awang, « Neolamarckia cadamba alkaloids as eco-friendly corrosion inhibitors for mild steel in 1 M HCl media », *Corrosion Science*, vol. 69, p. 292‑301, 2013.

[35] S. Nofrizal, A. A. Rahim, B. Saad, P. Bothi Raja, A. M. Shah, et S. Yahya, « Elucidation of the corrosion inhibition of mild steel in 1.0 M HCl by catechin monomers from commercial green tea extracts », *Metallurgical and Materials Transactions A*, vol. 43, nº 4, p. 1382‑1393, 2012.

[36] B. A. Shainyan, N. N. Chipanina, T. N. Aksamentova, L. P. Oznobikhina, G. N. Rosentsveig, et I. B. Rosentsveig, « Intramolecular hydrogen bonds in the sulfonamide derivatives of oxamide, dithiooxamide, and biuret. FT-IR and DFT study, AIM and NBO analysis », *Tetrahedron*, vol. 66, nº 44, Art. nº 44, oct. 2010, doi: 10.1016/j.tet.2010.08.076.

[37] S. J. Grabowski et J. M. Ugalde, « Bond Paths Show Preferable Interactions: Ab Initio and QTAIM Studies on the X–H···π Hydrogen Bond », *J. Phys. Chem. A*, vol. 114, nº 26, p. 7223‑7229, juill. 2010, doi: 10.1021/jp103047p.

[38] Z.-W. Wang, B. Li, Q.-B. Lin, et C.-Y. Hu, « Two-phase molecular dynamics model to simulate the migration of additives from polypropylene material to food », *International Journal of Heat and Mass Transfer*, vol. 122, p. 694‑706, 2018.

[39] M. Rezakazemi, T. A. Kurniawan, A. B. Albadarin, et S. Shirazian, « Molecular modeling investigation on mechanism of phenol removal from aqueous media by single-and multi-walled carbon nanotubes », *Journal of Molecular Liquids*, vol. 271, p. 24‑30, 2018.

[40] S. Benabid, A. F. Streit, Y. Benguerba, G. L. Dotto, A. Erto, et B. Ernst, « Molecular modeling of anionic and cationic dyes adsorption on sludge derived activated carbon », *Journal of molecular liquids*, vol. 289, p. 111119, 2019.

[41] L. E. I. Zhao, Y. Ding, Y. ZHANG, et C. U. I. Ping, « Constructions of coal and char molecular models based on the molecular simulation technology », *Journal of Fuel Chemistry and Technology*, vol. 45, n° 7, p. 769‑779, 2017.

[42] A. Klamt et F. Eckert, « Prediction of vapor liquid equilibria using COSMOtherm », *Fluid phase equilibria*, vol. 217, n° 1, p. 53‑57, 2004.

[43] M. Turchi, G. Lian, Q. Cai, I. Wood, J. Rabone, et M. Noro, « Multi-scale modelling of solute partition equilibria of micelle-water and microemulsion-water systems using molecular dynamics and COSMOtherm », in *Computer Aided Chemical Engineering*, Elsevier, 2017, p. 2773‑2778.

[44] S. Pirhadi, J. Sunseri, et D. R. Koes, « Open source molecular modeling », *Journal of Molecular Graphics and Modelling*, vol. 69, p. 127‑143, 2016.

[45] T. Aissaoui, Y. Benguerba, et I. M. AlNashef, « Theoretical investigation on the microstructure of triethylene glycol based deep eutectic solvents: COSMO-RS and TURBOMOLE prediction », *Journal of Molecular Structure*, vol. 1141, p. 451‑456, 2017.

Chapter III :

Results and Discussion

Part 1 : Corrosion Inhibition Performance of Cytisus Multiflorus Flower Extract (CMFE) on XC48 carbon Steel and 304L stainless steel in Sulfuric acidic medium

III.1. Electrochemical measurements:

III.1.1. Open circuit potential (OCP) measurements:

The variation of potential versus elapsed time during 30 min for the uninhibited and the inhibited (CMFE) solution is presented in Figure III.1. Based on the plots presented in Figure III.1, it can be observed that the XC48 carbon steel samples could achieve a quasi-stable open circuit potential under 30 min. Therefore, 30 min OCP measurement was assumed before performing all electrochemical.

In the case of an uninhibited solution, a decrease in potential E_{OCP} is observed after about 5 min immersion into H_2SO_4. This might be attributed to the dissolution of iron [1]. The behavior was different for the inhibited solution. The E_{OCP} was shifted to less negative potential values. No obvious fluctuation of E_{OCP} was observed in the measurement time frame, indicating that these interfaces seem to have increased corrosion resistance.

All the phenomena that happened in the presence of inhibitor are due to opposite processes at the metal/solution interface [2]. It is also noticed that, in most circumstances, the value of OCP in the presence of CMFE towards more positive potential (-450 mV for 500 ppm of (CMFE) in comparison with blank solution (-540 mV), which can be explained as the effective adsorption of inhibitor molecules on the metal surface [3].

The variation of the potential versus time for 30 minutes for both uninhibited and inhibited (CMFE) solutions is shown in Figure III.2. After just 30 minutes of aging, the open-circuit voltage of the 304L samples remained almost constant. In light of this, all electrochemical activities were based on a thirty-minute OCP measurement.

Due to the aggressive character of the acid, an uninhibited solution exhibited a decrease in the E_{OCP} potential (less negative potential values with a more electropositive cathode) and a considerable shift in the potential [4]. During the experiments, there was no noticeable change in E_{OCP}, indicating that the corrosion resistance of these interfaces improved. All behaviors seen in inhibitory settings may be attributed to metal/solution interface mechanism asymmetry [5]. Additionally, it is observed that the value of OCP in the presence of CMFE tends toward a less negative potential (-390 mV for -480 mV of CMFE versus -470 mV for the blank solution),

which can be attributed to the efficient adsorption of inhibitor molecules on the metal surface [6] and formation of the protective layer.

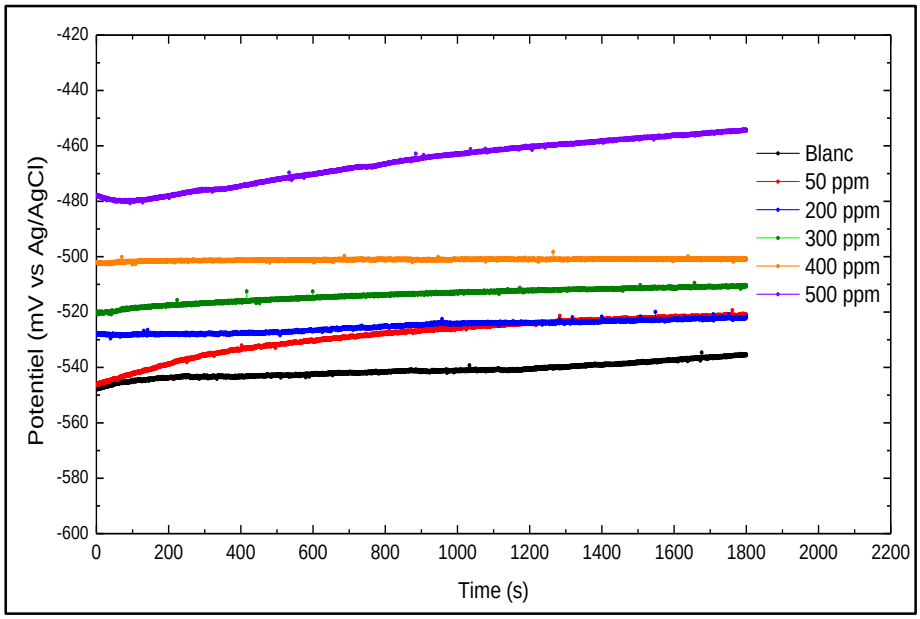

Figure III.1. Open circuit potential (OCP) of the XC 48 steel in 1M H_2SO_4 solutions with various concentrations of CMFE

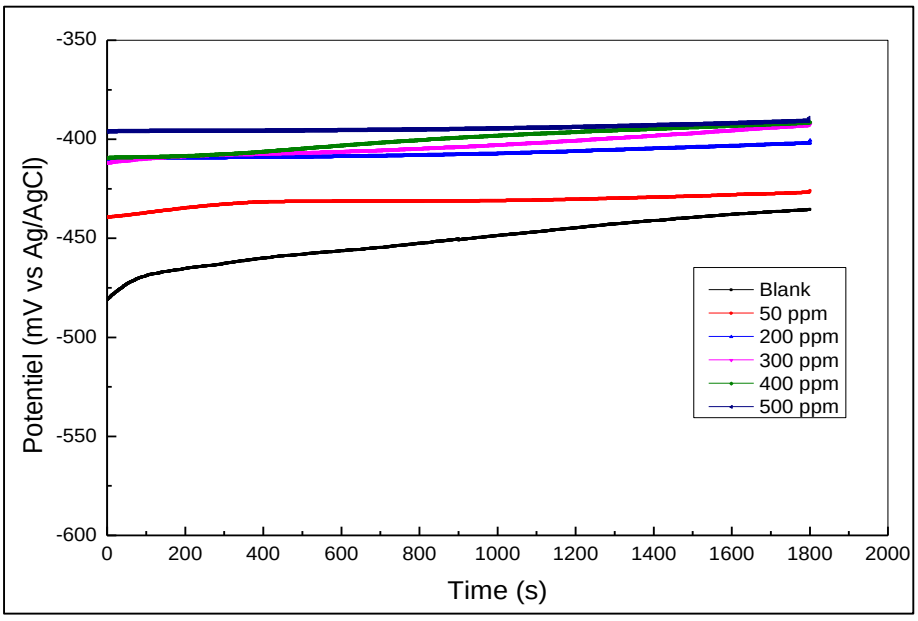

Figure III.2. Open circuit potential (OCP) curves of 304 L in 1M H_2SO_4 solutions with various concentrations of CMFE.

III.1.2. Polarization measurements:

The anodic and cathodic reactions' kinetics can be analyzed using potentiodynamic polarization measurements. The PDP curves of XC48 steel without and with different

concentrations of CMFE inhibitor are represented in Figure III.3. The kinetics parameters of the electrochemical reactions after the extrapolation of the Tafel curves are presented in Table III.1. The shifts in the E_{corr} values in the presence of CMFE is more negative with respect to blank. However, at a lower concentration (50ppm), this shift is towards a slightly positive side compared to the blank in the corrosion potential between 3 and 18 mV compared to the blank solution.

These values are less than the value of E_{corr} shift of ±85 mV, generally taken as a benchmark for an inhibitor to be classified as anodic or cathodic [3]. Hence (CMFE) officinal is extract could be considered to function as a mixed-type inhibitor. The corrosion potential E_{corr} of XC48 steel was around -493,90 mV vs. Saturated Calomel Electrode (SCE) with a corrosion current density of 232,686 µA/cm^2. Hydrogen evolution dominates at more negative potential than E_{corr}, increasing the cathodic currents [7]. A shift in potential, as compared to different concentrations, is observed for inhibitors in 500 ppm of CMFE with E_{corr} -490,638 mV vs. SCE. The presence of the film decreased additionally significantly both the anodic and cathodic current densities due to a restricted supply of oxygen and water, limiting their reduction. Consequently, the corrosion currents are reduced by two orders of magnitude compared to different inhibitor concentrations, resulting in i_{corr} 10.8691 µA/ cm^2. The coating's protection efficiency (PE) was determined from the polarization curve.

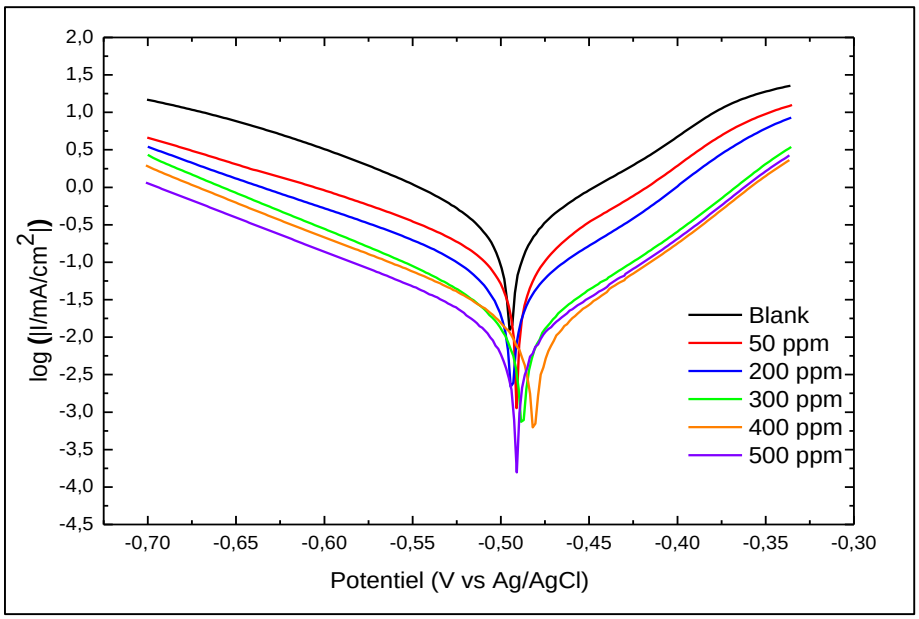

Figure III.3. Polarization curves of XC48 steel in 1M H_2SO_4 solutions with various concentrations of CMFE

The obtained result from Table III.1 reveals that the values of corrosion current density decrease and inhibition efficiency increase, respectively, as the CMFE concentration increases. At a concentration of 500 ppm, the corrosion current density and inhibition efficiencies are 8.518 µA/cm^2 and 95.91%, respectively.

Table III.1. Polarization parameters for XC48 steel corrosion in 1M H_2SO_4 in the absence and presence of CMFE;

Concentration (ppm)	E_{corr} (mV)	i_{corr} (mA/cm^2)	β_a (mV)	β_c (mV)	C_R (mmpy)	Rp (Ohm)	IE %
Blanc	-493.90	232.686	74	84.4	5.514	59.3	-
50	-490.98	105.82	77.7	114.4	2.508	166	64.27
200	-493.73	59.807	79.1	109.5	1.418	317	81.29
300	-487.71	18.826	82.3	93	0.446	970	93.88
400	-481.21	14.878	78.6	97.7	0.352	1 230	95.17
500	-490.63	8.518	68.7	78.5	0.201	1 453	95.91

The potentiodynamic polarization curves of 304L electrodes in 1M H_2SO_4 with various concentrations of CMFE are shown in Figure III.4. Corrosion potential (E_{corr}), corrosion current (i_{corr}), and Tafel's constant are the electrochemical properties listed in Table III.2.

Results from Table III.2 and polarization curves in Figure III.4 reveal little change in E_{corr} values over the investigated range of plant extract concentrations. E_{corr} values that shift by more than 85 mV away from the anode or towards the cathode compared to the blank solution have been used in previous work to categorize inhibitors as anodic or cathodic types [8]. If the shift is under 85 mV, the inhibitor is a transitional kind. *In the current study, ecorr shift values below 85 mV* suggest that CMFE is a mixed-type inhibitor.

Table III.2. Polarization parameters for 304 L corrosion in 1M H_2SO_4 in the absence and presence of CMFE

Concentration (ppm)	E_{corr} (mV)	i_{corr} (mA.cm^{-2})	βa (mV)	βc (mV)	CR (mmpy)	Rp (Ohm)	IE (%)
Blanc	-426,621	86,28	92,2	87,7	1,77692	181	--
50 ppm	-414,276	35,104	56,3	90,3	0,72296	322	59,31
200 ppm	-411,867	17,677	49,7	79,8	0,36406	658	79,51
300 ppm	-390,159	4,08	34,6	41,1	0,08402	1430	95,27
400 ppm	-386,957	3,296	39,6	49,2	0,06788	2062	96,17
500 ppm	-363,147	2,069	26,6	46,4	0,04261	2426	97,6

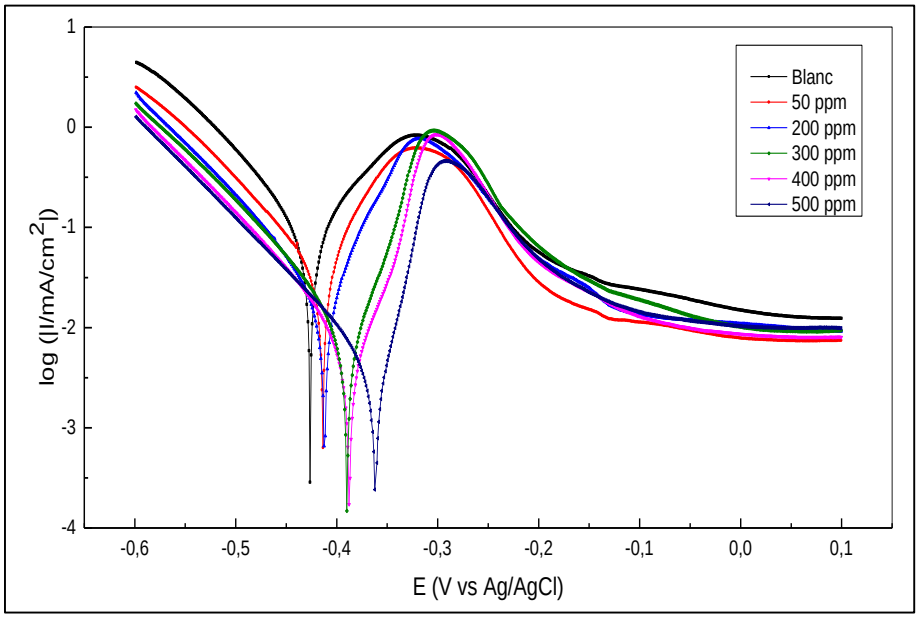

Figure III.4. Polarization curves of 304L in 1M H_2SO_4 solutions with various concentrations of CMFE

In addition, i_{corr} values dropped when the investigated plant extract was present. The effect was found to be more pronounced at higher plant extract concentrations, suggesting that this was produced by the organic components of the plant extract adsorbing to active sites on the surface of the 304L coupon. At 500 ppm of extract in 1M H_2SO_4, inhibition efficiencies of 97.6 percent were attained, demonstrating that CMFE significantly reduced corrosion rates.

These findings show that the extract effectively halts the corrosion of alloy 304L in the experimental medium.

III.1.3. Electrochemical impedance spectroscopy (EIS)

Figure III.5 illustrates the results obtained for EIS steel XC48 in 1M H_2SO_4 solutions interfaces with various CMFE amounts. The EIS experiments were conducted to evaluate the impedance of XC48 steel corrosion in 1M H_2SO_4 solution without and with various concentrations of the inhibitors. The recorded spectra were exemplified in Figure III.5 by the Nyquist plot. The result exhibits two distinguishable capacitive loops at f = 100.000 Hz - 0.1 Hz (i.e., high-frequency region) and f = 0.1 Hz to 0.01 Hz (i.e., low-frequency region). Their diameter increases with increasing inhibitor concentration. The first loop is greater in size. is flattened in shape and can be attributed to the charge transfer process. The second loop is located at a lower frequency. is smaller, and its shape indicates a diffusion process [9]. The observed diffusion process may have arisen due to the migration of the oxidant (i.e., the sulfate ions)

from the bulk solution through the CMFE layer to the metal surface or the diffusion of adsorbed inhibitor/corrosion products from the metal surface toward the bulk solution [9].

To evaluate the anti-corrosion behavior of the used inhibitor obtained by impedance measurements, the equivalents circuits of Figure III.6 represent the studied electrochemical interface were used to reproduce the experimental results [10-11]. This fitting procedure was applied between 100 kHz and 0.1 Hz to extrapolate faradic parameters.

In the first approach, the circuit of Figure III.6.a was used to reproduce the capacitive behavior of the recorded impedance. In this equivalent circuit, *Rs* is the non-compensated solution resistance. R_{ct} is the charge transfer resistance, and (Q_{dl}. n_{dl}) is the constant phase element. CPE is used in place of double-layer capacitance to account for the non-ideal behavior of the working electrode [12]. The agreement between the experimental (Z_{exp}) and the fitted impedance (Z_{fit}) was assessed by determining the error on the imaginary part according to the following equation [10-11]:

$$\varepsilon_{Z(im)} = 100 \frac{Z_{\exp}(im) - Z_{fit}(im)}{Z_{\exp}(im)} \quad \text{(III.1)}$$

The corresponding results were reproduced in Figure III.5. Using the equivalent circuit of Figure III.6.a, a good agreement was obtained with the blank system (red curve). However, for the 400 ppm inhibited system, the same circuit (Figure III.6.a) leads to an important and marked divergence on the imaginary part of the impedance, mainly above 1000 Hz (blue curve). As a result, another contribution must be considered to reproduce the experimental impedance data correctly. For inhibited system. the equivalent circuit of Figure III.6.b was therefore adopted. The corresponding error was also added to Figure III.7 (green curve). It was seen that the proposed equivalent circuit (Figure III.6.b) no longer induces a systematic error. In this circuit. The additional contribution consists of the CPE_{ad} (Q_{ad}. n_{ad}) and the resistance R_{ad} refereed to the adsorbed molecules of the used inhibitor on the XC48 steel surface [5]. Table III.3 lists the EIS parameters obtained from the fitting procedure using the equivalent circuit of Figure III.6. The computed parameters show a rise in the I_{EZ} (%) which indicates the presence of the CMFE adsorbed on the surface of XC48 steel working electrode [13]. The introduction of the inhibitors into 1M H_2SO_4 solution leads to an increase of both R_s and R_{ct} values compared to the blank. R_s is nearly constant for an inhibited acid solution with a value of 7.92 and 9.22 $cm^{2,}$ confirming a sufficient conductivity of all tested solutions [5,14].

In contrast, Q_{dl} and Q_{ad} decrease when the CMFE are progressively added to the 1M H_2SO_4 solution. The double-layer capacitance decreases due to the adsorption of the inhibitors molecules of lower dielectric constant on the metallic surface and the replacement of water molecules [15-16]. The decrease of Q_{ad}, which indicates that the adsorbed species slow the corrosion reaction, confirms the formation of a more protective and thicker layer slowing the corrosion process [17].

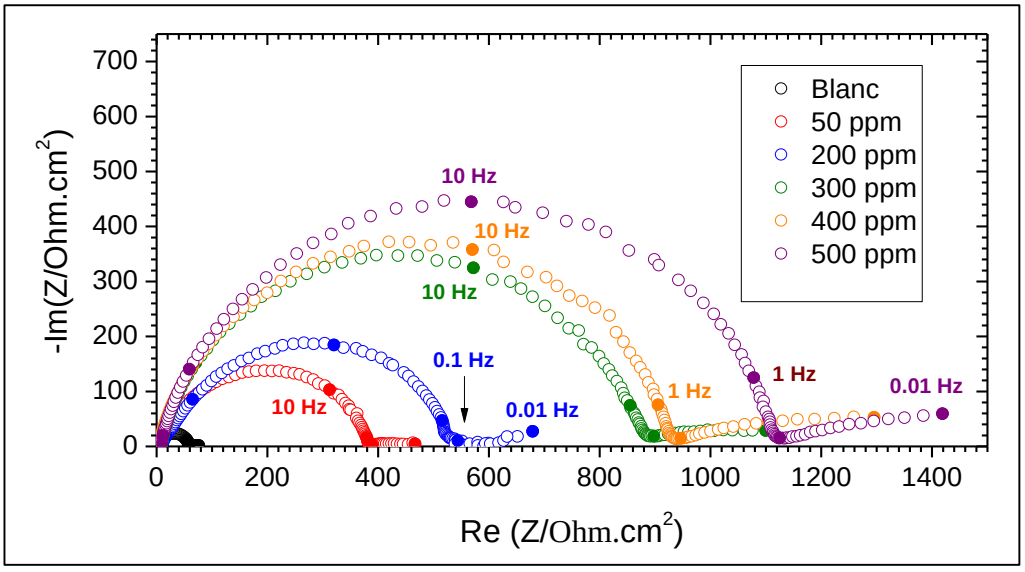

Figure III.5. Nyquist plot of XC 48 steel immersed in 1M H_2SO_4 solution without (Blank) and with different concentrations of CMFE.

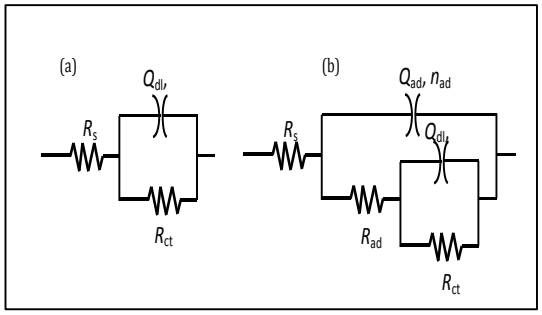

Figure III.6. Equivalents electric circuit (a) without inhibitor (Blank). (b) Solution containing diverse quantities of CMFE.

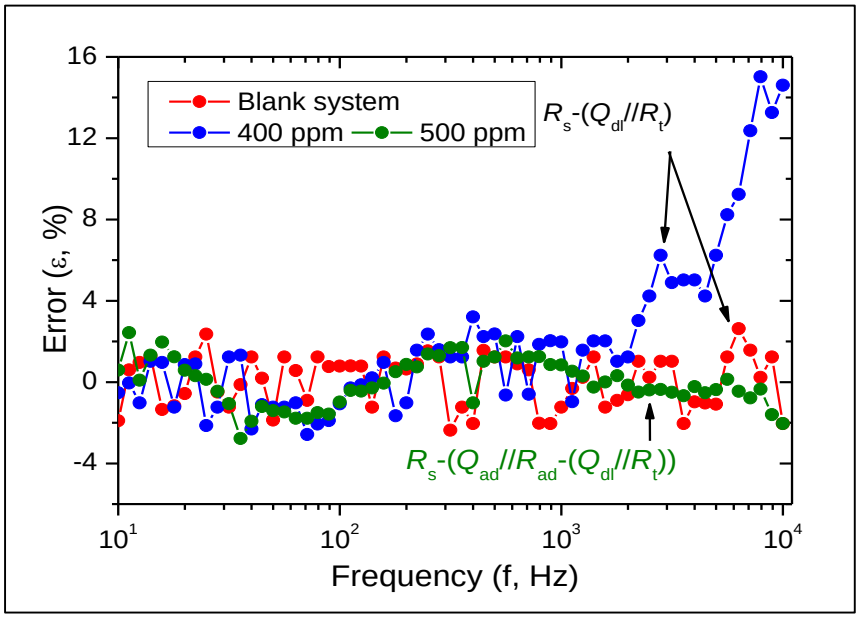

Figure III.7. Variation of the error on imaginary part as a function of frequency. Measurements were recorded on blank, 400 ppm, and 500 ppm inhibited systems.

Table III.3. Electrochemical impedance spectroscopy parameters for XC48 steel corrosion in 1M H_2SO_4 without and with different concentrations of CMFE.

C (ppm)	R_s (Ohm)	R_{ct} (Ohm)	n_{dl}	Q_{dl} ($\mu F.s^{nd-1}.cm^{-2}$)	R_{ad} (Ohm)	n_{ad}	Q_{ad} ($\mu F.s^{nf-1}.cm^{-2}$)	IE_Z (%)
Blank	5.14	53.22	0.93	90.4	-	-	-	-
50 ppm	8.36	284.07	0.71	51.8	94.28	0.94	11.0	81.26
200 ppm	8.02	474.30	0.75	54.0	53.47	0.92	11.5	88.78
300 ppm	8.76	829.20	0.72	25.2	49.55	0.98	6.03	93.58
400 ppm	7.92	899.56	0.73	26.4	43.27	0.99	5.78	94.08
500 ppm	8.02	1100.3	0.74	22.7	32.57	0.98	5.13	95.16

The impedance characteristics of a 304L electrode in 1 M HCl, both in the absence and presence of different doses of CMFE, are illustrated in Figure III.8 using Nyquist plots. A closer look at Figure III.8 reveals that the widths of the Nyquist plots were more remarkable when the extract was added to the 1 M H_2SO_4 solution. The extract may have acted as a barrier against corrosion by adsorbing onto the 304L surfaces and forming a layer that prevented further erosion [18]. The diameters grew with increasing extract concentrations.

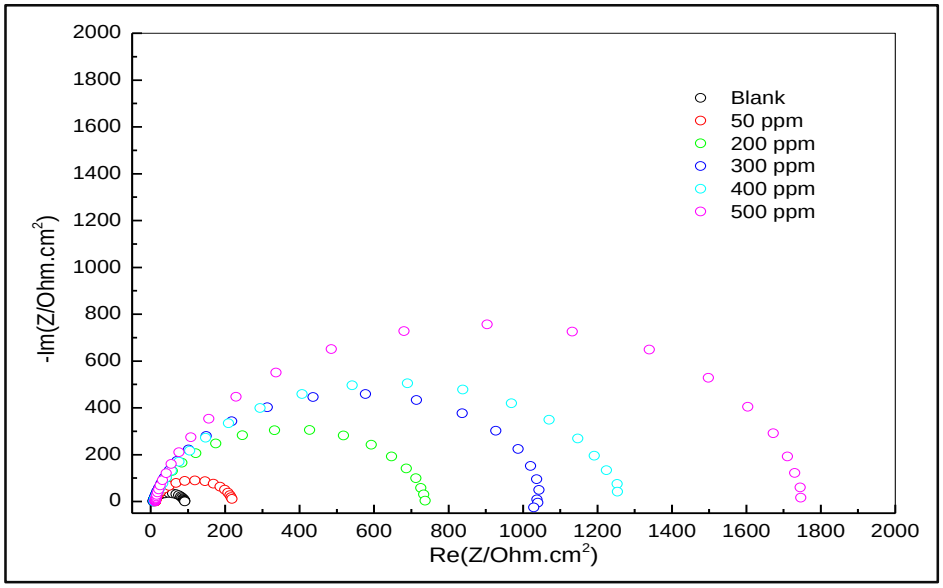

Figure III.8. Nyquist plot of 304L Stainless Steel immersed in 1M H2SO4 solution without (Blank) and with different concentrations of CMFE

Figure III.9.a depicts the equivalent circuit used for fitting impedance data. Depending on the value of ***n***, the constant phase element (CPE) can represent various impedances, including capacitance, inductance, resistance, and Warburg impedance. For example, if ***n = 1***, the CPE will show capacitance; if ***n = -1***, it will show inductance; if ***n = 0*** it will show resistance; and if ***n = 0.5***, it will show Warburg (Warburg impedance). The results showed that the CPE acted as a capacitor with n values between 0.8905 and 0.9989. This led to the following equation being developed to determine $\mathbf{C_{dl}}$ values for electrical double layers [5].

The maximum frequency at which the imaginary part of the impedance dominates is denoted by f_{max}. Figure III.9.b and Table III.4 demonstrate that the R_{ct} values in 1 M H_2SO_4 solution were much higher when the CMFE was present, going from 120,89 Ωcm^2 in the blank solution to 1749 Ωcm^2 in the solution containing 500 ppm extract.

The corrosion resistance of 304L in 1 M H_2SO_4 solution was improved with increased Rct values, as Cdl values decreased from 90,3647827 to 32,7701913 µF cm^{-2} [19]. This may be because the local dielectric constant decreased or the protective film thickness on the electrode surfaces increased. This finding showed that CMFE functioned by removing water molecules and other ions from the coupon surface, which reduced the electrode's electrical capacity by adsorption of organic compounds at the Metal/solution interface [20].

Table III.4. EIS parameters for 304L stainless steel corrosion in 1M H_2SO_4 without and with different concentrations of CMFE.

C (ppm)	R_s (Ohm)	R_{ct} (Ohm)	n_{dl}	Q_{dl} ($F.s^{nd-1}.cm^{-2}$)	R_{ad} (Ohm)	n_{ad}	Q_{ad} ($F.s^{nf-1}.cm^{-2}$)	IE_Z (%)
blank	6,846	84,12	0,906	2,10E-04				
50 ppm	12,65	206,2	0,923	1,38E-04	6,97E-07	0,106	7,84E-03	59,2
200 ppm	7,42	736,6	0,889	5,23E-05	1,36E-07	0,639	7,82E-05	88,57
300 ppm	7,377	1 077	0,885	5,55E-05	0,1314	0,080	4,30E-07	92,18
400 ppm	9,46	1260	0,863	6,24E-05	2,734	0,777	7,01E-06	93,32
500 ppm	12,02	1755	0,901	4,31E-05	2,115	0,222	8,94E-07	95,2

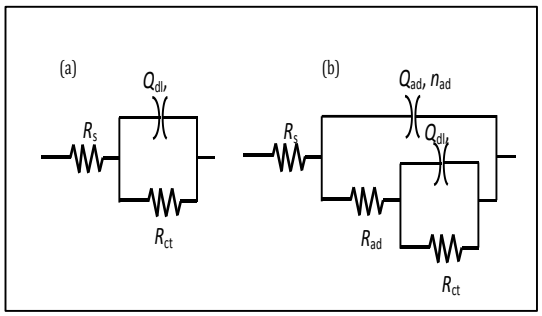

Figure III.9. Equivalent electric circuit (a) without inhibitor (Blank). (b) Solution containing diverse quantities of CMLE.

III.2. Surface characterizations

III.2.1. Scanning electron microscope (SEM)

The surface morphology of XC48 carbon steel is represented in Figure III.10.a, 10.b, and 10.c before and after immersing in 1M H_2SO_4 acidic solution in the presence and absence of an inhibitor. An aggressive attack is noted (Figure III.10.b) in the carbon steel surface's micrographs after immersion without inhibitor (Solution of 1M H_2SO_4 for 24h). The cracks and pits on the metal surface indicate that the solution's corrosive attack considerably damaged it. Meanwhile, adding 500 ppm of the inhibitor to the system (Figure III.10.c) shows a smooth and more compact surface, with very few notable cracks and pits, showing the metal was protected from the corrosive attack. The difference could easily be interpreted as the working electrode's steel surface was protected by the adsorbed CMFE molecules [7]. This demonstrates that an efficient protective layer of the tested inhibitor was adsorbed on the metal surface and played a useful role in protecting the surface steel against corrosion.

Figures.III.11.a, III.11.b, and III.11.c show the surface morphology of stainless steel before and after immersion in 1M H_2SO_4 acidic solution with and without an inhibitor. Without an inhibitor (Solution of 1M H_2SO_4 for 24h), the stainless-steel surface micrographs show vigorous assault following immersion (Figure III.11.b). It is clear from the metal's surface fractures and pits that the solution's corrosive assault was quite damaging. A smoother, more compact surface with less noticeable cracks and pits is seen when 500 ppm of the inhibitor is added to the solution (Figure III.11.c)), establishing that the metal was successfully shielded from the corrosive assault. The discrepancy may be explained by the fact that the working electrode is made of 304L stainless steel, immune to damage from the CMFE molecules that have been adsorbed on its surface [7]. This proves the tested inhibitor effectively adsorbs onto metal surfaces to prevent corrosion.

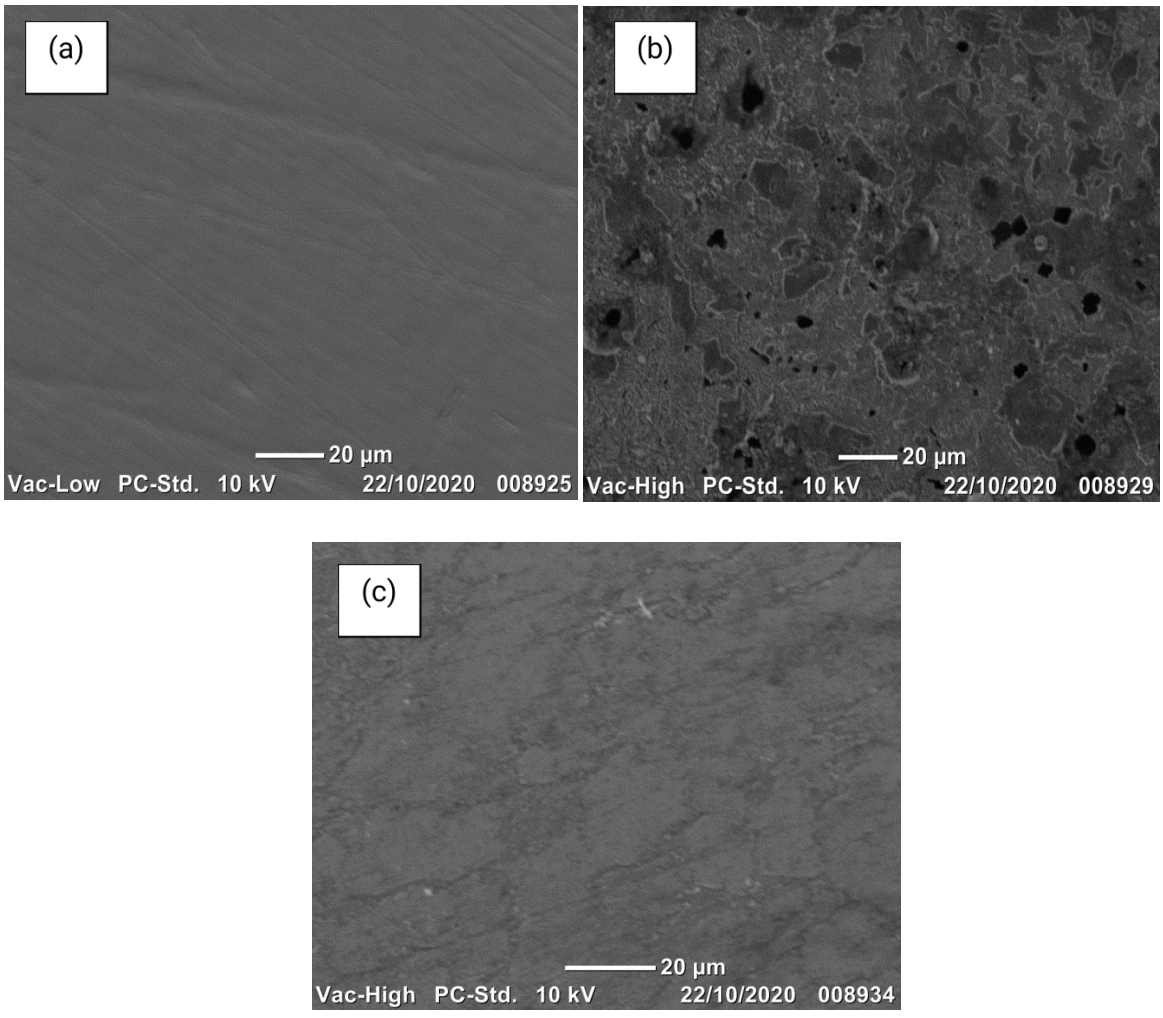

Figure III.10. SEM images of the XC48 surface a) before immersion. b) After immersion in an acidic solution without CMFE. c) After immersion in an acidic solution with CMFE (500 ppm).

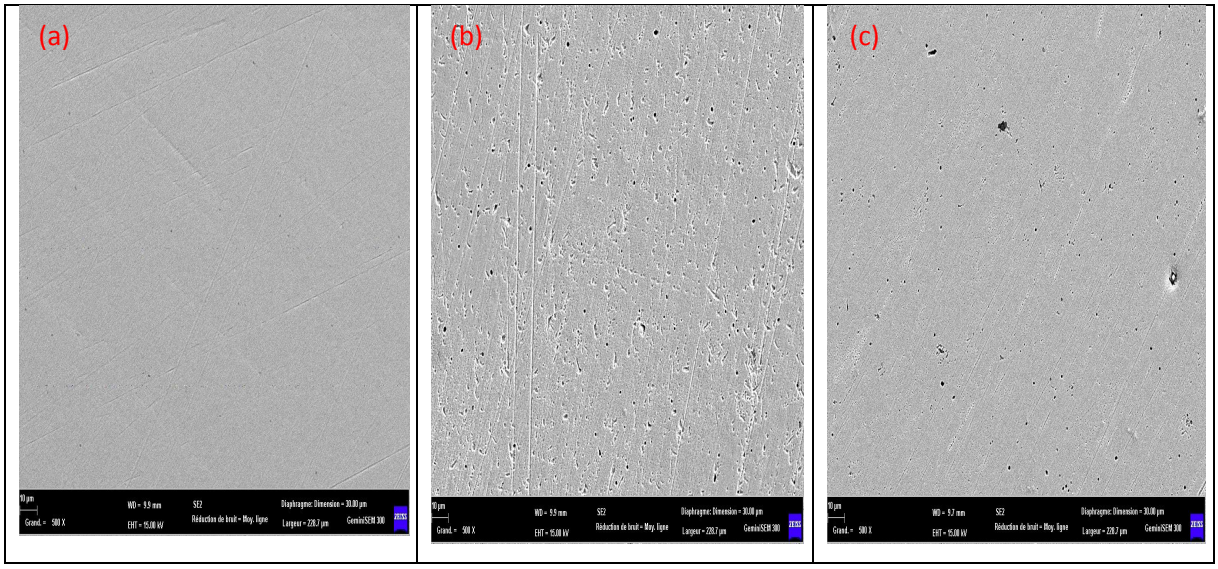

Figure III.11. SEM image of 304L coupon surfaces, (a) showing a polished surface, (b) surfaces immersed in 1M H_2SO_4 and (c) surfaces immersed in 1M H_2SO_4 containing 500 ppm concentration of CMFE

III.2.2. Fourier transform infrared spectroscopy

FTIR analyses were achieved on the pure extract (CMFE) and the surface protective film developed on the XC 48 steel after immersion in 1M H_2SO_4 acid solution at the optimum concentration. However, the FTIR was used to predict the CMFE extract's functional group (Figure III.12.a). The result was compared with surface protective film spectra (Figure III.12.b). As shown in (Figure III.12.a), an intensive band 3335 cm^{-1} appeared, which can be attributed to the O- H's symmetrical and asymmetrical stretching modes [21]. The two peaks at 2925 cm^{-1} and 2849 cm^{-1} are assigned to C-H stretching mode (élongation) [22]. The peak 1715 cm^{-1} corresponds to C—H elongation of the benzoic ring group. The stretching mode of C=O groups (benzoic ring) is indicated at peaks (1600 cm^{-1}, 1650 cm^{-1}, 1569 cm^{-1},1504 cm^{-1} and 1455 cm^{-1}) [23]. The absorption of 1266 cm^{-1} corresponds to C—C bending vibration and the bands observed at 1060 cm^{-1} is linked to C—O stretching**.** The presence of C—O—c bonds is testified by the stretching vibration at 1115 cm^{-1}. The FTIR spectrum of the layer formed on the metal surface shown in (Figure III.12.b) Indicates that the absorption peak of OH was shifted from 3350 cm^{-1} to about 3240 cm^{-1} [24]. Two peaks shifted to 2850 cm^{-1} corresponding to C—H of benzoic ring. The peak of 1715 cm^{-1} is also moved to about 1725 cm^{-1}, so it has been observed that approximately all peaks were shifted.

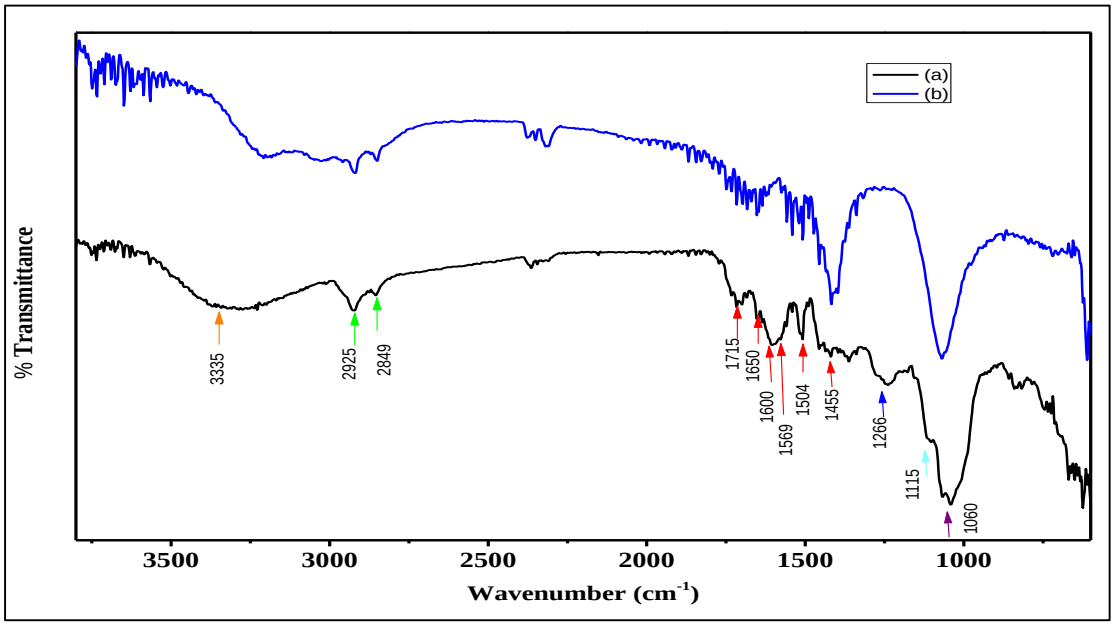

Figure III.12. FTIR spectra: (a) CMFE and (b) surface of XC48 steel after immersion in 1M H_2SO_4 solution containing 500 ppm of CMFE.

FTIR was used to examine the purity of the CMFE extract and the protective layer formed on the surface of the Inox 304L after it was immersed in a 1M H_2SO_4 acid solution. FTIR was used to predict the CMFE extract's functional group (Figure III.13.a) and compared to the spectra of surface protective films (Figure III.13.b).

An intense band at 3335 cm^{-1} [21] was discovered, attributed to O─H's symmetrical and asymmetrical stretching modes. At 2925 cm^{-1} and 2849 cm^{-1}, two peaks are ascribed to the C-H stretching mode (elongation) [22]. The peak at 1715 cm-1 reflects the C-H elongation in the benzoic ring group. The C=O group (benzoic ring) stretches at 1600, 1650, 1569, 1504, and 1455 cm^{-1} [23], as shown by peaks at those frequencies. The bands at 1060 cm^{-1} are related to C─O stretching, while the absorption at 1266 cm^{-1} is connected with C─C bending vibration. The stretching vibration at 1115 cm^{-1} is a signature of covalent carbon-oxygen bonding. C=O stretch peaks at 1715 cm^{-1} and peaks at 2925 cm^{-1} were initially ascribed to C-H of the benzoic ring, while OH stretch peaks at 3350 cm^{-1} were shifted to 3358 cm^{-1} in the FTIR spectrum of the layer produced on the metal surface [21]. Cross-ponding with a methyl group was seen at 1456 cm^{-1}, and vibrational peaks in the C-H bond at 1060 cm^{-1} were displaced to 1088 cm^{-1}. For this reason, CMFE is adsorption onto the surface of 304L.

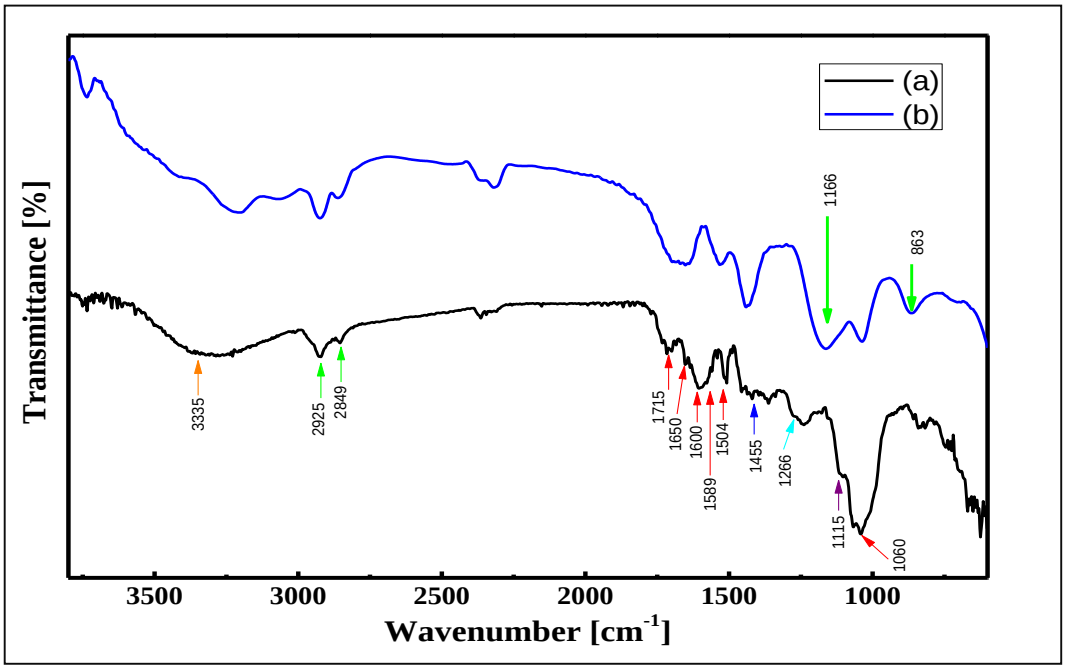

Figure III.13. FTIR spectra: (a) CMFE and (b) surface of 304L after immersion in 1M H_2SO_4 solution containing 500 ppm of CMFE.

III.2.3. X-ray diffraction

X-ray diffraction was used to detect the film product on the surface of XC48 steel. XRD analysis indicates the presence of a peak at 2θ of 45.2° related to metallic iron (Figure III.14.a). The X-ray spectra of the corrosion product formed on the steel surface immersed in 1M H_2SO_4 solution is shown in Figure III.14.b. The peaks at 16.3, 18.3, 23.5, 27.3, and 36.11° suggested the presence of Fe_3O_4 iron oxide and FeOOH, a minimal amount of brown film, which, due to Fe2O3 observed visually, leads to corrosion [25-26]. Figure III.14.c shows the X-ray diffraction patterns of XC48 steel immersed in the solution containing 500 ppm of CMFE. Compared to the spectrum of the steel surface immersed in 1M H_2SO_4 solution without inhibitor, which showed three phases of iron oxides (Fe_2O_3, Fe_3O_4, and FeOOH), this sample represented only a very weak Fe_2O_3 peak, which corresponds to the very slight oxidation of the XC48 steel in the presence of inhibitor. These observations reflect the adsorption of a protective film over the surface of XC48 steel in the presence of each plant extract [25,27,28].

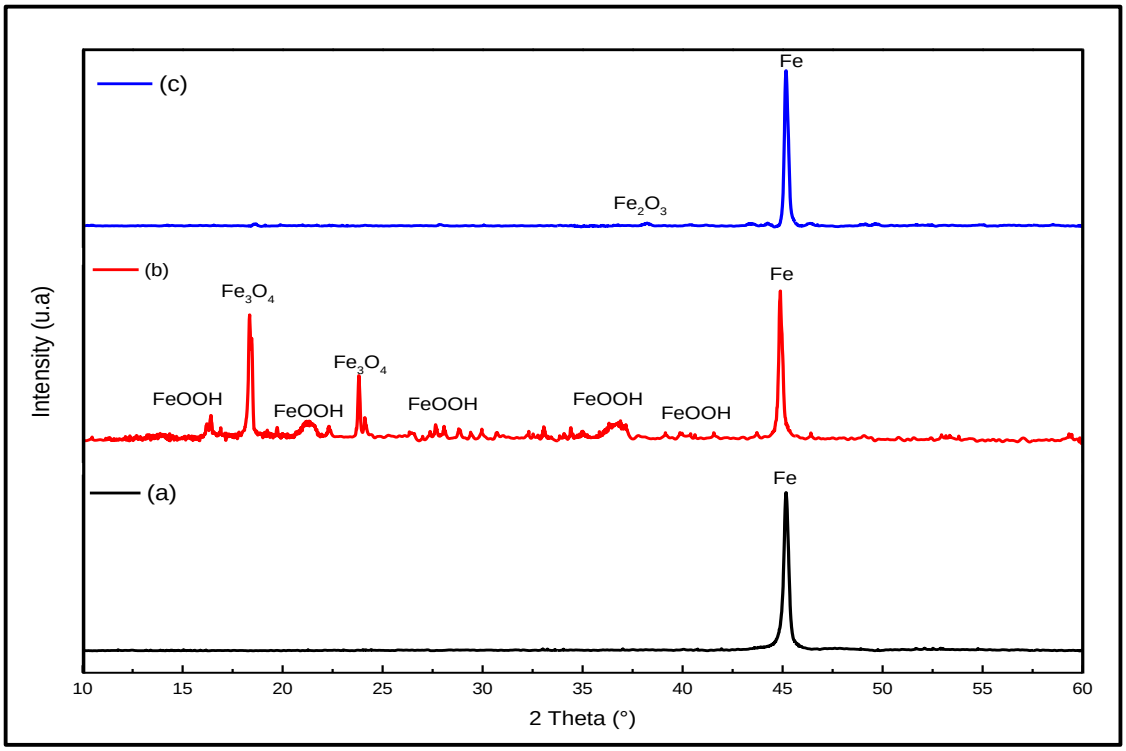

Figure III.14. X-ray diffraction pattern of XC48 steel; (a) before the experiment. (b) after 24 h of immersion in 1M H_2SO_4 solution and (c) after 24 h of immersion in 1M H_2SO_4 solution containing 500 ppm of the CMFE

X-ray diffraction (XRD) patterns of the stainless-steel surface of Alloy 304L immersed in 1M H_2SO_4 with and without the extract are shown side-by-side in Figure III.15. The ability to specify phase compositions is crucial for understanding corrosion processes (as opposed to elemental compositions). The phase compositions of damaged materials may provide insight into the corrosion process, allowing for the localization of the source of the corrosion within a facility and the identification of a feasible remedy [29]. The XRD pattern shows peaks at 44° related to Cr_2O_3 oxide, peak at 21° related to the $H_{15}Cr_1O_{15}S_2$ phase, peaks at 11°, 35° and 56° related to the FeOOH phase, and peaks at 23 ° and 33 ° related to $H_{3.5}Fe_1O_{3.25}$ phase as a result of the deterioration and breakdown of the 304L surface without the CMFE. The addition of the extract proves that iron oxide is not present. This result may be explained by the fact that CMFE extract has an inhibiting effect. It sped up the passivation process in 304L stainless steel and decreased the reactivity between anodic and cathodic species [30]. These findings show that a protective coating is being adsorbed onto the surface of the 304L stainless steel in the presence of each plant extract [31].

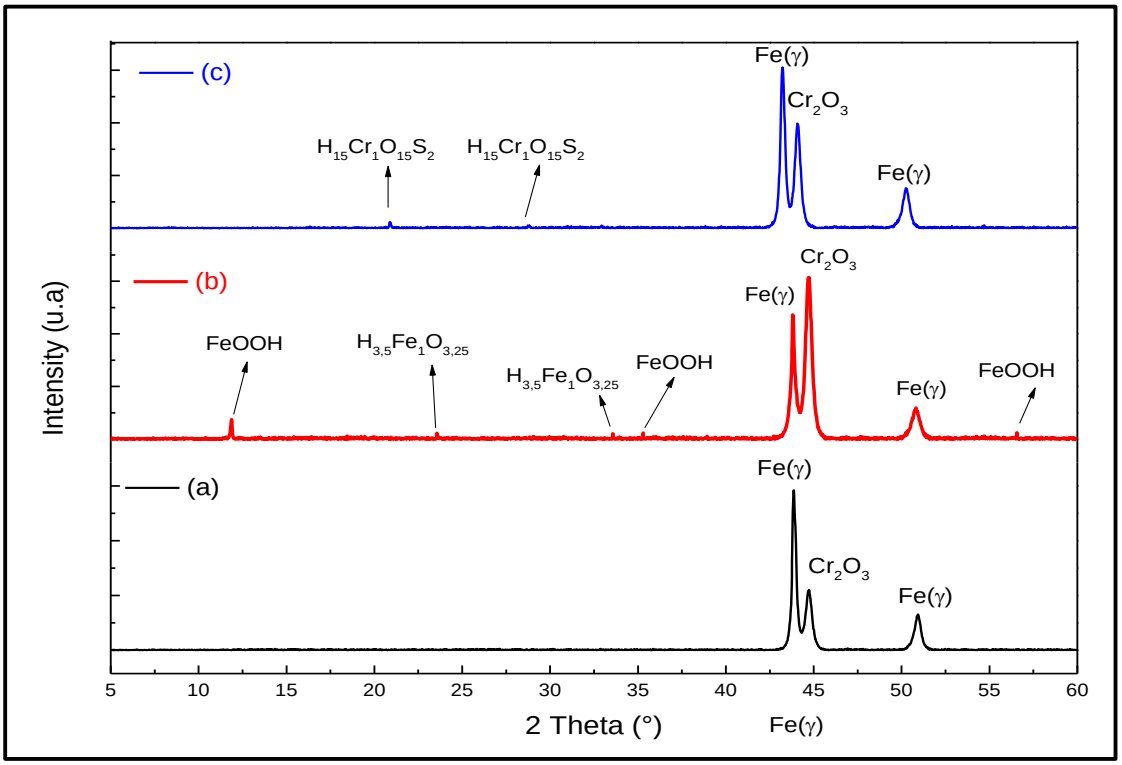

Figure III.15. X-ray diffraction pattern of 304L (a) before the experiment. (b) After 24 hours in 1M H_2SO_4 solution and (c) after 24 hours of immersion in a 1M H_2SO_4 with 500 ppm CMFE

III.2.4. XPS analysis

a. XPS analysis CMFE carbon steel

The XPS of the steel surface, which has been immersed in a solution of 1M H_2SO_4 in the presence of 500 ppm of CMFE for 24 hours, and of the analysis of the pure CMFE is shown in Figure III.16. The XPS spectra were obtained from pure CMFE (C 1s and O1s) and the CMFE-treated steel surface (C 1s, O 1s, S 2p and Fe 2p). The results from Table III.5 demonstrate a decrease in carbon content in pure CMFE at 73.29% to 44.18% in the metal surface treated by CMFE. These indicate the adsorption of CMFE on the steel surface. A deconvolution fitting procedure is used to represent complex forms for the related species in all XPS spectra are presented in Figure III.17.

The C1s core level spectra show four deconvoluted peaks. The first one assigned to the presence of –C=C / –C–C in aromatic rings [32], is located at 284.49 eV for pure CMFE (Figure III.17.a) and 284.58 eV for CMFE-treated carbon steel (Figure III.17.b). The second peak located at 286.03 eV for pure CMFE (Figure III.17.a) and 285.98 eV for both CMFE-treated carbon steel

(Figure III.17.b). can be attributed to the carbon atom bonded to hydrogen in C-H bonds [33] bonds and to sulfur in C-S bonds [34]. The third contribution appears at 287.42 eV and 287.08 eV for pure CMFE (Figure III.17.a) and CMFE-treated carbon steel (Figure III.17.a), respectively. These peaks correspond to the C-O with different intensities [13]. The peaks at 288.55 eV and 288.38 eV characterize the presence of a C=0 bond [35].

The deconvoluted O 1s spectrum for pure CMFE (Figure III.17.c) shows two main components at 531.15 eV and 533.33 eV, proving the presence of -C=O and–C–OH bonds, respectively [18]. The O 1s spectrum for CMFE-treated carbon steel could be fitted into four prominent peaks (Figure III.17.d). The first peak at 529.71 eV is attributed to oxygen in the Fe_2O_3 and/or Fe_3O_4 oxides bonded to Fe^{3+} [36]. The second peak at 530.60 eV is attributable to Fe-OH and Fe-O in the iron hydroxides and oxides [33]. The third peak at 531.31 eV. is attributed to the OH of FeOOH [36]. The latest peak can be due to the oxygen of the adsorbed water at 532.79 eV [37].

The S 2p high-resolution XPS spectra for XC48 steel after immersion in inhibited solution (Figure III.17.e) show one signal which corresponds to the doublet $2p_{3/2}$ and $2p_{1/2}$ in the 168.24 ev and 169.43 eV range characteristic of SO_4^{2-} ion [18].

The spectrum related to Fe 2p for CMFE-covered carbon steel surfaces shows two doublets (Figure III.17f). 710.58 eV (Fe $2p_{3/2}$) and 724.23 eV (Fe $2p_{1/2}$) related to high-energy ghost structures indicating subsequent steel surface oxidation. Three peaks constitute the deconvolution of the high-resolution Fe $2p_{3/2}$ XPS spectrum. The two prominent peaks at 710.41 eV and 712.76 eV are attributed to ferric compounds such as $Fe_2O_3/Fe_3O_4/FeSO_4$/FeOOH [37]. The last peak at BE=715.30 eV may be attributed to the Fe (III) satellite feature [38].

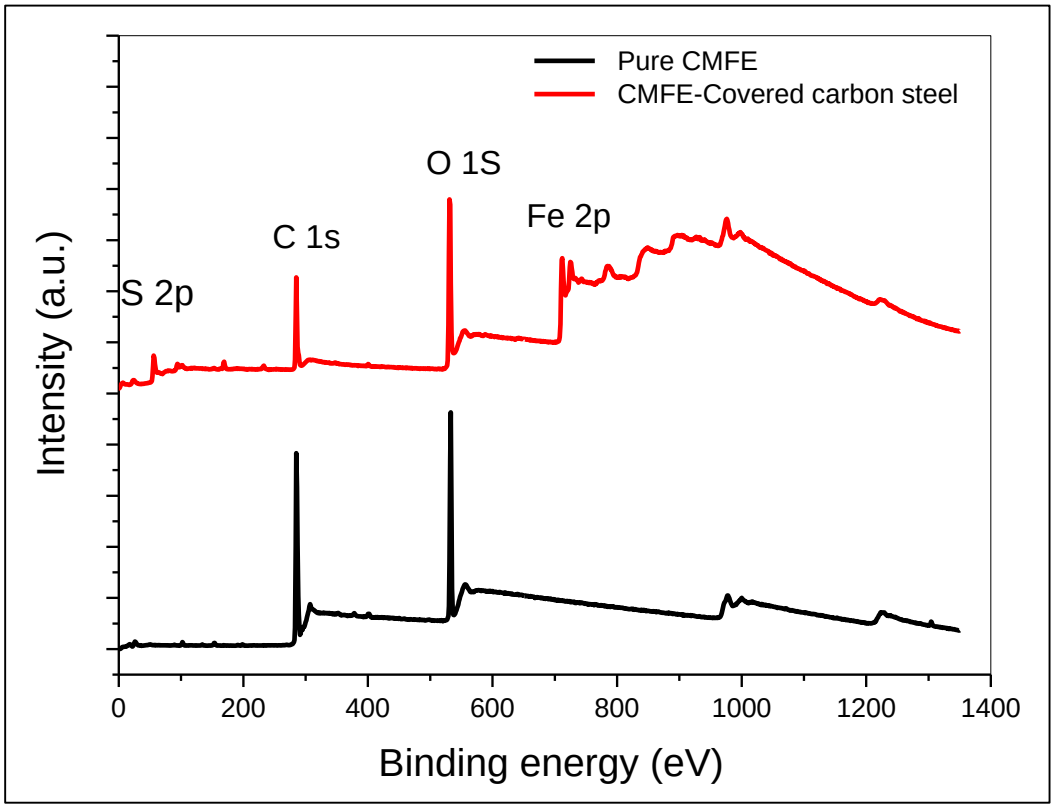

Figure III.16. XPS survey spectrum of pure CMFE and CMFE treated-carbon steel in 1M H_2SO_4.

Table III.5. The variation of the elemental composition of pure CMFE and CMFE-treated steel surface after 24h of immersion in 1M H_2SO_4.

Elemental composition (wt%)	C 1S	0 1S	Fe 2p	S 2p
CMFE	73.29	26.71	-	-
XC48- CMFE	44.18	40.53	13.14	2.15

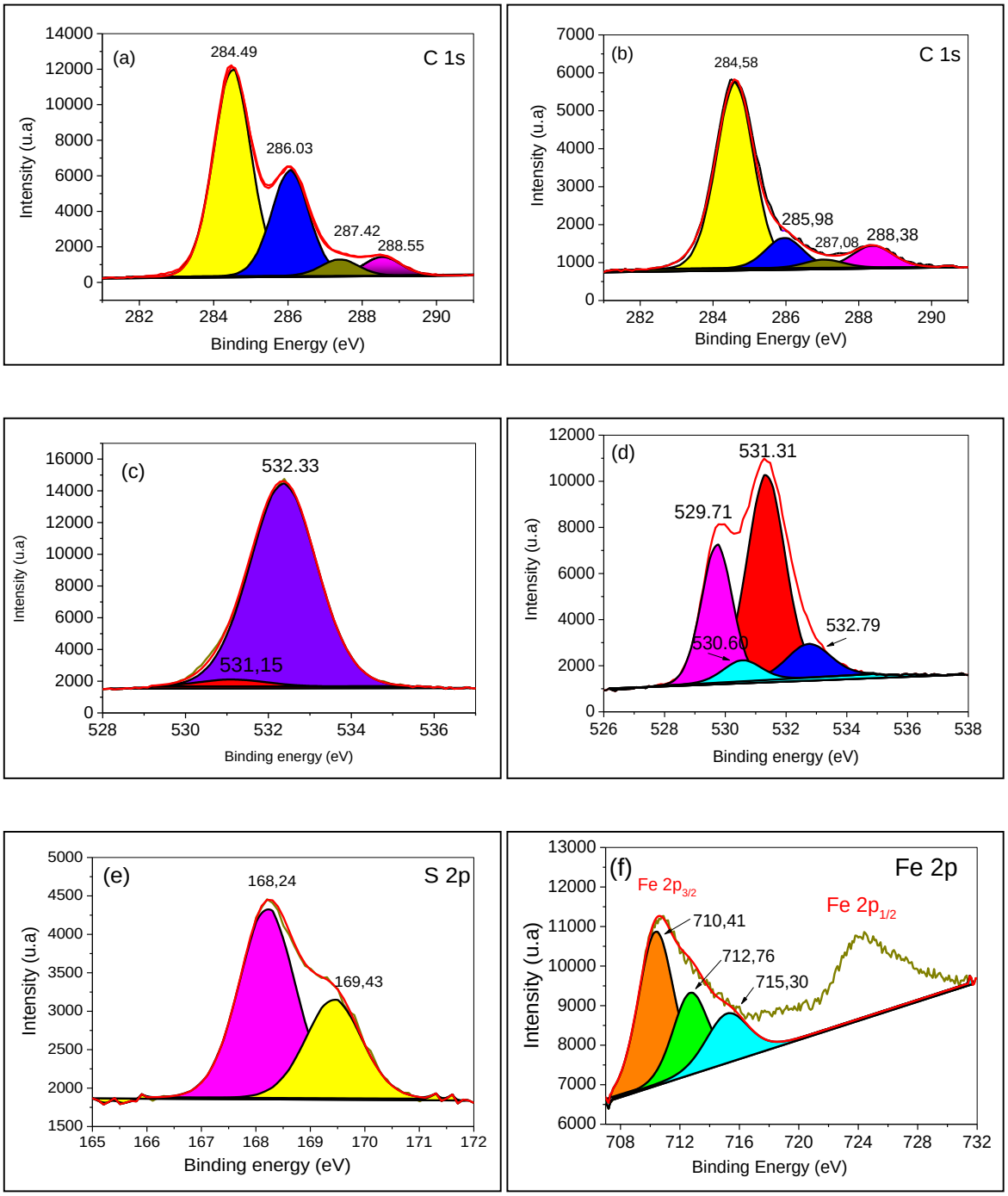

Figure III.17. The XPS deconvoluted profiles of pure CMFE (a) C 1s. (c) O 1s and for CMFE/Carbone steel (b) C 1s. (d) for O 1s. (e) S 2p and (f) Fe 2p1s. (e) S 2p and (f) Fe 2p

b. XPS analysis CMFE with 304L stainless steel

Figure III.18 displays the results of an XPS survey scan performed on pure CMFE and a 304L stainless steel (304L SS) surface treated with 500 ppm of CMFE at 298K after 24 hours of immersion in 1M H_2SO_4. Here we provide an X-ray photoelectron spectrum comparison of pure CMFE (C 1s and O 1s) and a CMFE-treated 304L SS surface (C 1s, O 1s, Cr 2p, Si 2p, Mn 2p, S 2p, and Fe 2p). After spraying CMFE over the surface of 304L SS, the carbon content dropped from 73.29 to 64.45 percent, as shown in Table III.6. As a result of these results, it is clear that CMFE has been adsorbed onto the surface of 304L SS. As seen in Figure III.18, using a deconvolution fitting approach, all XPS spectra display the intricate geometries characteristic of the related species.

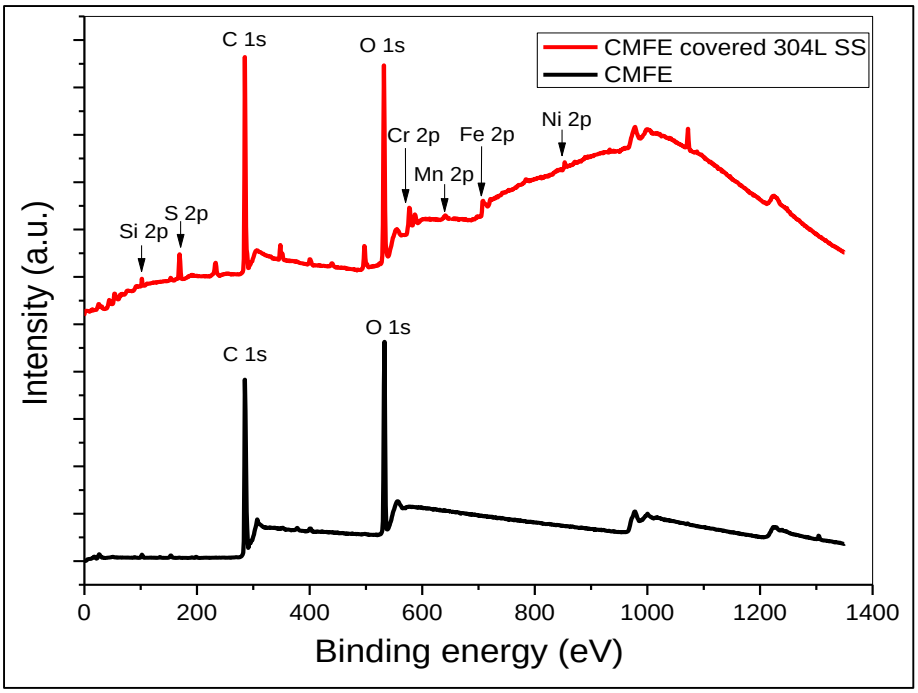

Figure III.18. XPS survey spectrum of pure CMFE and CMFE treated-304L stainless steel in 1M H_2SO_4.

Table III.6. Elemental composition after 24h of immersion in 1M H_2SO_4.

Elemental composition (wt%)	C 1s	0 1s	Cr 2p	Ni 2p	Si 2p	Mn 2p	S 2p	Fe 2p
Pure CMFE	73.29	26.71	-	-	-	-	-	-
CMFE-treated 304L SS surface	64.45	26.15	1.23	0.17	1.17	0.23	5.71	0.89

The spectrum of the C1s core level shows four distinct peaks. The presence of -C=C/-C-C in aromatic rings [39] places the first one at 284.49 eV for untreated CMFE (Figure III.19.a) and at 284.46 eV for CMFE-treated 304L stainless steel (Figure III.19.b). Carbon atoms bond to hydrogen as C-H [33] and to sulfur as C-S [34], accounting for the second peak at 286.03 eV for pure CMFE (Figure III.19.a) and 285.93 eV for both CMFE treated-304L stainless steel (Figure III.19.b). In pure CMFE (Figure III.19.a) and CMFE treated-304L stainless steel (Figure III.19.b), the third contribution emerges at 287.42 eV and 287.19 eV, respectively; these peaks correspond to the C-O with varying intensities [13]. The most recent peaks, at 288.55 eV and 288.45 eV, are indicative of the existence of a C=0 bond [35]. All the peaks mentioned above show that CMFE molecules were successfully adsorbed onto the 304L stainless steel surface.

Deconvolution of the O 1s spectra for pure CMFE (shown in Figure III.19.c) reveals two primary components at 531.15 and 533.33 eV, indicating the existence of -C=O and -C-OH bonds, respectively [18]. For CMFE-treated carbon steel, the O 1s spectra may be broken down into four peaks (Figure III.19.d). The oxygen atoms in Fe_2O_3 and/or Fe_3O_4 oxides bound to Fe^{3+} account for the first peak at 529.91 eV [36]. The OH of FeOOH is responsible for the second peak at 531.63 eV [36]. The latest peak at 533.55 eV [37] may be attributable to oxygen in the adsorbed water.

The XPS spectra of Cr 2p are shown in Figure III.19.e, with the strongest peak at a lower binding energy (577.52 eV) corresponding to chromium oxide (Cr_2O_3) and the second peak identified at 587.08 eV referring to chromium trioxide CrO_3 or potentially corresponding to metallic chromium [40].

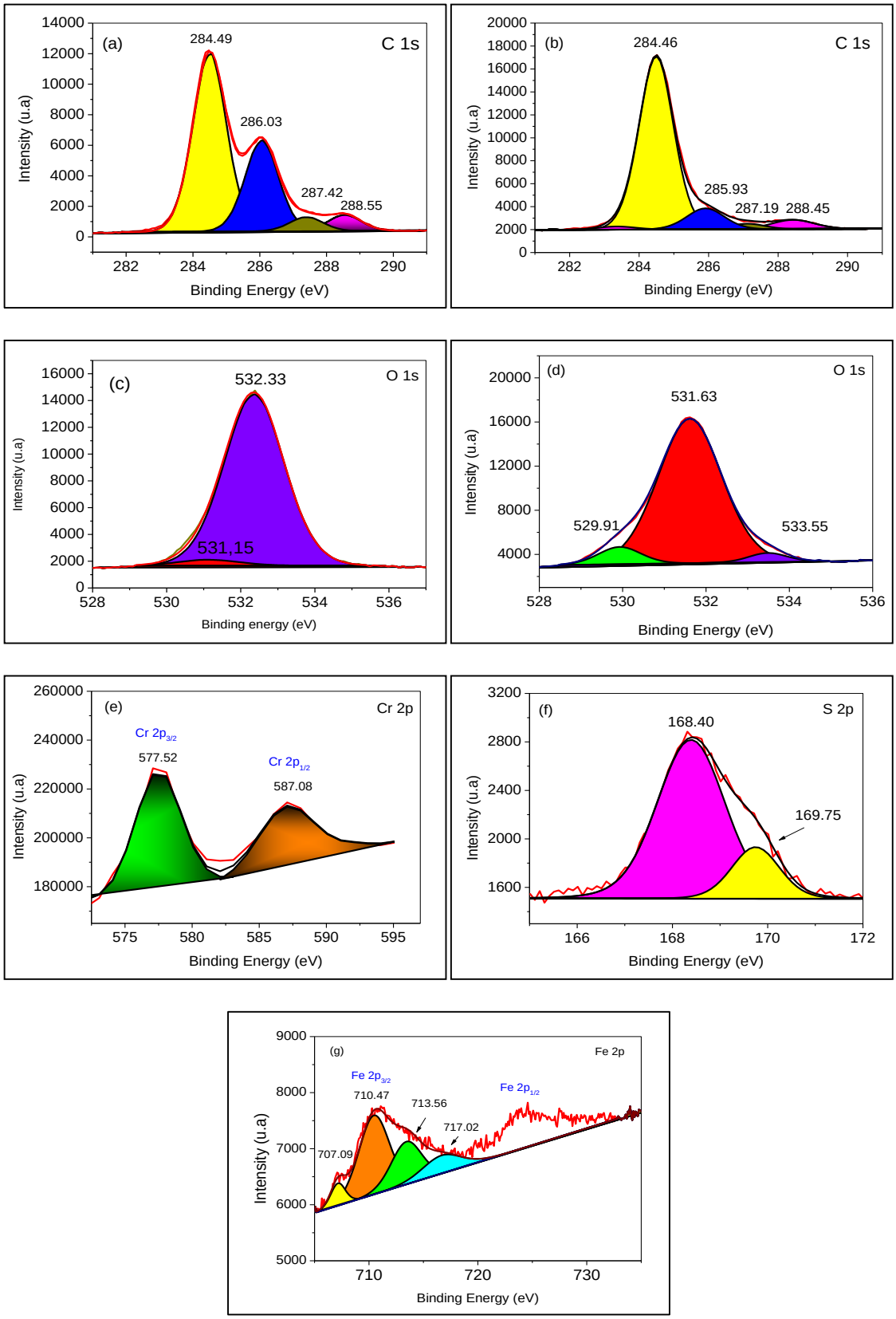

Figure III.19. The XPS deconvoluted profiles of pure CMFE (a) C 1s, (c) O 1s and for CMFE /304L stainless steel (b) C 1s, (d) for O 1s, Cr 2p (e) S 2p (f) and (g) Fe 2p

Part 2: Corrosion Inhibition Performance of Punica Granatum Peel Extract (PGPE) on Carbon Steel and 304L Stainless steel in Sulfuric acidic medium

III.3. Electrochemical measurements:

III.3.1. Polarization measurements:

The effect of the concentration of Punica granatum peel extract **(PGPE)** on the corrosion behavior of carbon steel in the 1M H_2SO_4 solution was studied by using anodic and cathodic polarization measurements after 30 min of the immersion time. Figure III.25 illustrates the potentiodynamic polarization curves for the alloy under study in the absence and presence of Punica granatum peel extract with different concentrations at 25°C.

As seen in the anodic branch (Figure III.20), we can point out the difficulty of recognizing the linear region of the Tafel law. Hence, the current densities are determined by extrapolating only the Tafel cathodic linear region to the corrosion potential. Several authors used This adjustment method for carbon steel materials in the hydrochloric acid medium [41].

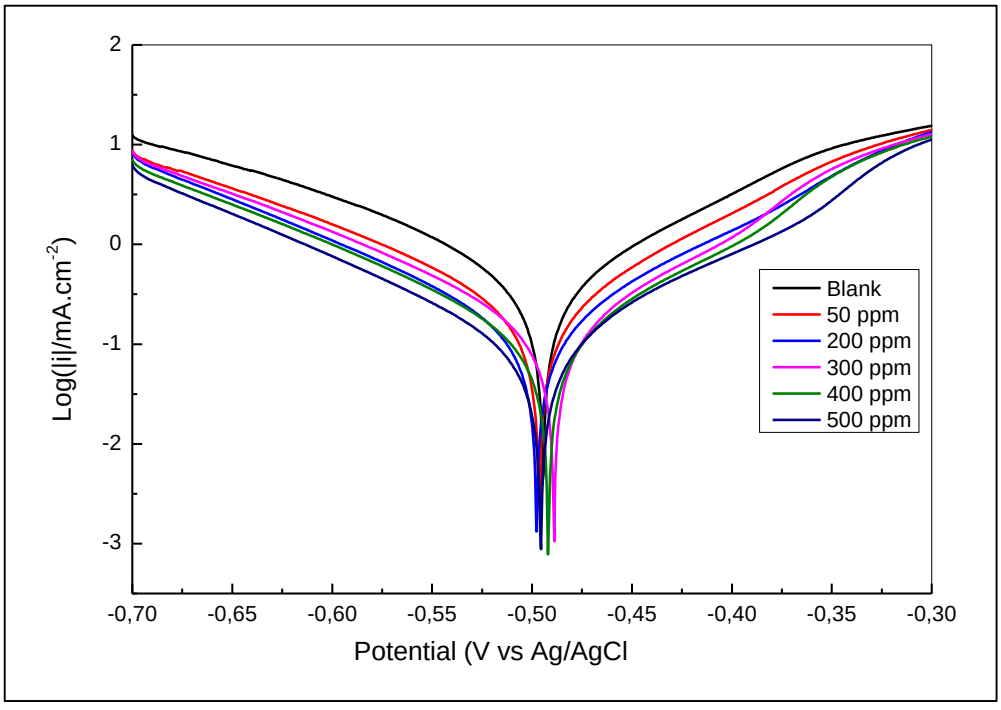

Figure III.20: Tafel polarization curves for XC48 carbon steel immersed in 1M H_2SO_4 with various concentrations of Punica granatum peel extract (PGPE).

The electrochemical corrosion kinetic data, such as corrosion potential (E_{corr}), cathodic and anodic tafel slopes (β_a, β_c), and corrosion current density i_{corr}, obtained by extrapolation of the tafel lines, are included in Table III.7.

Table III.7. Polarization parameters for carbon steel in 1M H_2SO_4 in Punica granatum peel extract (PGPE) absence and presence.

C (ppm)	E_{corr} (mV)	i_{corr} (mA.cm^{-2})	β_c (mV)	β_a (mV)	Corrosion rate (mmpy)	Rp (Ohm)	Correlation	Efficacity (%)
Blank	-494,493	517,48	139,9	116,7	12,0076	53,1	0,9999	
50 ppm	-507,013	245,391	131,3	111,3	5,69406	105	0,9995	49,4
200 ppm	-488,973	168,495	122,6	101,8	3,90976	138	0,9995	61,5
300 ppm	-497,697	158,738	121,1	99,8	3,68336	145	0,9996	63,3
400 ppm	-491,851	134,249	123,8	104,8	3,11512	177	0,9993	70
500 ppm	-495,625	112,807	125	109,7	2,61758	218	0,9992	75,6

It can be seen that the corrosion rate is reduced and ***IE*** is increased by increasing the concentration of the inhibitor [42]. Extracts at different concentrations lead to different anodic and cathodic tafel slopes and E_{corr} values, suggesting that these compounds behave as mixed-type (anodic/cathodic) inhibitors [43]. Increasing inhibition efficiency with increasing extract concentration shows inhibition occurs because of adsorption on the carbon steel surface [44]. It is clear from Table III.7 that the tafel cathodic slope (β_c) changes slightly in the presence of the Punica granatum peel extract, which outlines no significant effect of Punica granatum peel extract on the hydrogen reduction mechanism. Such a conclusion can be revealed in Figure III.20 from which the cathodic polarization curves are almost parallel. On the other hand, it is found that the value of I_{corr} decreases with the addition of the Punica granatum peel extract, which induces an increase in the inhibition efficiency as a function of the Punica granatum peel extract concentration. This is due to the increased blocked fraction of the alloy surface by adsorbing the active components in Punica granatum peel extract.

The representative potentiodynamic polarization curves of the 304L stainless steel electrode, obtained in 1M H_2SO_4 solution for various concentrations of Punica granatum peel extract, are summarized in Table III.8. Numerical values of corrosion variation current density (i_{corr}), corrosion potential (E_{corr}), Tafel anode slope (β_a), Tafel cathode slope (β_c), and percent efficiency.

Table III.8. Polarization parameters for 304 L stainless steel corrosion in 1M H_2SO_4 in the absence and presence of Punica granatum peel extract (PGPE)

	E_{corr} (mV)	i_{corr} (mA.cm^{-2})	βc (mV)	βa (mV)	corrosion rate (mmpy)	Rp (Ohm)	correlation	Efficacity (%)
Blank	-426,621	86,28	87,7	92,2	1,7769	181		
100 ppm	-363,712	17,579	91,2	32,8	0,362	469	0,9547	79,625
200 ppm	-364,25	16,811	93,1	33,6	0,3462	672	0,9843	80,515
300 ppm	-380,98	10,802	122,5	142,5	0,2224	1422	0,9998	87,48
400 ppm	-375,65	5,958	98,7	89,4	0,1227	2595	0,9997	93,094
500 ppm	-368,488	5,901	71,4	35,3	0,1215	3291	0,973	93,16

This shows that adding Punica granatum peel extract reduces the anodic dissolution and delays the hydrogen evolution reaction, indicating that PGPE extract is a mixed-type inhibitor and controls both: Anodic and cathodic reactions. Adding 500 ppm concentrations of PGPE extracts reduced (i_{corr}) from 130,253 µA to 9,39 µA. The anodic and cathodic Tafel slopes (β_a and β_c).

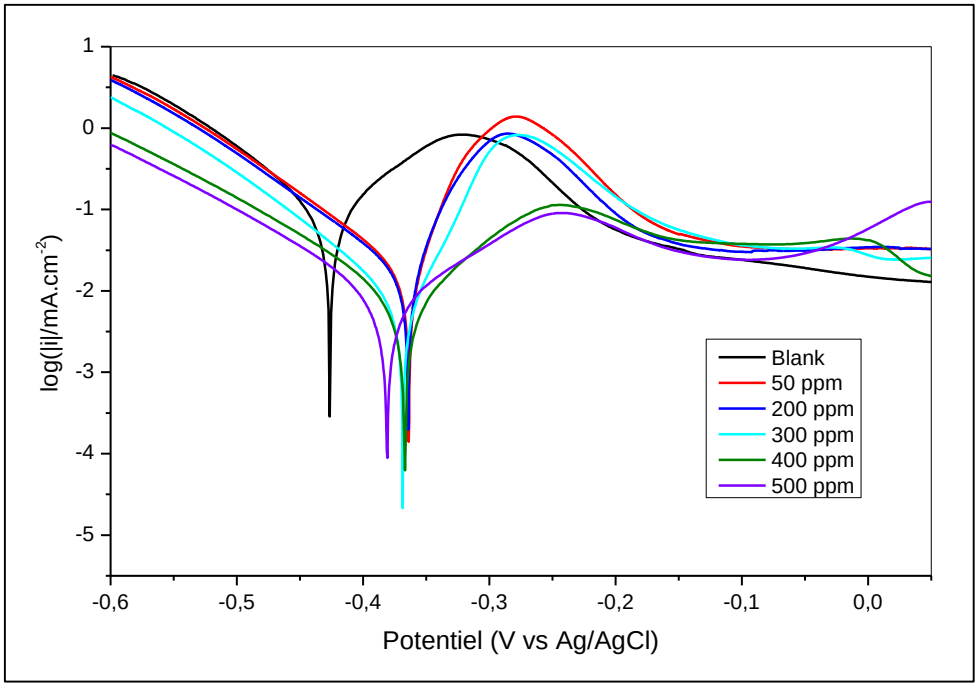

Figure III.21. Tafel polarization curves for 304L stainless steel immersed in 1 M H_2SO_4 with various concentrations of Punica granatum peel extract

These results indicate that Punica granatum peel extract increases inhibition efficiencies for 500 ppm and attainted 92,78% and reveals that the inhibition action is due to adsorption on the surface of the 304L stainless steel, and the adsorption is known to depend on the structure extract chemical. By comparing polarization curves (Figure III.21), we see that they change from one concentration to another, which may be due to the structure of the constituents of the PGP extract.

III.3.2. Electrochemical impedance spectroscopy (EIS)

III.3.1.a. EIS of carbon steel in 1M H_2SO_4 with and without PGPE

The Nyquist diagrams for studied carbon steel in 1M H_2SO_4 medium at 25°C, in the absence and presence of different Punica granatum peel extract concentrations, were plotted in E_{OCP} potential after 30 min of immersion as depicted in Figure III.22. It is evident from this figure that the impedance diagrams consist of a large capacitive loop at high frequency followed by an inductive loop at low frequency. In addition, the inductive semicircle diameter is considerably less than that observed in high frequencies. On the other hand, the impedance spectrum shows an approximately elliptical shape that is attributed to the frequency dispersion due to the roughness and inhomogeneity of the metal surface [45].

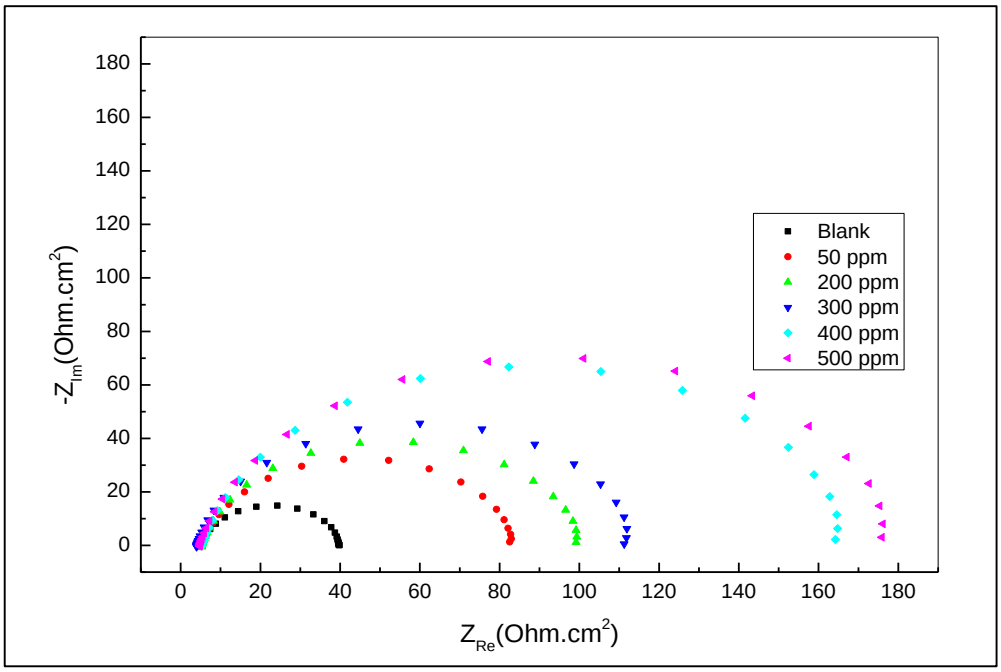

Figure III.22: Nyquist plot of carbon steel immersed in 1M H_2SO_4 solution without (Blank) and with different Punica granatum peel extract concentrations.

In the acidic media, similar impedance spectra have been reported in the corrosion literature for carbon steel and its alloys [46]. The addition of the Punica granatum peel extract does not affect the shape of the loops, indicating that no change in the corrosion mechanism of carbon steel has occurred. The impedance data is simulated using the equivalent circuit illustrated in Figure III.23. The components of this circuit are the electrolyte resistance (*R*s), charge transfer resistance (*Rt*), and constant phase element (CPE) for the used electrode, and *L* and *RL* represent the inductance and the inductive resistance associated with the inductive loop, respectively. Accordingly, the calculated impedance parameters are given in Table III.9.

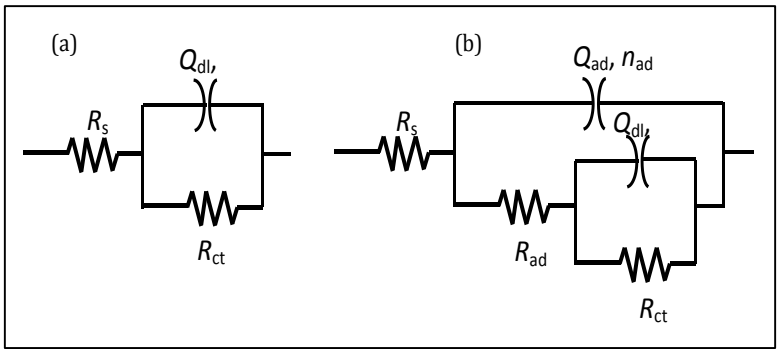

Figure III.23. Equivalent electric circuit (a) without inhibitor (Blank). (b) Solution containing diverse quantities of Punica granatum peel extract (PGPE).

As shown in Figure III.23 and from the values of χ^2 in Table III.5, a good fit by using the chosen equivalent circuit was obtained. This means that the adjusted data have good agreement with the experimental data. According to Table III.9, the *Rt* values increase with increasing Punica granatum peel extract concentration, resulting in an increase in IE attributed to the increase in organic inhibitory molecules (i.e., alkaloids) adsorbed on the surface of carbon steel. ***IE*** attains a maximum value equal to 82,50%, which confirms that Punica granatum peel extract has a good protection ability for carbon steel in 1M H_2SO_4 medium. The ***IE*** values computed from the EIS measurements agree with those found by the potentiodynamic technique. Besides, conferring to the obtained ***Q*** values in the presence of the tested inhibitor, it can be assumed that the Punica granatum peel extract active constituents were adsorbed onto the alloy surface to form a protective layer [47].

Table III.9. EIS parameters for carbon steel immersed in 1M H_2SO_4 solution without (Blank) and with different concentrations of Punica granatum peel extract (PGPE)

	R_S (Ohm)	R_{ct} (Ohm)	n_{dl}	Q_{dl} ($F.s^{nf-1}.cm^{-2}$)	R_{ad} (Ohm)	n_{ad}	Q_{ad} ($F.s^{nf-1}.cm^{-2}$)	IE (%)
Blank	2,775	30,67	0,875	1,50E-04				
50 ppm	4,061	74,35	0,861	6,92E-05	1,90	1	1,08E-03	58,75
200 ppm	5,287	95,71	0,869	1,10E-04	0,026	1	1,98E-02	67,96
300 ppm	4,012	109,9	0,878	7,10E-05	0,279	1	1,72E-03	72,09
400 ppm	5,267	162,7	0,868	7,85E-05	0,976	0,958	6,59E-04	81,15
500 ppm	4,73	175,3	0,863	6,11E-05	0,621	0,984	8,58E-03	82,50

III.3.2.b. EIS of 304L stainless steel in 1M H_2SO_4 with and without PGPE

Electrochemical impedance spectroscopy was used to determine the behavior of the metal/solution interface in the absence and presence of inhibitors. The representative Nyquist plots of the 304L stainless steel electrode were obtained in 1M H_2SO_4 solution in the absence and presence of various concentrations of PGP extract.

It is clear that the diameter of the half circle increases with increasing concentration of the extract, at a maximum value of 95,87% in 1 M H_2SO_4, which indicates an increase in the corrosion resistance of the metal.

In addition, the highest concentration of PGPE inhibitor (500 ppm) results in a much larger half-circle diameter than the other four lower concentrations of PGPE shown in Figure III.24. These diagrams have a similar shape in all tested concentrations, indicating that almost a change in the corrosion mechanism occurs due to the addition of inhibitors [48]. The circuit consists of a constant phase element (CPE) Q, in parallel with a resistor Rct presented in Figure III.25. The use of a CPE type impedance has been widely described [49-51]: n -1 Z_{CPE} [Q(jw)] the equation above provides information on the degree of non-ideality in capacitive behavior. Its value makes it possible to differentiate the behavior of an ideal capacitor (n = 1) and a CPE (n <1) [52].

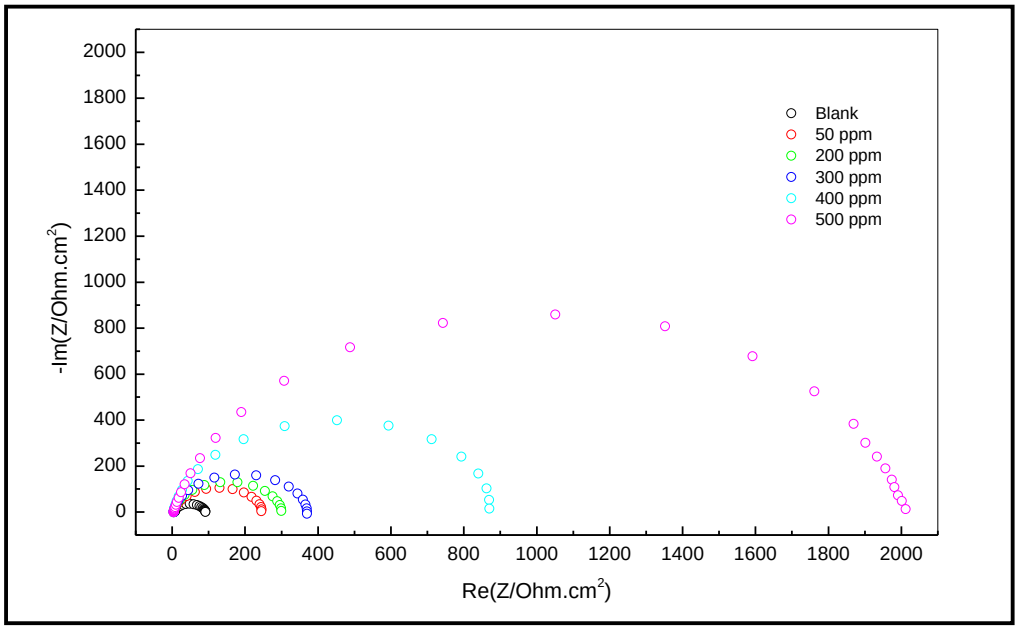

Figure III.24. Nyquist plots of the 304L immersed in 1M H_2SO_4 with various concentrations of PGPE

Impedance data of 304L stainless steel in 1M H_2SO_4 medium without and with different concentrations of the PGPE extract for the concentrations extracted in 1M H_2SO_4 medium are recorded and presented in Tables III.16 and respectively; it can be seen that the presence of PG improves the values of Rct and reduces the Cd1 values. The decrease in Cd1 is due to the adsorption of PGPE on the metal surface to form an adhesive film. It suggests that the coverage of the metal surface with this film decreases the local dielectric constant and/or increases the thickness of the double -3 layer mentioned in the work done [53-55].

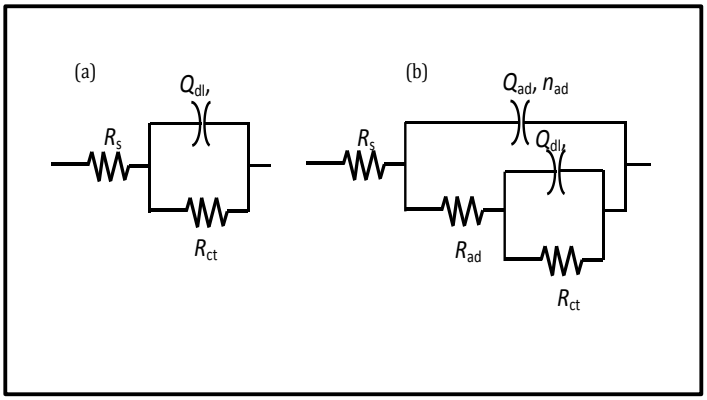

Figure III.25. Equivalent electric circuit (a) without inhibitor (Blank). (b) Solution containing diverse quantities of Punica granatum peel extract.

Table III.16. EIS parameters of impedance for 304L stainless steel in 1M H_2SO_4 with and without PGPE extract concentration.

	R_S (Ohm)	R_{at} (Ohm)	n_{dl}	Q_{dl} ($F.s^{nf-1}.cm^{-2}$)	R_{ad} (Ohm)	n_{ad}	Q_{ad} ($F.s^{nf-1}.cm^{-2}$)	*IE %*
Blanc	6,846	84,12	0,906	0,2096				
50 ppm	4,358	242,9	0,910	1,10E-04	0,7243	0,943	2,42E-06	65,368
200 ppm	4,582	295,8	0,929	1,49E-04	0,132	0,499	1,85E-04	71,561
300 ppm	4,522	366,3	0,934	1,61E-04	0,283	0,950	2,85E-09	77,035
400 ppm	3,878	891,9	0,918	6,34E-05	0,2562	0,724	7,93E-03	90,568
500 ppm	2,085	2037	0,880	4,98E-05	0,7496	0,936	3,69E-03	95,87

III.4. Surface characterization

III.4.1. SEM Observations

The SEM images of corroded carbon steel and 304L stainless steel surface examined the effect of inhibitors on the corrosion process. Figure III.26 and Figure III.27 show the SEM image of carbon steel and 304L stainless steel samples after 24 hours of immersion in 1M H_2SO_4 solution in the absence and presence of inhibitors. This micrograph reveals that the metal surface was strongly damaged in the absence of the inhibitor due to the metal dissolution in an aggressive solution, and many cracks with high depth were distributed all over the surface (Figure III.26.a).

Examination of Figure III.26.a and Figure III.27.a observed that the very strong corroded (crack and pits) and uneven (heavy damage) metal surface was obtained when the metal was immersed in 1M H2SO4 without inhibitor. In the presence of inhibitor Punica granatum peel extract 500 ppm, the metal surface shows Figure III.26.b and Figure III.27.b smoother (carbon steel surface and 304L stainless steel are covered with the protective layer formed by the inhibitor) with clear different morphology (surface covered means no pits and cracks). However, the corrosion rate is reduced in inhibited solutions because the electrode surface is almost corrosion-free due to the inhibitor's adsorption on the carbon steel surface and 304L surface.

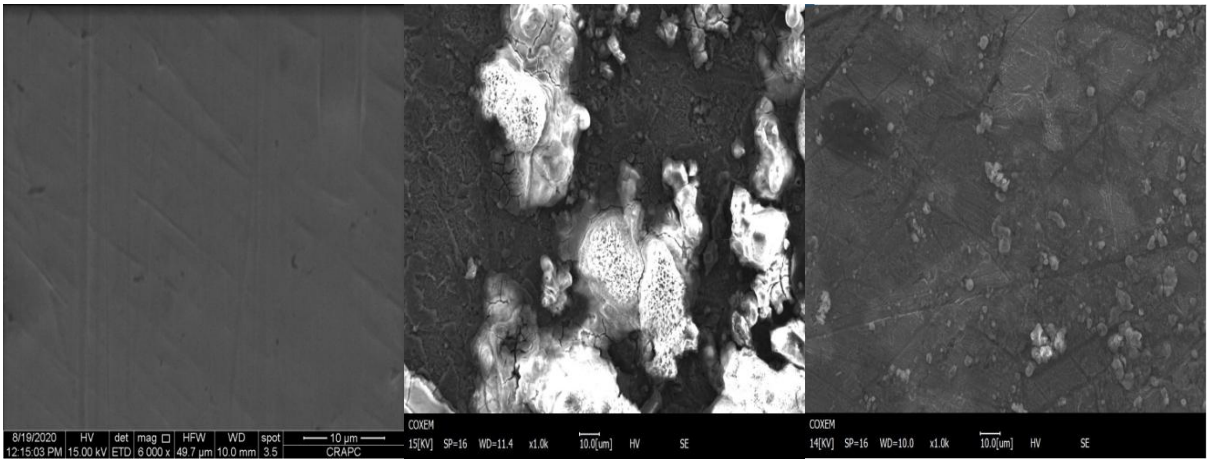

(a) **(b)** **(c)**

Figure III.26. SEM images of the carbon steel surface: a) showing a polished surface,(b) immersion in 1M H_2SO_4. c) After immersion in1M H_2SO_4 containing 500 ppm of PGPE

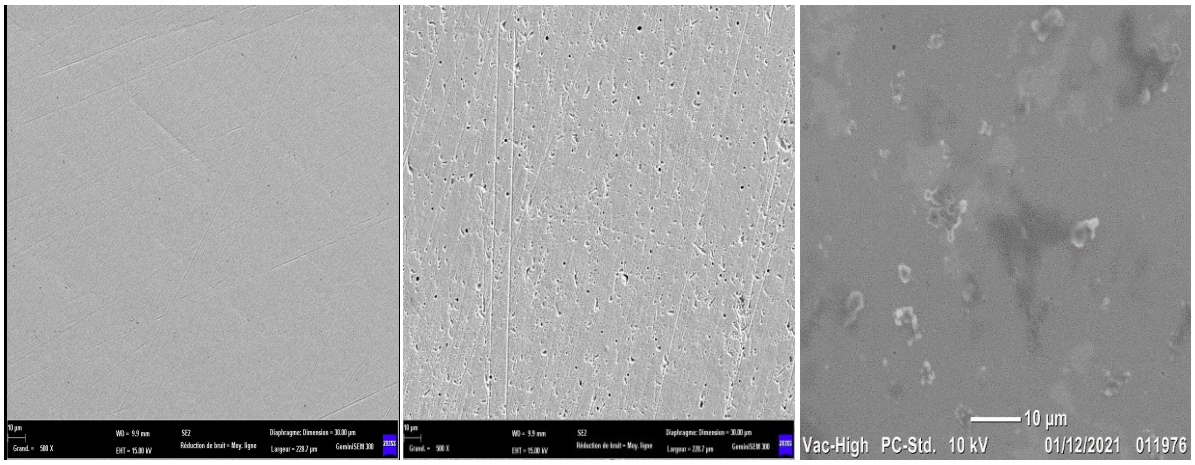

(a) (b) (c)

Figure III.27. SEM images of the 304L surface: a) showing a polished surface, b) immersion in 1M H_2SO_4. c) After immersion in 1M H_2SO_4 containing 500 ppm of PGPE.

III.4.2. Fourier transform infrared spectroscopy

FTIR analyses were achieved on the pure extract (PGPE) and the surface protective film developed on the XC 48 steel after immersion in 1M H_2SO_4 acid solution at the optimum concentration. However, the FTIR was used to predict the functional group present in the PGPE extract (Fig.III.28.a and Fig.III.29.a), and then compared with spectra of the surface protective film (Fig.III.28.b and Fig.III.29.b).

FTIR spectra of PGP extract (Fig.III.28.a and Fig.III.29.a), which contain bands corresponding to 3346.33 cm^{-1}, 3229.04 $cm^{-1,}$ can be assigned to the hydroxyl group (O─H stretch) and a strong band around 1707.47 cm^{-1} which reveal the presence of carbonyl (C=O) stretching vibration respectively [56-57]. Peaks at 2924.44 cm^{-1} and 2852.94 cm^{-1} indicate

carboxylic acids stretch alkane (C─H). The peaks at 1608.8 cm^{-1} and 1507.26 cm^{-1} C=C aromatic compounds. The peak at 1444.34 cm^{-1} C=C, 1317.07 cm^{-1} O─H. The peak at 1174.06 cm^{-1} indicates the presence of C─F, and 1029.63 cm^{-1} indicates the C─ OH bonding in alcohols [58]. The 875 cm-1 and 579.16 cm-1 peaks correspond to the C─H group of alkanes [59].

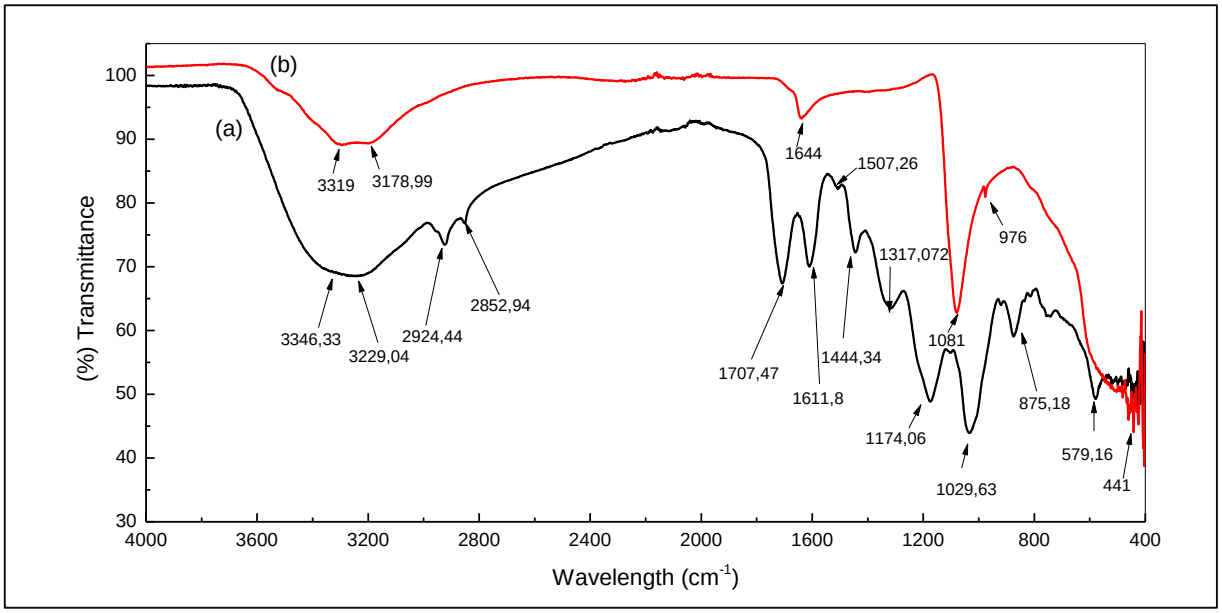

Figure III.28. FTIR spectra: (a) PGPE and (b) surface of XC48 steel after immersion in 1M H_2SO_4 solution containing 500 ppm of PGPE.

The FTIR spectrum of the thin film formed on the surface of the XC 48 carbon steel after immersing the coupon in 1M H_2SO_4 containing 500 ppm of PGPE for 24 hours is shown in Figure III.28.b. The spectrum has a bond at 3319 and 3178.99 cm^{-1} due to the O─H hydroxyl group and 1644 cm^{-1} corresponding to the C=C bond [59-60]. The peak at 1081 cm^{-1} is due to the oxygen atom present in the aromatic ring. The peak observed at 441 cm^{-1} is attributed to the bending of the C─H group of alkanes. Phytochemicals present in the Punica granatum peel extract contain heteroatoms, which are believed to get adsorbed on the surface of the steel substrate making bonds with Fe^{2+} ions and thus acting as a potent corrosion inhibitor [61].

FTIR was used to examine the purity of the PGP extract and the protective layer formed on the surface of the 304L stainless steel after being immersed in a 1M H2SO4 acid solution for 24 hours. FTIR was used to predict the functional group in PGP extract (Fig.III.29.a), and compared to the spectra of surface protective films (Fig.III.29.b).

Figure III.29.b shows that there is a presence of the compound of PGP extract pure in the protective film on the surface of the 304L samples immersed in the H_2SO_4 solution in the presence of the PGP extract of 500 ppm with a low transmittance intensity in some peak.

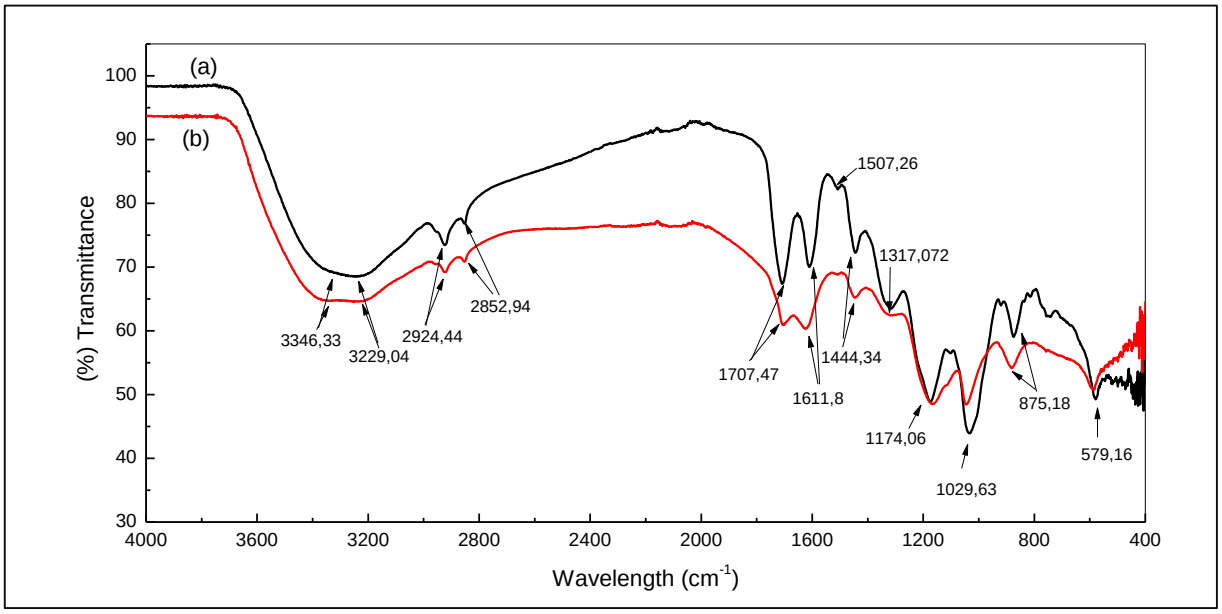

Figure III.29. FTIR spectra: (a) PGPE and (b) surface of 304L after immersion in 1M H_2SO_4 solution containing 500 ppm of PGPE.

III.4.3. X-ray diffraction

X-ray diffraction was carried out to determine the film product formed on the surface of XC48 steel. XRD analysis reveals the presence of a peak at 2θ of 44.7° associated to the iron phase (Figure III.30.a). The XRD diffractogram of the corrosion product formed on the steel surface immersed in 1M H_2SO_4 solution is shown in Figure III.30.b. The presence of peaks at 22.34°, 16.22°, and 26.16° suggest the formation of Fe_3O_4 iron oxide, FeOOH, and a very small amount of brown film, which is related to Fe_2O_3 observed visually and, therefore, leads to corrosion [25-26]. Figure III.30.c XRD diffractogram of XC48 steel immersed in 1M H_2SO_4 solution containing 500 ppm of PGPE. Compared to the sample surface immersed in 1M H_2SO_4 solution without inhibitor which presented three types of iron oxides (Fe_2O_3, Fe_3O_4 and FeOOH), this sample presents a very weak Fe_2O_3 peak, which corresponds to a slight corrosion of the XC48 steel in the presence of inhibitor. These results reflect the adsorption of a protective film on the surface of XC48 steel in the presence of plant extracts [25, 27-28].

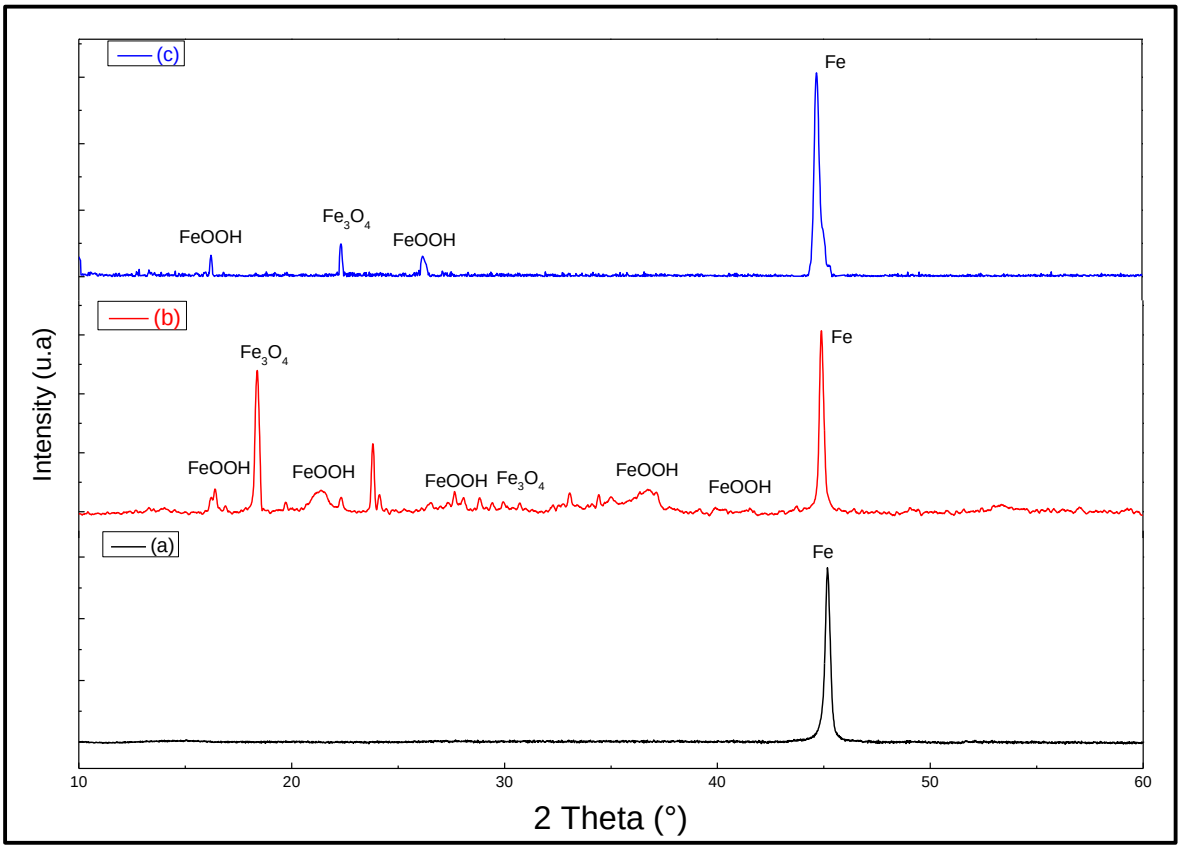

Figure III.30. XRD diffractogram of XC48 steel; (a) Before experiment. (b) After 24 h of immersion in 1M H_2SO_4 solution. (c) After immersion in 1M H_2SO_4 with 500 ppm of PGPE.

X-ray diffraction diffractograms of 304L stainless steel immersed in 1M H_2SO_4solution with and without plant extract are shown in Figure III.31. It is well known that determining phase compositions is essential for understanding corrosion processes (as opposed to elemental compositions). The phase compositions of corroded materials may offer insight into the corrosion process, permitting the localization of corrosion sources within a facility and the identification of a good remedy [29]. The XRD pattern shows peaks at 44° related to Cr_2O_3 oxide, peak at 21° related to $H_{15}Cr_1O_{15}S_2$ phase, peaks at 11°, 35° and 56° related to $HFeO_2$ phase and peaks at 23 ° and 33 ° related to $H_{3.5}Fe_1O_{3.25}$ phase as a result of the deterioration and breakdown of the 304L surface without the PGPE.

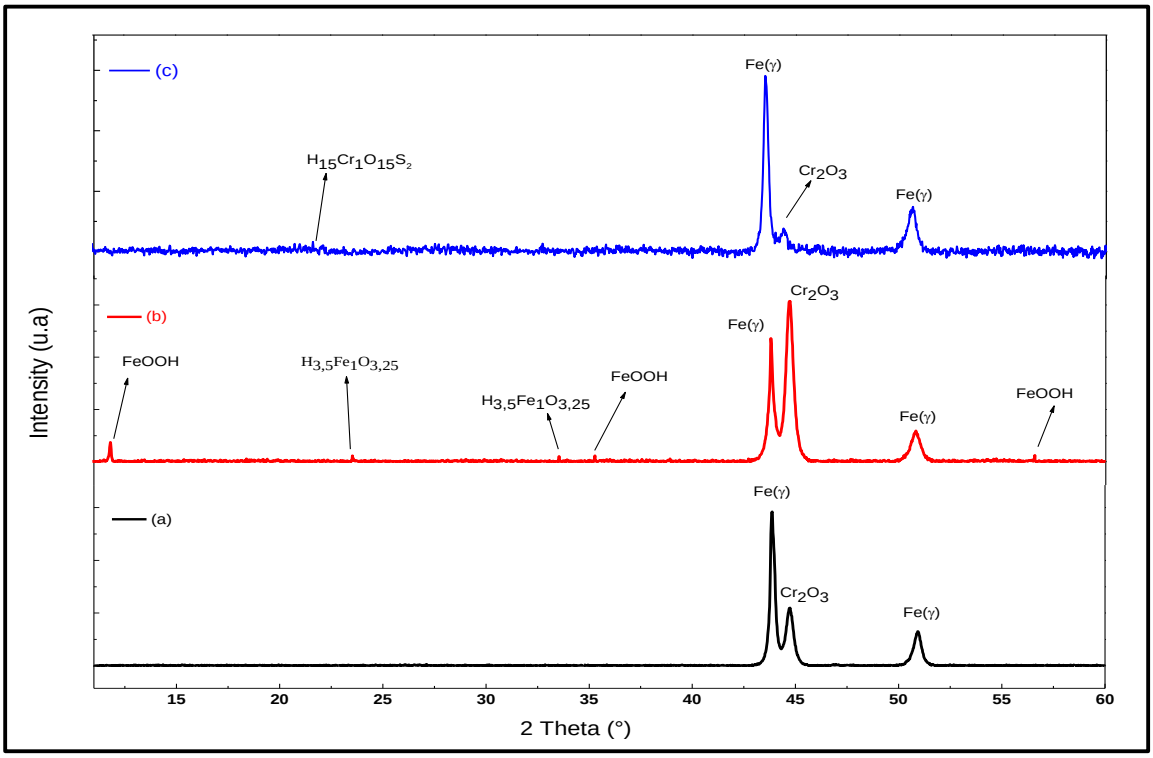

Figure III.31.X-ray diffractogram of 304L stainless steel: (a) Before the experiment. (b) After immersion in 1M H_2SO_4 solution. (c) After immersion in a 1M H_2SO_4 with 500 ppm PGPE

The addition of the plant extract to the solution significantly affects the corrosion process; the absence of iron oxide explains this. As a result, the PGPE extract has an inhibiting effect. It accelerates the passivation process of 304L stainless steel and decreases the reactivity between anodic and cathodic species [30]. These findings show that a protective film was adsorbed onto the surface of the 304L stainless steel in the presence of plant extract [31].

III.5. Conclusion

After the electrochemical study and analysis of the results, we found that the two plant extracts (PGPE and CMFE) inhibit the corrosion of the two metals (XC48 and 304L stainless steel). The results of the analyzes using the infrared spectrum and microscopic scanning showed the presence of the two extracts compounds on the surfaces.

Reference

[1] M. Abdallah, H. M. Altass, A. S. Al-Gorair, J. H. Al-Fahemi, B. A. A. L. Jahdaly, et K. A. Soliman, « Natural nutmeg oil as a green corrosion inhibitor for carbon steel in 1.0 M HCl solution: Chemical, electrochemical, and computational methods », *J. Mol. Liq.*, vol. 323, p. 115036, févr. 2021, doi: 10.1016/j.molliq.2020.115036.

[2] L. Boucherit, T. Douadi, N. Chafai, M. Al-Noaimi, et S. Chafaa, « The inhibition Activity of 1,10 -bis(2-formylphenyl)-1,4,7,10- tetraoxadecane (Ald) and its Schiff base (L) on the Corrosion of Carbon Steel in HCl: Experimental and Theoretical Studies », *Int. J. Electrochem. Sci.*, vol. 13, mars 2018, doi: 10.20964/2018.04.59.

[3] Jun Tang *et al.*, « Electrochemical Behavior of Jasmine Tea Extract as Corrosion Inhibitor for Carbon Steel in Hydrochloric Acid Solution », *Int. J. Electrochem. Sci.,* p. 3625‑3642, 2018.

[4] P. B. Raja et M. G. Sethuraman, « Natural products as corrosion inhibitor for metals in corrosive media—a review », *Mater. Lett.*, vol. 62, n° 1, Art. n° 1, 2008.

[5] A. Belakhdar *et al.*, « Computational and experimental studies on the efficiency of Rosmarinus officinalis polyphenols as green corrosion inhibitors for XC48 steel in acidic medium. », 2020.

[6] J. Aljourani, K. Raeissi, et M. A. Golozar, « Benzimidazole and its derivatives as corrosion inhibitors for mild steel in 1M HCl solution », *Corros. Sci.*, vol. 51, n° 8, Art. n° 8, 2009.

[7] H. Ferkous, S. Djellali, R. Sahraoui, Y. Benguerba, H. Behloul, et A. Çukurovali, « Corrosion inhibition of mild steel by 2-(2-methoxybenzylidene) hydrazine-1-carbothioamide in hydrochloric acid solution: Experimental measurements and quantum chemical calculations », *J. Mol. Liq.*, vol. 307, p. 112957, juin 2020, doi: 10.1016/j.molliq.2020.112957.

[8] B. E. A. Rani et B. B. J. Basu, « Green Inhibitors for Corrosion Protection of Metals and Alloys: An Overview », *International Journal of Corrosion*, 26 septembre 2011. https://www.hindawi.com/journals/ijc/2012/380217/ (consulté le 7 novembre 2020).

[9] Z. Panossian, N. L. de Almeida, R. M. Ferreira de Sousa, G. de Souza Pimenta, et L. B. Schmidt Marques, « Corrosion of carbon steel pipes and tanks by concentrated sulfuric acid », *Corrosion Science*, p. 1‑11, 2012.

[10] W. Ebdelly, S. Ben Hassan, X. R. Novoa, et Y. Ben Amor, « Inhibition of carbon steel corrosion in calcareous chloride solution by Eruca Sativa extract », *Physicochemical problems of materials protection*, p. 519‑602, 2019.

[11] Y. Ben Amor *et al.*, « Electrochemical study of the tarnish layer of silver deposited on glass », *Electrochimica Acta*, p. 89, 2014.

[12] H. Lahbib, S. Ben Hassen, H. Gerengi, et Y. Ben Amor, « Inhibition effect of Cynara cardunculus leaf extract on corrosion of St37 steel immersed in seawater with and without bleach solution », 2020.

[13] Nor Zakiah Nor Hashim, El Hassane Anouar, Karimah Kassimc, Hamizah Mohd Zaki, Abdulrahman I. Alharthi, et Zaidi Embonge, « XPS and DFT investigations of corrosion inhibition of substituted benzylidene Schiff bases on mild steel in hydrochloric acid. », *Applied surface Science*, p. 861-877., 2019.

[14] Q Qu *et al.*, « Corrosion behavior of cold rolled steel in artificial seawater in the presence of Bacillus subtilis C », *Corrosion Science*, p. 321‑329, 2015.

[15] Lgaz .H *et al.*, « Evaluation of 2-Mercaptobenzimidazole Derivatives as Corrosion Inhibitors for Mild Steel in Hydrochloric Acid. », *Metals*, p. 1‑14, 2020.

[16] Zou C, Yan X, Qin Y, Wang M, et Liu Y, « Inhibiting evaluation of b-Cyclodextrin-modified acrylamide polymer on alloy steel in sulfuric solution. », *Corrosion Science*, p. 445-454., 2014.

[17] Gerengi .H, Uygur .I, Solomon .MM, Yildiz .M, et Goksu .H, « Evaluation of the inhibitive effect of Diospyros kaki (Persimmon) leaves extract on St37 steel corrosion in acid medium », *Sustain. Chem. Pharm*, p. 57‑66, 2016.

[18] H. Lahbib, S. Ben Hassen, H. Gerengi, M. Rizvi, et Y. Ben Amor, « Corrosion inhibition performance of dwarf palm and Cynaracardunculus leaves extract for St37 steel in 15% H 2 SO 4 : a comparative study », *J. Adhes. Sci. Technol*, p. 1‑32, septembre 2020.

[19] H. Ferkous, S. Djellali, R. Sahraoui, H. Behloul, K. Saoud, et A. Çukurovali, « Electrochemical Impedance Spectroscopy and Adsorption Study of Carbon Steel in 1 M HCl Solution Containing 2-(2-Methoxybenzylidene) Hydrazine-1-Carbothioamide », in *Recent Advances in Environmental Science from the Euro-Mediterranean and Surrounding Regions (2nd Edition)*, Springer, Cham, 2021, p. 53‑58. doi: 10.1007/978-3-030-51210-1_9.

[20] H. Ferkous, M. Zerroug, M. A. Chaouch, M. Radjai, H. Majdoub, et A. Bouzid, « Green Corrosion Inhibitor for Carbon Steel in 1 M HCl: A Comparative Study of Polysaccharides Extracted from Prickly Pear Nopals of Opuntia Ficus-Indica (Peel and Pulp) », in *Recent Advances in Environmental Science from the Euro-Mediterranean and Surrounding Regions*, Springer, Cham, 2018, p. 1293‑1296. doi: 10.1007/978-3-319-70548-4_380.

[21] R. Ashokkumar et M. Ramaswamy, « Phytochemical screening by FTIR spectroscopic analysis of leaf extracts of selected Indian medicinal plants », *Int. J. Curr. Microbiol. Appl. Sci.*, p. 395-406., 2014.

[22] S. Chitra et B. Anand, « Surface morphological and FTIR spectroscopic information on the corrosion inhibition of drugs on mild steel in chloride environment », *J. Chem. Pharm. Sci*, p. 453‑456, 2017.

[23] P. Jain, A. Soni, P. Jain, et J. Bhawsar, « Phytochemical analysis of Mentha spicata plant extract using UV-VIS, FTIR and GC/MS technique ». 5 novembre 2016.

[24] R. Haldhar, D. Prasad, et A. Saxena, « Myristica fragrans extract as an eco-friendly corrosion inhibitor for mild steel in 0.5 M H2SO4 solution », *J. Environ. Chem. Eng.*, vol. 6, n° 2, p. 2290‑2301, avr. 2018, doi: 10.1016/j.jece.2018.03.023.

[25] Z. Meriem *et al.*, « Experimental and theoretical evaluation of the adsorption process of some polyphenols and their corrosion inhibitory properties on mild steel in acidic media », *J. Environ. Chem. Eng.*, vol. 9, n° 6, p. 106482, déc. 2021, doi: 10.1016/j.jece.2021.106482.

[26] D. K. Verma et F. Khan, « Corrosion inhibition of mild steel in hydrochloric acid using extract of glycine max leaves », *Res. Chem. Intermed.*, vol. 42, n° 4, Art. n° 4, avr. 2016, doi: 10.1007/s11164-015-2227-7.

[27] P. Muthukrishnan, B. Jeyaprabha, et P. Prakash, « Adsorption and corrosion inhibiting behavior of Lannea coromandelica leaf extract on mild steel corrosion », *Arab. J. Chem.*, vol. 10, p. S2343‑S2354, mai 2017, doi: 10.1016/j.arabjc.2013.08.011.

[28] M. Pitchaipillai, K. Raj, J. Balasubramanian, et P. Periakaruppan, « Benevolent behavior of Kleinia grandiflora leaf extract as a green corrosion inhibitor for mild steel in sulfuric acid solution », *Int. J. Miner. Metall. Mater.*, vol. 21, n° 11, p. 1083‑1095, nov. 2014, doi: 10.1007/s12613-014-1013-7.

[29] O. Ofuyekpone, O. Utu, et B. Onyekpe, « Corrosion inhibition for alloy 304L (UNS S30403) in H2SO4 1M solution by Centrosema pubescens leaves extract », *Appl. Surf. Sci. Adv.*, vol. 3, p. 100061, mars 2021, doi: 10.1016/j.apsadv.2021.100061.

[30] R. T. Loto, C. A. Loto, A. P. I. Popoola, et T. Fedotova, « Inhibition effect of butan-1-ol on the corrosion behavior of austenitic stainless steel (Type 304) in dilute sulfuric acid », *Arab. J. Chem.*, vol. 12, n° 8, Art. n° 8, déc. 2019, doi: 10.1016/j.arabjc.2014.12.024.

[31] W. Ebdelly, S. Ben Hassen, X. R. Nóvoa, et Y. Ben Amor, « Inhibition of carbon steel corrosion in neutral calcareous synthetic water by Eruca sativa extract », *Prot. Met. Phys. Chem. Surf.*, vol. 55, n° 3, Art. n° 3, 2019.

[32] M. Tourabi, K. Nohair, M. Traisnel, C. Jama, et F. Bentiss, « Electrochemical and XPS studies of the corrosion inhibition of carbon steel in hydrochloric acid pickling solutions by 3,5-bis(2-thienylmethyl)-4-amino-1,2,4-triazole », *Corros. Sci.*, vol. 75, p. 123‑133, oct. 2013, doi: 10.1016/j.corsci.2013.05.023.

[33] X. Luo, X. Pan, S. Yuan, S. Du, C. Zhang, et Y. Liu, « Corrosion inhibition of mild steel in simulated seawater solution by a green eco-friendly mixture of glucomannan (GL) and bisquaternary ammonium salt (BQAS) », *Corros. Sci.*, vol. 125, p. 139‑151, août 2017, doi: 10.1016/j.corsci.2017.06.013.

[34] M. Bouanis, M. Tourabi, A. Nyassi, A. Zarrouk, C. Jama, et F. Bentiss, « Corrosion inhibition performance of 2,5-bis(4-dimethylaminophenyl)-1,3,4-oxadiazole for carbon steel in HCl solution: Gravimetric, electrochemical and XPS studies », *Appl. Surf. Sci.*, vol. 389, p. 952‑966, déc. 2016, doi: 10.1016/j.apsusc.2016.07.115.

[35] M. Cui, Y. Yu, et Y. Zheng, « Effective Corrosion Inhibition of Carbon Steel in Hydrochloric Acid by Dopamine-Produced Carbon Dots », *Polymers*, vol. 13, n° 12, Art. n° 12, janv. 2021, doi: 10.3390/polym13121923.

[36] W. Temesghen et P. Sherwood, « Analytical utility of valence band X-ray photoelectron spectroscopy of iron and its oxides, with spectral interpretation by cluster and band structure calculations », *Anal. Bioanal. Chem.*, vol. 373, n° 7, p. 601‑608, août 2002, doi: 10.1007/s00216-002-1362-3.

[37] K. Babić-Samardžija, C. Lupu, N. Hackerman, A. R. Barron, et A. Luttge, « Inhibitive Properties and Surface Morphology of a Group of Heterocyclic Diazoles as Inhibitors for Acidic Iron Corrosion », *Langmuir*, vol. 21, n° 26, p. 12187‑12196, déc. 2005, doi: 10.1021/la051766l.

[38] A. Galtayries, R. Warocquier-Clérout, M.-D. Nagel, et P. Marcus, « Fibronectin adsorption on Fe–Cr alloy studied by XPS », *Surf. Interface Anal.*, vol. 38, n° 4, p. 186‑190, 2006, doi: 10.1002/sia.2295.

[39] C. Boulechfar *et al.*, « DFT/molecular scale, MD simulation and assessment of the eco-friendly anti-corrosion performance of a novel Schiff base on XC38 carbon steel in acidic medium », *J. Mol. Liq.*, vol. 344, p. 117874, 2021.

[40] E. E. El-Katori, M. I. Nessim, M. A. Deyab, et K. Shalabi, « Electrochemical, XPS and theoretical examination on the corrosion inhibition efficacy of stainless steel via novel imidazolium ionic liquids in acidic solution », *J. Mol. Liq.*, vol. 337, p. 116467, sept. 2021, doi: 10.1016/j.molliq.2021.116467.

[41] T. Salman, « Comparison and Evaluation studies for corrosion inhibition of mild steel in hydrochloric acid solution by some thiadiazole derivatives », *Wulfenia*, vol. 23, p. 46‑58, janv. 2016.

[42] S. Hassani, K. Roberts, S. Shirazi, J. Shadley, E. Rybicki, et C. Joia, « Characterization and Prediction of Chemical Inhibition Performance for Erosion-Corrosion Conditions in Sweet Oil and Gas Production », *Corrosion*, vol. 68, p. 885‑896, oct. 2012, doi: 10.5006/0546.

[43] R. Aslam *et al.*, « Corrosion inhibition of steel using different families of organic compounds: Past and present progress », *J. Mol. Liq.*, vol. 348, p. 118373, févr. 2022, doi: 10.1016/j.molliq.2021.118373.

[44] C. Lai, B. Xie, L. Zou, X. Zheng, X. Ma, et S. Zhu, « Adsorption and corrosion inhibition of mild steel in hydrochloric acid solution by S-allyl-O,O'-dialkyldithiophosphates », *Results Phys.*, vol. 7, p. 3434‑3443, janv. 2017, doi: 10.1016/j.rinp.2017.09.012.

[45] M. Chadili *et al.*, « Corrosion Inhibition of 3003 Aluminum Alloy in Molar Hydrochloric Acid Solution by Olive Oil Mill Liquid By-Product », *Int. J. Corros.*, vol. 2021, p. 6662395, janv. 2021, doi: 10.1155/2021/6662395.

[46] H. Awad, « The corrosion and inhibition of Zn-Al alloy in acidic media by pyridine and its methyl-containing derivatives », *Anti-Corros. Methods Mater.*, vol. 53, p. 110‑117, mars 2006, doi: 10.1108/00035590610650811.

[47] C. Arinzechukwu Maduabuchi, C. Ogukwe, K. Oguzie, N. Chukwuemeka, et E. Oguzie, « Corrosion Inhibition and Adsorption Behavior of Punica granatum Extract on Mild Steel in Acidic Environments: Experimental and Theoretical Studies », *Ind. Eng. Chem. Res.*, vol. 51, p. 668‑677, janv. 2012, doi: 10.1021/ie201941f.

[48] H. Ma *et al.*, « Evaluation of polyphenol anthocyanin-enriched extracts of blackberry, black raspberry, blueberry, cranberry, red raspberry, and strawberry for free radical scavenging, reactive carbonyl species trapping, anti-glycation, anti-β-amyloid aggregation, and microglial neuroprotective effects », *Int. J. Mol. Sci.*, vol. 19, n° 2, Art. n° 2, 2018.

[49] F. E.-T. Heakal, S. A. Rizk, et A. E. Elkholy, « Characterization of newly synthesized pyrimidine derivatives for corrosion inhibition as inferred from computational chemical analysis », *J. Mol. Struct.*, vol. 1152, p. 328‑336, 2018.

[50] J. Sun *et al.*, « Effect of cranberry (Vaccinium macrocarpon) oligosaccharides on the formation of advanced glycation end-products », *J. Berry Res.*, vol. 6, n° 2, Art. n° 2, 2016.

[51] Y. Zhang, H. Ma, W. Liu, T. Yuan, et N. P. Seeram, « New antiglycative compounds from cumin (Cuminum cyminum) spice », *J. Agric. Food Chem.*, vol. 63, n° 46, Art. n° 46, 2015.

[52] F. Bentiss, M. Lebrini, H. Vezin, et M. Lagrenée, « Experimental and theoretical study of 3-pyridyl-substituted 1, 2, 4-thiadiazole and 1, 3, 4-thiadiazole as corrosion inhibitors of mild steel in acidic media », *Mater. Chem. Phys.*, vol. 87, n° 1, Art. n° 1, 2004.

[53] S. Banerjee, V. Srivastava, et M. M. Singh, « Chemically modified natural polysaccharide as green corrosion inhibitor for mild steel in acidic medium », *Corros. Sci.*, vol. 59, p. 35‑41, 2012.

[54] S. Tamil Selvi, V. Raman, et N. Rajendran, « Corrosion inhibition of mild steel by benzotriazole derivatives in acidic medium », *J. Appl. Electrochem.*, vol. 33, n° 12, Art. n° 12, 2003.

[55] H.-L. Wang, H.-B. Fan, et J.-S. Zheng, « Corrosion inhibition of mild steel in hydrochloric acid solution by a mercapto-triazole compound », *Mater. Chem. Phys.*, vol. 77, n° 3, Art. n° 3, 2003.

[56] R. G. Saratale, H. S. Shin, G. Kumar, G. Benelli, D.-S. Kim, et G. D. Saratale, « Exploiting antidiabetic activity of silver nanoparticles synthesized using Punica granatum leaves and anticancer potential against human liver cancer cells (HepG2) », *Artif. Cells Nanomedicine Biotechnol.*, vol. 46, n° 1, p. 211‑222, janv. 2018, doi: 10.1080/21691401.2017.1337031.

[57] M. N. Sharif, F. Ansari, A. Malik, Q. Ali, Z. Hasan, et N. U. Khan, « Fourier-Transform Infrared Spectroscopy, Antioxidant, Phytochemical and Antibacterial Screening of N-Hexane Extracts of Punica granatum, A Medicinal Plant », *Genet. Mol. Res. GMR*, vol. 19, p. gmr16039989, oct. 2020.

[58] M. J. Al et G. J. Mohammed, « Anti-bacterial, Antifungal Activity and Chemical Analysis of Punica grantanum (Pomegranate peel) Using GC-MS and FTIR Spectroscopy ».

[59] M. Sharif, F. Ansari, A. Malik, Q. Ali, Z. Hasan, et N. U. H. Khan, « Fourier-Transform Infrared Spectroscopy, Antioxidant, Phytochemical and Antibacterial Screening of N-Hexane Extracts of Punica granatum, A Medicinal Plant », 2018.

[60] M. Shahsavari, A. Imani, et E. Asselin, « Pomegranate arils extract as a green corrosion inhibitor for mild steel: effect of concentration and temperature in hydrochloric acid », *Mater. Res. Express*, 2022.

[61] N. Bhardwaj, P. Sharma, L. Guo, O. Dagdag, et V. Kumar, « Molecular dynamic simulation, quantum chemical calculation and electrochemical behaviour of Punica granatum peel extract as eco-friendly corrosion inhibitor for stainless steel (SS-410) in acidic medium », *J. Mol. Liq.*, vol. 346, p. 118237, 2022.

Chapter IV

Theoretical study

IV. Theoretical study

IV.1. Quantum molecular descriptors of CMFE (QMDs)

IV.1.1. Theoretical study of CMFE with 304L stainless steel and XC48 carbon steel

The frontier molecular orbital, which can be used to study chemical reactivity and kinetic stability, is the essential molecular orbital in a molecule. The frontier molecular orbitals are the highest occupied molecular orbital (HOMO) and the lowest unoccupied molecular orbital (LUMO). Electronic absorption, the transition from the ground to the first excited state, is primarily explained by one-electron excitation from HOMO to LUMO. The system's kinetic stability increases as the HOMO-LUMO distance widens. As a result, it takes more energy to pass electrons from the ground state HOMO to the excited state LUMO. For each compound. Table IV.1 lists the measured orbital energies, with the HOMO-LUMO gap (E_{gap}), as well as other chemical descriptors, i.e., chemical potential (μ), global hardness (η), and electrophilicity index (ω)) for CMFE and pure cluster components of Fe_{20} and 304L stainless steel.

Table IV.1 shows that 304L and Fe20 have the highest HOMO energy and Rutin the highest LUMO energy, which means that the two metals (Fe20 and 304L) cluster is the more electron donator and Rutin is the more electron acceptor. Consequently, Rutin shows the highest inhibiting activity.

Table IV.1. Global reactivity descriptors CMFE

Isomer	E_{HOMO} (eV)	E_{LUMO} (eV)	Gap (eV)	χ	η	ω	ΔN_{max}
304L	-4.601	-4.592	0.009	4,597	0,005	2347.535	919,4000
Fe_{20}	-4.139	-4.072	0.067	4.106	0.033	252.824	124,4242
DHF	-6.938	-3.277	3.661	5.107	1.830	7.125	2,7907
CGP	-6.927	-3.380	3.547	5.154	1.774	7.489	2,9052
Rutin	-6.684	-3.194	3.490	4.939	1.745	6.991	2,8303

The 304L steel molecule has the lowest energy gap (0.009 eV) and the lowest hardness of any molecule. It is also the most reactive (0.005 eV), followed by the Fe_{20} molecule (energy gap 0.067 eV and $\boldsymbol{\eta}$ = 0.033 eV). Both DHF and CGP inhibitor molecules show gap energies that are comparable to each other, which indicates that their effect on the corrosion behavior of

the 304L and Fe_{20} cluster metal surfaces is similar. Rutin has also been found to be less reactive than the other ingredients. This result also shows that CGP and DHF are more stable than Rutin. Parr et al. [1-2] developed the global electrophilicity index (ω) based on thermodynamic properties and calculated the beneficial shift in energy when a chemical system reaches saturation by adding electrons. The energy loss is caused by the flow of electrons from the donor (HOMO) to the acceptor (LUMO) in molecules.

Isomer	Optimized structure	HOMO	LUMO	Sigma-surface
Fe_{20}	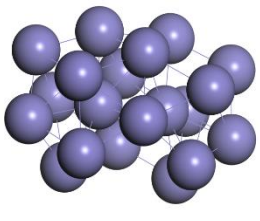	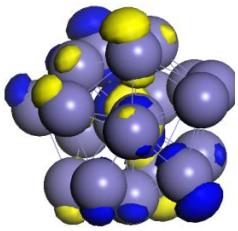	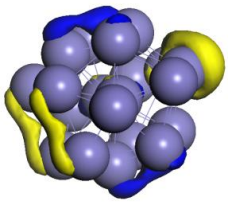	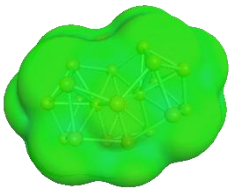
304L	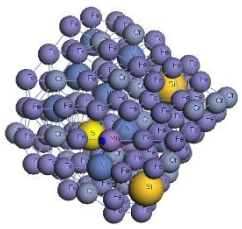	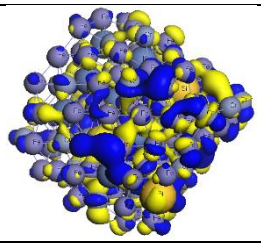	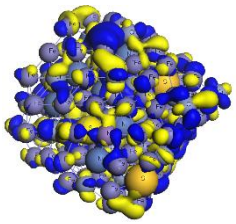	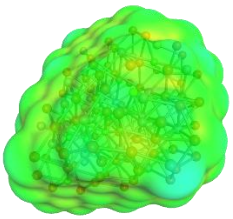
CGP	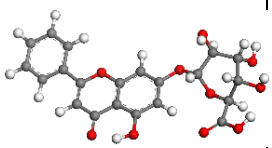	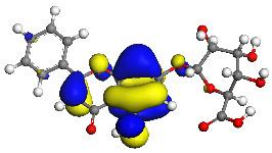	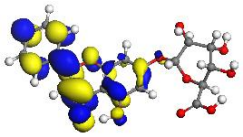	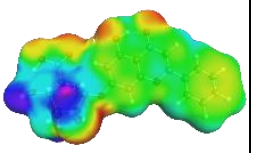
DHF	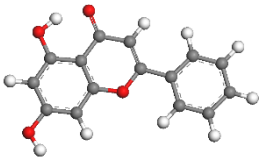	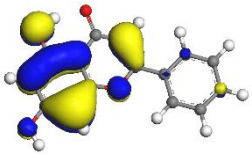	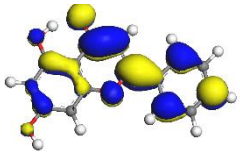	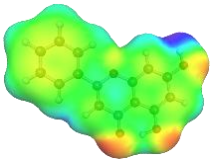
Rutin	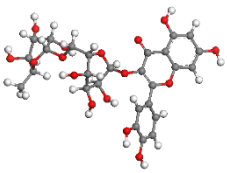	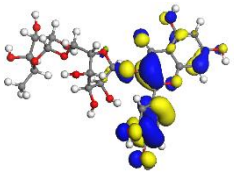	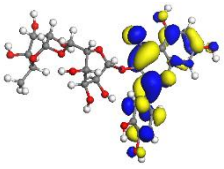	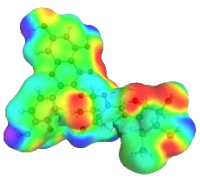

Figure IV.1. DFT global reactivity descriptors and COSMO-RS results.

The high value of E_{HOMO} demonstrates that 304L and Fe_{20} clusters can act as electron donors (it has the greatest electrophilicity index, which is 2347.535eV and 252.842 eV,

respectively). According to Table IV.1, the 304L and Fe_{20} cluster molecules are electron donors, whereas the inhibitory molecules are electron acceptors. The E_{LUMO} energy that is the greatest among the three inhibitors correlates to the inhibition efficiency that is the highest (the highest electron acceptor ability). This demonstrates that the DHF is the CMFE extract constituent responsible for the most excellent inhibition. The fact that the DHF has the largest ΔN_{max} proves it is an acceptor.

Figure IV.1 depicts the HOMO and LUMO regions, which indicate the ability to act as either an electron donor or an electron acceptor. The 304L cluster's surface may be nonpolar, and also that of the Fe_{20} cluster, as seen by the Cosmo surfaces' green color. Hydrogen bond acceptor (HBA) regions in red and donor (HBD) regions in blue may be seen.

The HOMO was found to be located on the conjugated π-bonds of the phenylchromane in the three molecules DHF, CGP, and Rutin (See Figure IV.1). The LUMO was concentrated on the phenylchromane simple bonds of the three molecules. Table IV.1 also gives the HOMO and LUMO of the Fe_{20} cluster and 304L.

If $\Delta N_{max} > 0$, an inhibitor molecule transfers its ***e-*** to a metal and vice versa if $\Delta N_{max} < 0$ [3]. From Table IV.1, all the calculated values of the ΔN_{max} of the three molecules are less than zero. This confirms the molecule's electron-accepting character already demonstrated. Rutin with the lowest ΔN_{max} is the more electron acceptor from the iron surface (electrons donator).

According to the simple charge transfer model for donation and back-donation of charges proposed recently by Gomez et al. [1], an electronic back-donation process might be occurring governing the interaction between the inhibitor molecule and the metal surface. The concept establishes that if both processes occur, namely charge transfer to the molecule and back-donation from the molecule, the energy change is directly proportional to the hardness of the molecule, as indicated in the following expression. $\Delta E_{Back\text{-}donation} = -\eta/4$.

The $\Delta E_{Back\text{-}donation}$ implies that when $\eta > 0$ and $\Delta E_{Back\text{-}donation} < 0$, the charge transfer to a molecule, followed by a back-donation from the molecule, is energetically favored. Hence, it is possible to compare the stabilization among inhibiting molecules in this context since there will be an interaction with the same metal. Then, it is expected that it will decrease as the hardness increases. Consequently, the back-donation is so pronounced for the Rutin molecule.

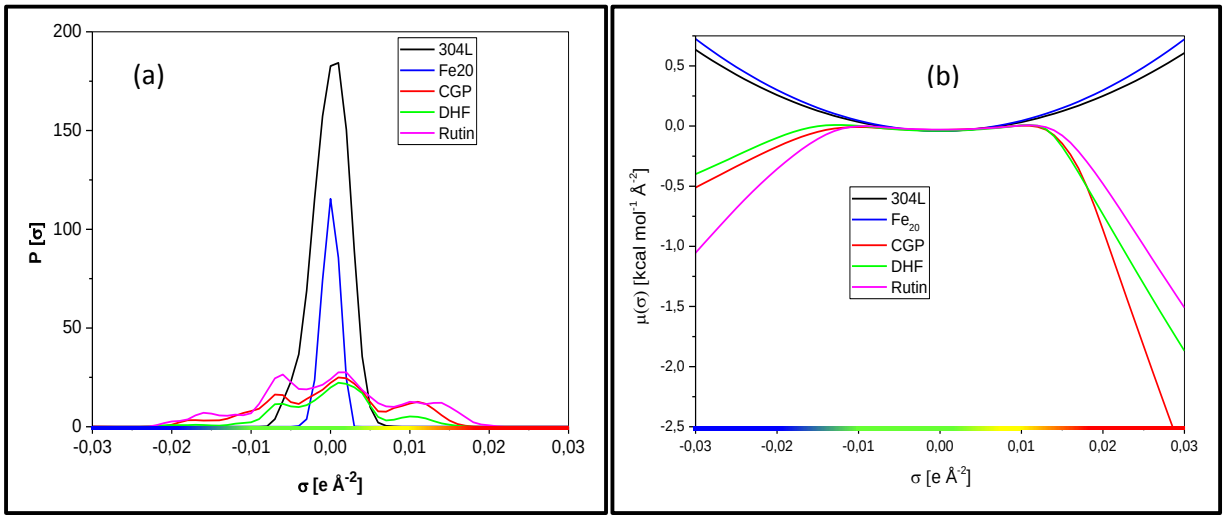

Figure IV.2. Surface polarity and potentials of Fe20 cluster and 304L in CMFE major compounds

Figure IV.2 shows the charge distribution of the binary interacting system. It is noted that the green surface is for the non-polar regions of the complex. The red one is for the hydrogen bond acceptor (HBA) region, and finally, the blue region is for the hydrogen bond donor (HBD) region [4].

The relative probability distributions (σ-profiles) of the inhibitor, 304L and the Fe cluster (Fe_{20}) and their related σ-potentials are depicted in Figure IV.2. $P(\sigma)$ denotes the number of molecular surface segments having a specific screening charge density σ [5-6].

$\sigma > 0$ represents the surfaces of negative polarity. Whereas $\sigma < 0$ is for positive polarity surfaces [7-8]. $\sigma \approx 0$ is the non-polar (hydrophobic) areas. As a result the profile curves can be separated into three sections: the HBD (hydrogen bond donor) zone ($-0.025 < \sigma < -0.010$) the non-polar zone ($-0.010 < \sigma < +0.010$) and the HBA (hydrogen bond acceptor) region ($+0.010 < \sigma < +0.025$).

In Figure IV.2.a, the three inhibitor molecules are found to be mostly non-polar (green-colored surfaces) with σ ϵ [-0.01, 0.01] au. The iron cluster Fe_{20} is, as expected, completely non-polar. The adsorption is expected to be in the non-polar region, as concluded from Figure IV.2.b. It is noticed that chemical potential is always positive in the polar regions (non-spontaneous phenomena). The chemical potential for the four molecules is less than zero in the non-polar region which suggests that the interaction forces are Van der Waals type. This confirms that the only possible interaction is with nonpolar groups or molecule chemisorption (chemical bound) as will be revealed by the AIM study.

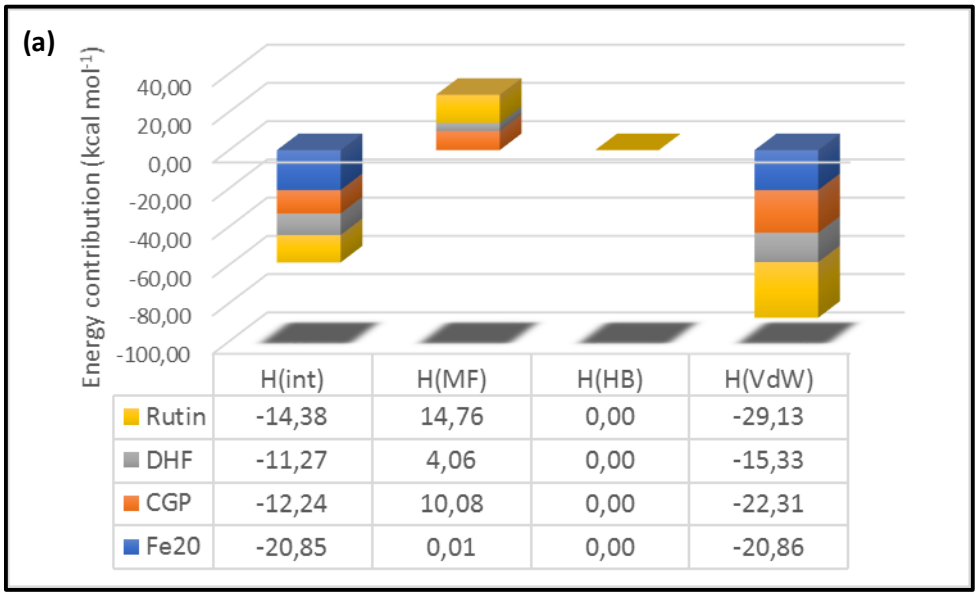

	H(int)	H(MF)	H(HB)	H(VdW)
Rutin	-14,38	14,76	0,00	-29,13
DHF	-11,27	4,06	0,00	-15,33
CGP	-12,24	10,08	0,00	-22,31
Fe20	-20,85	0,01	0,00	-20,86

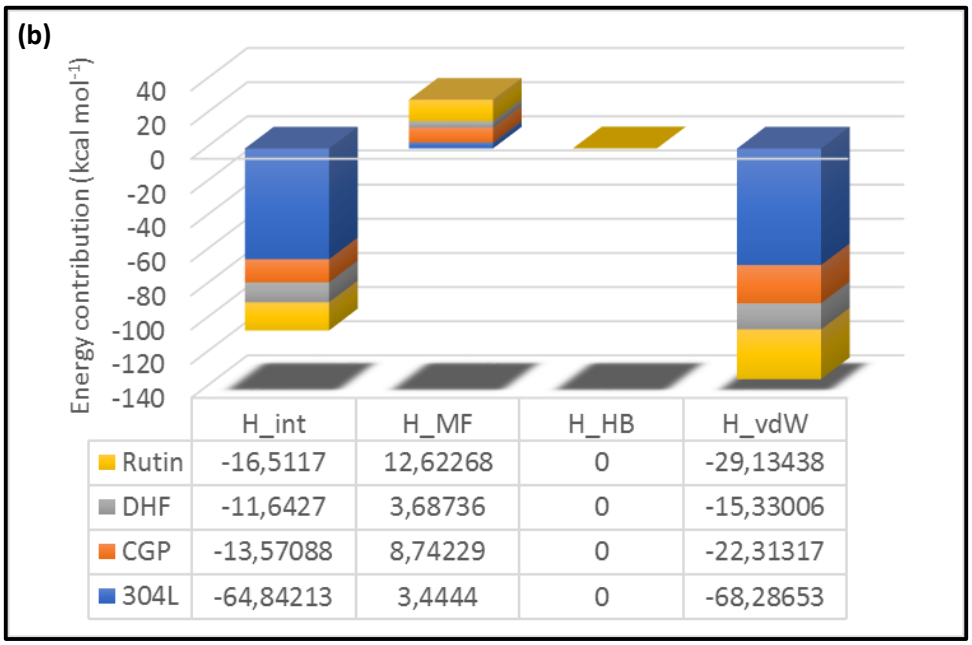

	H_int	H_MF	H_HB	H_vdW
Rutin	-16,5117	12,62268	0	-29,13438
DHF	-11,6427	3,68736	0	-15,33006
CGP	-13,57088	8,74229	0	-22,31317
304L	-64,84213	3,4444	0	-68,28653

Figure IV.3. Interaction energies of : (a) system inhibitor-Fe_{20} cluster (b) system inhibitor-304L

Figure IV.3 shows that the large contributing interaction energy in mixing the inhibitor with Fe_{20} cluster and 304L cluster is Van der Waals type. The contributions of electrostatic (H_{misfit}) and hydrogen bonding (H_{HB}) enthalpies were found to be negligible for the first type of interaction energy and null for the second one (no Hydrogen bonding).

A molecular graph of the optimized CMFE-Fe_{20} cluster complex is presented in Figure IV.4, while in Table IV.2, the topological parameters at BCP of interaction contacts are listed.

Table IV.2. The topological parameters at BCP of interaction contacts

	BCP	ρ_c (Ha)	$\nabla^2\rho(r)$ (Ha)	G (Ha)	V (Ha)	E_{HB} (eV)	H=G+V (Ha)	G/|V|
DHF@Fe_{20}	53	5.77E-03	8.13E-03	1.89E-03	-1.74E-03	-2.37E-02	1.44E-04	1.08E+00
	145	5.25E-02	1.27E-01	4.24E-02	-5.29E-02	-7.19E-01	-1.05E-02	8.01E-01
	154	1.64E-02	2.66E-02	7.47E-03	-8.30E-03	-1.13E-01	-8.26E-04	9.00E-01
	177	3.83E-02	1.05E-01	2.99E-02	-3.37E-02	-4.59E-01	-3.79E-03	8.88E-01
CGP@Fe_{20}	97	7.92E-02	3.95E-01	1.08E-01	-1.17E-01	-1.59E+00	-9.03E-03	9.23E-01
	154	4.63E-03	9.06E-03	1.88E-03	-1.49E-03	-2.03E-02	3.86E-04	1.26E+00
	191	5.87E-02	1.52E-01	5.07E-02	-6.36E-02	-8.65E-01	-1.29E-02	7.98E-01
Rutin@Fe_{20}	126	1.17E-02	1.16E-01	2.10E-02	-1.31E-02	-1.79E-01	7.90E-03	1.60E+00
	136	8.49E-04	6.40E-03	1.09E-03	-5.77E-04	-7.85E-03	5.11E-04	1.89E+00
	185	2.26E-01	4.41E-02	2.49E-01	-4.86E-01	-6.61E+00	-2.38E-01	5.11E-01
	178	2.77E-04	5.40E-03	9.03E-04	-4.57E-04	-6.21E-03	4.46E-04	1.98E+00
	218	3.24E-03	7.86E-02	1.33E-02	-6.96E-03	-9.47E-02	6.35E-03	1.91E+00

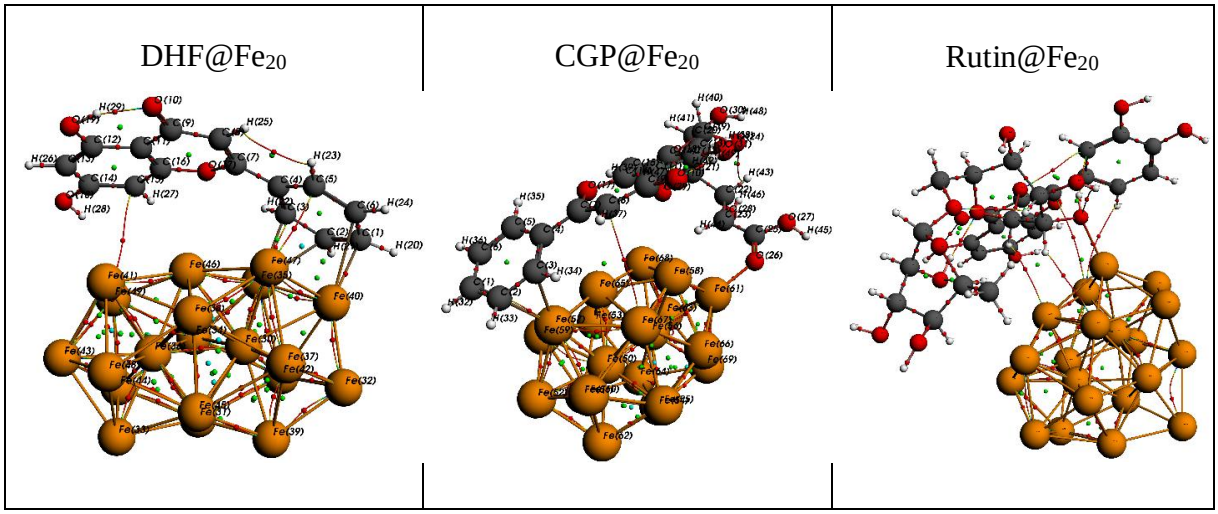

Figure IV.4. Molecular graph of the optimized molecules-XC48 cluster

From the results in Table IV.2. the calculated values of $\rho(r)$ in BCPs are quite low, and $\nabla^2\rho(r)$ are positive. This indicates the occurrence of Hydrogen bonds (HBs) interaction in the case of the twelve BCPs bonds. On the other hand, the positive values of $\nabla^2\rho_{BCP}$ and H_{BCP} indicates the weak molecular interaction (electrostatic, G/|V|>1) between the BCPs atoms (for DHF@Fe_{20}: BCP 53; for CGP@Fe_{20}: BCP 154 and for Rutin@Fe_{20}:BCPs 126, 136, 178 and 218). The $E_{HB} < 0$ is characteristic of weak hydrogen bonding [8].

On the contrary, for DHF@Fe_{20}: BCPs 145, 154, and 177; CGP@Fe_{20}: BCPs 97 and 191, and for Rutin@Fe_{20}:BCP 185, Close inspection of the energetic AIM parameters reveals that the intermolecular hydrogen bonds in the gas phase have positive $\nabla^2\rho_{BCP}$ and a negative H_{BCP} shows a partially covalent character of the investigated interactions (G/|V|<1). The values of ρ_{BCP} and $\nabla^2\rho_{BCP}$ of intermolecular HB interactions are well correlated with the hydrogen bond energies strength calculated by the Espinosa method [9]. It is known that high electron density corresponds to the strongest HB with a shorter H-bond distance, and low electron density corresponds to the weakest HB with a longer H-bond distance [10].

IV.1.2. Monte Carlo (MC) simulations of CMFE

The inhibitors are adsorbed on the Fe(110) and 304L surfaces with an almost flat orientation, as it is shown. The inhibitor molecule (green colored) and metal surface interact with the donor-acceptor, which results in parallel adsorption of the inhibitor molecule. The inhibitor molecule has π-electrons, which provide many electrons to the unoccupied $d_{orbitals}$ of iron. On the other hand, the phenyl rings p-anti-bonding empty orbitals can accept an electron from the 4s or 3d orbitals of iron to produce feedback bonds. Many large-scale organic corrosion inhibitors, such as those described in refs [11-12], have this parallel arrangement on steel surfaces, where the p–d hybridization plays a prominent role. However, small inhibitory molecules can chemisorb perpendicular to the iron surface with unsaturated heteroatoms via s molecular orbitals [11]. The values for adsorption-desorption and deformation energy are listed in Table IV.3.

Table IV.3. Adsorption energies (kcal mol^{-1}) of the inhibition system

Energy		**Fe_{20}**	**304L**
Total Energy		1.28E+03	1.28E+03
Adsorption Energy (E_{ads})		-3.34E+03	-3.34E+03
Rigid Adsorption Energy (E_{ra})		-58.001	-61.2936
Deformation Energy (E_{def})		-3.28E+03	-3.28E+03
dEad/dNi (Desorption Energy)	CGP	-304.681	-307.338
	DHF	-271.169	-268.843
	Rutin	-75.912	-105.767
	H_2O	-16.499	-16.499
	H_3O^+	-24.909	-24.908
	SO_4^{2-}	-54.878	-54.880

The results show that the three inhibitor molecules adsorb well on the iron surface in an acidic aqueous solution (CGP has slightly stronger adsorption energy in gas (isolated)) and liquid state). Moreover, the strength of the adsorption is proportional to the solution's acidity. All adsorption energies were negative, indicating that the adsorption is exothermic and spontaneous.

According to the principle of higher absolute values of the adsorption energy, the order of inhibitory efficiency of the studied complexes is the following: [CGP] > [DHF] > [Rutin] against corrosion of Fe_{20} and 304L steel in 100 H_2O + 10 H_2SO_4 solution.

The optimal adsorption arrangement of inhibitors on metal surfaces (XC48 and 304L) is shown in Figure IV.5.

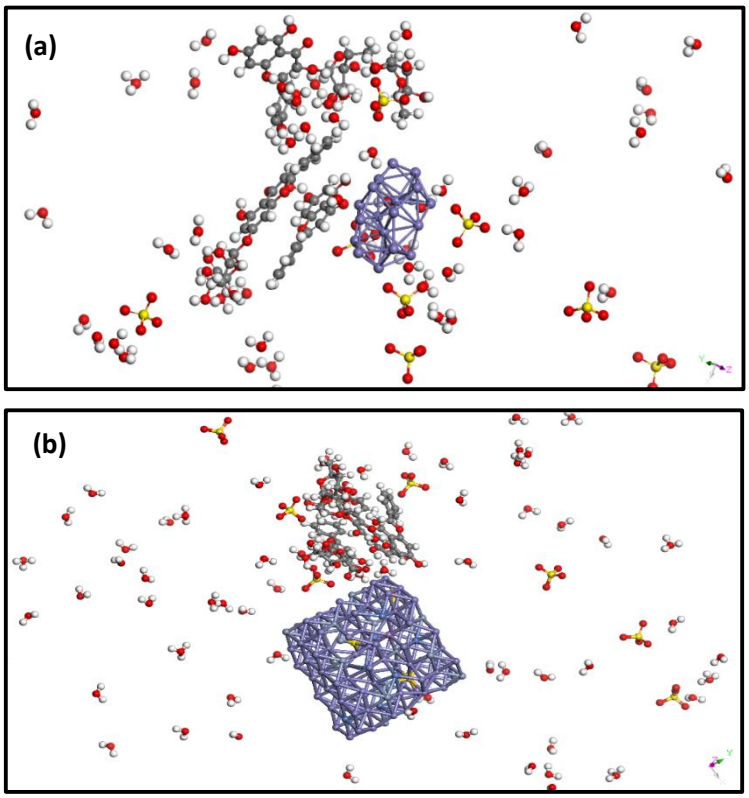

Figure IV.5. Extract's main components adsorption on (a) Fe_{20} clusters (b) 304L clusters

Furthermore, the magnitude of E_{ads} may be used to determine the adsorption system stability. E_{ads}' greater absolute values are associated with more potent inhibitor-Fe(110) interactions and higher corrosion inhibition effectiveness.

The adsorption mechanism of the inhibitors on the surface of the 304L-steel was elucidated using MD simulations. Table IV.4 shows that the adsorption of inhibitor molecules onto the surface of 304L material leads to a strong interaction. In addition, each inhibitor

molecule was found either parallel to or nearly flat on the metal surface. More research into the interaction and binding energies associated with inhibitor adsorption is likely required before we learn anything valuable about the 304L-inhibitor relationship. It's worth noting that the DHF inhibitor compound had the most negative interaction energy among all the chemicals studied. This study supports the hypothesis of a previous study that DHF may adsorb preferentially on the iron surface.

Table IV.4. Molecular Dynamic simulation results for the inhibition systems with 304L

	DHF	CGP	Rutin
E_{tot}	18944.43	18016.02	16288.30
E_{304L}	18841.42	17883.04	16087.79
E_{inh}	124.39	152.66	213.53
E_{int}	-21.38	-19.7	-13.02
Optimized structure	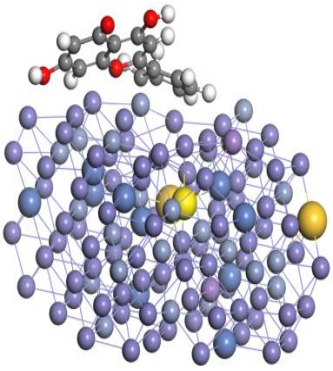	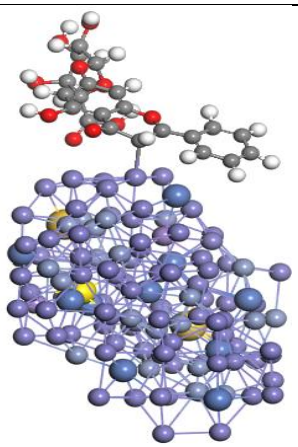	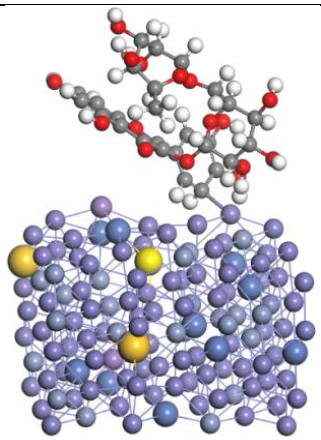

IV.2. Quantum molecular descriptors of PGPE (QMDs)

IV.2.1. Theoretical study of PGPE with XC48 and 304L

The optimal structures of the examined systems are shown in Figure IV.6. Table IV.5 contains the calculated orbital energies for the metal complexes (304L) and the Fe35 carbon steel cluster, as well as the various chemical descriptors, such as μ, η and χ. The energy gap value plays a crucial role in determining the adsorption of inhibitor molecules on metal surfaces, making it an essential factor to consider. Reactivity and inhibition efficiency worsen with increasing gap values [13-14]. The inhibitory activity improves as the energy is necessary to take an electron out of the hight occupied molecular orbital (HOMO) [15]. A "soft" molecule in chemistry possesses a small gap value, indicating strong chemical reactivity and poor kinetic

stability [16]. Organic compounds are regarded as efficient corrosion inhibitors if they offer electrons to the empty orbit of a metal and accept free electrons from a metal [17-18].

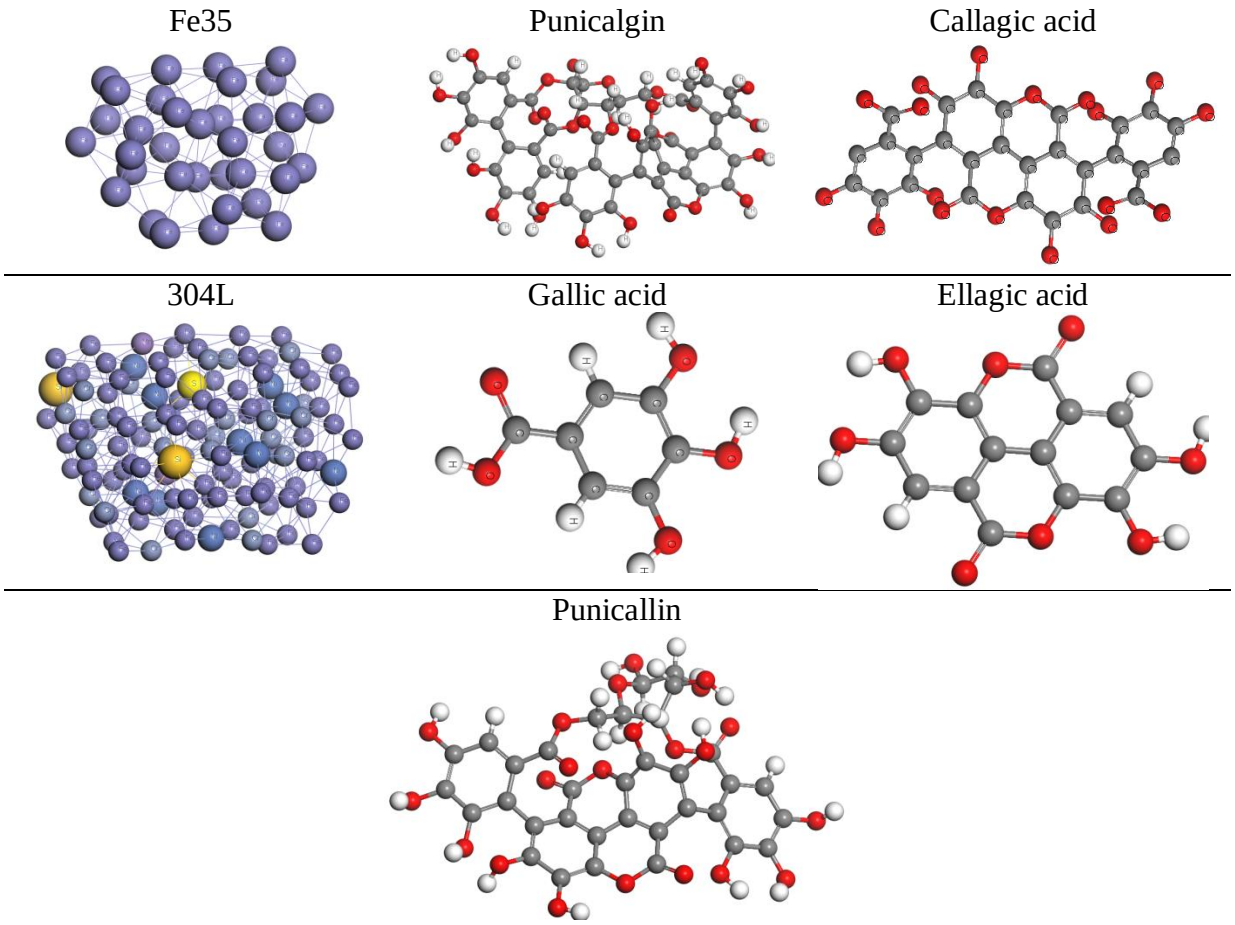

Figure IV.6. Optimized structures of XC48 carbon steel, 304L stainless steel and the PGPE compounds

Table IV.5 indicates that 304L stainless steel has the lowest gap (at 0.009 eV). Thus, it is a minor reactive inhibitor. The Galic Acid had the highest gap at 3.229 eV. These results show that Galic acid is the most stable molecule in the system according to the minimum energy gap theory, and due to its low hardness and small gap according to gap energy, steels and compounds are arranged as follows: 304L, XC48, Punicalin, Punicalgin, Gallagic acid, Ellagic acid, and finally Galic Acid.

To quantify the positive energy shift that occurs when a chemical system approaches saturation by adding electrons, the electrophilicity index (ω) is established by Parr et al. [19].

Table IV.5. Global reactivity descriptors PGPE

	HOMO(eV)	LUMO(eV)	GAP(ev)	X	η	ω	ΔN_{max}
Punicalin	- 5.139	- 3.216	1.923	4.177	0.962	9.074	4.345
Ellagicacid	- 5.432	- 2.771	2.661	4.102	1.331	6.322	3.083
Gallagicacid	- 5.324	- 2.826	2.497	4.075	1.249	6.649	3.263
GalicAcid	- 5.407	- 2.178	3.229	3.792	1.615	4.454	2.349
Punicalgin	- 5.248	- 2.888	2.360	4.068	1.180	7.014	3.448
Fe35	- 4.565	- 4.549	0.015	4.557	0.008	1348.383	591.770
304L	- 4.601	- 4.592	0.009	4.596	0.005	2250.349	979.197

Table IV.5 shows that electron flow will be from Punicalin, Punicalgin, Gallagic acid, Ellagic acid, and Galic Acid to iron and 304L (positive ΔN). The chemical potentials will still be unbalanced until this electron flow stops. The number of electrons given up by the inhibitor molecule to the metal atom was determined using Pearson's electronegativity scale [20].

The computed electron transfer (ΔN) from inhibitor to 304L and XC 48 were estimated and presented in Table IV.5. The ΔN values can be inferred that electron donation plays a significant role in the efficiency with which inhibition occurs. E_{HOMO} = - 5.139 eV and E_{LUMO} = - 3.216 eV for Punicalin, respectively, show that it has the greatest and lowest inhibition efficiencies. Furthermore, it has demonstrated inhibitors can create a feedback connection by accepting electrons from the metal's *d*-orbital that are not occupied. Thus, the potential for building a feedback link should be determined by the magnitude of E_{LUMO}. When the E_{LUMO} energy is small, it is easier for electrons in the metal's *d*-orbital to be accepted, followed by Punicalin, with the lowest energy at - 3.216 eV.

The overall hardness is proportional to obtain values for "$\Delta E_{Back\text{-}donation}$", thus the correct formula is "-η/4" with η>0 for all molecules, $\Delta E_{Back\text{-}donation} < 0$ [21]. Upon receiving a charge, a molecule may donate that charge to another atom, causing a net energy gain. Since all inhibitory chemicals will interact with the same metal, evaluating their stabilization against each other will be possible. Back-donation is preferred for Punicalin since its expected effectiveness as an inhibitor decreases with increasing hardness: [Punicalin] > [Punicalgin] > [Gallagic acid] > [Ellagic acid] > [Galic Acid].

In the Ellagic acid, Gallagic acid, and Gallic Acid structures, the HOMO and LUMO were located through most of the molecule (Table IV.6).

Table IV.6. Frontier molecular orbitals of the molecules.

	HOMO	LUMO	ESP
Punicalin	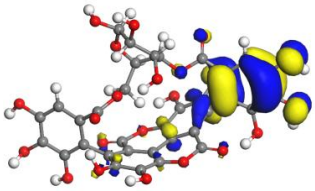	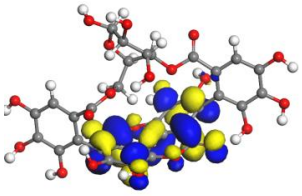	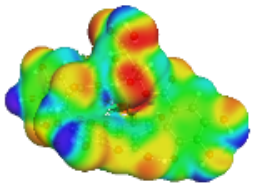
Ellagic acid	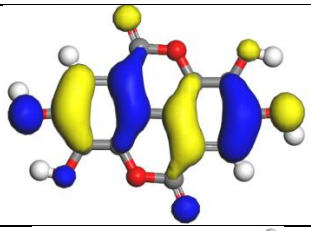	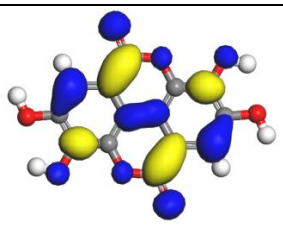	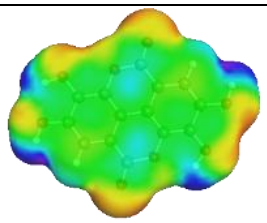
Gallagic acid	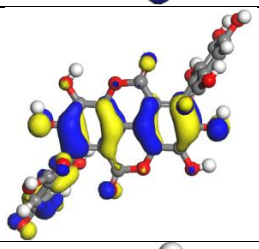	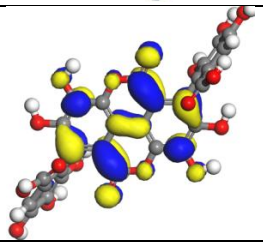	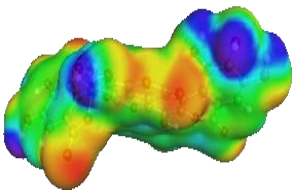
Gallic Acid	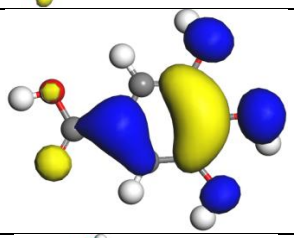	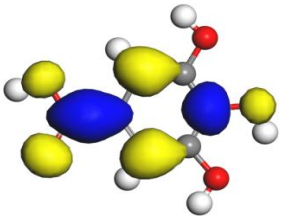	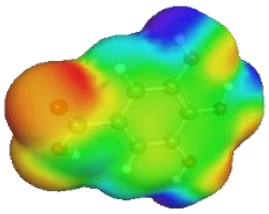
Punicalgin	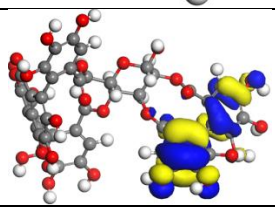	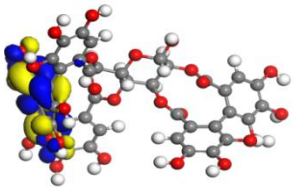	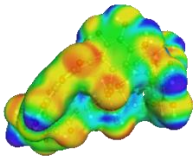
Fe35	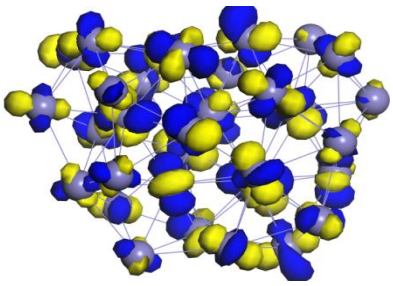	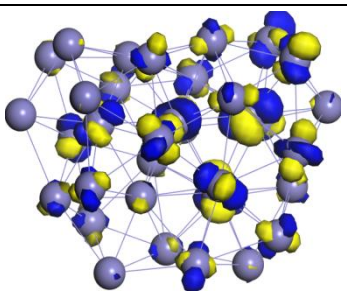	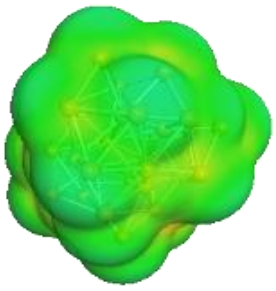
304L	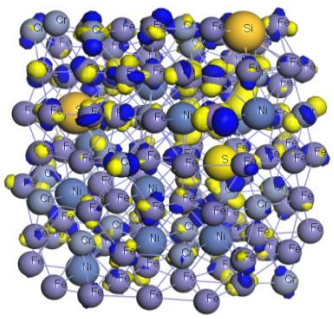	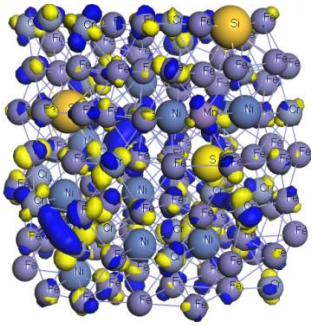	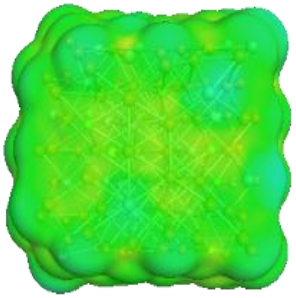

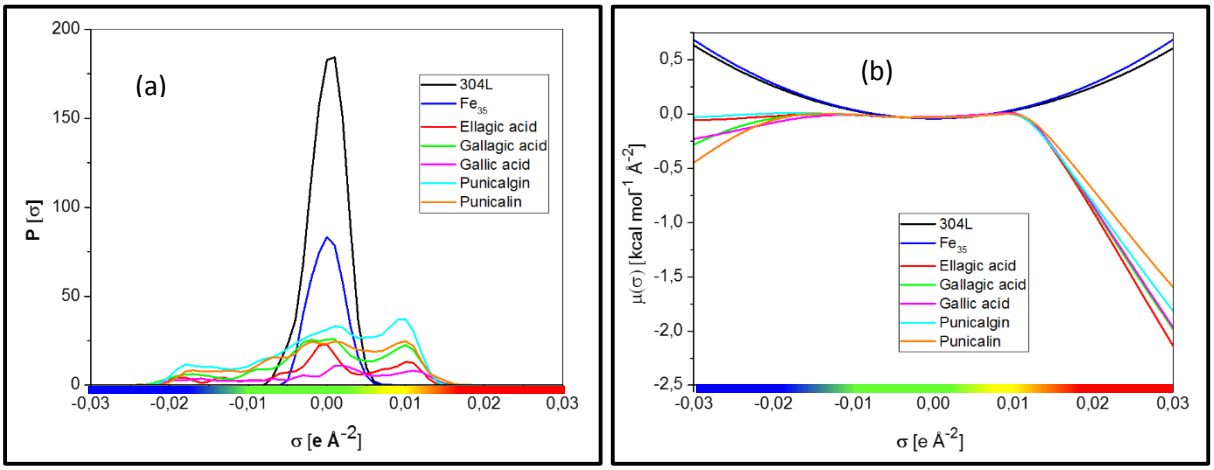

Figure IV.7. COSMO-RS study: surface polarity and potentials

Figure IV.7 illustrates the distribution of charges in the binary interacting system. The green surface in the figure represents the non-polar regions of the complex. The red region corresponds to the hydrogen bond acceptor (HBA) region, while the blue region represents the hydrogen bond donor (HBD) region [4].

In Figure IV.7.a, it can be observed that the three inhibitor molecules are predominantly non-polar, indicated by the green-colored surfaces, with a charge density range of $\sigma \in$ [-0.01, 0.01] au. As expected, the iron cluster Fe20 is completely non-polar. The adsorption is expected to occur in the non-polar region, as deduced from Figure IV.7.b.

The relative probability distributions (σ-profiles) of the inhibitor, 304L, and the Fe cluster (Fe35), along with their corresponding σ-potentials, are depicted in Figure IV.7. The parameter P(σ) represents the number of molecular surface segments with a specific screening charge density σ [5-6].

The positive polarity surfaces are represented by $\sigma>0$, while the negative polarity surfaces are denoted by $\sigma<0$ [7-8]. The charge density $\sigma \approx 0$ corresponds to the non-polar (hydrophobic) areas. Consequently, the profile curves can be divided into three sections: the hydrogen bond donor (HBD) zone ($-0.025<\sigma<-0.010$), the non-polar area ($-0.010<\sigma<+0.010$), and the hydrogen bond acceptor (HBA) region ($+0.010<\sigma<+0.025$).

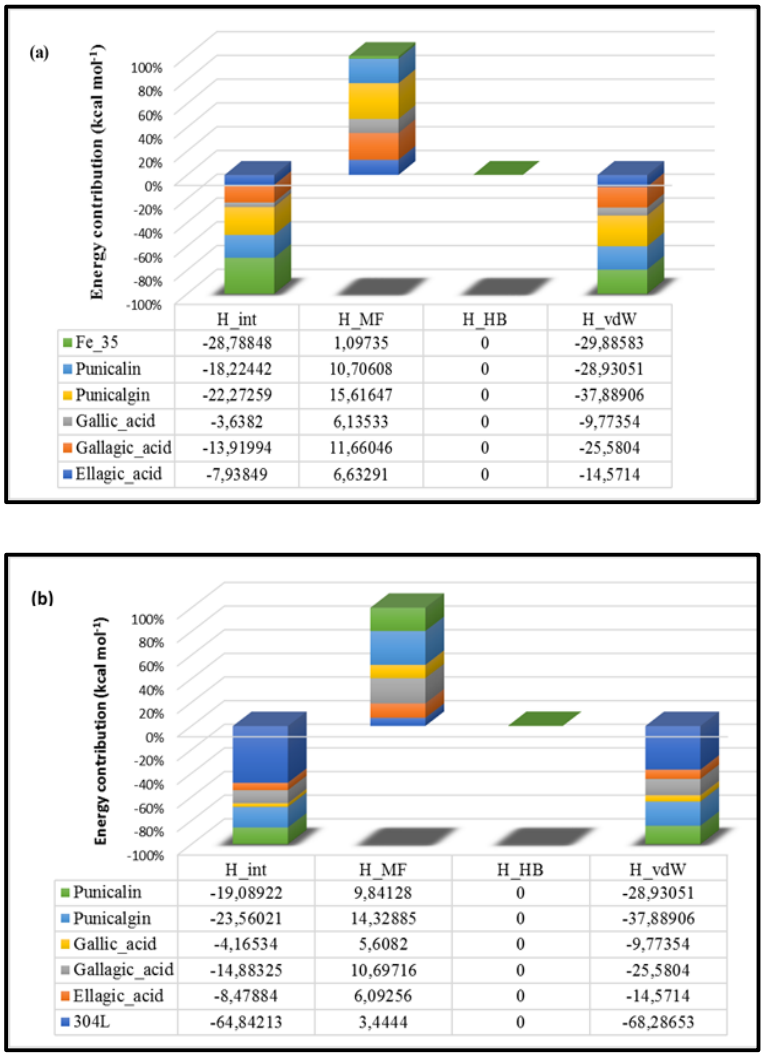

	H_int	H_MF	H_HB	H_vdW
Fe_35	-28,78848	1,09735	0	-29,88583
Punicalin	-18,22442	10,70608	0	-28,93051
Punicalgin	-22,27259	15,61647	0	-37,88906
Gallic_acid	-3,6382	6,13533	0	-9,77354
Gallagic_acid	-13,91994	11,66046	0	-25,5804
Ellagic_acid	-7,93849	6,63291	0	-14,5714

	H_int	H_MF	H_HB	H_vdW
Punicalin	-19,08922	9,84128	0	-28,93051
Punicalgin	-23,56021	14,32885	0	-37,88906
Gallic_acid	-4,16534	5,6082	0	-9,77354
Gallagic_acid	-14,88325	10,69716	0	-25,5804
Ellagic_acid	-8,47884	6,09256	0	-14,5714
304L	-64,84213	3,4444	0	-68,28653

Figure IV.8. Interaction energies of the PGPE system inhibitor-304L cluster

Based on the findings presented in Figure IV.8, it can be observed that the Van der Waals interaction energy contributes significantly to the mixing of the inhibitor with both the Fe35 cluster and the 304L cluster. Specifically, the Van der Waals interaction energy is the primary contributor to the overall contact energy in these interactions.

Interestingly, it was discovered that the contributions of hydrogen bonding (HB) and electrostatic (Hmisfit) enthalpies were found to be null for the second type of interaction energy, where no hydrogen bonding occurs. This means there is no significant involvement of hydrogen bonding or electrostatic interactions in this particular type of interaction.

Although hydrogen bonding and electrostatic contributions were present for the first type of interaction energy, their magnitudes were negligible. In other words, while they

contribute to the overall interaction, their impact is relatively small compared to the dominant Van der Waals interaction energy.

IV.2.2. Monte Carlo (M.C.) simulations of PGPE

A Monte Carlo simulation was conducted to investigate the physical adsorption of various complexes on an iron (110) surface, as shown in Table IV.7. this study focused on physical forces, specifically Van der Waals and electrostatic interactions. The stability of the adsorption system was assessed based on the adsorption energy (Eads), where a higher absolute value indicates stronger inhibitor-Fe (110) interactions and more efficient corrosion inhibition.

The study results revealed that Punicalagin with 10 H_2SO_4 exhibited the best complex, displaying active interactions with the 304L surface. Following the principle of higher absolute values of the adsorption energy, the inhibitory efficiency of the studied complexes can be ranked as follows: [Punicalagin]>[Punicalin]>[Gallagic_acid]>[Ellagic_acid]>[Gallic_acid] against the corrosion of Fe_{35} and 304L steel in both 5 H_2SO_4 and 10 H_2SO_4 solutions.

Table IV.7. Adsorption energies (kcal/mol) of the extract's main components on the Fe35 and 304L at different acid concentrations

Energy \ Structures		Fe_{35}		304L	
		5 H_2SO_4	10 H_2SO_4	5 H_2SO_4	10 H_2SO_4
Total Energy		1321.260	1861.000	1313.594	1870.435
Adsorption energy		-8285.024	-8814.623	-8292.691	-8805.189
Rigid adsorption energy		-53.437	-56.096	-61.478	-54.856
DeformationEnergy		-8231.587	-8758.527	-8231.213	-8750.332
dEad/dNi (Desorption Energy)	Punicalagin	-1741.665	-1750.064	-1760.225	-1720.472
	Gallagic_acid	-811.995	-823.237	-816.278	-824.337
	Gallic_acid	-197.817	-197.054	-206.446	-196.487
	Ellagic_acid	-360.739	-362.695	-365.848	-361.079
	Punicalin	-1367.387	-1351.970	-1358.706	-1348.864
	H_30^+	-54.828	-54.829	-54.828	-54.825
	SO_4^{2-}	-25.409	-25.409	-25.409	-25.409
	H_2O	-16.499	-16.499	-16.499	-16.499

The optimal adsorption arrangement of PGPE inhibitors on metal surfaces (XC48 and 304L) is shown in Figure IV.9.

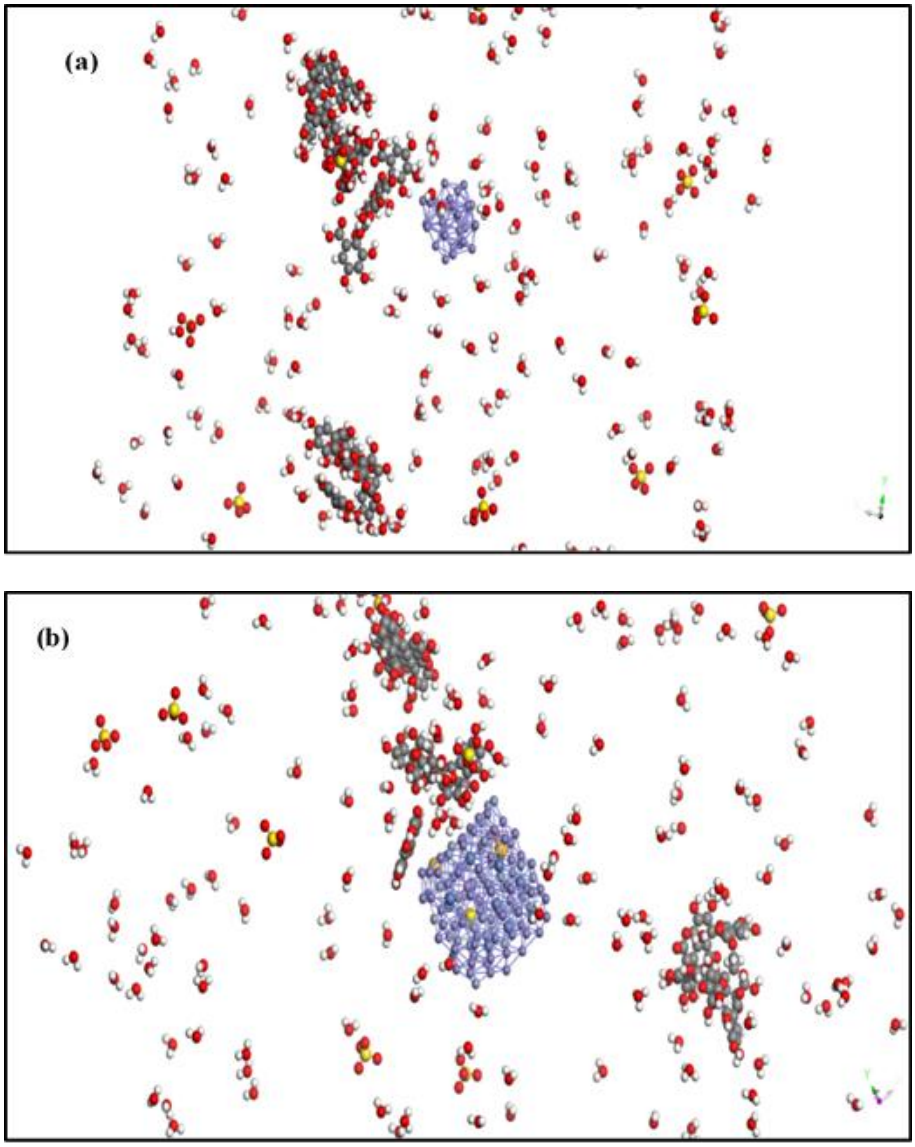

Figure IV.9. Extract's main components adsorption on the two iron clusters

IV.3. Conclusion

In conclusion, the electrochemical study and analysis findings in this chapter demonstrate the corrosion inhibition properties of two plant extracts, namely PGPE and CMFE, on the metals XC48 and 304L stainless steel. The results indicate that these plant extracts effectively inhibit the corrosion process of both metals.

Further investigations using infrared spectrum analysis and microscopic scanning have provided valuable insights. The presence of compounds from the two extracts on the metal surfaces has been confirmed through these analyses. Additionally, Monte Carlo simulations have supported and validated these experimental observations.

This chapter provides comprehensive evidence of the corrosion-inhibitory effects of PGPE and CMFE extracts on XC48 and 304L stainless steel. The extracts' compounds on the metal surfaces indicate their potential role in forming a protective layer and inhibiting corrosion. These findings contribute to the understanding and development natural extract-based corrosion inhibitors for various metal systems.

Reference

[1] B. Gómez, N. V. Likhanova, M. A. Domínguez-Aguilar, R. Martínez-Palou, A. Vela, et J. L. Gázquez, « Quantum Chemical Study of the Inhibitive Properties of 2-Pyridyl-Azoles », *J. Phys. Chem. B*, vol. 110, n° 18, Art. n° 18, mai 2006, doi: 10.1021/jp057143y.

[2] R. G. Parr et R. G. Pearson, « Absolute hardness: companion parameter to absolute electronegativity », *ACS Publications*, 1 mai 2002. https://pubs.acs.org/doi/pdf/10.1021/ja00364a005 (consulté le 17 octobre 2021).

[3] H. Ferkous, S. Djellali, R. Sahraoui, Y. Benguerba, H. Behloul, et A. Çukurovali, « Corrosion inhibition of mild steel by 2-(2-methoxybenzylidene) hydrazine-1-carbothioamide in hydrochloric acid solution: Experimental measurements and quantum chemical calculations », *J. Mol. Liq.*, vol. 307, p. 112957, juin 2020, doi: 10.1016/j.molliq.2020.112957.

[4] W. Bououden *et al.*, « Surface adsorption of Crizotinib on carbon and boron nitride nanotubes as Anti-Cancer drug Carriers: COSMO-RS and DFT molecular insights », *J. Mol. Liq.*, vol. 338, p. 116666, sept. 2021, doi: 10.1016/j.molliq.2021.116666.

[5] A. S. Darwish *et al.*, « Multicomponent extraction of aromatics and heteroaromatics from diesel using acidic eutectic solvents: Experimental and COSMO-RS predictions », *J. Mol. Liq.*, vol. 336, p. 116575, août 2021, doi: 10.1016/j.molliq.2021.116575.

[6] T. Lemaoui *et al.*, « Predicting the density and viscosity of hydrophobic eutectic solvents: towards the development of sustainable solvents », *Green Chem.*, vol. 22, n° 23, p. 8511‑8530, déc. 2020, doi: 10.1039/D0GC03077E.

[7] T. Lemaoui *et al.*, « Molecular-Based Guide to Predict the pH of Eutectic Solvents: Promoting an Efficient Design Approach for New Green Solvents », *ACS Sustain. Chem. Eng.*, vol. 9, n° 17, p. 5783‑5808, mai 2021, doi: 10.1021/acssuschemeng.0c07367.

[8] M. Yoosefian, A. Pakpour, et N. Etminan, « Nanofilter platform based on functionalized carbon nanotubes for adsorption and elimination of Acrolein, a toxicant in cigarette smoke », *Appl. Surf. Sci.*, vol. 444, p. 598‑603, juin 2018, doi: 10.1016/j.apsusc.2018.03.108.

[9] H. Ghiassi et H. Raissi, « Investigation of adsorption properties of CS_2 on interior and exterior surfaces of single-walled silicon-carbide nanotubes and effect of applied electric field: electronic structure, charge density and NMR studies », *RSC Adv.*, vol. 5, n° 102, p. 84022‑84037, oct. 2015, doi: 10.1039/c5ra06459g.

[10] N. Ding, X. Chen, et C.-M. Lawrence Wu, « Interactions between polybrominated diphenyl ethers and graphene surface: a DFT and MD investigation », *Environ. Sci. Nano*, vol. 1, n° 1, p. 55‑63, 2014, doi: 10.1039/C3EN00037K.

[11] A. Dutta, S. Kr. Saha, P. Banerjee, et D. Sukul, « Correlating electronic structure with corrosion inhibition potentiality of some bis-benzimidazole derivatives for mild steel in hydrochloric acid: Combined experimental and theoretical studies », *Corros. Sci.*, vol. 98, p. 541‑550, sept. 2015, doi: 10.1016/j.corsci.2015.05.065.

[12] N. Kovačević et A. Kokalj, « Chemistry of the interaction between azole type corrosion inhibitor molecules and metal surfaces », *Mater. Chem. Phys.*, vol. 137, n° 1, p. 331‑339, nov. 2012, doi: 10.1016/j.matchemphys.2012.09.030.

[13] S. Boudjelida, S. Djellali, H. Ferkous, Y. Benguerba, I. Chikouche, et M. Carraro, « Physicochemical Properties and Atomic-Scale Interactions in Polyaniline (Emeraldine

Base)/Starch Bio-Based Composites: Experimental and Computational Investigations », *Polymers*, vol. 14, n° 8, p. 1505, avr. 2022, doi: 10.3390/polym14081505.

[14] H. Ferkous *et al.*, « The Removal of a Textile Dye from an Aqueous Solution Using a Biocomposite Adsorbent », *Polymers*, vol. 14, n° 12, p. 2396, juin 2022, doi: 10.3390/polym14122396.

[15] H. Behloul *et al.*, « New insights on the adsorption of CI-Reactive Red 141 dye using activated carbon prepared from the ZnCl2-treated waste cotton fibers: Statistical physics, DFT, COSMO-RS, and AIM studies », *J. Mol. Liq.*, vol. 364, p. 119956, oct. 2022, doi: 10.1016/j.molliq.2022.119956.

[16] M. Abdallah, H. M. Altass, A. S. Al-Gorair, J. H. Al-Fahemi, B. A. A. L. Jahdaly, et K. A. Soliman, « Natural nutmeg oil as a green corrosion inhibitor for carbon steel in 1.0 M HCl solution: Chemical, electrochemical, and computational methods », *J. Mol. Liq.*, vol. 323, p. 115036, févr. 2021, doi: 10.1016/j.molliq.2020.115036.

[17] E. Ech-chihbi *et al.*, « Experimental and computational studies on the inhibition performance of the organic compound "2-phenylimidazo [1,2-a]pyrimidine-3-carbaldehyde" against the corrosion of carbon steel in 1.0 M HCl solution », *Surf. Interfaces*, vol. 9, p. 206‑217, déc. 2017, doi: 10.1016/j.surfin.2017.09.012.

[18] F. El-Hajjaji *et al.*, « Experimental and quantum studies of newly synthesized pyridazinium derivatives on mild steel in hydrochloric acid medium », *Mater. Today Proc.*, vol. 13, p. 822‑831, 2019, doi: 10.1016/j.matpr.2019.04.045.

[19] R. G. Parr, L. v. Szentpály, et S. Liu, « Electrophilicity Index », *J. Am. Chem. Soc.*, vol. 121, n° 9, p. 1922‑1924, mars 1999, doi: 10.1021/ja983494x.

[20] R. G. Pearson, « Absolute electronegativity and hardness: applications to organic chemistry », *ACS Publications*, 1 mai 2002. https://pubs.acs.org/doi/pdf/10.1021/jo00267a034 (consulté le 4 juin 2023).

[21] A. Kahlouche *et al.*, « Molecular insights through the experimental and theoretical study of the anticorrosion power of a new eco-friendly Cytisus multiflorus flowers extract in a 1 M sulfuric acid », *J. Mol. Liq.*, vol. 347, p. 118397, 2022, doi: https://doi.org/10.1016/j.molliq.2021.118397.

General Conclusion

The present work was devoted to studying the corrosion inhibition of XC48 carbon steel and 304L stainless steel, in an aggressive environment of sulfuric acid at 1M, investigated by potentiodynamic polarization and electrochemical impedance spectroscopy (EIS) methods. Scanning electron microscopy (SEM) with X-ray photoelectron spectroscopy (XPS) and X-ray diffraction (XRD) analysis were performed to analyze the metal surface. Fourier-transform infrared spectroscopy with attenuated total reflectance (FT-IR/ATR) was applied to investigate the adsorption behavior. Finally, the experimental results were confirmed using density functional theory (DFT) calculations.

This study examines the inhibitory property of some green products, such; as Cytisus multiflorus extract (CMFE) and Punica granatum extract (PGPE). The essential objective of this manuscript is to add to the literature other natural, biodegradable, non-toxic, less expensive, and available inhibitors with significant inhibitory efficacy.

Cytisus Multiflorus is a species (Leguminosae-cytiseae), a broad and diverse genus found around the Mediterranean, particularly in North Africa and Europe. This genus of plants has bioactive, antiparasitic, and antioxidant properties with a high concentration of phenolic compounds.

Pomegranate (Punica granatum) is one of the essential fruits grown in Turkey, Iran, the USA, the Middle East, and Mediterranean and Arabic countries. It is originated from southeast Asia. Extracts from various parts of the plant have exhibited antioxidant, antibacterial, and antifungal activities. The peeling part of pomegranate contains hydroxyl, carbonyl, and aromatic groups with a considerable amount of punicalagin, punicalin, granatin A, granatin B, maleic acid, ursolic acid, gallic acid, and antioxidant materials. These substances with influential constitutive chemical groups in their structure could show corrosion inhibition performance.

The polarization curves obtained indicate that the addition of the tested inhibitors to the corrosive medium causes a decrease in the corrosion rate. They also show that the inhibitor molecules tested can be classified as mixed inhibitors. The evaluation of the inhibitory power revealed that CMFE and PGPE are the most effective inhibitor; their inhibitory efficiency reaches 75.6% and 97.60% at a concentration of 500 ppm in XC48 carbon steel and 304L stainless steel, respectively.

The electrochemical impedance spectra of the inhibitors studied show that the values of the charge transfer resistance and the film resistance formed at the metal/solution interface increase with increasing inhibitor concentration. This is assigned to the adsorption of these inhibitors to the metal surface. The values of inhibitory efficacy, estimated by electrochemical impedance spectroscopy and the potentiodynamic method, are in good agreement.

Scanning electron microscopy (SEM) images of XC48 carbon steel and 304L stainless steel immersed in a sulfuric acid containing CMFE and PGPE show a less corroded surface, indicating that these molecules have adsorbed onto the metal surface and forming a barrier between these inhibitors and metal surface.

The XRD spectrum of carbon steel immersed in 1M H_2SO_4 solution containing CMFE and PGPE (500 ppm), on the other hand, shows prominent peaks which are typical of the metal, and the absence of the peaks of the oxides are explained by the adsorption of our extracts (CMFE and PGPE) on the metal surface, leading to the creation of a protective layer on the surface of the steels.

FT-IR and XPS results confirmed the development of a protective layer comprising CMFE and PGPE molecules with iron.

DFT calculations give a better insight into the reactivity of the CMFE and PGPE with respect to XC48 carbon steel and 304L stainless steel at a good correlation with the experimental results.

Journal of Molecular Liquids 347 (2022) 118397

Contents lists available at ScienceDirect

Journal of Molecular Liquids

journal homepage: www.elsevier.com/locate/molliq

Molecular insights through the experimental and theoretical study of the anticorrosion power of a new eco-friendly *Cytisus multiflorus* flowers extract in a 1 M sulfuric acid

Abdesalem Kahlouche [a,b], Hana Ferkous [c,d], Amel Delimi [c,d], Souad Djellali [e], Krishna Kumar Yadav [f], Ahmed M. Fallatah [g], Byong-Hun Jeon [h], Krid Ferial [a], Chérifa Boulechfar [c], Yasser Ben Amor [i,j], Yacine Benguerba [k,*]

[a] *Laboratoire de Génie Chimique et Environnement de Skikda (LGCES), Faculté de Technologie, Université de Skikda, 21000, Algeria*
[b] *Research Centre in Industrial Technologies – CRTI, P.O. Box 64, Cheraga 16014 Algiers, Algeria*
[c] *Laboratoire de Génie méncanique et Matériaux, Faculté de Technologie, Université de Skikda, 21000, Algeria*
[d] *Département de Technologie, Université de Skikda, 21000 Skikda, Algeria*
[e] *Laboratoire de Physico-Chimie des Hauts Polymères (LPCHP), Faculty of Technology, University Ferhat Abbas Setif1, 19000 Setif, Algeria*
[f] *Faculty of Science and Technology, Madhyanchal Professional University, Ratibad, Bhopal 462044, India*
[g] *Department of Chemistry College of Science, Taif University, PO Box 11099, Taif 21944, Saudi Arabia*
[h] *Department of Earth Resources and Environmental Engineering, Hanyang University, Seoul 04763, Republic of Korea*
[i] *Higher Institute of Environmental Sciences and Technology, Carthage University, BP.1003 Hammam-Lif, 2050 Ben Arous, Tunisia*
[j] *Laboratory of Wastewaters and Environment, Centre of Water Researches and Technologies (CERTE) Technopark of Borj Cedria PB 273, Soliman 8020, Tunisia*
[k] *Department of Process Engineering, Faculty of Technology, University Ferhat Abbas Setif 1, Setif 19000, Algeria*

ARTICLE INFO

Article history:
Received 3 December 2021
Revised 21 December 2021
Accepted 22 December 2021
Available online 28 December 2021

Keywords:
Carbon steel
Corrosion
Inhibitor
Cytisus Multiflorus
WL
PDP
EIS
SEM
ATR
XPS
DFT
XRD

ABSTRACT

The use of *Cytisus Multiflorus* Flowers Extract (CMFE) as a carbon steel corrosion inhibitor in 1 M H_2SO_4 solution was investigated by potentiodynamic polarization and electrochemical impedance spectroscopy (EIS) methods. Potentiodynamic polarization curves indicated that CMFE behaves as a mixed-type inhibitor. Quantum chemical parameters were also calculated, which provided a reasonable theoretical explanation for the adsorption and inhibition behavior of CMFE on the carbon steel. The presence of CMFE leads to the formation of a protective film revealed by the Scanning Electron Microscope (SEM) and attenuated total reflectance (FTIR-ATR). The process of corrosion inhibition of carbon steel by CMFE in a 1 M H_2SO_4 was studied by X-ray photoelectron spectroscopy (XPS) and X-ray diffraction (XRD) analysis. The Density Functional Theory (DFT) and molecular dynamics (MD) studies are conducted to explore the connection between quantum calculations and experimental findings.

1. Introduction

Steel and alloys are the most widely used metals in various fields in the daily life of people in the world. Due to its physical and mechanical excellent properties [1,2], it is used in different industrial sectors such as the automobile industry and machinery in the military and aerospace industries due to its low cost [3,4]. However, mild steel corrodes upon contact with acids, such as its use in an acidic environment used in pickling and descaling processes and chemical industries, such as sulfuric acid, hydrochloric acid, and other acids [5,6].

Nowadays, one of the essential topics in industrial and academic studies is the corrosion phenomenon of mild steel in acidic media [7]. Corrosion inhibitors can be classified into three classes cathodic, anodic or mixed type [8]. During the past last decades, various types of anti-corrosion methods used plasma electrolytic

* Corresponding author.
E-mail address: yacinebenguerba@univ-setif.dz (Y. Benguerba).

https://doi.org/10.1016/j.molliq.2021.118397
0167-7322/

oxidation [9,10], physical vapor and chemical vapor deposition [11,12], electrodeposition [13,14], applying polymeric and organic coatings [15,16] and using corrosion inhibitors [17], are among the most widely used methods of protecting metals from corrosion in acidic environments. Due to its low cost, non-toxic nature, and the presence of different heterocyclic atoms, double conjugate bonds, polar groups, and aromatic rings, plant extracts are highly effective environmental inhibitors in various industries [11]. The corrosion inhibition property of organic compounds having highly electron-dense hetero-atoms such as N, S, and O is well established. To date, a large number of plant extracts have been reported. Various plant parts, such as seeds, leaves, flowers, and fruits, have been used as anti-corrosion factors [4].

Apricot juice [18] Calendula officinalis flower heads [19] Dardagan Fruit [20] Garlic [11], inox. Glycine max meal [21] *Hymenaea stigonocarpa* fruit shell [22].

Cytisus Multiflorus is a species (Leguminosae-cytiseae), a broad and diverse genus found around the Mediterranean, particularly in North Africa and Europe. This genus of plants has bioactive, anti-parasitic and antioxidant properties with a high concentration of phenolic compound [23].

However, this study aims to investigate the inhibitory effect of CMFE(CMFE) regarding the corrosion of hard steels in sulfuric acid H_2SO_4. Therefore, the inhibition efficiency was determined by adapting weight loss measurement, open circuit polarization, potentiodynamic polarization (PDP) experiments, and electrochemical impedance spectroscopy (EIS). Scanning electron microscopy (SEM) with X-ray photoelectron spectroscopy (XPS) and X-ray diffraction (XRD) analysis was were performed to analyze the metal surface. Fourier-transform infrared spectroscopy with attenuated total reflectance (FT-IR/ATR) were applied to investigate the adsorption behavior. Thus, Adsorption isotherms were also plotted. In addition, the activation parameters of the corrosion process were acquired using Arrhenius and transition-state plots. The theoretical findings of quantum chemistry calculations and MD simulations were compared with experimental data as part of our study to better understand corrosion mechanisms (see Table 1 and Table 2).

2. Materials and methods

2.1. Inhibitor extract

The Cytisus multiflorus flowers (CMF) were collected in March 2019 from the region of Collo in the Northeastern Algeria. The flowers of C. multiflorus (5 g) were grounded and defatted with 150 ml of n-hexane, for three times. The residue was extracted with 150 ml of an 80% ethanol solution (v/v) at room temperature for 1 h then the resulting mixture was filtered. The residue was removed in the same conditions three more times, and the filtrated solutions were combined, concentrated, and freeze-dried. For subsequent use, the dried extract (ethanolic extract) of C. multiflorus was stored in a vacuum at a desiccator in the dark. This procedure was performed in triplicate [24].

2.2. Metal sample

In the experiments regarding the corrosion process, XC48 Steel was used to prepare specimens and the working electrode. They helped in applying gravimetric and electrochemical studies, before each experiment, the samples were mechanically polished (using emery paper with a mesh/in grade from 400 to 2400), cleaned with double distilled water, and with acetone and finally dried in hot air before being immersed in the corrosive electrolyte. For the electrochemical studies the samples cut and embedded in an inert resin with a 0.5 cm^2 exposed surface section.

2.3. Working solutions

A solution of 1 M H_2SO_4 was prepared from analytical grade H_2SO_4 (purty 98%) and distilled water both in the presence and absence of the inhibitor to be the aggressive electrolyte solution. A variety of 50 ppm to 500 ppm was considered the working concentration of inhibitors in 1 M of H_2SO_4. Double distilled water was employed in the preparation of several concentration test solutions.

2.4. Electromechanical measurements

The electrochemical experiments were carried out by using a traditional 3-electrode (carbon steel as a working electrode WE, the platinum counter-electrode CE, and a saturated Ag/AgCl as the reference electrode RE).EIS measurements were carried out on a potentiostat–galvanostat (SP 300) coupled with a computer equipped with EC-Lab software. Before the measurement, the WE was immersed for one hour in the corrosive solution (1 M H_2SO_4). A great aid in achieving the curves of potentiodynamic polarization was the automatic change in the potential from −200 to +200 mV with a scan rate of 0.5 $mV.s^{-1}$. Following equa-

Table 1
Major chemical structures of CMF components [23].

	CGP	DHF	Rutin
name	chrysin-7-O-b-D-glucopyranoside (Molecular Formula: $C_{21}H_{18}O_{10}$ Molecular Weight 430,4 g/mol)	(7) Dihydroxyflavone isomer of chrysin (Molecular Formula: $C_{15}H_{10}O_4$ Molecular Weight: 254.2 g/mol)	(4.5) Rutin (Molecular Formula: $C_{27}H_{30}O_{16}$ Molecular Weight: 610.5 g/mol) (Rutin)
Compound	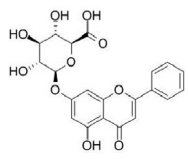	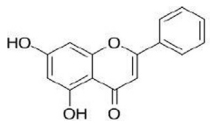	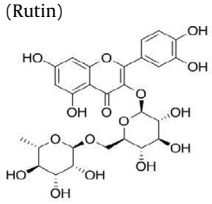

Table 2
Chemical composition of XC48 carbon steel.

Element	C	SI	Mn	P	Cr	Mo	Ni	Fe
% wt	0.440	0.187	0.610	0.0090	0.040	0.001	0.011	98.703

tion (1), corrosion inhibition efficiency was calculated, the Tafel exploration approach was used [25]:

$$E_{icorr}(\%) = \frac{\left(i^0_{corr} - i_{corr}\right)}{i^0_{corr}} \times 100 \quad (1)$$

Where i^0_{corr} is the uninhibited solution current density and i_{corr} the inhibited solution current density.

The Stern-Geary correlation was employed as shown by equation to indicate the polarization resistance R_p (Ω cm^2):

$$R_p = \frac{\beta_a \beta_c}{2.30 i_{corr}(\beta_a + \beta_c)} \quad (2)$$

Where β_a and β_c respectively are the anodic and cathodic Tafel slopes respectively.

The Values of polarization resistance were employed according to equation in order to determine CMFE inhibition efficiency:

$$E_{Rp}(\%) = \frac{\left(R_p - R^0_p\right)}{R_p} \times 100 \quad (3)$$

Where R^0_p and R_p represent the values for system's polarization resistance before and after inhibitor addition.

The EIS measurements were carried out at an open circuit potential with a frequency window of 50 to 10 mHz and an amplitude of 10 mV. The data obtained was used to determine inhibition efficiency (E_{EIS}) by employing the following formula [26]:

$$E_{EIS}(\%) = \frac{\left(R_{ct} - R^0_{ct}\right)}{R_{ct}} \times 100 \quad (4)$$

Surface coverage degree was also determined by:

$$\theta = \frac{(R_{ct} - R^0_{ct})}{R_{ct}} \quad (5)$$

While R^0_{ct} and R_{ct} indicate the charge transfer resistance before and after inhibitor (CMFF) addition.

2.5. Surface characterization

The cylindrical carbon steel samples of (Diameter: D = 15 mm and Thickness H = 2 mm) are prepared and used in the following surface analyzes:

2.5.1. SEM analysis

SEM could be used to monitor the change in corrosion process on the carbon steel surface in both cases of inhibitor existence and its non-existence. The samples were immersed in the corrosive solution (H_2SO_4, 100 ml, 1 M in both existence and absence of the CMFE inhibitor (500 ppm) for 24 h at room temperature. After that, the samples were extracted and cleaned with double distilled water and dried soon after. The SEM analysis was performed using FEI Quanta 250 model instrument while applying an acceleration voltage of 20 kVolts.

2.5.2. Fourier transform infrared spectroscopy

Fourier transform infrared spectroscopy analysis was adopted to detect the presence of the specific functional groups of the CMF Extract inhibitor. Attenuated Total Reflectance Fourier-transform infrared spectroscopy (ATR-FTIR) measurements were performed with a FT/IR 4200 Jasco operated in the wavelength range 4000–400 cm^{-1}.

2.5.3. X-Ray diffraction (XRD)

Our theoretical study has characterized the XC48 carbon steel surface before immersion in aggressive solutions in presence and absence of the inhibitor by X-ray diffraction using Bruker D8 Advance A25 instrument.

2.5.4. XPS analysis

The corrosion inhibition obtained results were verified by X-rays photoelectron (XPS) analysis on the pure CMFE and the steel surface. The latter was treated with 500 ppm CMFE at 298 K after 24 h of immersion in 1 M H_2SO_4 to determine the inhibited interface's chemical composition. The sample was collected and washed shortly with double distilled water. XPS measurements on Kratos Axis Ultra have been carried out with AlKα (1486.6 eV) radiation for surface study. At 20 eV pass energy with a resolution of 0.9 eV, the high-resolution spectra were acquired. The C 1s line of 284.4 eV was used to correct the energy charge shift's binding energies.

2.6. Theoretical study

2.6.1. Quantum chemical calculations

The DFT-B3LYB method was employed to optimize the CMFE compound and carry out the Quantum chemical calculations; with the basis set TZVP while using the Turbomole program package [27]. On the other hand, Materials Studio (MS) for further DFT computations at the level of generalized gradient approximation (GGA-BP) and the basis for double numeric polarization (DNP) are to be carried out [28]. Calculations were conducted in a liquid phase as a conductor-like screening model for real-solutions (COSMO-RS) [27,28]. Fukui functions, combined with dual description calculation, were calculated using the Dmol3 module to investigate nucleophilicity and electrophilicity [28].

Equations of hardness η and electronegativity χ (chemical potential μ) have been given based on the ground state energies of ionization (I) and the electron affinity (A) values for CMFE [28].

$$\chi = -\mu = \frac{I + A}{2} \quad (6)$$

$$\eta = \frac{I - A}{2} \quad (7)$$

$$I = -E_{HOMO} \quad (8)$$

$$A = -E_{LUMO} \quad (9)$$

Softness (σ), known as the multiplicative inverse of the hardness, is commonly recognized as a parameter closely related to the polarizability.

$$\sigma = 1/\eta \quad (10)$$

The chemical proton affinity (PA) is proportional to the chemical potential value, which means calculating the chemical potential is considered a test for proton affinity. The electrophilicity index (ω) of ions, atoms, and molecules is calculated from the electronegativity and hardness values [28].

$$\omega = \frac{\chi^2}{2\eta} \quad (11)$$

The fraction of electrons transferred (ΔN) is calculated in corrosion studies by the next formula [28].

$$\Delta N = [\chi_{Fe} - \chi_{inh}]/[2(\eta_{Fe} + \eta_{inh})] \quad (12)$$

The atom in molecule (AIM) characteristics were calculated using ADF software [63]. The def-TZVP basis set was used for molecular structure optimization in the DFT-B3LYP [63]. Materials Studio 2017 was utilized with molecular mechanics and Monte Carlo simulations to better understand the interactions between the inhibitors and steel surfaces.

2.6.2. MD simulations

The Material Studio' Forcite module was used to carry out MD [32]. The iron structure was imported from the software database. It was then cleaved along (1 1 0) plane, and a slab of 15 Å length was obtained. The MD model consists of two layers: a top layer for the solvent; and a frozen bottom layer of Fe(1 1 0). The solvent layer was constructed using one inhibitor molecule, chloride (10) ions with their counter ions, hydronium (10), and water molecules (1 0 0). Both layers were placed in a simulation box (15.20 × 18.1 69 × 43.43 $Å^3$). The system was first optimized using the SMART minimizer algorithm until the energies and temperature reached a steady-state under periodic boundary conditions and the COMPASS force field. Electrostatic interactions were calculated using the Ewald summation technique with an Ewald precision of 1.0×10^{-4} kcal mol^{-1} and a buffer width of 0.5 Å. The atom-based summation approach was used to calculate the Van der Waals interactions, a cut-off of 15.5 Å and the buffer width of 0.5 Å. The simulation model was submitted to MD after the optimization step, performed using the Andersen thermostat method under the canonical NTV set (constant N, T, and V) at T = 298 K [32]. The simulation was performed with a time step of 1 fs and a full time of 2 ns. On MD's trajectory after simulation, the radial distribution function, also known as the pair correlation function, was determined to study the interaction between the inhibitory molecule and iron surface.

3. Results and discussion

3.1. Electrochemical measurements:

3.1.1. Open circuit potential (OCP) measurements

The variation of potential versus elapsed time during 30 min for the uninhibited and the inhibited (CMFE) solution is presented in Fig. 1. It can be observed that the mild steel samples could achieve a quasi-stable open circuit potential under 30 min. Therefore, 30 min OCP measurement was assumed prior to performing all electrochemical.

In the case of uninhibited solution, a decrease in potential E_{OCP} is observed after about 5 min immersion into H_2SO_4 this might be attributed to the dissolution of iron [29]. The behavior was different for the inhibited solution. The E_{OCP} was shifted to more positive potential values and no obvious fluctuation of E_{OCP} was observed in the measurement time frame, indicating that these interfaces seem to have an increased corrosion resistance.

All the phenomena happened in the presence of inhibitor are due to opposite processes existed at the metal/solution interface [30]. It is also noticed that, in most circumstances, the value of OCP in the presence of CMFE towards more positive potential (-450 mV for 500 ppm of (CMFE) in comparison with blank solution (-540 mV), which can be explained as the effective adsorption of inhibitor molecules on the metal surface [31].

3.1.2. Polarization measurements

The anodic and cathodic reactions kinetics can be analyzed using potentiodynamic polarization measurements. The PDP curves of XC48 steel without and with different concentrations of CMFE inhibitor are represented in Fig. 2. The kinetics parameters of the electrochemical reactions after the extrapolation of the Tafel curves are presented in Table 3. The obtained result from Table 3 reveals that the values of corrosion current density decreases and inhibition efficiency increases respectively as the CMFE concertations increases. At a concentration of 500 ppm, the corrosion current density and inhibition efficiency are 8.518 μA/cm^2 and 96.339% respectively. The shifts in the E_{corr} values in presence of CMFE is more negative with respect to blank. However, at lower concertation (50 ppm), this shift is towards slight positive side as compared to the blank. In the corrosion potential between 3 and 18 mV in comparison to the blank solution. These values are less than the value of E_{corr} shift of ± 85 mV generally taken as a benchmark for an inhibitor to be classified as anodic or cathodic, [31] hence (CMFE) officinalis extact could be considered to function as a mixed-type inhibitor. The corrosion potential E_{corr} of XC48 steel was found to be around −493,90 m V vs. Saturated Calomel Electrode (SCE) with a corrosion current density 232,686 μA/cm^2. Hydrogen evolution dominates at more negative potential than E_{corr}, resulting in an increase in the cathodic currents [32]. A shift in potential, as compared to different concentrations is observed for of inhibitor in 500 ppm of CMFE with E_{corr} − 490,638 m V vs. SCE. The presence of the film decreased additionally significantly both the anodic and cathodic current densities due to a restricted supply of oxygen and water, limiting their reduction. Consequently, the corrosion currents are reduced by two orders of mag-

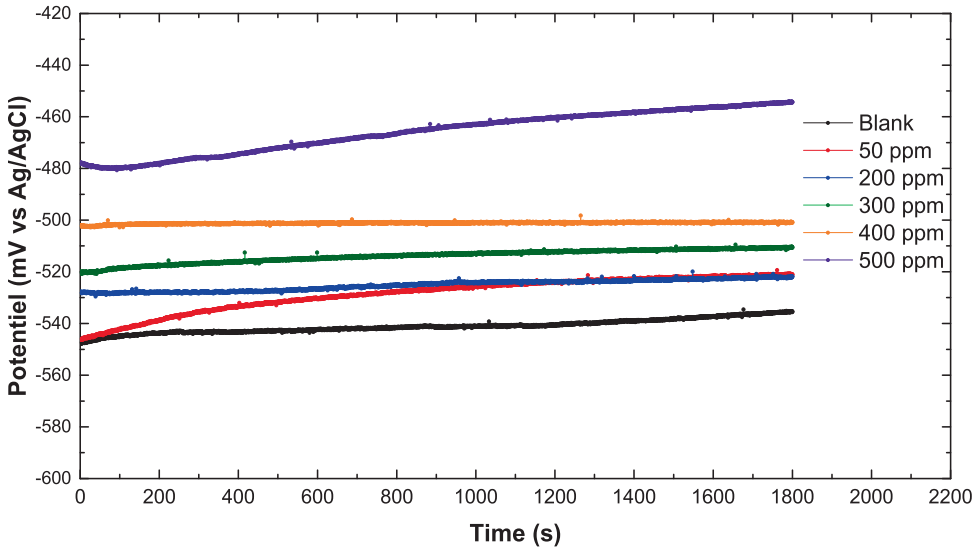

Fig. 1. Open circuit potential (OCP) of the XC 48 steel at different concentrations of CMFE.

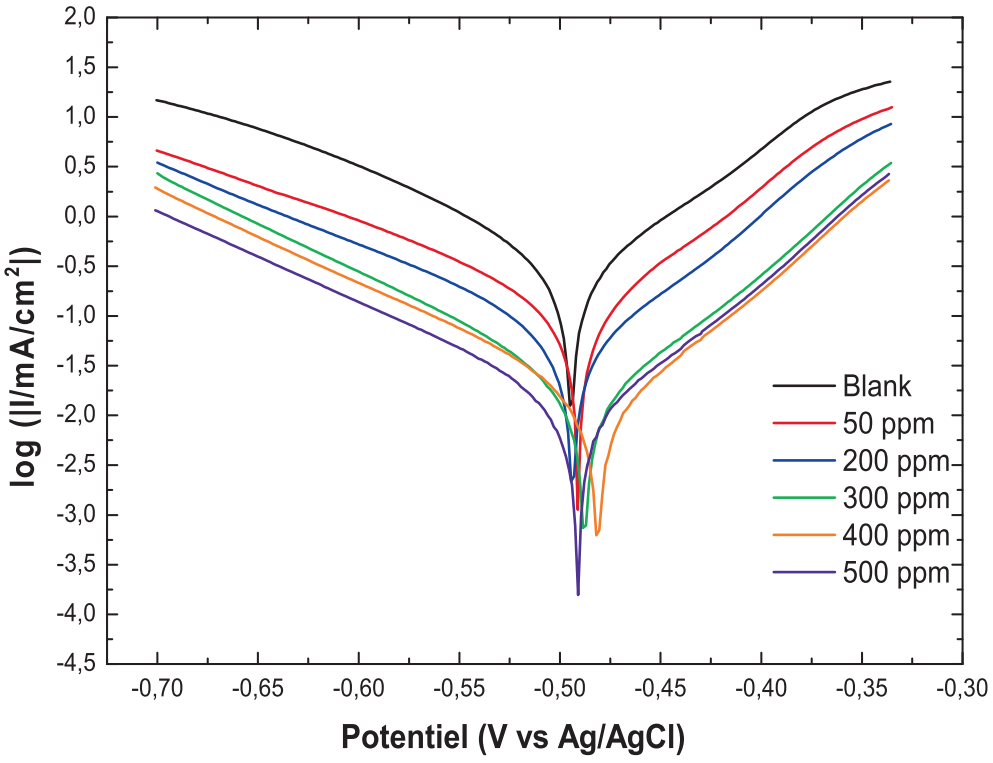

Fig. 2. Polarization curves of XC48 steel in 1 M H_2SO_4 solutions with various concentration of CMFE.

Table 3
Polarization parameters for XC48 steel corrosion in 1 M H_2SO_4 in the absence and presence of CMFE;

Concentration(ppm)	E_{corr} *(mV)*	I_{corr} *(μA/cm²)*	β_a *(mV)*	β_c *(mV)*	C_R *(mmpy)*	*Rp (Ohm)*	*θ*	IE_{Rp} *%*
Blanc	−493.90	232.686	74	84.4	5.5149	59.3	0.9998	–
50	−490.98	105.82	77.7	114.4	2.50804	166	0.9984	64.27
200	−493.73	59.807	79.1	109.5	1.41849	317	0.9999	81.29
300	−487.71	18.826	82.3	93	0.446196	970	0.9997	93.88
400	−481.21	14.878	78.6	97.7	0.352624	1 230	0.9998	95.17
500	−490.63	8.518	68.7	78.5	0.201885	1 453	0.9997	95.91

nitude compared to different concentrations of inhibitor and results in i_{corr} 10,8691 μA/cm². The protection efficiency (PE) of the coating was determined from the polarization curve.

3.1.3. Electrochemical impedance spectroscopy (EIS)

Fig. 3 illustrate the results obtained for EIS steel XC48 in 1 M H_2SO_4 solutions interfaces, with various CMFE amounts. The EIS experiments were conducted in order to evaluat the impedance of XC48 steel corrosion in 1 M H_2SO_4 solution without and with various concentrations of the inhibitors. The recorded spectra were exemplified in Fig. 3 by Nyquist plot. The obtained result exhibits two distinguishable capacitive loops at f = 100.000 Hz – 0.1 Hz (i.e high frequency region) and f = 0.1 Hz to 0.01 Hz (i.e low frequency region). Their diameter increases with increasing inhibitor concentration. The first loop greater in size is flattened in shape and can be attributed to the charge transfer process. The second loop located at lower frequency is smaller and its shape indicating the presence of a diffusion process [33]. The observed diffusion process may have arisen due to the migration of the oxidant (i.e., the sulphate ions) from the bulk solution through the CMFE layer to the metal surface or the diffusion of adsorbed inhibitor/corrosion products from the metal surface toward the bulk solution [33].

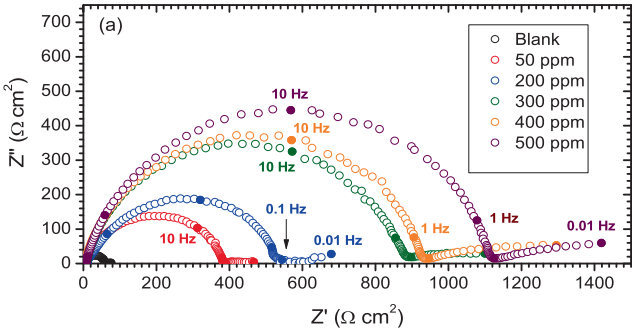

Fig. 3. Nyquist plot of XC48 steel immersed in 1 M H_2SO_4 solution without (Blank) and with different concentrations of CMFE.

To evaluate the anticorrosion behavior of the used inhibitor obtained by impedance measurements the equivalents circuits of Fig. 4 representing the studied electrochemical interface were used to reproduce the experimental results [34,35]. This fitting procedure was applied between 100 kHz and 0.1 Hz to extrapolate faradic parameters. The agreement between the experimental and

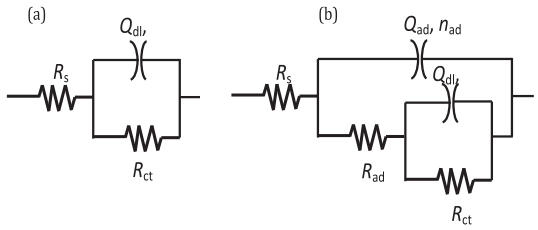

Fig. 4. Equivalent electric circuit (a) without inhibitor (Blank). (b) Solution containing diverse quantities of CMFE.

calculated points is based on the χ^2 function defined elsewhere [35].

With nf the number of the frequency. The fitting quality q is determined by:

$$q = \sqrt{\frac{\chi^2}{2 \cdot nf}} \tag{13}$$

When q close to 1. the fitting quality is considered satisfactory (Table 4).

In first approach. The circuit of Fig. 4.a was used to reproduce the capacitive behavior of the recorded impedance. In this equivalent circuit Rs is the non-compensated solution resistance. R_{ct} is the charge transfer resistance and (Q_{dl}. n_{dl}) is the constant phase element. CPE used in place of double layer capacitance to account for the non-ideal behavior of the working electrode [34]. The agreement between experimental (Z_{exp}) and the fitted impedance (Z_{fit}) was assessed by determining the error on imaginary part according to the following equation [35,36]:

$$\varepsilon_{Z(im)} = 100\frac{Z_{\exp}(im) - Z_{fit}(im)}{Z_{\exp}(im)} \tag{14}$$

The corresponding results were reproduced in Fig. 5. Using the equivalent circuit of Fig. 4.a, a good agreement was obtained with the blank system (red curve). However for 400 ppm inhibited system. the same circuit (Fig. 4.a) leads to an important and marked divergences on the imaginary part of the impedance mainly above 1000 Hz (blue curve). As a result another contribution must be considered to correctly reproduce the experimental impedance data. For inhibited system the equivalent circuit of Fig. 4.b was therefore adopted. The corresponding error was also added to the Fig. 5 (green curve). It was clearly seen that the proposed equivalent circuit (Fig. 4.b) no longer induces a systematic error. In this circuit the additional contribution consist of the CPE_{ad} (Q_{ad}. n_{ad}) and the resistance R_{ad} refereed to the adsorbed molecules of the used inhibitor on the XC48 steel surface [37].

Table 4 lists the EIS parameters obtained from the fitting procedure using the equivalent circuit of Fig. 4. The computed parameters show a rise in the I_{EZ} (%) which indicates the presence of the CMFE adsorbed on the surface of XC48 steel working electrode [38]. The introduction of the inhibitors into 1 M H_2SO_4 solution leads to an increase of both R_s and R_{ct} values compared to the blank. R_s is nearly constant for inhibited acid solution with value varying between 7.92 and 9.22 .cm^2 confirming a sufficient conductivity of all tested solutions [37,39]. In contrast, Q_{dl} and Q_{ad} decrease when the CMFE is progressively added to the 1 M H_2SO_4 solution. The decrease of the double layer capacitance is due to the adsorption of the inhibitors molecules of lower dielectric constant on the metallic surface and replacement of water molecules [40,41]. The decrease of Q_{ad}, which indicates that the corrosion reaction is slowed by the adsorbed species. Confirm the formation of a more protective and a thicker layer slowing the corrosion process [42].

3.2. Scanning electron microscope (SEM)

The surface morphology of XC48 carbon steel is represented in Fig. 6.a, 6.b and 6.c before and after immersing in 1 M H_2SO_4 acidic solution in presence and absence of inhibitor. An aggressive attack is noted (Fig. 6.b) in carbon steel surface's micrographs after immersion in the absence of inhibitor (Solution of 1 M H_2SO_4 for 24 h). The cracks and pits on the metal surface indicate that the solution's corrosive attack considerably damaged it. Meanwhile, adding 500 ppm of the inhibitor to the system (Fig. 6.c) shows a smooth and more compact surface, with very few notable cracks and pits; showing that the metal was indeed protected from the corrosive attack. The difference could easily be interpreted as the working electrode's steel surface was protected by the adsorbed CMFE molecules [32]. This demonstrates that an efficient protective layer of the tested inhibitor was adsorbed on the metal surface, and played a useful role in protecting the surface steel against corrosion.

3.3. Fourier transform infrared spectroscopy

FTIR analyses were achieved on the pure extract (CMFE) and the surface protective film developed on the XC 48 steel after immersion in 1 M H_2SO_4 acid solution at the optimum concentration. However, the FTIR was used to predict the functional group present in CMFE extract (Fig. 7.a) and then compared with spectra of surface protective film (Fig. 7.b). As shown in (Fig. 7.a) an intensive band 3335 cm^{-1} appeared. Which can be attributed to symmetrical and and asymmetrical stretching modes of O–H [43]. The two peaks at 2925 cm^{-1} and 2849 cm^{-1} are assigned to C—H stretching mode (élongation) [44]. The peak 1715 cm^{-1} corresponds to C—H elongation of the benzoic ring group. Stretching mode of C=O groups (benzoic ring) is indicated at peaks (1600 cm^{-1}, 1650 cm^{-1}, 1569 cm^{-1}, 1504 cm^{-1} and 1455 cm^{-1}) [45]. The absorption 1266 cm^{-1} corresponds to C—C bending vibration and the bands observed at 1060 cm^{-1} is linked to C—O stretching.The presence of C—O—c bonds is testified by the stretching vibration at 1115 cm^{-1}. The FTIR spectrum of the layer formed on the metal surface shown in (Fig 0.7.b) Indicates that the absorption peak of OH was shifted from 3350 cm^{-1} to about 3240 cm^{-1} [46]. Two peaks shifted to 2850 cm^{-1}corresponding to C—H of benzoic ring. The peak of 1715 cm^{-1} is also moved to about 1725 cm^{-1}, so it has been observed that approximately all peaks were shifted.

Table 4
EIS parameters for XC48 steel corrosion in 1 M H_2SO_4 without and with different concentrations of CMFE.

	R_s (cm^2)	R_{ct} (cm^2)	n_{dl}	Q_{dl} (μF.s^{nd-1}.cm^{-2})	R_{ad} (cm^2)	n_{ad}	Q_{ad} (μF.s^{nf-1}. cm^{-2})	IE_Z (%)
Blank	5.14	**53.22**	0.93	90.4	–	–	–	–
50 ppm	8.36	**284.07**	0.71	51.8	94.28	0.94	11.0	81.26
200 ppm	8.02	474.30	0.75	54.0	53.47	0.92	11.5	88.78
300 ppm	8.76	829.20	0.72	25.2	49.55	0.98	6.03	93.58
400 ppm	7.92	899.56	0.73	26.4	43.27	0.99	5.78	94.08
500 ppm	8.02	1100.3	0.74	22.7	32.57	0.98	5.13	95.16

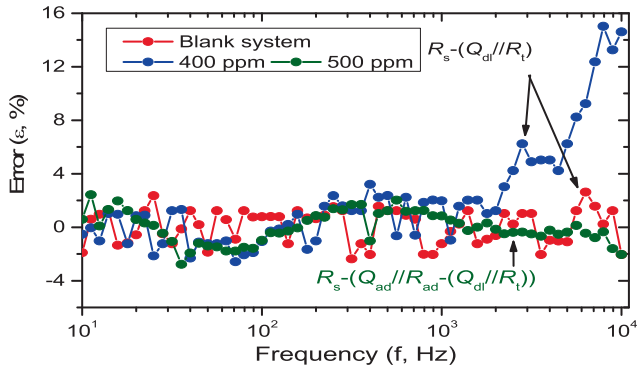

Fig. 5. Variation of the error on imaginary part as a function of frequency. Measurements recorded on blank, 400 ppm and 500 ppm inhibited systems.

These observations suggested that molecules of (CMFE) extract were adsorbed on the surface of the steel.

3.4. X-ray diffraction

X-ray diffraction was used to detect the film product on the surface of XC48 steel. XRD analysis indicates the presence of a peak at 2θ of 45.2° related to metallic iron (Fig. 8.a). The X-ray spectra of the corrosion product formed on the steel surface immersed in 1 M H_2SO_4 solution is shown in Fig. 8.b. The peaks at 16.3, 18.3, 23.5, 27.3 and 36.11 suggested the presence of Fe_3O_4 iron oxide, FeOOH and a very small amount of brown film. Which due to Fe_2O_3 observed visually and consequently leads to corrosion [47,48]. Fig. 8.c shows the X-ray diffraction patterns of XC48 steel immersed in the solution containing 500 ppm of CMF. Compared to the spectrum of the steel surface immersed in 1 M H2SO4 solution without inhibitor which showed three phases of iron oxides (Fe_2O_3, Fe_3O_4 and FeOOH), this sample represented only a very weak Fe_2O_3 peak, which corresponds to the very sligh oxidation of the XC48 steel in the presence of inhibitor. These observations clearly reflect the adsorption of a protective film over the surface of XC48 steel in the presence of each plant extracts [49–51].

3.5. XPS analysis

The XPS survey scan of pure CMFE and steel surface was treated by 500 ppm of CMFE at 298 K after 24 h of immersion in 1 M H_2SO_4 are shown in Fig. 9. The XPS spectra were obtained from pure CMFE (C 1s. and O1s) and the CMFE-treated steel surface (C 1s. O 1s. S 2p and Fe 2p). The results from Table 5 demonstrate a decrease in carbon content in pure CMFE at 73.29% to 44.18% in the metal surface treated by CMFE. These indicate the adsorption of CMFE on the steel surface. A deconvolution fitting procedure is used to represent complex forms for the related species in all XPS spectras are presented in Fig. 10.

The C1s core level spectra show four deconvoluted peaks. The first one. assigned to the presence of–C═C/–C–C in aromatic rings [52], is located at 284.49 eV for pure CMFE (Fig. 10.a) and

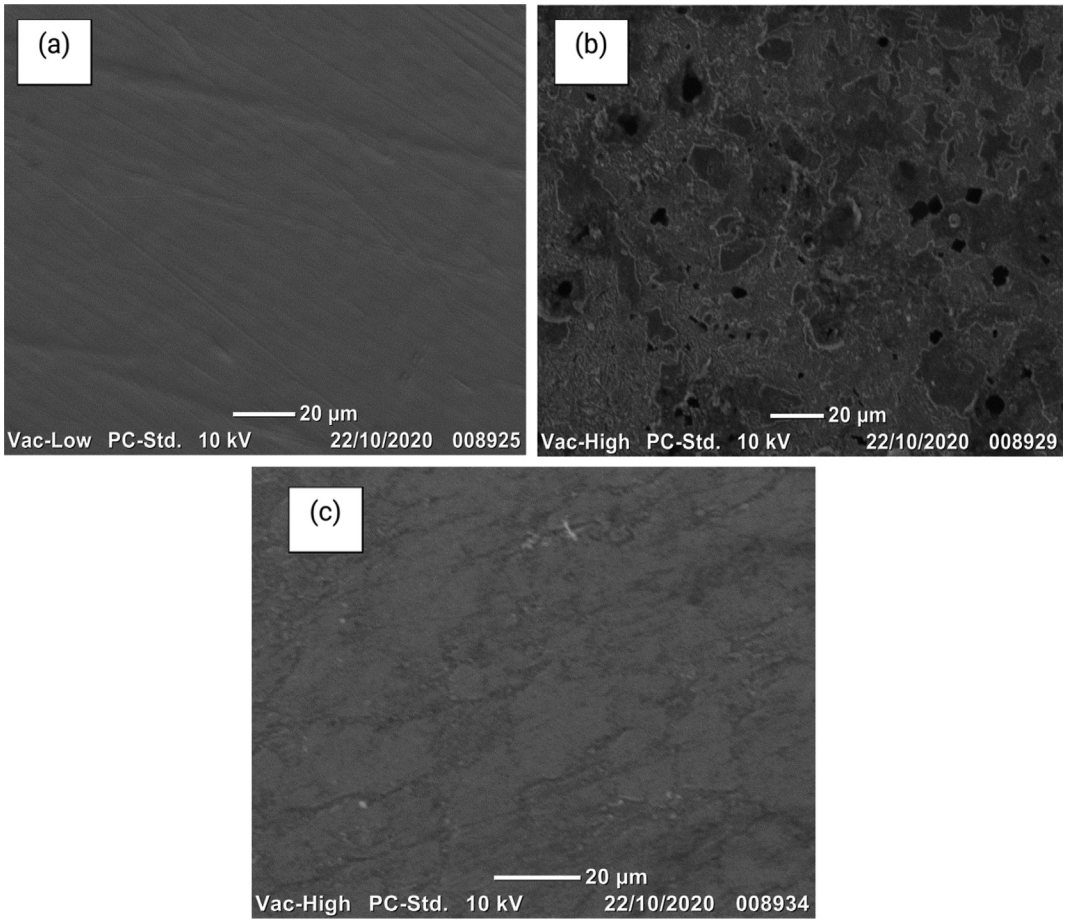

Fig. 6. SEM images of the XC48 surface a) Before immersion. b) After immersion in acidic solution without CMFE. c) After immersion in acidic solution with CMFE (500 ppm).

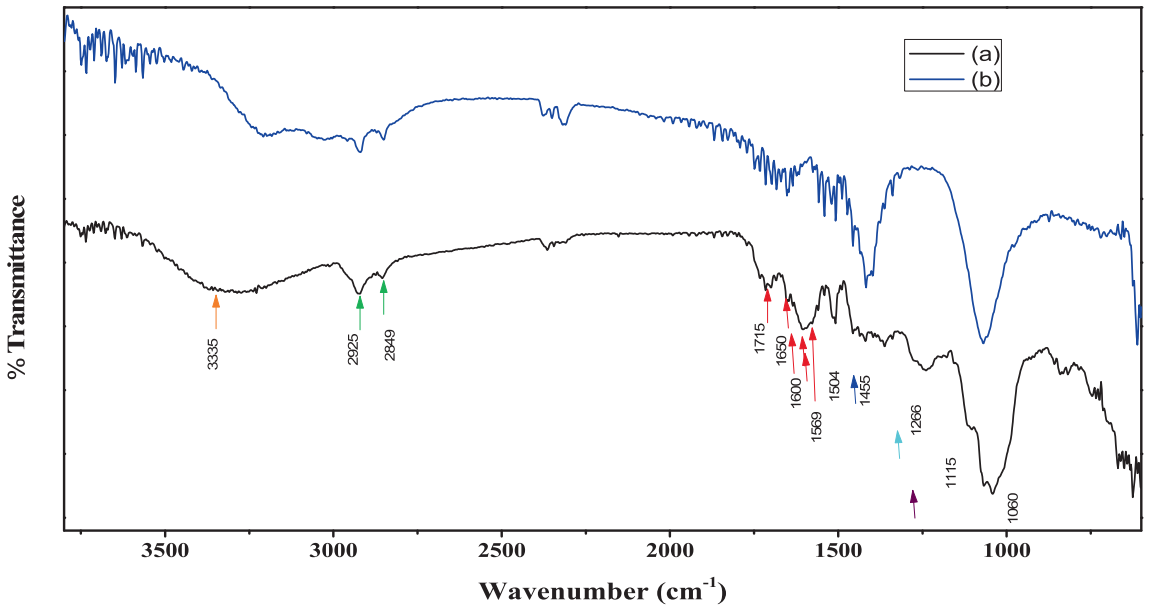

Fig. 7. FTIR spectra: (a) CMF extract and (b) surface of XC48 steel after immersion in 1 M H_2SO_4 solution containing 500 ppm of CMF extract.

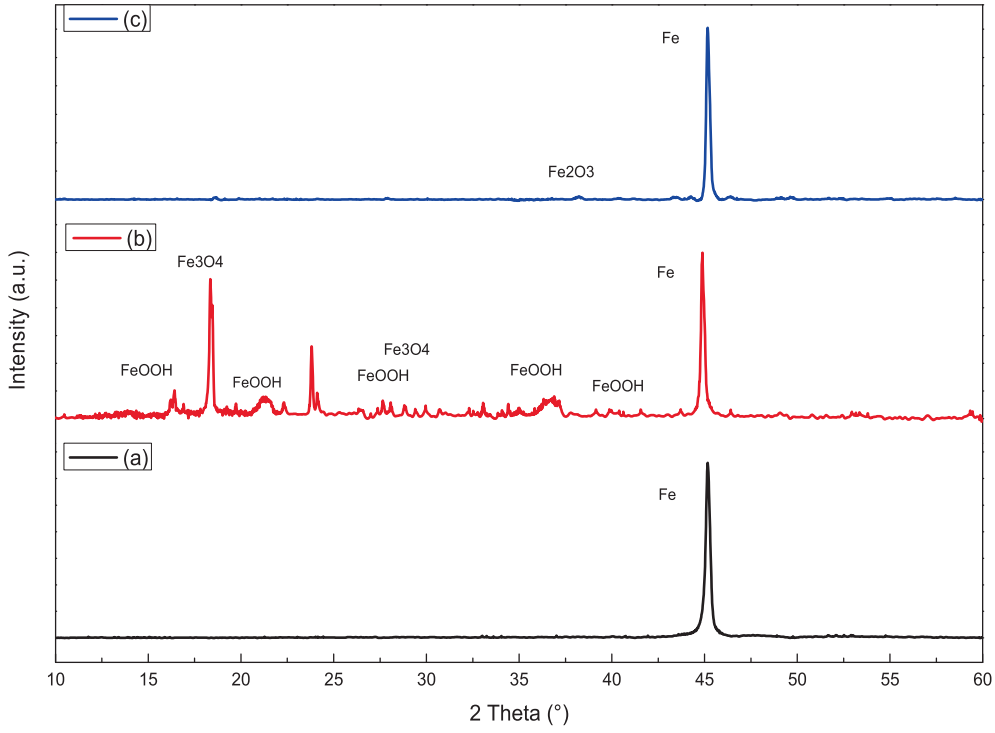

Fig. 8. XRD pattern of XC48 steel; (a) before experiment. (b) After 24 h of immersion in 1 M H_2SO_4 solution. and (c) after 24 h of immersion in 1 M H_2SO_4 solution containing 500 ppm of the CMFE.

284.58 eV for CMFE-treated carbon steel (Fig. 10.b). The second peak located at 286.03 eV for pure CMFE (Fig. 10.a) and 285.98 eV for both CMFE-treated carbon steel (Fig. 10.b). Can be attributed to the carbon atom bonded to hydrogen in C–H bonds [53] bonds and to sulfur in C-S bonds [54]. The third contribution appears at 287.42 eV and 287.08 eV for pure CMFE (Fig. 10.a) and CMFE-treated carbon steel (Fig. 10.b), respectively. These peaks correspond to the C–O with different intensities [38]. The peaks at 288.55 eV and 288.38 eV characterise the presence of C=0 bond [55].

The deconvoluted O 1s spectrum for pure CMFE (Fig. 10.c) shows two main components located at 531.15 and 533.33 eV.

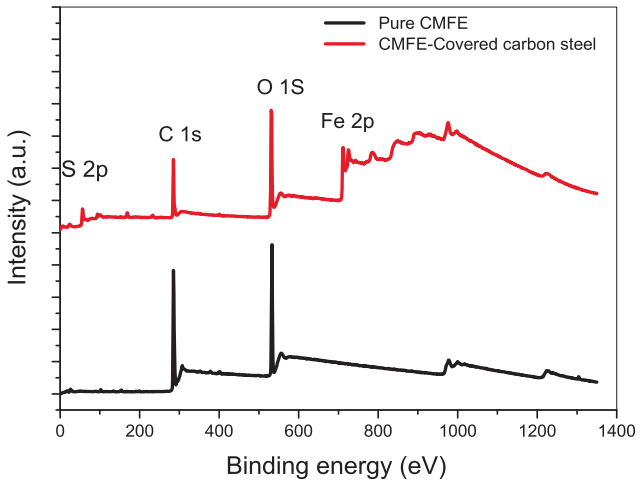

Fig. 9. XPS survey spectrum of pure CMFE and CMFE treated-carbon steel in 1 M H_2SO_4.

Table 5
The variation of elemental composition of pure CMFE and CMFE-treated steel surface after 24 h of immersion in 1 M H_2SO_4.

Elemental composition (wt%)	C 1S	0 1S	Fe 2p	S 2p
Cryt	73.29	26.71	–	–
XC48- Cryt	44.18	40.53	13.14	2.15

Which proves the presence of -C═O and –C–OH bonds. respectively [56]. The O 1s spectrum for CMFE-treated carbon steel could be fitted into four prominent peaks (Fig. 10.d). The first peak at 529.71 eV is attributed to oxygen in the Fe_2O_3 and/or Fe_3O_4 oxides bonded to Fe^{3+} [57]. The second peak located at 530.60 eV is attributable to Fe-OH and Fe-O in the iron hydroxides and oxides [53]. The third peak at 531.31 eV is attributed to OH of FeOOH [57]. The lalest peak can be due to the oxygen of the adsorbed water at 532.79 eV [58].

The S 2p high-resolution XPS spectra for XC48 steel after immersion in inhibited solution (Fig. 10.e) show one signal which corresponds to the doublet $2p_{3/2}$ and $2p_{1/2}$ in the 168.24–169.43 eV range characteristic of SO_4^{2-} ion [56].

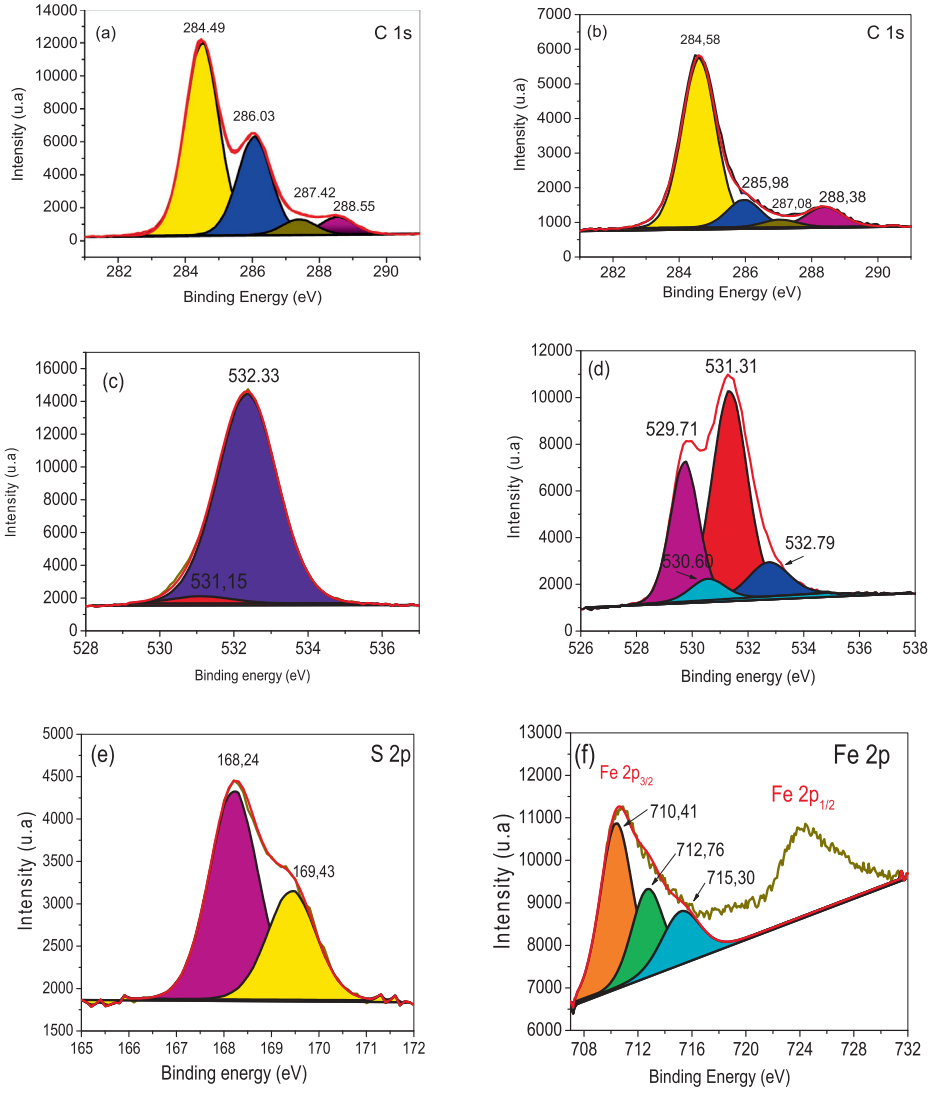

Fig. 10. The XPS deconvoluted profiles of pure CMFE (a) C 1s. (c) O 1s and for CMFE/Carbone steel (b) C 1s. (d) for O 1s. (e) S 2p and (f) Fe 2p1s. (e) S 2p and (f) Fe 2p.

Table 6
Global reactivity descriptors.

Isomer	E_{HOMO} (eV)	E_{LUMO} (eV)	Gap (eV)	χ	η	ω	ΔN
Fe_{20}	−4.139	−4.072	0.067	4.106	0.033	252.824	0.000
DHF	−6.938	−3.277	3.661	5.107	1.830	7.125	−0.139
CGP	−6.927	−3.380	3.547	5.154	1.774	7.489	−0.149
Rutin	−6.684	−3.194	3.490	4.939	1.745	6.991	−0.239

The spectrum related to Fe 2p for CMFE-covered carbon steel surfaces shows two doublets (Fig. 10.f). 710.58 eV (Fe $2p_{3/2}$) and 724.23 eV (Fe $2p_{1/2}$) related to high-energy ghost structures indicating subsequent steel surface oxidation. Three peaks constitute the deconvolution of the high-resolution Fe $2p_{3/2}$ XPS spectrum. The two prominent peaks at 710.41 eV and 712.76 eV are attributed to ferric compounds such as $Fe_2O_3/Fe_3O_4/FeSO_4/FeOOH$ [58].

Table 7
Frontiers molecular orbitals.

Isomer	HOMO	LUMO
Fe_{20}	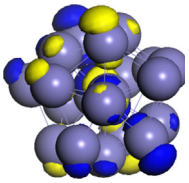	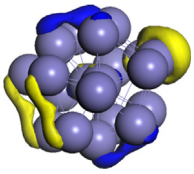
DHF	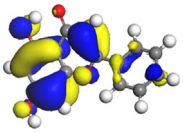	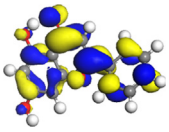
CGP	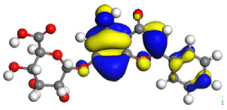	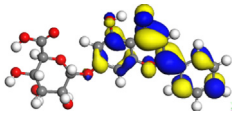
Rutin	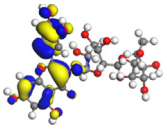	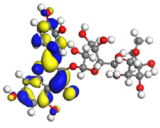

The last peak at BE = 715.30 eV may be attributed to the Fe (III) satellite feature [59].

3.6. Quantum chemical study

The frontier molecular orbitals which can be used to study the chemical reactivity and kinetic stability, are the essential molecular orbitals in a molecule. The frontier molecular orbitals are the highest occupied molecular orbital (HOMO) and the lowest unoccupied molecular orbital (LUMO). Electronic absorption or the transition from the ground to the first excited state is primarily explained by one-electron excitation from HOMO to LUMO. The system's kinetic stability increases as the HOMO-LUMO distance widens. As a result, it takes more energy to pass electrons from the ground state HOMO to the excited state LUMO. For each compound. Table 6 lists the measured orbital energies. with the HOMO-LUMO gap (E_{gap}), as well as other chemical descriptors i.e., chemical potential (μ), global hardness (η) and electrophilicity index (ω)) for CMFE and Fe cluster pure components.

Table 6 shows that Fe_{20} has the highest HOMO energy and Rutin the highest LUMO energy, which means that iron cluster is the more electron donator and Rutin is the more electron acceptor. Consequently, Rutin shows the highest inhibiting activity.

The highest HOMO-LUMO gap and hardness were calculated for the iron surface and the three selected molecules. Fe cluster was found to be the most reactive because of its lowest gap and hardness followed by Rutin with 0.067 and 3.49 eV, respectively. This results also show that CGP and DHF are more stable than Rutin.. Parr et al. [60,61] developed the global electrophilicity index (ω) based on thermodynamic properties and calculates the beneficial shift in energy when a chemical system reaches saturation by adding electrons. The energy loss is caused by the flow of electrons from the donor (HOMO) to the acceptor (LUMO) in molecules.

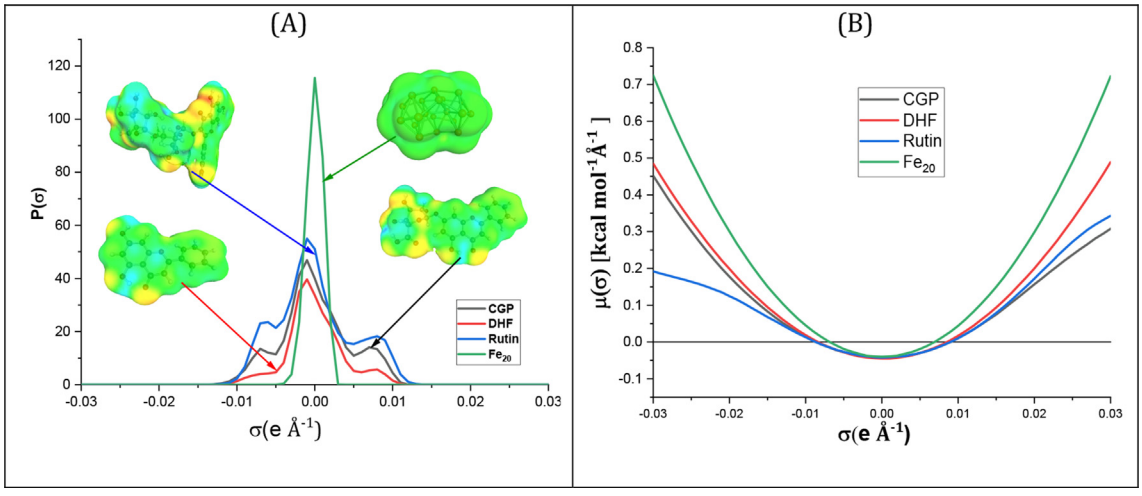

Fig. 11. COSMO-RS study: surfaces, polarities, and potentials.

It is noted that if $\Delta N > 0$ an inhibitor molecule transfers its e- to a metal and vice versa if $\Delta N < 0$ [32]. From Table 6, all the calculated values of the ΔN of the three molecules are less than zero. This confirms the molecules electron-accepting character already demonstrated. Rutin with the lowest ΔN is found to be the more electron acceptor from iron surface (electrons donator).

According to the simple charge transfer model for donation and back-donation of charges proposed recently by Gomez et al., [62] an electronic back-donation process might be occurring governing the interaction between the inhibitor molecule and the metal surface. The concept establishes that if both processes occur, namely charge transfer to the molecule and back-donation from the molecule, the energy change is directly proportional to the hardness of the molecule, as indicated in the following expression. $\Delta E_{Back\text{-}donation} = -\eta/4$.

The $\Delta E_{Back\text{-}donation}$ implies that when $\eta > 0$ and $\Delta E_{Back\text{-}donation} < 0$ the charge transfer to a molecule, followed by a back-donation from the molecule, is energetically favored. In this context, hence, it is possible to compare the stabilization among inhibiting molecules, since there will be an interaction with the same metal, then, it is expected that it will decrease as the hardness increases. Consequently, the back-donation is so pronounced for the Rutin molecule.

The HOMO was found to be located on the conjugated π-bonds of the phenylchromane in the the three molecules DHF, CGP, and Rutin (See Table 7). The LUMO was concentrated on the phenylchromane simple bonds of the three molecules. Table 7 also gives the HOMO and LUMO of the Fe cluster.

Fig. 11 shows the charge distribution of the binary interacting system. It is noted that the green surface is for the non-polar regions of the complex. The red one is for the hydrogen bond acceptor (HBA) region and finally. The blue region is for the hydrogen bond donor (HBD) region [63].

The relative probability distributions (σ-profiles) of the inhibitor and the Fe cluster (Fe_{20}) and their related σ-potentials are depicted in Fig. 11. $P(\sigma)$ denotes the number of molecular surface segments having a specific screening charge density σ [64,65]. $\sigma > 0$ represent the surfaces of negative polarity. whereas $\sigma < 0$

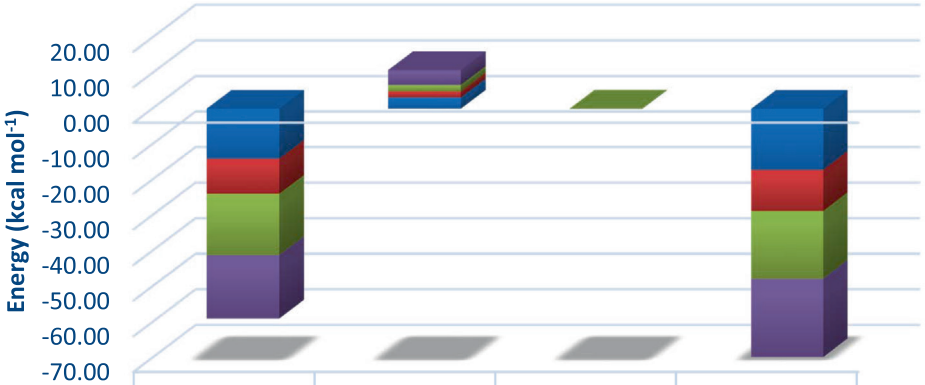

	H(int)	H(MF)	H(HB)	H(VdW)
Rutin	-17.77	4.18	-5.35E-03	-21.95
Fe20	-17.26	1.81	0.00E+00	-19.07
DHF	-9.84	1.74	-2.30E-04	-11.58
CGP	-14.06	3.12	-5.00E-04	-17.18

Fig. 12. Interaction energies of the system inhibitor-Fe_{20} cluster.

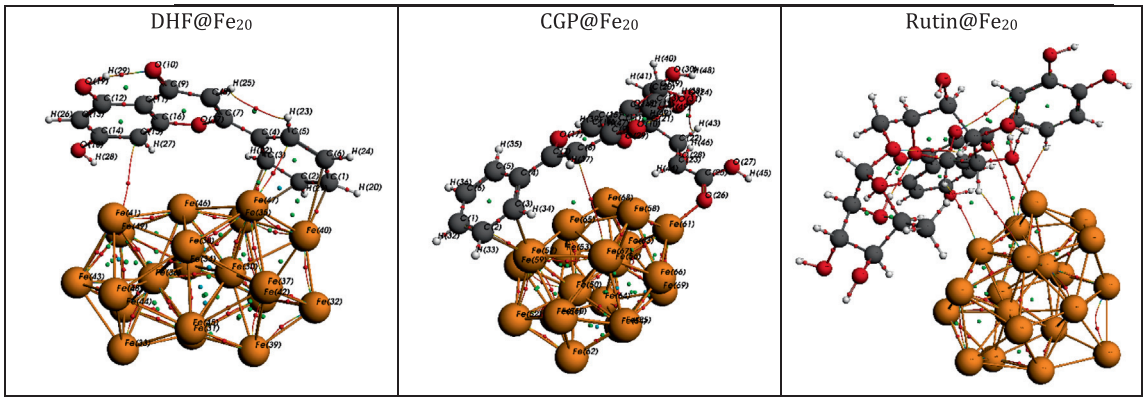

Fig. 13. Molecular graph of the optimized molecules-Fe_{20} cluster.

is for positive polarity surfaces [66,67]. $\sigma \approx 0$ is the non-polar (hydrophobic) areas. As a result. the profile curves can be separated into three sections: the HBD (hydrogen bond donor) zone ($-0.025 < \sigma < -0.010$). The non-polar zone ($-0.010 < \sigma < +0.010$). and the HBA (hydrogen bond acceptor) region ($+0.010 < \sigma < +0.025$).

In Fig. 11(a), the three inhibitor molecules are found to be mostly non-polar (green colored surfaces) with $\sigma \in$[-0.01, 0.01] au. The iron cluster Fe_{20} is as expected completely non-polar. The adsorption is expected to be in the non-polar region as concluded from Fig. 11(b). It is noticed that chemical potential is always positive in the polar regions (non-spontaneous phenomena). The chemical potential for the four molecules is less than zero in the non-polar region which suggests that the interaction forces are Van der Waals type. This confirms that the only possible interaction is with nonpolar groups or molecule chemisorption (chemical bound) as will be revealed by the AIM study.

Fig. 12 shows that the large contributing interaction energy in mixing the inhibitor with Iron cluster is Van der Waals type. The contributions of electrostatic (H_{misfit}) and hydrogen bonding (H_{HB}) enthalpies were found to be negligeable for the first type of interaction energy and null for the second one (no Hydrogen bonding).

A molecular graph of the optimized CMFE-Fe cluster complex is presented in Fig. 13, while in Table 8 the topological parameters at BCP of interaction contacts are listed.

From the results in Table 8 the calculated values of $\rho(r)$ in BCPs are quite low values and $\nabla^2\rho(r)$ are positive. Which indicates the occurrence of Hydrogen bonds (HBs) interaction in the case of the twelve BCPs bonds. On the other hand, the positive values of $\nabla^2\rho_{BCP}$ and H_{BCP} indicate the weak molecular interaction (electrostatic, G/|V|>1) between the BCPs atoms (for DHF@Fe_{20}:BCP 53; for CGP@Fe_{20}:BCP 154 and for Rutin@Fe_{20}:BCPs 126, 136, 178 and 218). The $E_{HB} < 0$ is characteristic of weak hydrogen bonding [68].

Table 8
The topological parameters at BCP of interaction contacts.

	BCP	ρ_c (Ha)	$\nabla^2\rho(r)$ (Ha)	G (Ha)	V (Ha)	E_{HB} (eV)	H = G + V (Ha)	G/|V|
DHF@Fe_{20}	53	5.77E−03	8.13E−03	1.89E−03	−1.74E−03	−2.37E−02	1.44E−04	1.08E + 00
	145	5.25E−02	1.27E−01	4.24E−02	−5.29E−02	−7.19E−01	−1.05E−02	8.01E−01
	154	1.64E−02	2.66E−02	7.47E−03	−8.30E−03	−1.13E−01	−8.26E−04	9.00E−01
	177	3.83E−02	1.05E−01	2.99E−02	−3.37E−02	−4.59E−01	−3.79E−03	8.88E−01
CGP@Fe_{20}	97	7.92E−02	3.95E−01	1.08E−01	−1.17E−01	−1.59E + 00	−9.03E−03	9.23E−01
	154	4.63E−03	9.06E−03	1.88E−03	−1.49E−03	−2.03E−02	3.86E−04	1.26E + 00
	191	5.87E−02	1.52E−01	5.07E−02	−6.36E−02	−8.65E−01	−1.29E−02	7.98E−01
Rutin@Fe_{20}	126	1.17E−02	1.16E−01	2.10E−02	−1.31E−02	−1.79E−01	7.90E−03	1.60E + 00
	136	8.49E−04	6.40E−03	1.09E−03	−5.77E−04	−7.85E−03	5.11E−04	1.89E + 00
	185	2.26E−01	4.41E−02	2.49E−01	−4.86E−01	−6.61E + 00	−2.38E−01	5.11E−01
	178	2.77E−04	5.40E−03	9.03E−04	−4.57E−04	−6.21E−03	4.46E−04	1.98E + 00
	218	3.24E−03	7.86E−02	1.33E−02	−6.96E−03	−9.47E−02	6.35E−03	1.91E + 00

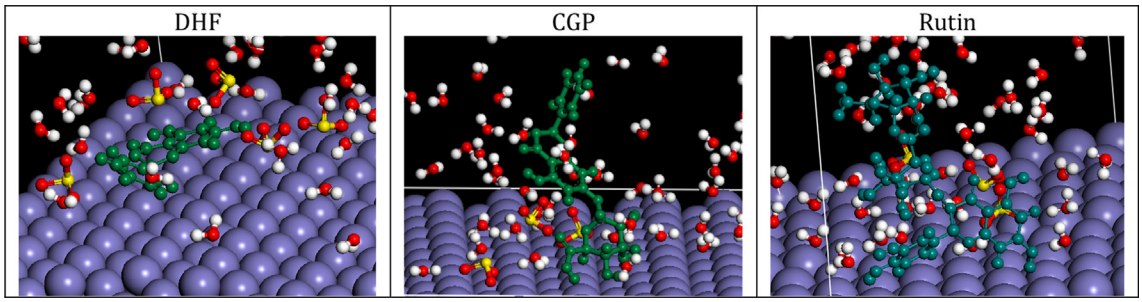

Fig. 14. MCS study results: a) Steel (blue)/carbon (grey)/ (O: red; H: white/inhibitor (green). (For interpretation of the references to colour in this figure legend, the reader is referred to the web version of this article.)

Table 9
Adsorption energies (kcal mol^{-1}) of the inhibition system.

		Energy				$\frac{dE_{ad}}{dN_i}$			
		Total	E_{ad}	E_{ra}	E_{def}	Inhibitor	H_2O	H^+	SO_4^{2-}
Inhibitor in water (1OO H_2O)	DHF	9.50	−1323.72	−34.84	−1288.87	−86.63	−9.95		
	CGP	29.41	−1354.59	−40.27	−1314.31	−119.69	−10.61		
	Rutin	59.33	−1335.55	−38.07	−1297.48	−102.48	−10.23		
Inhibitor in acidic medium (1OO H_2O + 10 H_2SO_4)	DHF	−9.61	−2671.99	−56.09	−2615.90	−91.32	−9.74	−28.04	−76.18
	CGP	18.73	−2694.44	−47.84	−2646.59	−114.23	−10.10	−28.59	−73.87
	Rutin	39.73	−2684.32	−58.42	−2625.90	−91.05	−10.17	−28.39	−76.88

On the contrary for DHF@Fe_{20}:BCPs 145, 154 and 177; CGP@Fe_{20}:BCPs 97 and 191 and for Rutin@Fe_{20}:BCP 185, Close inspection of the energetic AIM parameters reveals that the intermolecular hydrogen bonds in gas phase have positive $\nabla^2\rho_{BCP}$ and a negative H_{BCP} which show partially covalent character of the investigated interactions (G/|V|<1). The values of ρ_{BCP} and $\nabla^2\rho_{BCP}$ of intermolecular HB interactions are well correlated with the hydrogen bond energies strength which is calculated by Espinosa method [69]. It is known that the high electron density corresponds to the strongest HB with shorter H-bond distance and low electron density corresponds to the weakest HB with longer H-bond distance [70].

Fig. 14 depicts the inhibitors' optimal adsorption arrangement on the Fe(1 1 0) surface.

The inhibitors are adsorbed on the Fe(1 1 0) surface with an almost flat orientation. As it is shown. The inhibitor molecule (green colored) and metal surface engage in a donor–acceptor interaction. which results in parallel adsorption of the inhibitor molecule. The inhibitor molecule has π-electrons. which provide a high number of electrons to the unoccupied $d_{orbitals}$ of iron. On the other hand. the phenyl rings p-antibonding empty orbitals can accept an electron from the 4s or 3d orbitals of iron to produce feedback bonds. Many large-scale organic corrosion inhibitors, such as those described in refs [71–73], have this parallel arrangement on steel surface, in which the p–d hybridization plays a prominent role. However, small inhibitory molecules. Can chemisorb perpendicular to the iron surface with unsaturated heteroatoms via s molecular orbitals [71]. The values for adsorption–desorption and deformation energy are listed in Table 9. The results show that the three inhibitor molecules adsorb well on the iron surface in an acidic aqueous solution (CGP have a slight stronger adsorption energy in gas (isolated)) and liquid state). Moreover, the strength of the adsorption is proportional to the acidity of the solution. All of the adsorption energies were negative, indicating that the adsorption is exothermic and spontaneous.

Furthermore, the magnitude of E_{ads} may be used to determine the adsorption system stability. E_{ads}' greater absolute values are associated with more potent inhibitor–Fe(1 1 0) interactions and higher corrosion inhibition effectiveness.

4. Conclusion

CMFE was used in this research as an anti-corrosion additive to prevent the corrosion of carbon steel XC48 in H2SO4 solution. The CMFE as a mixed-type corrosion inhibitor, has been shown to suppress the cathodic and anodic reactions of XC48 carbon steel in electrochemical studies. At 500 ppm, the extract had a 95.91% anti-corrosion effectiveness. Furthermore, quantum chemistry proved that CMFE's inhibitory effectiveness was closely linked to its HOMO and LUMO energies. As an electron donor, it may lead to the formation of a stable organic coating on the metal surface, which would prevent corrosion in acidic solutions. Furthermore, practical testing and theoretical calculations were shown to be in excellent agreement with SEM observations, XPS and FT-IR analyses.

Declaration of Competing Interest

The authors declare that they have no known competing financial interests or personal relationships that could have appeared to influence the work reported in this paper.

Acknowledgement

Taif University research supporting Project number (TURSP-2020/46), Taif University, Taif, Saudi Arabia.

References

[1] H.M. Abd El-Lateef, M.A. Abo-Riya, A.H. Tantawy, Empirical and quantum chemical studies on the corrosion inhibition performance of some novel synthesized cationic gemini surfactants on carbon steel pipelines in acid pickling processes, Corros. Sci. 108 (2016) 94–110.
[2] X. Li, S. Deng, Inhibition effect of Dendrocalamus brandisii leaves extract on aluminum in HCl, H3PO4 solutions, Corros. Sci. 65 (2012) 299–308.
[3] S. El-Maksoud, The effect of organic compounds on the electrochemical behaviour of steel in acidic media. A review, Int. J. Electrochem. Sci., 3 (mai 2008) 528–555..
[4] M. Prabakaran, S.-H. Kim, K. Kalaiselvi, V. Hemapriya, I.-M. Chung, Highly efficient Ligularia fischeri green extract for the protection against corrosion of mild steel in acidic medium: Electrochemical and spectroscopic investigations, J. Taiwan Inst. Chem. Eng. 59 (2016) 553–562.
[5] P. Mourya, S. Banerjee, M.M. Singh, Corrosion inhibition of mild steel in acidic solution by Tagetes erecta (Marigold flower) extract as a green inhibitor, Corros. Sci. 85 (2014) 352–363.
[6] Q. Wang, B. Tan, H. Bao, Y. Xie, Y. Mou, P. Li, D. Chen, Y. Shi, X. Li, W. Yang, Evaluation of Ficus tikoua leaves extract as an eco-friendly corrosion inhibitor for carbon steel in HCl media, Bioelectrochemistry 128 (2019) 49–55.
[7] M. Behpour, S.M. Ghoreishi, N. Soltani, M. Salavati-Niasari, M. Hamadanian, A. Gandomi, Electrochemical and theoretical investigation on the corrosion inhibition of mild steel by thiosalicylaldehyde derivatives in hydrochloric acid solution, Corros. Sci. 50 (8) (2008) 2172–2181.
[8] A. Miralrio, A. Vázquez, Plant Extracts as Green Corrosion Inhibitors for Different Metal Surfaces and Corrosive Media: A Review, Processes, 8 (août 2020) 942, http://doi.org/10.3390/pr8080942..
[9] R.C. Barik, J.A. Wharton, R.J.K. Wood, K.R. Stokes, R.L. Jones, Corrosion, erosion and erosion–corrosion performance of plasma electrolytic oxidation (PEO) deposited Al_2O_3 coatings, Surf. Coat. Technol., 199 (2) (sept. 2005) 158–167, http://doi.org/10.1016/j.surfcoat.2004.09.038..
[10] A.L. Yerokhin, X. Nie, A. Leyland, A. Matthews, Characterisation of oxide films produced by plasma electrolytic oxidation of a Ti–6Al–4V alloy, Surf. Coat. Technol., 130 (2) (août 2000) 195–206, http://doi.org/10.1016/S0257-8972(00)00719-2..
[11] M.P. Asfia, M. Rezaei, G. Bahlakeh, Corrosion prevention of AISI 304 stainless steel in hydrochloric acid medium using garlic extract as a green corrosion inhibitor: Electrochemical and theoretical studies, J. Mol. Liq. 315 (2020) 113679, https://doi.org/10.1016/j.molliq.2020.113679.
[12] C. Keawhan, P. Wongpanya, N. Witit-anun, P. Songsiriritthigul, Corrosion behavior of AISI 4140 steel surface coated by physical vapor deposition, J. Met. Mater. Miner., vol. 22 (1) (juin 2012) Art. n° 1, Consulté le: janv. 18, 2021. [En ligne]. Disponible sur: http://www.jmmm.material.chula.ac.th/index.php/jmmm/article/view/25..
[13] R.T. loto, C.A. Loto, M. Akinyele, Effect of ginger, pomegranate and celery extracts on zinc electrodeposition, surface morphology and corrosion inhibition of mild steel, Alex. Eng. J., vol. 59 (2) 933–941, avr. 2020, http://doi.org/10.1016/j.aej.2020.03.014..
[14] C.-X. Wang, X.-F. Zhang, A non-particle and fluorine-free superhydrophobic surface based on one-step electrodeposition of dodecyltrimethoxysilane on mild steel for corrosion protection, Corros. Sci. 163 (2020) 108284, https://doi.org/10.1016/j.corsci.2019.108284.
[15] A.F. Baldissera, C.A. Ferreira, Coatings based on electronic conducting polymers for corrosion protection of metals, Prog. Org. Coat. 75 (3) (2012) 241–247.
[16] R. Selvaraj, M. Selvaraj, S.V.K. Iyer, Studies on the evaluation of the performance of organic coatings used for the prevention of corrosion of steel rebars in concrete structures, Prog. Org. Coat. 64 (4) (2009) 454–459.
[17] C. Verma, L.O. Olasunkanmi, E.E. Ebenso, M.A. Quraishi, Substituents effect on corrosion inhibition performance of organic compounds in aggressive ionic solutions: A review, J. Mol. Liq. 251 (2018) 100–118.
[18] A.S. Yaro, A.A. Khadom, R.K. Wael, Apricot juice as green corrosion inhibitor of mild steel in phosphoric acid, Alexandria Eng. J. 52 (1) (2013) 129–135.
[19] M.A. El-Hashemy, A. Sallam, The inhibitive action of Calendula officinalis flower heads extract for mild steel corrosion in 1 M HCl solution, J. Mater. Res. Technol. 9 (6) (2020) 13509–13523.
[20] A. Sedik, D. Lerari, A. Salci, S. Athmani, K. Bachari, İ.H. Gecibesler, R. Solmaz, Dardagan Fruit extract as eco-friendly corrosion inhibitor for mild steel in 1 M HCl: Electrochemical and surface morphological studies, J. Taiwan Inst. Chem. Eng. 107 (2020) 189–200.
[21] K.C.d.S.d. Lima, V.M. Paiva, D. Perrone, B. Ripper, G. Simões, M.L.M. Rocco, A.G. d. Veiga, E. D'Elia, Glycine max meal extracts as corrosion inhibitor for mild steel in sulphuric acid solution, J. Mater. Res. Technol. 9 (6) (2020) 12756–12772.

[22] E.d.B. Policarpi, A. Spinelli, Application of Hymenaea stigonocarpa fruit shell extract as eco-friendly corrosion inhibitor for steel in sulfuric acid, J. Taiwan Inst. Chem. Eng. 116 (2020) 215–222.
[23] O.R. Pereira, A.M.S. Silva, M.R.M. Domingues, S.M. Cardoso, Identification of phenolic constituents of Cytisus multiflorus, Food Chem. 131 (2) (2012) 652–659.
[24] O.R. Pereira et al., Cytisus multiflorus: source of antioxidant polyphenols, 11º Encontro Quím. Aliment., 2012, Consulté le: sept. 06, 2021. [En ligne]. Disponible sur: https://bibliotecadigital.ipb.pt/handle/10198/8268..
[25] Z. Tao, S. Zhang, W. Li, B. Hou, Corrosion inhibition of mild steel in acidic solution by some oxo-triazole derivatives, Corros. Sci., (nov. 2009) 2588–2595..
[26] H. Zarrok, A. Zarrouk, B. Hammouti, R. Salghi, C. Jama, F. Bentiss, Corrosion control of carbon steel in phosphoric acid by purpald – Weight loss, electrochemical and XPS studies, Corros. Sci. 64 (2012) 243–252.
[27] B.A. Shainyan, N.N. Chipanina, T.N. Aksamentova, L.P. Oznobikhina, G.N. Rosentsveig, I.B. Rosentsveig, Intramolecular hydrogen bonds in the sulfonamide derivatives of oxamide, dithiooxamide, and biuret. FT-IR and DFT study, AIM and NBO analysis, Tetrahedron 66 (44) (2010) 8551–8556.
[28] S.J. Grabowski, J.M. Ugalde, Bond Paths Show Preferable Interactions: Ab Initio and QTAIM Studies on the X−H···π Hydrogen Bond, J. Phys. Chem. A 114 (26) (2010) 7223–7229.
[29] M. Abdallah, H.M. Altass, A.S. Al-Gorair, J.H. Al-Fahemi, B.A.A.L. Jahdaly, K.A. Soliman, Natural nutmeg oil as a green corrosion inhibitor for carbon steel in 1.0 M HCl solution: Chemical, electrochemical, and computational methods, J. Mol. Liq., 323 (févr. 2021) 115036, http://doi.org/10.1016/j.molliq.2020.115036..
[30] L. Boucherit, T. Douadi, N. Chafai, M. Al-Noaimi, et S. Chafaa, The inhibition Activity of 1,10 - bis(2-formylphenyl)-1,4,7,10- tetraoxadecane (Ald) and its Schiff base (L) on the Corrosion of Carbon Steel in HCl: Experimental and Theoretical Studies, Int. J. Electrochem. Sci., 13 (mars 2018), http://doi.org/10.20964/2018.04.59..
[31] Jun Tang et al., Electrochemical Behavior of Jasmine Tea Extract as Corrosion Inhibitor for Carbon Steel in Hydrochloric Acid Solution, Int. J. Electrochem. Sci., (2018) 3625–3642..
[32] H. Ferkous, S. Djellali, R. Sahraoui, Y. Benguerba, H. Behloul, et A. Çukurovali, Corrosion inhibition of mild steel by 2-(2-methoxybenzylidene) hydrazine-1-carbothioamide in hydrochloric acid solution: Experimental measurements and quantum chemical calculations, J. Mol. Liq., 307 (juin 2020) 112957, http://doi.org/10.1016/j.molliq.2020.112957..
[33] Z. Panossian, N.L. de Almeida, R.M. Ferreira de Sousa, G. de Souza Pimenta, L.B. Schmidt Marques, Corrosion of carbon steel pipes and tanks by concentrated sulfuric acid, Corros. Sci., (2012) 1–11..
[34] H. Lahbib, S. Ben Hassen, H. Gerengi, Y. Ben Amor, Inhibition effect of Cynara cardunculus leaf extract on corrosion of St37 steel immersed in seawater with and without bleach solution, (2020)..
[35] W. Ebdelly, S. Ben Hassan, X.R. Novoa, et Y. Ben Amor, Inhibition of carbon steel corrosion in calcareous chloride solution by Eruca Sativa extract, Physicochemical problems of materials protection, (2019) 519–602..
[36] Y. Ben Amor et al., Electrochemical study of the tarnish layer of silver deposited on glass, Electrochimica Acta, (2014) 89..
[37] A. Belakhdar et al., Computational and experimental studies on the efficiency of Rosmarinus officinalis polyphenols as green corrosion inhibitors for XC48 steel in acidic medium, (2020)..
[38] N.Z.N. Hashim, E.H. Anouar, K. Kassim, H.M. Zaki, A.I. Alharthi, Z. Embong, « XPS and DFT investigations of corrosion inhibition of substituted benzylidene Schiff bases on mild steel in hydrochloric acid, Appl. Surf. Sci. 476 (2019) 861–877.
[39] Q. Qu et al., Corrosion behavior of cold rolled steel in artificial seawater in the presence of Bacillus subtilis C, Corros. Sci. (2015) 321–329.
[40] H. Lgaz, S. Masroor, M. Chafiq, M. Damej, A. Brahmia, R. Salghi, M. Benmessaoud, I.H. Ali, M.M. Alghamdi, A. Chaouiki, I.-M. Chung, Evaluation of 2-Mercaptobenzimidazole Derivatives as Corrosion Inhibitors for Mild Steel in Hydrochloric Acid, Metals 10 (3) (2020) 357, https://doi.org/10.3390/met10030357.
[41] C. Zou, X. Yan, Y. Qin, M. Wang, Y. Liu, Inhibiting evaluation of b-Cyclodextrin-modified acrylamide polymer on alloy steel in sulfuric solution, Corros. Sci. (2014) 445–454.
[42] H. Gerengi, I. Uygur, M. Solomon, M. Yildiz, H. Goksu, Evaluation of the inhibitive effect of Diospyros kaki (Persimmon) leaves extract on St37 steel corrosion in acid medium, Sustain. Chem. Pharm 4 (2016) 57–66.
[43] R. Ashokkumar, M. Ramaswamy, Phytochemical screening by FTIR spectroscopic analysis of leaf extracts of selected Indian medicinal plants, Int. J. Curr. Microbiol. Appl. Sci., (2014) 395–406..
[44] S. Chitra, B. Anand, Surface morphological and FTIR spectroscopic information on the corrosion inhibition of drugs on mild steel in chloride environment, J. Chem. Pharm. Sci., (2017) 453–456..
[45] P. Jain, A. Soni, P. Jain, J. Bhawsar, Phytochemical analysis of Mentha spicata plant extract using UV-VIS, FTIR and GC/MS technique, nov. 05, 2016..
[46] R. Haldhar, D. Prasad, A. Saxena, Myristica fragrans extract as an eco-friendly corrosion inhibitor for mild steel in 0.5 M H2SO4 solution, J. Environ. Chem. Eng. 6 (2) (2018) 2290–2301.
[47] D. Gopi, E.-S. Sherif, V. Manivannan, D. Rajeswari, M. Surendiran, L. Kavitha, Corrosion and Corrosion Inhibition of Mild Steel in Groundwater at Different Temperatures by Newly Synthesized Benzotriazole and Phosphono Derivatives, Ind. Eng. Chem. Res. 53 (11) (2014) 4286–4294.
[48] D.K. Verma, F. Khan, Corrosion inhibition of mild steel in hydrochloric acid using extract of glycine max leaves, Res Chem Intermed 42 (4) (2016) 3489–3506.
[49] Z. Meriem, F. Hana, D. Souad, B. Abderrazak, M.A. Amin, R. Leila, A. Belakhdar, B.-H. Jeon, C. Boulechfar, Y. Benguerba, Experimental and theoretical evaluation of the adsorption process of some polyphenols and their corrosion inhibitory properties on mild steel in acidic media, J. Environ. Chem. Eng. 9 (6) (2021) 106482, https://doi.org/10.1016/j.jece:2021.106482.
[50] P. Muthukrishnan, B. Jeyaprabha, P. Prakash, Adsorption and corrosion inhibiting behavior of Lannea coromandelica leaf extract on mild steel corrosion, Arabian J. Chem. 10 (2017) S2343–S2354.
[51] M. Pitchaipillai, K. Raj, J. Balasubramanian, P. Periakaruppan, Benevolent behavior of Kleinia grandiflora leaf extract as a green corrosion inhibitor for mild steel in sulfuric acid solution, Int. J. Miner. Metall. Mater. 21 (11) (2014) 1083–1095.
[52] M. Tourabi, K. Nohair, M. Traisnel, C. Jama, F. Bentiss, Electrochemical and XPS studies of the corrosion inhibition of carbon steel in hydrochloric acid pickling solutions by 3,5-bis(2-thienylmethyl)-4-amino-1,2,4-triazole, Corros. Sci. 75 (2013) 123–133.
[53] X. Luo, X. Pan, S. Yuan, S. Du, C. Zhang, Y. Liu, Corrosion inhibition of mild steel in simulated seawater solution by a green eco-friendly mixture of glucomannan (GL) and bisquaternary ammonium salt (BQAS), Corros. Sci. 125 (2017) 139–151.
[54] M. Bouanis, M. Tourabi, A. Nyassi, A. Zarrouk, C. Jama, F. Bentiss, Corrosion inhibition performance of 2,5-bis(4-dimethylaminophenyl)-1,3,4-oxadiazole for carbon steel in HCl solution: Gravimetric, electrochemical and XPS studies, Appl. Surf. Sci. 389 (2016) 952–966.
[55] M. Cui, Y. Yu, Y. Zheng, Effective Corrosion Inhibition of Carbon Steel in Hydrochloric Acid by Dopamine-Produced Carbon Dots, Polymers 13 (12) (2021), https://doi.org/10.3390/polym13121923.
[56] H. Lahbib, S. Ben Hassen, H. Gerengi, M. Rizvi, Y. Ben Amor, Corrosion inhibition performance of dwarf palm and Cynaracardunculus leaves extract for St37 steel in 15% H 2 SO 4 : a comparative study, J. Adhes. Sci. Technol., (sept. 2020) 1–32..
[57] W. Temesghen, P. Sherwood, Analytical utility of valence band X-ray photoelectron spectroscopy of iron and its oxides, with spectral interpretation by cluster and band structure calculations, Anal. Bioanal. Chem. 373 (7) (2002) 601–608.
[58] K. Babić-Samardžija, C. Lupu, N. Hackerman, A.R. Barron, A. Luttge, Inhibitive Properties and Surface Morphology of a Group of Heterocyclic Diazoles as Inhibitors for Acidic Iron Corrosion, Langmuir 21 (26) (2005) 12187–12196.
[59] A. Galtayries, R. Warocquier-Clérout, M.-D. Nagel, P. Marcus, Fibronectin adsorption on Fe–Cr alloy studied by XPS, Surf. Interface Anal. 38 (4) (2006) 186–190, https://doi.org/10.1002/sia.2295.
[60] R.G. Parr, C. Hill, N. Carolina, Electrophilicity Index, 121 (9) (1999) 1922–1924 http://doi.org/10.1021/ja983494x..
[61] R.G. Parr, R.G. Pearson, Absolute Hardness : Companion Parameter to Absolute Electronegativity, (1983) 7512–7516..
[62] B. Gomez, N.V. Likhanova, M.A. Dominguez-Aguilar, R. Martinez-Palou, A. Vela, J.L. Gasquez, Quantum chemical study of the inhibitive properties of 2-pyridyl-azoles, J. Phys. Chem. B. 110 (18) (2006) 8928–8934, https://doi.org/10.1021/jp057143y.
[63] W. Bououden, Y. Benguerba, A.S. Darwish, A. Attoui, T. Lemaoui, M. Balsamo, A. Erto, I.M. Alnashef, Surface adsorption of Crizotinib on carbon and boron nitride nanotubes as Anti-Cancer drug Carriers: COSMO-RS and DFT molecular insights, J. Mol. Liq. 338 (2021) 116666, https://doi.org/10.1016/j.molliq.2021.116666.
[64] T. Lemaoui, A.S. Darwish, A. Attoui, F. Abu Hatab, N.E.H. Hammoudi, Y. Benguerba, L.F. Vega, I.M. Alnashef, Predicting the density and viscosity of hydrophobic eutectic solvents: towards the development of sustainable solvents, Green Chem. 22 (23) (2020) 8511–8530.
[65] T. Lemaoui et al., Prediction of Electrical Conductivity of Deep Eutectic Solvents Using COSMO-RS Sigma Profiles as Molecular Descriptors: A Quantitative Structure–Property Relationship Study | Industrial & Engineering Chemistry Research, 2020, https://pubs.acs.org/doi/abs/10.1021/acs.iecr.0c02542 (consulté le oct. 14, 2021)..
[66] A.S. Darwish, F. Abu Hatab, T. Lemaoui, O. A. Z. Ibrahim, G. Almustafa, B. Zhuman, S. E. E. Warrag, M.K. Hadj-Kali, Y. Benguerba, I.M. Alnashef, Multicomponent extraction of aromatics and heteroaromatics from diesel using acidic eutectic solvents: Experimental and COSMO-RS predictions, J. Mol. Liq. 336 (2021) 116575, https://doi.org/10.1016/j.molliq.2021.116575.
[67] T. Lemaoui, F. Abu Hatab, A.S. Darwish, A. Attoui, N.E.H. Hammoudi, G. Almustafa, M. Benaicha, Y. Benguerba, I.M. Alnashef, Molecular-Based Guide to Predict the pH of Eutectic Solvents: Promoting an Efficient Design Approach for New Green Solvents, ACS Sustain. Chem. Eng. 9 (17) (2021) 5783–5808.
[68] M. Yoosefian, A. Pakpour, N. Etminan, Nanofilter platform based on functionalized carbon nanotubes for adsorption and elimination of Acrolein, a toxicant in cigarette smoke, Appl. Surf. Sci. 444 (2018) 598–603.
[69] Z. Hasanzade, H. Raissi, Solvent/co-solvent effects on the electronic properties and adsorption mechanism of anticancer drug Thioguanine on Graphene oxide surface as a nanocarrier: Density functional theory investigation and a molecular dynamics, Appl. Surf. Sci. 422 (2017) 1030–1041.

[70] H. Ghiassi, H. Raissi, Investigation of adsorption properties of CS_2 on interior and exterior surfaces of single-walled silicon-carbide nanotubes and effect of applied electric field: electronic structure, charge density and NMR studies, RSC Adv., 5 (102) (oct. 2015) 84022–84037, http://doi.org/10.1039/c5ra06459g..
[71] N. Ding, X. Chen, C.-M. Lawrence Wu, Interactions between polybrominated diphenyl ethers and graphene surface: a DFT and MD investigation, Environ. Sci. Nano 1 (1) (2014) 55–63, https://doi.org/10.1039/C3EN00037K.
[72] A. Dutta, S.K. Saha, P. Banerjee, D. Sukul, Correlating electronic structure with corrosion inhibition potentiality of some bis-benzimidazole derivatives for mild steel in hydrochloric acid: Combined experimental and theoretical studies, Corros. Sci. 98 (2015) 541–550.
[73] N. Kovačević, A. Kokalj, Chemistry of the interaction between azole type corrosion inhibitor molecules and metal surfaces, Mater. Chem. Phys. 137 (1) (2012) 331–339.